

**Total Synthesis of Terpenoid Natural Products: A Platform for Discovery in Chemical Biology and  
for the Development of New Chemical Methods**

by

James Annand

A dissertation submitted in partial fulfillment  
of the requirements for the degree of  
Doctor of Philosophy  
(Chemical Biology)  
in the University of Michigan  
2019

Doctoral Committee:

Associate Professor Corinna S. Schindler, Chair  
Professor Anna K. Mapp  
Professor John Montgomery  
Professor John P. Wolfe

James Annand

[jannand@umich.edu](mailto:jannand@umich.edu)

ORCID iD: [0000-0002-2026-9985](https://orcid.org/0000-0002-2026-9985)

© James Annand 2019

## **Dedication**

This thesis is dedicated to the undergraduates, graduate students, and postdocs that worked in the Schindler group between 2014 and 2019 without whom none of this work would be possible.

## **Acknowledgements**

I would like to specifically acknowledge the collaborators who worked on this thesis work with me. The work described in chapter 2 was done in collaboration with Dr. Paul Bruno, Dr. Andrew Henderson, Dr. Kyle Cole, Aaron Maurais, Max Kuang, Lynne Balsius, Professor Anna Mapp, Professor Angela Koehler, Professor Eranthie Weerapana, Professor Kristen Verhey. This work was enabled by the Swanson Biotechnology Center High Throughput Sciences Core at the Koch Integrative Cancer Research Institute at MIT as well as the Microscopy and Imaging Analysis Laboratory at the Biomedical Sciences Research Building at the University of Michigan. The work described in chapter 3 was done in collaboration with Dr. Paul Riehl, Max Kuang, and Dr. Danielle Schultz. This work was enabled by the Catalysis and Enabling Technology group at Merck Process Chemistry. The work described in chapter 4 was done in collaboration with Dr. Yvonne DePorre and Dr. Sukanta Bar. All work described was done under the guidance and with the support of my advisor Professor Corinna Schindler and with the advisement of my committee members through the years, Professor Anna Mapp, Professor John Montgomery, Professor John Wolfe, Professor Brent Martin, and Professor Matthew Soellner.



## Table of Contents

Dedication	ii
Acknowledgements	iii
List of Figures	viii
List of Appendices	xvi
Abstract	xvii
Chapter 1 Introduction	1
Chapter 1.1 Nuclear Factor-kappaB(NF-κB)	1
Chapter 1.1.1 NF-κB structure and function	1
Chapter 1.1.2 IKK kinases and NF-κB regulation	3
Chapter 1.1.3 NF-κB pathway activation	9
Chapter 1.1.4 Physiological consequences of NF-κB related dysregulation	12
Chapter 1.1.5 Inhibitors and inhibition of the NF-κB pathway	14
Chapter 1.2 Michael accepting enones as bioactive molecules and covalent inhibitors	19
Chapter 1 Bibliography	28
Chapter 2 Gibberellins as Inhibitors of the NF-κB Pathway	33
Chapter 2.1 Introduction	33
Chapter 2.1.1 Gibberellic acid ( <b>2-1</b> ) isolation and biosynthesis	33
Chapter 2.1.2 Gibberellic acid ( <b>2-1</b> ) synthesis	36
Chapter 2.1.3 Gibberellic acid ( <b>2-1</b> ) biological activity	39

Chapter 2.1.4 Pharbinilic acid ( <b>2-5</b> ) isolation and biological activity	43
Chapter 2.2 Synthesis and biological evaluation of pharbinilic acid ( <b>2-5</b> )	44
Chapter 2.3 Evaluation of gibberellins as NF- $\kappa$ B pathway inhibitors	49
Chapter 2.3.1 Structure Activity Relationship (SAR) studies—synthesis and NF- $\kappa$ B pathway inhibition	49
Chapter 2.3.2 Structure Activity Relationship (SAR) studies—HTS Cell Titre Glo	54
Chapter 2.3.3 NF- $\kappa$ B nuclear translocation studies—highlighting a potential MoA	56
Chapter 2.3.4 Pulldown studies and proteomics	60
Chapter 2.4 Conclusions and mechanistic hypothesis	65
Chapter 2 Bibliography	66
Chapter 3 Efforts Towards the Unified Synthesis of the <i>ent</i> -Kaurene Diterpenoids	69
Chapter 3.1 Introduction	69
Chapter 3.1.1 <i>ent</i> -Kaurene history and biosynthesis	69
Chapter 3.1.2 Selected biological activities of <i>ent</i> -kaurene diterpenoids	72
Chapter 3.1.3 <i>ent</i> -Kaurene classifications	79
Chapter 3.1.4 Selected syntheses towards the <i>ent</i> -kaurene diterpenoids	82
Chapter 3.2 Retrosynthetic analysis for a unified approach to the <i>ent</i> -kaurene diterpenoids	97
Chapter 3.2.1 Eriocalyxin B as a retrosynthetic target	97
Chapter 3.2.2 Retrosynthetic analysis highlights a common intermediate to the <i>ent</i> -kaurene diterpenoids	100
Chapter 3.2.3 Model system studies towards synthesizing a common intermediate to the <i>ent</i> -kaurene diterpenoids	104
Chapter 3.3 The synthesis of a common intermediate towards the <i>ent</i> -kaurene diterpenoids	110

Chapter 3.3.1 Synthesis of the A ring fragment	110
Chapter 3.3.2 Synthesis of the C ring fragment	115
Chapter 3.3.3 Combining the A ring and C ring fragments towards a common intermediate to the <i>ent</i> -kaurenes	117
Chapter 3 Bibliography	120
Chapter 4 Lewis Base-Catalyzed Reductive Aldol Reaction to Access Quaternary Carbons	124
Chapter 4.1 Introduction	124
Chapter 4.2 Reaction optimization and diastereoselectivity	129
Chapter 4.3 Substrate scope and derivitization	134
Chapter 4 Bibliography	141
Appendices	144
Appendix 1 Chapter 2 Supplementary Information	144
Appendix 2 Chapter 3 Supplementary Information	153
Appendix Bibliography	166

## **List of Figures**

Figure 1.1 Protein maps of key NF- $\kappa$ B family members.	2
Figure 1.2 In the canonical NF- $\kappa$ B pathway IKK $\alpha$ , IKK $\beta$ , and NEMO phosphorylate inhibition complex which signals for proteolytic processing and provides active complexes which are actively imported into the nucleus where they bind DNA and signal for the transcription of genes.	5
Figure 1.3 In the noncanonical NF- $\kappa$ B pathway IKK $\alpha$ dimers phosphorylate p100 for proteolytic processing and provides active complexes which are actively imported into the nucleus where they bind DNA.	6
Figure 1.4 Transcriptionally inactive subunits of NF- $\kappa$ B can fall under two paradigms of activity.	7
Figure 1.5 Common activation modes of canonical and noncanonical NF- $\kappa$ B pathway activity.	9
Figure 1.6 A common motif in TAK1 control is to phosphorylate and degrade ubiquitinases like RIP1 or TRAF6. This prevents RIP1 or TRAF6 from ubiquitinating and degrading TAK1.	10
Figure 1.7 In noncanonical NF- $\kappa$ B activation TNFR superfamily receptors like CD40R recruit cIAP to the membrane,	11
Figure 1.8 Anti-inflammatory molecules with characterized activity against the NF- $\kappa$ B pathway.	15
Figure 1.9 Pharmaceutically developed IKK inhibitors.	16
Figure 1.10 Protease inhibitors that have been shown to inhibit the NF- $\kappa$ B pathway.	17

Figure 1.11 The general scheme of a Michael addition between a reactive thiol with an enone.	19
Figure 1.12 Successful examples of overcoming apparent PAINs to advance natural products to specific and active pharmaceuticals.	21
Figure 1.13 Michael acceptors in recently approved pharmaceuticals.	23
Figure 1.14 Kazusamycin A ( <b>1-35</b> ) and related analogs with their reported IC <sub>50</sub> values against HPAC cells.	24
Figure 1.15 Elephantopin ( <b>1-40</b> ) possesses 3 electronically similar, but conformationally distinct Michael acceptors providing a case study in the consequences of enone confirmation on reactivity.	24
Figure 1.16 Strategies for handling overly reactive exocyclic Michael acceptors (red).	26
Figure 2.1 Selected gibberellin diterpenoids.	34
Figure 2.2 The first step in gibberellin biosynthesis is the conversion of GGPP ( <b>2-7</b> ) to <i>ent</i> -CPP ( <b>2-8</b> ).	34
Figure 2.3 The biosynthesis of gibberellic acid ( <b>2-1</b> ) from <i>ent</i> -kaurene ( <b>2-10</b> ) and GA <sub>12</sub> ( <b>2-6</b> ).	36
Figure 2.4 Highlights from Corey's 1978 synthesis of gibberellic acid ( <b>2-1</b> ).	37
Figure 2.5 Side reactions from gibberellic acid ( <b>2-1</b> ) include Wagner Meerwein rearrangements, eliminations, and aromatizations.	38
Figure 2.6 Bioactive gibberellins bind the nuclear receptor GID1, which induces a conformational change, which allows GID1 to recruit and promote the degradation of DELLA proteins.	41
Figure 2.7 Structure of GA-13315 ( <b>2-28</b> ).	42

Figure 2.8 Pharbinilic acid ( <b>2-5</b> ) isolation and biological activity.	43
Figure 2.9 Retrosynthetic analysis of pharbinilic acid ( <b>2-5</b> ).	44
Figure 2.10 A synthesis of key intermediate <b>2-30</b> .	45
Figure 2.11 Key precedent by Wang and coworkers inspired and attempted oxidative coupling of <b>2-42</b> .	46
Figure 2.12 The completion of the total synthesis of pharbinilic acid ( <b>2-5</b> ).	47
Figure 2.13 Initial biological evaluation of synthetic gibberellins as inhibitors of the NF-kB pathway as determined by a Luciferase reporter gene assay.	48
Figure 2.14 Quantitative PCR analysis of NF-kB controlled gene MIP3a shows that <b>2-30</b> inhibits NF-kB driven transcription.	49
Figure 2.15 SAR studies around functionalizing the B ring carboxylic acid.	50
Figure 2.16 SAR studies around the H9 epimeric state in allogibberellins	51
Figure 2.17 SAR studies around the H9 epimeric state in C/D ring epimerized allogibberellins.	51
Figure 2.18 SAR studies around the H9 epimeric state in native C/D ring allogibberellins.	52
Figure 2.19 SAR studies around the native C/D ring enones.	53
Figure 2.20 SAR studies around epimerizing the C/D ring juncture with halogen electrophiles.	53
Figure 2.21 Hierarchical clustering of HTS Cell Titre Glo cell viability assays cluster NF-kB inhibiting gibberellins and the positive control MG-132.	54
Figure 2.22 Enone <b>2-30</b> selectively kills cell lines derived from inflammatory cancers or lymphoma as determine by a HTS Cell Titre Glo cell viability assay.	55
Figure 2.23 Immunohistochemical staining of HUVEC cells.	57

Figure 2.24 Immunohistochemical staining and confocal microscopy of Hek-293T cells upon treatment with DMSO, <b>2-36</b> , or <b>2-30</b> in the presence or absence of induction by IL-1 $\beta$ .	58
Figure 2.25 Immunohistochemical staining and confocal microscopy of Hek-293T in the presence or absence of NF- $\kappa$ B pathway induction by IL-1 $\beta$ .	59
Figure 2.26 Hek-293T cells in the absence or presence of induction by IL-1 $\beta$ and the absence or presence of treatment with <b>2-36</b> or <b>2-30</b> were fractioned and analyzed by Western blotting for the presence of pathway members.	60
Figure 2.27 Synthesis of the first generation of pulldown probe molecules.	60
Figure 2.28 Silver stained protein gel of Hek-293T Nutravadin pulldowns using biotinylated analogs of <b>2-36</b> and <b>2-30</b> .	61
Figure 2.29 Western blotting of Hek-293T cells pulled down with 5 $\mu$ M <b>2-86</b> .	62
Figure 2.30 Treatment of Hek-293T cell lysates with alkyne <b>2-56</b> followed by clicking onto a fluorescent azide and running on a gel.	63
Figure 2.31 Results of SILAC mass spectrometry competition pulldown experiments in which Hek-293T are pretreated with 10 $\mu$ M of a synthetic gibberellin, or DMSO, before being pulled down with <b>2-56</b> .	64
Figure 2.32 Results of SILAC mass spectrometry competition pulldown experiments in which Hek-293T are pretreated with 10 $\mu$ M of a synthetic gibberellin, or DMSO, before being pulled down with <b>2-56</b> .	65
Figure 3.1 Parent structures for the kaurene diterpenoids.	69
Figure 3.2 Some of the earliest studied <i>ent</i> -kaurene diterpenoids.	70
Figure 3.3 The first step in kaurene biosynthesis is the conversion of GGPP ( <b>3-6</b> ) to CPP ( <b>3-7</b> ) or <i>ent</i> -CPP ( <b>3-8</b> ).	71

Figure 3.4 The formation of <i>ent</i> -kaurene ( <b>3-2</b> ) from <i>ent</i> -CPP ( <b>3-7</b> ).	72
Figure 3.5 <i>ent</i> -Kaurene diterpenoids that bear an exocyclic Michael acceptor (blue) are also found to be active against Gram positive bacteria.	74
Figure 3.6 Several <i>ent</i> -kaurene diterpenoids have well studied biological activities against oncogenic pathways.	77
Figure 3.7 <i>ent</i> -Kaurene diterpenoids that bear exocyclic Michael acceptors are found to be generally cytotoxic towards cancer derived cell lines.	78
Figure 3.8 Published medicinal chemistry indicates that ablating reactive exocyclic Michael acceptors enhances selectivity.	79
Figure 3.9 Two major classifications of <i>ent</i> -kaurene diterpenoids pertain to their oxidation pattern at C <sub>20</sub> .	80
Figure 3.10 Three major classification of <i>ent</i> -kaurene diterpenoids that pertain to the disconnections across the tetracyclic core structure.	81
Figure 3.11 Highlights from Ireland's 1966 synthesis of kaurene.	82
Figure 3.12 Highlights from Fujita's 1972 relay synthesis of enmein ( <b>3-3</b> ).	83
Figure 3.13 Highlights from Ziegler's 1977 racemic synthesis of steviol methyl ester ( <b>3-52</b> ).	84
Figure 3.14 Highlights from Sniders's 1998 racemic synthesis of isosteviol ( <b>3-55</b> ).	85
Figure 3.15 Highlights from Baran's 2013 enantioselective synthesis of steviol ( <b>3-5</b> ).	86
Figure 3.16 Highlights from Mander's 1986 racemic synthesis of 15-Desoxy-effusin ( <b>3-69</b> ).	87
Figure 3.17 Synthetic route towards the Riesman group's common intermediate to select <i>ent</i> -kaurene diterpenoids <b>3-78</b> .	88
Figure 3.18 Intermediate <b>3-78</b> is converted to maecrystal Z ( <b>3-25</b> ) as well as (-)-trichorabdal A ( <b>3-26</b> ) and (-)-longikaurin E ( <b>3-27</b> ).	89



Figure 3.19 Structural features of maoecrystal V ( <b>3-28</b> ).	90
Figure 3.20 Key disconnections by Baran, Yang, and Zakarian in early studies towards maoecrystal V ( <b>3-28</b> ) take advantage of oxidative dearomatization-Diels-Alder sequences.	92
Figure 3.21 Key disconnections by Danishefsky along with Nicolaou and Chen in early studies towards maoecrystal V ( <b>3-28</b> ) take advantage of generating an enolate diene for a Diels-Alder reaction.	93
Figure 3.22 Highlights from Thomson's 2014 enantioselective synthesis of maoecrystal V ( <b>3-28</b> ).	95
Figure 3.23 Highlights from Baran's 2016 enantioselective synthesis of maoecrystal V ( <b>3-28</b> ).	96
Figure 3.24 1990 semi-synthesis of eriocalyxin B ( <b>3-19</b> ) from oridonin ( <b>3-17</b> ).	99
Figure 3.25 Lee group's 2018 synthesis of eriocalyxin B ( <b>3-19</b> ).	100
Figure 3.26 Retrosynthetic analysis of eriocalyxin B ( <b>3-19</b> ) provides spirocyclic lactone <b>3-120</b> .	101
Figure 3.27 Common intermediate <b>3-127</b> could be converted to laxiflorin B ( <b>3-32</b> ) and thus to a wide variety of <i>ent</i> -kaurene diterpenoids bearing a common scaffold.	102
Figure 3.28 Common intermediate <b>3-127</b> could be converted <i>ent</i> -kaurene diterpenoids that lack the connectivity of the C/D ring with and without attachment between C <sub>6</sub> and C <sub>7</sub> .	103
Figure 3.29 A convergent strategy to <b>3-127</b> would allow for extension of the initial synthetic efforts to additional <i>ent</i> -kaurenes depending on the oxidation state of precursors used.	104
Figure 3.30 The first approach towards a common intermediate to the <i>ent</i> -kaurene diterpenoids.	105
Figure 3.31 The second approach towards a common intermediate to the <i>ent</i> -kaurene	

diterpenoids.	106
Figure 3.32 The third approach towards a common intermediate to the <i>ent</i> -kaurene diterpenoids.	107
Figure 3.33 The fourth approach towards the <i>ent</i> -kaurene diterpenoids successfully provides the desired product.	109
Figure 3.34 First approach to A ring fragment <b>3-184</b> .	110
Figure 3.35 Second approach to A ring fragment <b>3-184</b> .	111
Figure 3.36 Successful synthesis of <b>3-188</b> .	112
Figure 3.37 Attempts to do a directed C-H oxidation towards <b>3-197</b> .	113
Figure 3.38 Initial results via an oxidation, isomerization strategy towards <b>3-209</b> .	114
Figure 3.39 Current strategy towards A ring fragment <b>3-217</b> .	115
Figure 3.40 Current strategy towards C ring fragment <b>3-225</b> .	116
Figure 3.41 Methodology required to determine the enantiomeric excess of <b>3-225</b> .	117
Figure 3.42 The synthesis of Mizoroki-Heck substrate <b>3-230</b> .	117
Figure 3.43 Current efforts towards the optimization of a Mizoroki-Heck reaction towards <b>3-231</b> and <b>3-232</b> .	118
Figure 4.1 Synthetic strategies towards atropurpuran ( <b>4-4</b> ) and isopalhinine A ( <b>4-5</b> ) rely on common core structure and common intermediate <b>4-3</b> .	125
Figure 4.2 A retrosynthetic analysis of isopalhinine A ( <b>4-5</b> ) reveals a challenging aldol disconnection to provide <b>4-6</b> from <b>4-7</b> .	125
Figure 4.3 A reductive aldol reaction would provide regioselectivity towards the formation of <b>4-6</b> .	126

Figure 4.4 Literature precedents highlight underexplored substrates for a reductive aldol methodology.	127
Figure 4.5 Denmark's proposed transition states account for stereodivergent outcomes based upon relative equivalencies of silenol ether <b>4-14</b> and phosphoramidate.	128
Figure 4.6 Optimization of the triaryl phosphine oxide Lewis base catalyst.	130
Figure 4.7 Two possible closed transition state models exist, a chair-like transition state and a boat-like transition state.	133
Figure 4.8 Substrate scope for lactone Michael acceptors and aryl or vinyl aldehydes.	134
Figure 4.9 Substrate scope for lactam Michael acceptors and aryl or vinyl aldehydes.	136
Figure 4.10 Deuterium incorporation experiments highlight the challenges with aliphatic aldehyde electrophiles.	137
Figure 4.11 Substrate scope of lactones and lactams with pivaldehyde <b>4-72</b> .	138
Figure 4.12 Results of the reductive aldol reaction of morpholine amides.	139
Figure 4.13 Derivatization of the reductive aldol products leads to useful synthetic building blocks bearing all carbon quaternary stereocenters.	140
Figure S1 Dose response curves of synthetic gibberellins against a variety of cell lines as determined by a Cell Titre Glo viability assay.	150
Figure S2 Dose response curves of active inhibitor <b>2-30</b> and inactive analog <b>2-36</b> against a variety of cell lines as determined by a Cell Titre Glo viability assay.	151
Figure S3 Merck Heck monodentate ligands.	158
Figure S4 HTE screens of Heck ligands under palladium catalyzed Heck reaction conditions.	159

Figure S5 The structures of Merck's A-ligands which were compiled based upon their ability to promote myriad cross-coupling reactions.	160
Figure S6 Merck's B-ligands which were selected based upon their ability to promote myriad cross-coupling reactions.	161
Figure S7 HTE screens of Heck A/B ligands under palladium and nickel catalyzed Heck reaction conditions.	162
Figure S8 HTE screens of selected ligands in nickel catalyzed Heck reaction conditions.	163
Figure S9 HTE follow up investigations in nickel catalyzed photochemical Heck reaction conditions.	164
Figure S10 HTE follow up investigations in nickel catalyzed photochemical Heck reaction conditions.	165

## **List of Appendices**

Appendix 1 Chapter 2 Supplementary Information	144
Appendix 2 Chapter 3 Supplementary Information	153
Appendix Bibliography	166

## Abstract

Natural product synthesis exists today as a crucible for method development, a test of strategic disconnections, and, perhaps most importantly, a means of generating bioactive small molecules and testing biological hypotheses. Indeed, many small molecule diterpenoids, upon isolation from plant material, are tested for their ability to serve as cytotoxins in cancer and for their ability to reduce signals of inflammation. These diterpenoids often bear sterically complex, densely functionalized cage-like core structures, making their synthesis a significant endeavor and providing opportunities for the development of new methods and strategic disconnections. NF- $\kappa$ B is a family of transcription factors that drive both inflammation and cancer cell survival, and many diterpenoids that were shown to have anti-cancer anti-inflammatory activities have also been shown to interact with this pathway. The focus of this thesis work has been to apply synthetic approaches to the challenge of studying if, and how, small molecule diterpenoids inhibit the NF- $\kappa$ B pathway. The aromatic gibberellin, pharbinilic acid, was selected as a synthetic target based upon its structural homology to a known NF- $\kappa$ B binder and based upon its anti-cancer and anti-inflammatory properties. In the course of the first successful synthesis of this molecule a potent, selective inhibitor of the NF- $\kappa$ B pathway was discovered and demonstrated to have thousand-fold selectivity for killing inflammatory cancer derived cell lines over cell lines derived from healthy fibroblasts. A unified approach to the bioactive *ent*-kaurene diterpenoids is disclosed. These studies were initiated in order to differentiate between specific activities inherent to the diverse cage-like structures of these molecules and those misattributed to pan assay interfering enone moieties present in many such molecules. Of particular interest is

the synthesis of ericalyxin B it has been shown to covalently label the DNA binding domain of NF- $\kappa$ B. Finally, the development of a new method to enable a key disconnection towards the synthesis of the terpene alkaloid isopalhinine A is discussed.

## Chapter 1 Introduction

### Chapter 1.1 Nuclear Factor-kappaB (NF-κB)

#### Chapter 1.1.1 NF-κB structure and function

NF-κB was discovered in 1986 as a protein that bound to a specific DNA sequence in B lymphocytes and it was named for the gene it effected and the cell line it was found in, nuclear factor binding near the κ-light chain gene in B cells.<sup>1</sup> In my favorite piece of NF-κB trivia David Baltimore, one of the discoverers of NF-κB, apologized for giving it a name so difficult to type saying “Had we realized that NF-κB would have a wide role in inflammation and other natural and pathological processes, we might have found a simpler designation for ease of typing.”<sup>2</sup>

NF-κB is a transcription factor that is not one, but a family of five, closely related proteins. These proteins, to make matters worse, are referred to often by different names and are RelA (p65), RelB, c-Rel, p105/p50 (NFκB1), and p100/p52 (NFκB2). What unites these proteins is the possession of a Rel homology domain (RHD, Figure 1.1). This 300 amino acid domain has three functions.<sup>3,4</sup> First, it enables sequence specific DNA binding to a nearly palindromic sequence namely 5'-GGGRNWYYCC-3' (R = purine, N = any base, W = adenine or thymine, Y = pyrimidine). Second, it allows for binding to ankyrin rich repeats in inhibitory proteins. Third, it allows for characteristic dimerization. All NF-κB family members exist as dimers, either homodimers (excepting RelB) or heterodimers. 13 of 15 dimeric proteins have been identified *in vivo* and likely have differential selectivities in terms of specific gene activation.<sup>2</sup>



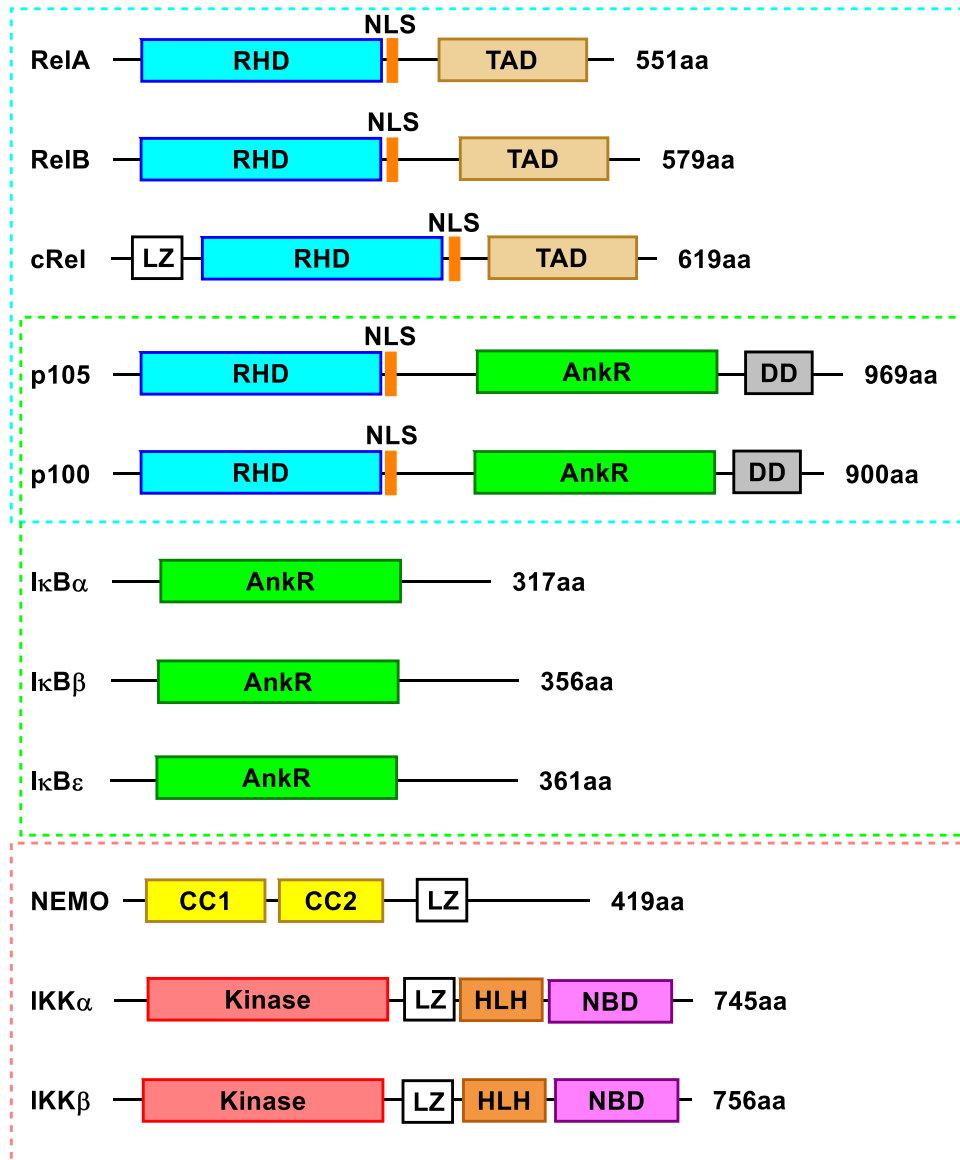


**Figure 1.1-** Protein maps of key NF- $\kappa$ B family members. RHD = Rel Homology Domain. NLS = Nuclear Localization Sequence. TAD = TransActivation Domain. LZ = Leucine Zipper. AnkR = Ankyrin Repeats. DD = Death Domain. CC1 = Coiled-Coil domain 1. CC2 = Coiled-Coil domain 2. Kinase = Kinase domain. HLH = Helix-Loop-Helix region. NBD = NEMO-Binding Domain.

Of the five NF- $\kappa$ B family members only three of the, RelA, RelB, and c-Rel, contain transactivating domains. These transactivating domains are required for recruiting the transcriptional machinery necessary for inducing the transcription of target genes.<sup>5</sup> Thus it is typically only dimers of NF- $\kappa$ B that contain RelA, RelB, or c-Rel that are activating while homo-

and heterodimers of p50 and p52 are silencing<sup>6</sup> though there are reports of co-transcriptional regulators such as Bcl-3 binding to p50:p52 heterodimers and facilitating gene activation.<sup>7</sup>

The genes associated with NF- $\kappa$ B are myriad and a catalog of genes characterized to be activated by NF- $\kappa$ B, current as of 2010, can be found at [bu.edu/nf-kb/gene-resources/target-genes/](http://bu.edu/nf-kb/gene-resources/target-genes/). This pathway is so well studied because genes that it controls have biologically and pathologically critical functions including immune cell differentiation and control, inflammation, and all stages of cancer development and survival. These functions will be covered in more detail in this document (see Chapter 1.1.4).

#### Chapter 1.1.2 IKK kinases and NF- $\kappa$ B regulation

One striking feature of NF- $\kappa$ B is the speed with which it can be activated and controlled.<sup>7</sup> This is important because NF- $\kappa$ B activates the immune response so it must be able to adapt quickly when required. The genius to the transcription factor lies in the way it is controlled. NF- $\kappa$ B is uniformly expressed in mammalian cells and are kept locked in the cytoplasm by a feature of the RHD which enables binding of NF- $\kappa$ B subunits to the ankyrin repeats (AnkR) subunits of inhibitors of NF- $\kappa$ B (I $\kappa$ B), the most well characterized of which is I $\kappa$ B $\alpha$ .<sup>8</sup> Upon binding an I $\kappa$ B the nuclear localization sequence (NLS) and the DNA binding domain (DBD) of NF- $\kappa$ B subunits are blocked preventing them from being transported to the nucleus and even were they in the nucleus preventing them from binding DNA and activating genes.

Non-transcriptionally active NF- $\kappa$ B subunits, p105/p50 and p100/p52, must be proteolytically processed before they can be translocated to the nucleus and bind DNA. This is a result of their AnkR regions which themselves are inhibitors of NF- $\kappa$ B (I $\kappa$ B $\gamma$  and I $\kappa$ B $\delta$  respectively). These regions are proteolytically cleaved before the active subunits, p50 and p52, can be a part of an active NF- $\kappa$ B dimer. In the case of p50 this processing is constitutively active

and occurs largely as p105 is being translated, though some cytosolic p105 can be detected.<sup>9</sup> For p100 this proteolytic processing is more tightly regulated and will be discussed in more detail below.

The transcriptionally active subunits of NF- $\kappa$ B are thought to be controlled in two major ways. The first is the canonical pathway (Figure 1.2). In this activation mode an I $\kappa$ B, the most well studied and characterized of which is I $\kappa$ B $\alpha$ , binds the RHD of a transcriptionally active NF- $\kappa$ B family member, typically RelA, then c-Rel, less frequently RelB, preventing it from entering the nucleus and binding DNA. In these complexes NF- $\kappa$ B is typically dimerized with a transcriptionally inactive subunit, typically p50, rarely p52, and occasionally another active subunit, RelA, c-Rel, or RelB.<sup>10</sup> In the case of inhibition by I $\kappa$ B $\alpha$ , I $\kappa$ B $\beta$ , or I $\kappa$ B $\epsilon$  the inhibitory protein must be ubiquitinated and proteolytically degraded before transcriptionally active NF- $\kappa$ B can be transported to the nucleus.

In all so-called canonical NF- $\kappa$ B pathways the protein complex that is responsible for activating the I $\kappa$ B for degradation is made up of three distinct I $\kappa$ B kinases (IKKs). This complex, which is made up of IKK $\alpha$ , IKK $\beta$  and NF- $\kappa$ B essential modifier (NEMO or IKK $\gamma$ ), phosphorylates an N-terminal serine on I $\kappa$ B leading to its degradation. It has also been observed that this IKK $\beta$ , IKK $\alpha$ , NEMO complex can activate NF- $\kappa$ B complexes that are inhibited by unprocessed p105, such as p105:RelA or p105:c-Rel dimers.<sup>11-13</sup> In all such canonical signaling it has been shown that IKK $\beta$  and NEMO are essential for pathway activation while IKK $\alpha$  appears to play more of a supporting role.<sup>14</sup>

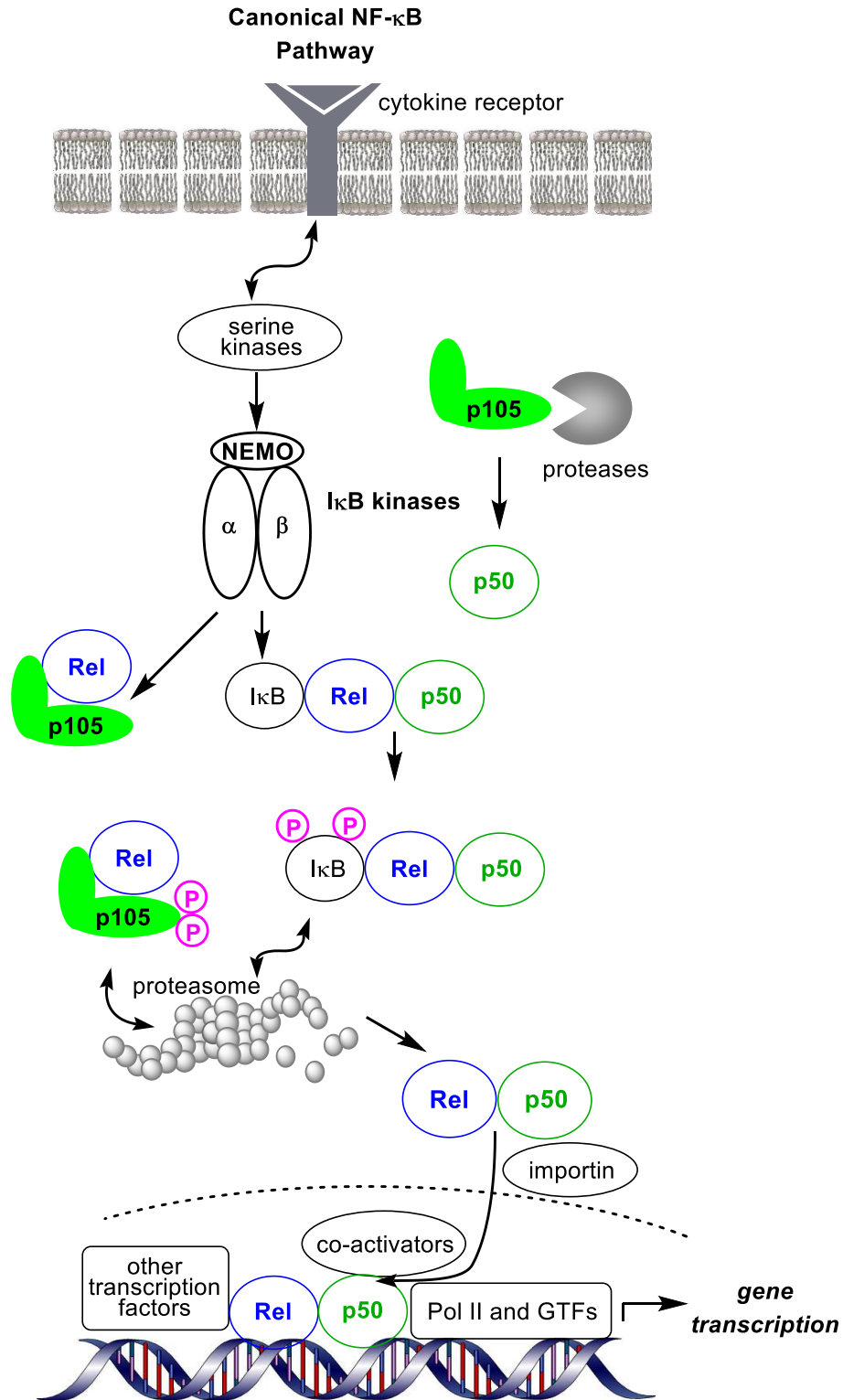


**Figure 1.2-** In the canonical NF- $\kappa$ B pathway IKK $\alpha$ , IKK $\beta$ , and NEMO phosphorylate inhibition complex which signals for proteolytic processing and provides active complexes which are actively imported into the nucleus where they bind DNA and signal for the transcription of genes.

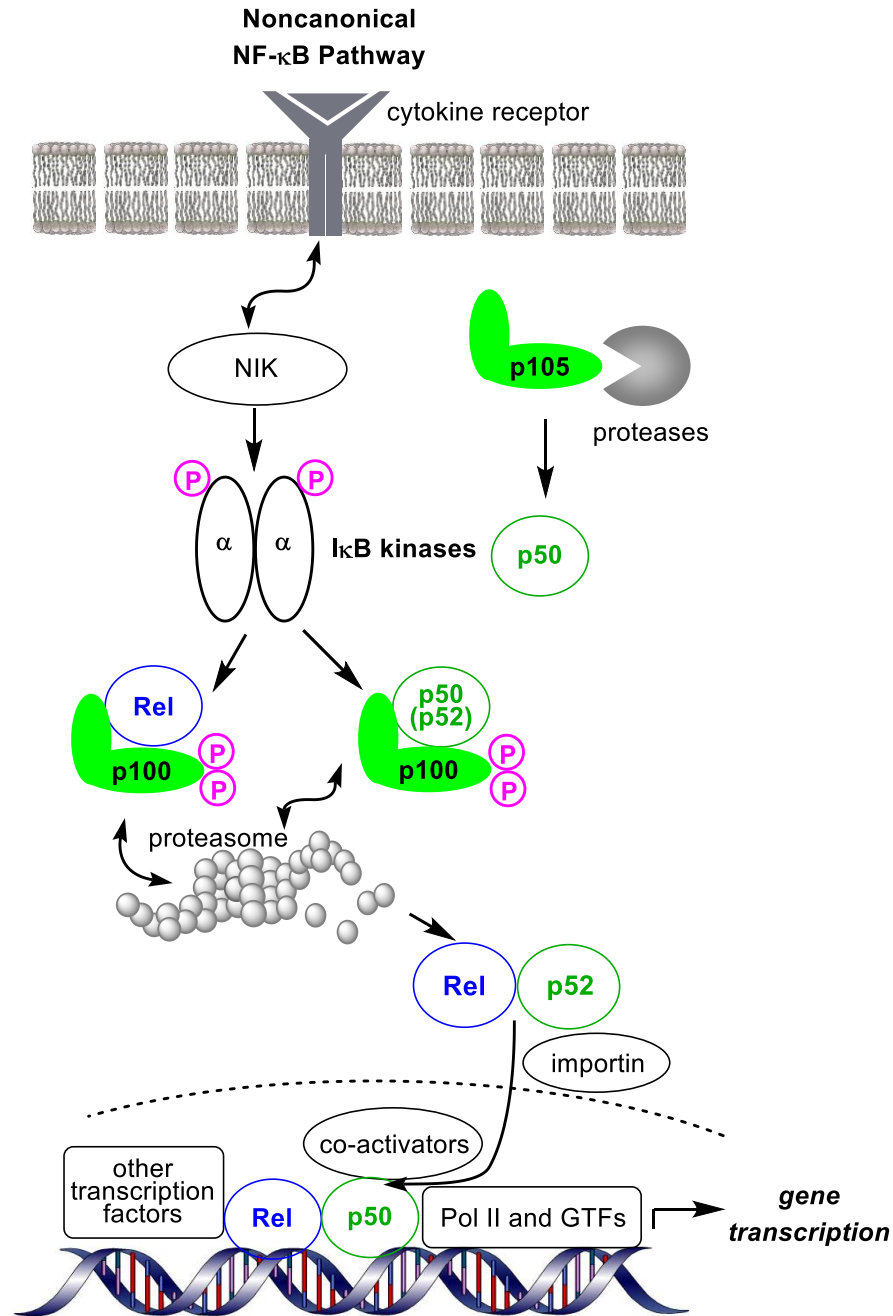


**Figure 1.3-** In the noncanonical NF-κB pathway IKKα dimers phosphorylate p100 for proteolytic processing and provides active complexes which are actively imported into the nucleus where they bind DNA.

In so-called noncanonical NF-κB dimers of IKKα are activated by NF-κB inducing kinase (NIK) and the activated IKKα dimers then phosphorylate p100 (Figure 1.3). p100 unlike, p105 is not co-translationally processed so translated p100 in the cytosol dimerizes, typically

with RelB but also with p50, processed p52, and the other Rel's. These dimers of unprocessed p100 are inhibited by the Ankr in p100 until activated dimers of IKK $\alpha$  phosphorylate p100 and signal for its proteolytic processing into uninhibited complexes.<sup>15</sup>

Other modes of NF- $\kappa$ B signaling exist but are far less well studied. Among the more prominent modes is how homo- and heterodimers of p50 and p52 effect NF- $\kappa$ B pathway inhibition (Figure 1.4). Specifically, a transcriptional co-activator, Bcl-3, binds transcriptionally inactive NF- $\kappa$ B dimers that contain p52.<sup>16</sup> Unlike other Bcl family proteins, Bcl-3 contains a TAD which, upon phosphorylation in the nucleus by IKK $\alpha$  or IKK $\beta$ , can activate genes which had been silenced and lead to oncogenic gene transcription specifically Bcl-3 phosphorylation by nuclear IKKs promotes cell proliferation and migration.<sup>17</sup>

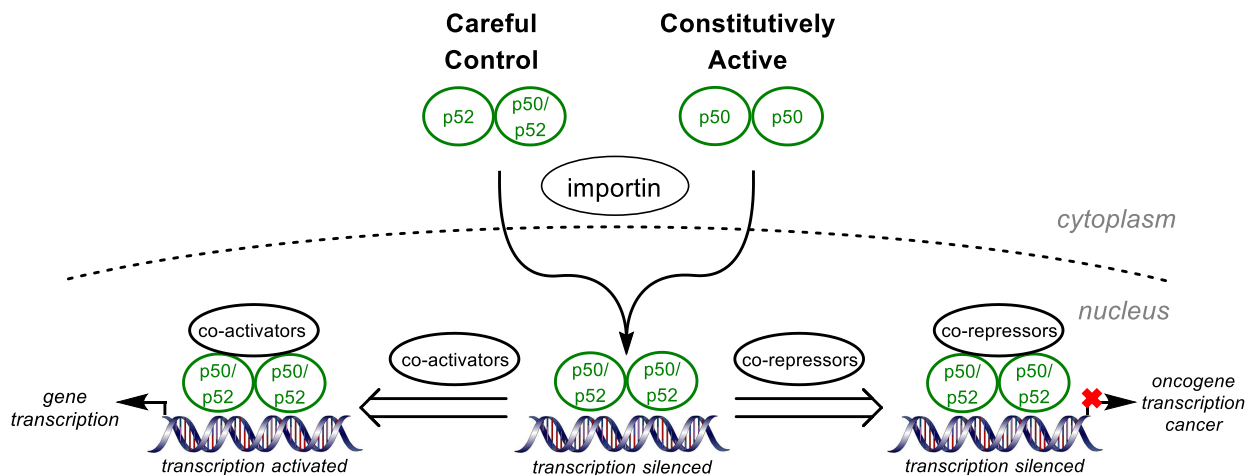


**Figure 1.4-** Transcriptionally inactive subunits of NF- $\kappa$ B can fall under two paradigms of activity. Homodimers of p50 are constitutively activate and dimers of p52 are carefully controlled by noncanonical NF- $\kappa$ B pathway signalling. These dimers bind NF- $\kappa$ B and silence NF- $\kappa$ B gene transcription. These complexes can be modified by co-repressors which stabilize DNA:protein complexes and prevent transcription. These complexes can also bind co-activators which allow for silenced genes to become activated.

This mode of activations dovetails nicely into a discussion of non-cytostolic modes of IKK activity. For decades the study of IKK was relegated to how they are activated and assembled to phosphorylate and activate NF- $\kappa$ B signaling (*vide supra*).<sup>10</sup> IKK $\alpha$  has been shown

to constitutively translocate to and from the nucleus in an equilibrium that favors cytosolic localization.<sup>18</sup> However, upon NF- $\kappa$ B pathway stimulation, in particular by TNF $\alpha$ , lymphotoxin  $\beta$ , and CD40, IKK $\alpha$  is shifted towards nuclear localization.<sup>19</sup> IKK $\alpha$  has been shown to modulate histones by phosphorylating histone 3 freeing NF- $\kappa$ B controlled genes and allowing for their transcription.<sup>20,21</sup> IKK $\alpha$  translocation has been shown to be critical in apoptosis, cell cycle progression, and tumor progression in colorectal,<sup>22,23</sup> breast,<sup>24,25</sup> pancreatic,<sup>26</sup> gastric,<sup>27</sup> osteosarcoma,<sup>28</sup> and prostate cancers.<sup>29</sup> In general IKK $\alpha$  functions in the nucleus by affecting the co-translational machinery shifting equilibrium towards the transcription of NF- $\kappa$ B controlled genes by phosphorylating and deactivating repressor complexes and phosphorylating and activating activator complexes.<sup>30</sup>

### Chapter 1.1.3 NF- $\kappa$ B pathway activation

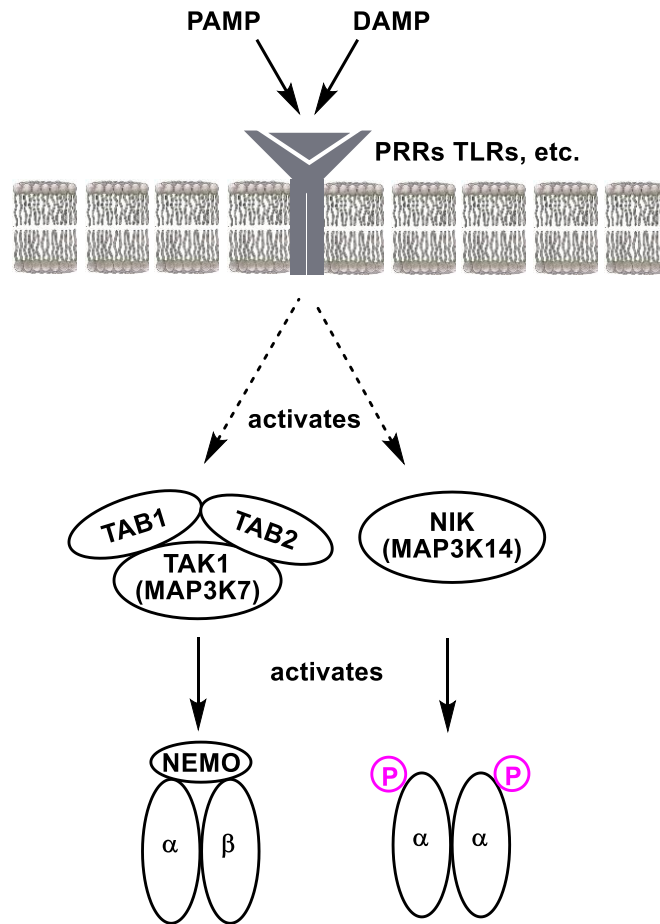


**Figure 1.5-** Common activation modes of canonical and noncanonical NF- $\kappa$ B pathway activity. Pattern Recognition Receptors (PRR) and Toll-Like Receptors (TLR) recognize Pattern-Associated Molecular Patterns (PAMP) or Damage-Associated Molecular Patterns (DAMP). This ultimately leads to the activation of Transforming growth factor- $\beta$  Activated Kinase 1 (TAK1) as well as activation of NF- $\kappa$ B Inducing Kinase (NIK).

A whole host of PRRs, TNFRs, and TLRs can recognize ligands and set off a host of cascades that are united by a set of kinases, typically TAK1, which activates the trimeric canonical IKK complexes as well as NIK which activates the dimeric noncanonical IKK complexes.<sup>15</sup> These regulatory pathways are complex and typically function by inhibiting ubiquitin ligases that degrade TAK1 or NIK.



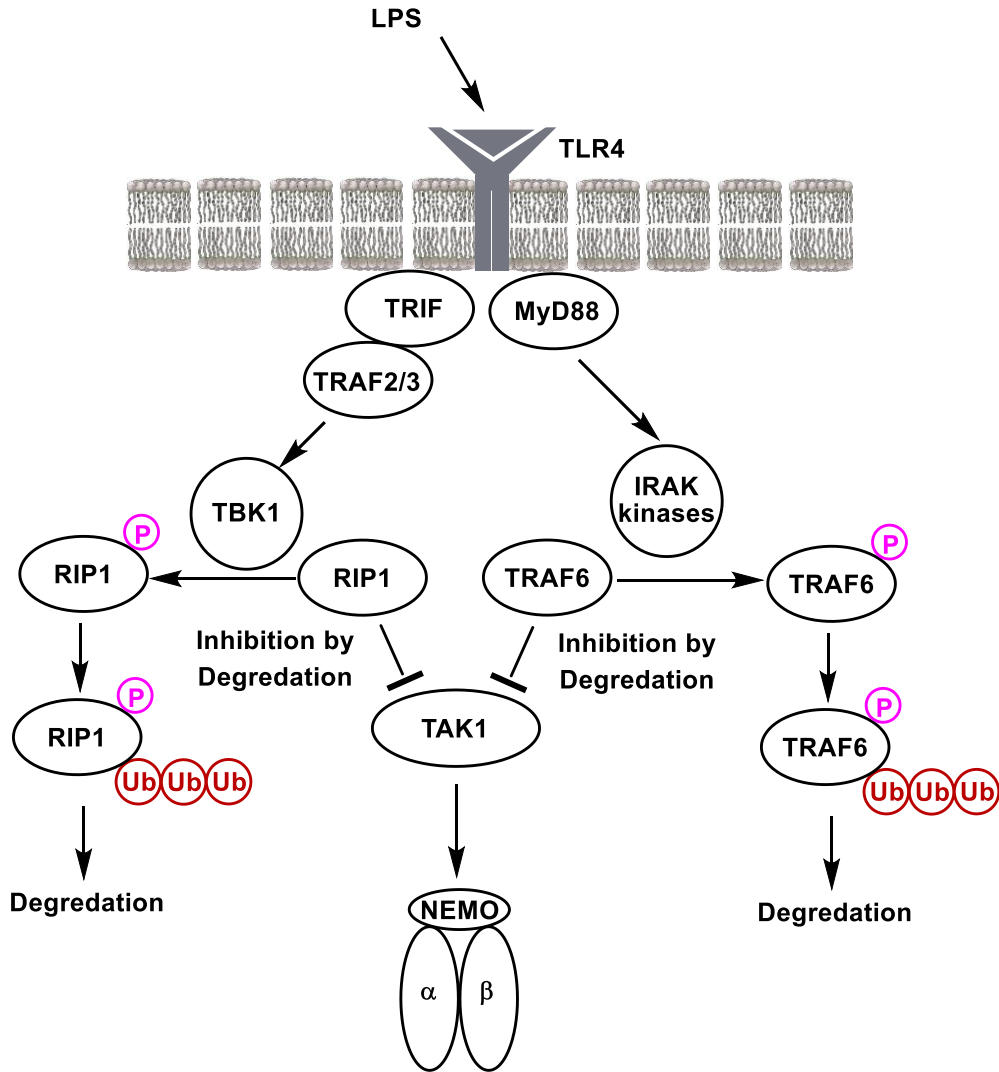


**Figure 1.6-** A common motif in TAK1 control is to phosphorylate and degrade ubiquitinases like RIP1 or TRAF6. This prevents RIP1 or TRAF6 from ubiquitinating and degrading TAK1.

For example, when TLR4 is activated by Lipopolysaccharide (LPS) it recruits and activates MyD88 and TRIF.<sup>31</sup> Activation of MyD88 leads to the activation of the IRAK kinases the effect of which is the phosphorylation, ubiquitinylation and proteolytic degradation of TRAF6 which itself ubiquitinylates and degrades TAK1. Recruitment of TRIF leads to the sequestration of TRAF2/3/ This leads to the activation of TBK1. When TBK1 is not initiating IFN signaling, it phosphorylates and leads to the ubiquitinylation and degradation of RIP1

which itself would ubiquitinate and degrade TAK1. As inhibitory signaling events are reduced, TAK1 is allowed to persist in the cytosol which can initiate NF- $\kappa$ B signaling.

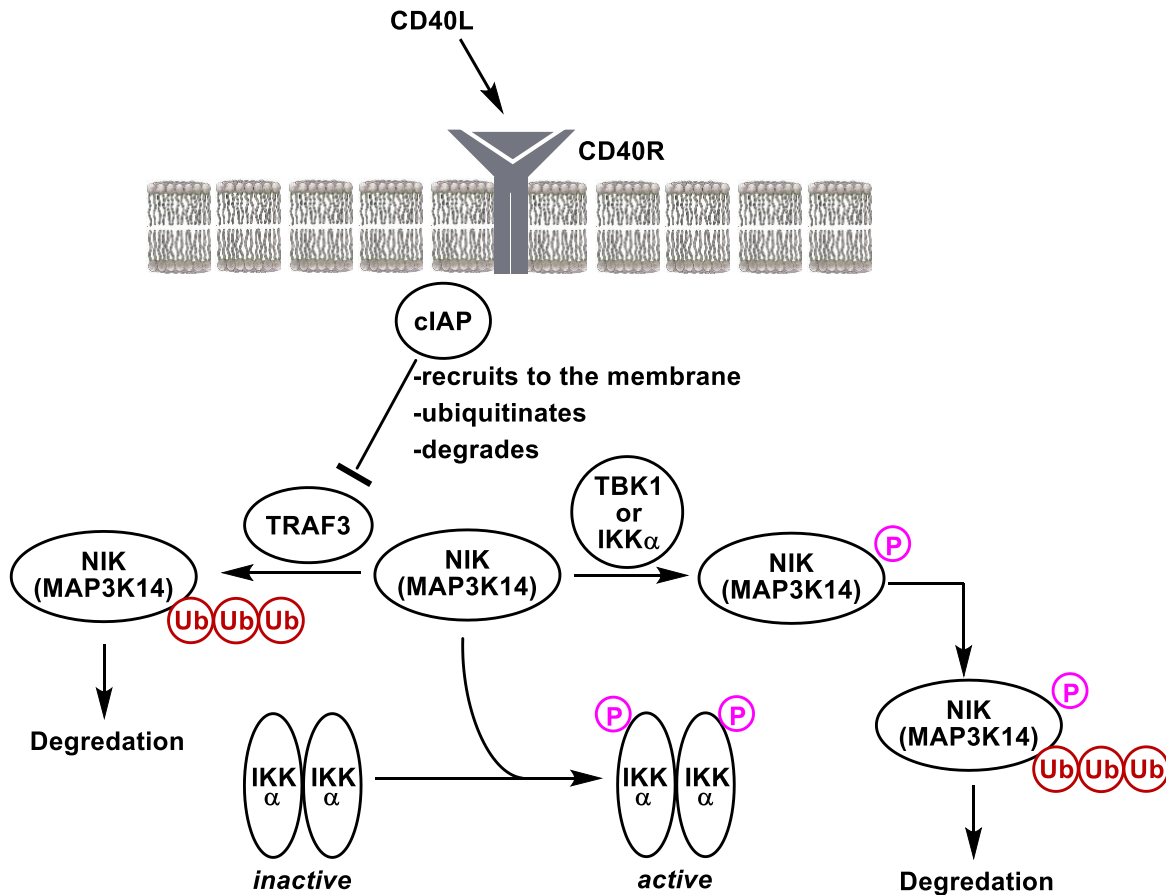


**Figure 1.7-** In noncanonical NF- $\kappa$ B activation TNFR superfamily receptors like CD40R recruit cIAP to the membrane, which in turn recruits and signals for degradation TRAF2, which is responsible for ubiquitinyolating NIK which is the kinase that activated noncanonical NF- $\kappa$ B. Alternatively NIK can become phosphorylated, including by active IKK $\alpha$ , which also leads to degradation of NIK.

In an example of noncanonical NF- $\kappa$ B pathway signaling, TNFR superfamily receptors, like CD40, can recruit cIAP to the membrane.<sup>32</sup> cIAP, in turn, recruits TRAF3 to the membrane and causes its degradation. TRAF3 is predominantly the ubiquitin ligase that's responsible for the degradation of NIK.<sup>33</sup> If TRAF3 activity is reduced NIK can also become inhibited by a cascade that is initiated by phosphorylation by kinases including TBK1, which is involved in *activating* canonical NF- $\kappa$ B signaling, as well as IKK $\alpha$  itself. This provides a negative feedback loop in healthy cells limiting noncanonical NF- $\kappa$ B signaling.<sup>34</sup> Which is not a unique feature of

NF- $\kappa$ B pathway activity as NF- $\kappa$ B also controls for the expression of I $\kappa$ Bs providing for negative feedback loops in the case of a transient activating signal, and cyclical activity in the case of chronic activating signals.<sup>7</sup>

#### Chapter 1.1.4 Physiological consequences of NF- $\kappa$ B related dysregulation

So why do we care about NF- $\kappa$ B? Why is the discoverer of NF- $\kappa$ B apologizing for making it so hard to type?<sup>2</sup> Why were there more than 25,000 papers published on NF- $\kappa$ B as of 2006?<sup>10</sup> The answer to all of these questions are related to 3 predominant consequences of NF- $\kappa$ B dysregulation. First, NF- $\kappa$ B controls for immune cell differentiation, thus dysregulation of NF- $\kappa$ B can cause aberrant immune cell activity and the development of immune disorders and cancer. Second, NF- $\kappa$ B is a key driver in extrinsic inflammation, as observed by the promotion of pro-inflammatory cytokines like IL-1 $\beta$  or TNF $\alpha$ , and the intrinsic inflammation pathway, by controlling the expression of NLRP3. As such NF- $\kappa$ B is implicated in every inflammatory disease from arthritis to multiple sclerosis to obesity. Third, NF- $\kappa$ B has been implicated in every stage of tumor development from initiation to metastasis to survival, even angiogenesis. As such the study of the NF- $\kappa$ B pathway and NF- $\kappa$ B mediated gene expression has allowed researchers to identify mechanisms of pathogenicity and elucidate new targets for therapeutic intervention.

First NF- $\kappa$ B is a driver in immune cell differentiation. In macrophages activation of PRRs in response to pathogen associated molecular patterns (PAMPs) or damage associated molecular patterns (DAMPs) NF- $\kappa$ B is activating leading to polarization and differentiation to both M1 and M2 macrophages.<sup>35</sup> This helps drive the differentiation of T cells into Th1 and Th17 cells<sup>36</sup> and promotes the production of inflammatory cytokines IL-10 and IL-13 which are necessary for wound healing.<sup>37</sup> Additionally, the signaling through antigen presenting dendritic cells hinges on NF- $\kappa$ B activity<sup>38</sup> and maturation of CD4<sup>+</sup> helper T cells (Th) relies on canonical NF- $\kappa$ B

signaling.<sup>39</sup> Mice bearing mutations in canonical NF- $\kappa$ B signaling have impaired allergen antigen responses.<sup>36</sup> Mice bearing noncanonical NF- $\kappa$ B pathway loss of function (LOF) mutations have impaired abilities to develop memory T cells and have significantly reduced neuroinflammation.<sup>40</sup>

With such a profound effect on immune cells it should not be surprising that NF- $\kappa$ B pathway dysregulation is at the core of many auto-immune disease phenotypes. These include systemic lupus erythematosus,<sup>41</sup> severe combined immunodeficiency (SCID),<sup>42</sup> combined variable immune deficiency (CVID),<sup>43</sup> combined immune deficiency (CID),<sup>44</sup> anhidrotic ectodermal dysplasia with immune deficiency (EDA-ID),<sup>45</sup> psoriasis,<sup>46</sup> and many more.<sup>1</sup>

If NF- $\kappa$ B is affecting immune cell differentiation and function it should not be surprising to see that NF- $\kappa$ B dysregulation also plays a driving role in many inflammatory disorders. Canonical<sup>47</sup> and noncanonical<sup>48</sup> NF- $\kappa$ B dysregulation has been shown to be important for the progression and development of rheumatoid arthritis. Inhibition of NF- $\kappa$ B has been shown *in vivo* to ameliorate the effects of the disease.<sup>49</sup> Genome wide association studies have shown that NF- $\kappa$ B pathway members likely play a role in multiple sclerosis.<sup>50-52</sup> Genetic intervention and pathway inhibition in murine MS models have shown that NF- $\kappa$ B inhibition reduces the severity of MS.<sup>53,54</sup> In inflammatory bowel disease (IBD) and Crohn's disease, NF- $\kappa$ B is constitutively active.<sup>55,56</sup> Inhibition of the NF- $\kappa$ B pathway, either using inhibitory oligonucleotides<sup>57,58</sup> or by genetic intervention<sup>59</sup> inhibits inflammatory colitis and treats IBD. Noncanonical NF- $\kappa$ B inflammatory activity has even been linked to inflammatory metabolic diseases such as type-2 diabetes<sup>60,61</sup> and obesity.<sup>62</sup>

Given the link between inflammation and cancer and the importance of inflammation in tumor microenvironments<sup>63</sup> it should not be surprising that NF- $\kappa$ B is implicated in cancer as

well.<sup>64</sup> Intuitively this makes sense as inflammatory cytokines, such as  $\text{TNF}\alpha$ , are pro-apoptotic in nature, inducing apoptosis through the TNFR1 associated death domain (TRADD).<sup>65</sup> This allows for damaged cells in the case of an infection or wound to be destroyed and ultimately replaced with a healthy cell. However, healthy cells in an inflammatory environment, such as immune cells for example, need to have a mechanism to overcome this pro-apoptotic signal. As such, NF- $\kappa$ B, which promotes and responds to inflammatory signaling, also controls for pro-survival or anti-apoptotic proteins, such as Bcl-XL, to allow healthy cells to survive in inflammatory environments. It is not surprising that in cancer, which is characterized by abnormal cell survival and inflammation, NF- $\kappa$ B is often over expressed, constitutively active and necessary for survival.<sup>64</sup> Indeed the NF- $\kappa$ B pathway is associated with tumor initiation<sup>66</sup>, angiogenesis<sup>67</sup> and metastasis<sup>68</sup> as well. NF- $\kappa$ B activity and mutations have proven critical to cancer survival and development in lymphoma, either Burkitt's,<sup>69</sup> Hodgkin's,<sup>69</sup> B cell,<sup>70</sup> or T cell,<sup>71</sup> in breast carcinoma,<sup>72,73</sup> colorectal cancer,<sup>74</sup> non-small cell lung cancer,<sup>75</sup> ovarian cancer,<sup>76</sup> multiple myeloma,<sup>77</sup> nasopharyngeal carcinoma,<sup>78</sup> prostate carcinoma,<sup>79</sup> and glioma<sup>80</sup> to name a handful of cases. This has prompted the community to consider the NF- $\kappa$ B pathway as a target for the development of novel anti-cancer therapeutics.<sup>81</sup>

#### Chapter 1.1.5 Inhibitors and inhibition of the NF- $\kappa$ B pathway

So, if you're reading this and you're thinking 'why haven't I heard of a widespread commercial direct NF- $\kappa$ B inhibitor?' A part of this is that the oldest characterized activity of NF- $\kappa$ B is its inflammatory activity. While chronic inflammation is certainly worth developing therapeutics for, consider what would happen if you greatly suppressed NF- $\kappa$ B activity across an entire organism for a prolonged period of time. NF- $\kappa$ B controls immune cell differentiation, its required for embryonic development, it is necessary for epithelial cell integrity and polarization,

completely inhibiting NF- $\kappa$ B chronically is probably not going to be a therapeutically useful strategy.

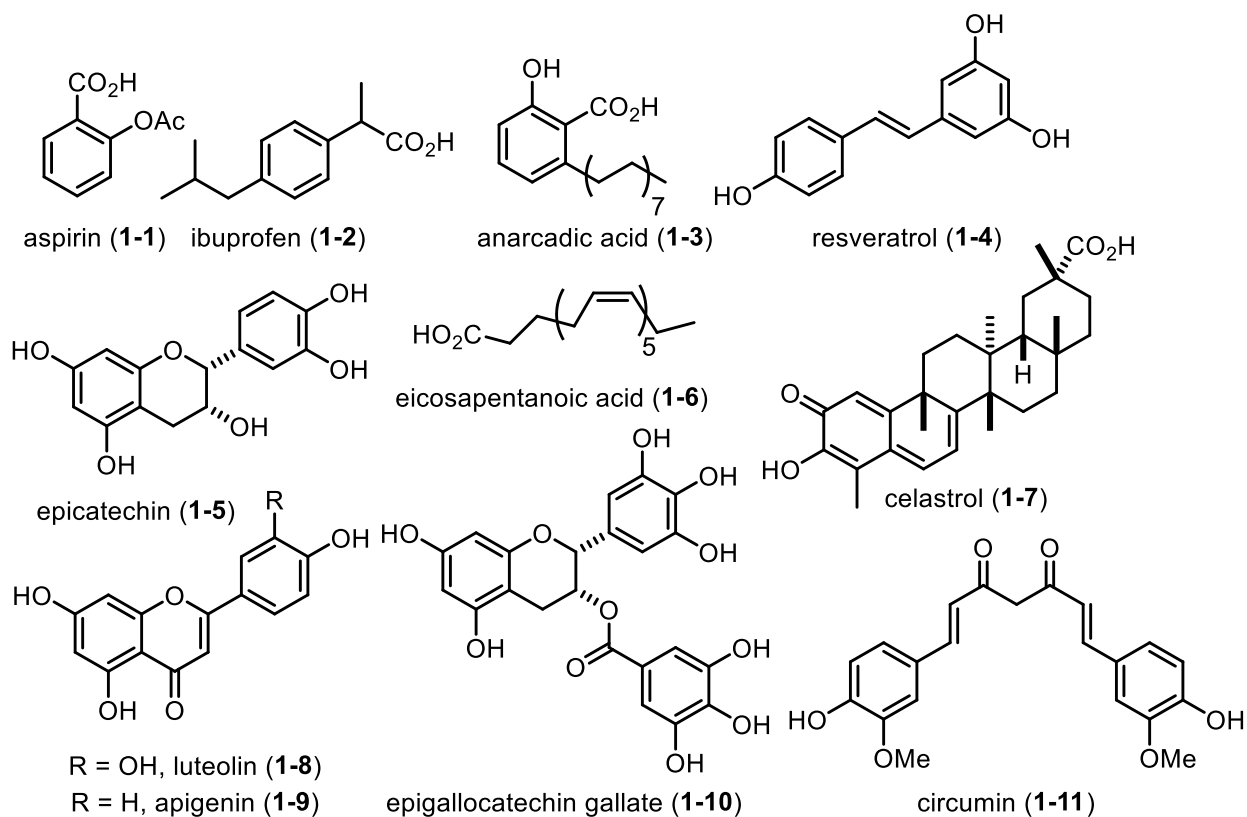


**Figure 1.8-** Anti-inflammatory molecules with characterized activity against the NF- $\kappa$ B pathway.

That being said, many anti-inflammatory therapeutics and small molecules do work on the NF- $\kappa$ B pathway but as modulators or depressors rather than complete inhibitors (Figure 1.8). NSAIDs, such as aspirin (1-1) or ibuprofen (1-2), inhibit COX-2 an NF- $\kappa$ B controlled protein that initiates prostaglandin mediated inflammatory signaling. Other anti-inflammatory small molecules have been shown to have effect on the NF- $\kappa$ B pathway such as epigallocatechin gallate (1-10), eicosapentanoic acid (1-6), curcumin (1-11), and luteolin (1-8). Apigenin (1-9) and anarcadic acid (1-3) have been shown to suppress IKK activity. Resveratrol (1-4), for what it's worth, has been shown to inhibit RelA phosphorylation. Epicatechin (1-5) inhibits nuclear translocation of RelA. Celestrol (1-7) inhibits DNA binding to NF- $\kappa$ B.<sup>82-84</sup> However very

specific and potent inhibitors of NF- $\kappa$ B pathway activity have not been developed for chronic inflammation.

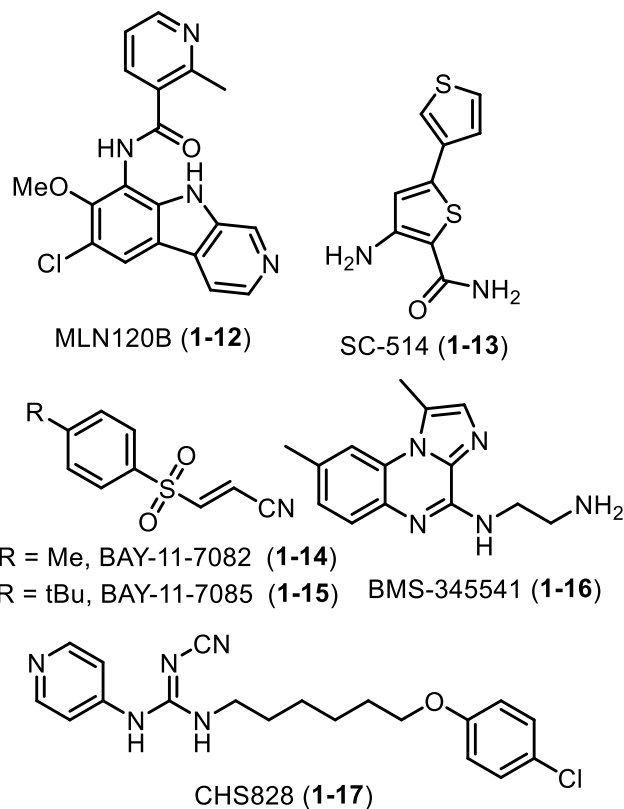


**Figure 1.9-** Pharmaceutically developed IKK inhibitors.

The importance of NF- $\kappa$ B to cancer development and survival along with the observation that 20% of cancer is strongly linked to underlying inflammation,<sup>85</sup> suggest that NF- $\kappa$ B might be an excellent target for cancer therapy.<sup>86</sup> Additionally a chemotherapeutic use of NF- $\kappa$ B would be an acute treatment which would avoid some of the consequences for long term pathway inhibition. As such IKK, which is 1) a kinase and 2) a central regulator and activator of NF- $\kappa$ B signaling, has been a target of intensive research into therapeutic inhibition. As of 2010,<sup>86</sup> BAY-11-7082 (1-14),<sup>87</sup> BAY-11-7085 (1-15),<sup>87</sup> MLN120B (1-12),<sup>88</sup> BMS-345541 (1-16),<sup>89</sup> SC-514 (1-13),<sup>90</sup> and CHS828 (1-17)<sup>91</sup> had been developed as IKK inhibitors both for use alone and in

combination with other therapies. Unfortunately, none of these inhibitors have been approved for therapeutic use.<sup>92</sup>

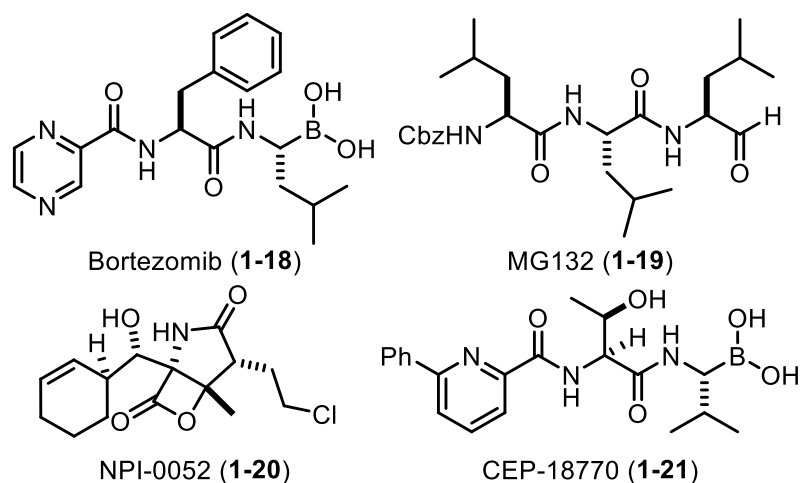


**Figure 1.10-** Protease inhibitors that have been shown to inhibit the NF- $\kappa$ B pathway.

Other modes of potential NF- $\kappa$ B pathway inhibition by small molecules have been explored, most prominently protease inhibitors which prevent I $\kappa$ B degradation and hopefully induce cell death. One such example, bortezomib (**1-18**), is actually mild enough that it can be used for treatment of myeloma alone<sup>93</sup> or as a part of a combination therapy in a wide variety of tumor cells in model studies<sup>94</sup> and clinically in breast,<sup>95</sup> head and neck cancers,<sup>96</sup> and non-small cell lung cancers.<sup>97</sup> Broad spectrum proteasome inhibitors, such as MG132 (**1-19**),<sup>98</sup> are too general to be useful as a potential therapeutic and though new proteasome inhibiting molecules such as NPI-0052 (**1-20**) and CEP-18770 (**1-21**)<sup>92</sup> have been investigated alone and in concert with other therapeutic agents none have become approved therapeutics. To make matters more complicated the lone FDA approved NF- $\kappa$ B protease inhibitor, bortezomib, has demonstrated potential as an NF- $\kappa$ B activator, of all things.<sup>99</sup>

Other interesting modes of inhibition include peptide-based inhibitors. Mapp and coworkers produced a synthetic loop peptide that inhibited canonical NF- $\kappa$ B signaling by



interfering in the canonical IKK complex.<sup>100</sup> SN-50 is a synthetic analog to the nuclear translocation domain of p50 and outcompetes native p50 for translocation increasing the sensitivity of ovarian cancer to cisplatin treatment.<sup>101</sup> A peptide that mimicks the NEMO binding domain reduces tumors in a canine model of relapsed diffuse B cell lymphoma.<sup>102</sup> Though it bears saying that peptide based therapeutics suffer from clinical challenges including cell permeability, oral bioavailability and poor plasma half-lives.<sup>103</sup> Similarly excellent viral based gene therapy approaches for NF- $\kappa$ B pathway inhibition have been explored but there have been as of yet no examples of clinically relevant gene therapy much less in the NF- $\kappa$ B space.<sup>104,105</sup>

If I would summarize my thoughts, based on the literature record, I have reviewed, I would say that the NF- $\kappa$ B pathway is important to understanding biochemical underpinnings to disease states. It is undeniable that inhibiting the NF- $\kappa$ B pathway can have beneficial effects in disease models. However, NF- $\kappa$ B controls for its own inhibition and in many cell types is protective rather than destructive. Existing small molecule inhibitors with well characterized activities have proven ineffective therapeutics. Small molecules that are efficient therapeutics, such as **1-18**, have a confluence of effects, inhibiting NF- $\kappa$ B in some ways but promoting it in others.

This seems like a promising area of research and potential benefit. The discovery of molecules that perturb the kinetics of the pathway could be beneficial to patients. However, the current popular modes of inhibition, general proteasome inhibitors, and signaling kinase inhibitors are not effective therapeutic strategies. Basic and academic research that is conducted in the space of NF- $\kappa$ B pathway inhibition or modulation might be best spent in less traditional areas such as protein-protein interactions, targeting protein DNA complexes, effecting NF- $\kappa$ B

co-transcriptional machinery, or effecting NF- $\kappa$ B gene related histone modulation. One potentially untapped resource in this regard is the area of natural product chemistry.

## Chapter 1.2 Michael accepting enones as bioactive molecules and covalent inhibitors

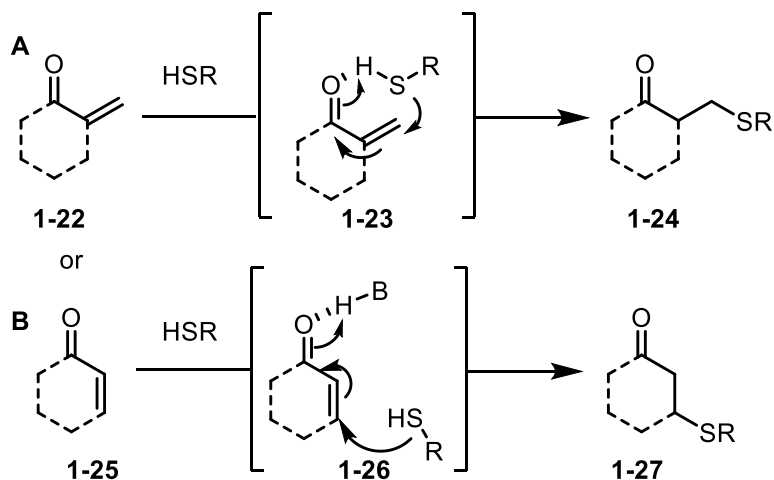


**Figure 1.11-** The general scheme of a Michael addition between a reactive thiol with an enone. This can readily occur out of an **A** syn or **B** trans configured enone

The first thing one should consider when working with electrophilic enones is that they are Michael acceptors, or in a more chemistry-oriented vernacular, they are capable of undergoing conjugate addition by nucleophiles (Figure 1.11). This is particularly important in biological contexts as thiols are suitably soft nucleophiles to undergo, often functionally irreversible, addition to an enone. This means that cysteine thiol, and every protein with a solvent exposed cysteine residue, can be covalently labeled by any molecule that contains a suitably reactive enone.

This has caused enones to be considered by hit-to-lead medicinal chemists a PAIN (Pan Assay INterference compound).<sup>106</sup> Practically this means that enones are overrepresented in screening efforts as low micromolar assay hits which often cannot be improved by SAR as they are not the result of specific interactions. Enones are not alone in this activity, catechols, quinones, peroxides, epoxides, and orthophenolic Mannich bases are also PAINs, to name a few.

Even natural product scaffolds are not immune to the designation of being a PAIN, despite being presumably evolved to interact with a specific or narrow subset of targets.<sup>107</sup> For example epigallocatechin gallate (**1-10**) continues to be and has frequently been published to be bioactive and has even been the subject of many clinical trials all without success.<sup>108</sup> Curcumin (**1-11**) has been considered by some as a “privileged biological scaffold” however close consideration of its chemical properties indicates that it is redox active, chelates metals, and irreversibly binds nucleophilic cysteines all in a scaffold not predisposed to make specific interactions with specific targets. It is certainly these PAIN effects that make **1-11** so well studied and not a function of privileged interactions with a specific subset of targets.<sup>109-112</sup> Molecules like resveratrol (**1-4**) similarly are PAINs as they interfere with membrane integrity causing very nonspecific signaling events.<sup>113</sup> Celastrol (**1-7**) similarly has been shown to provide a positive result in 61 of 216 primary screens and 29 of 62 follow up screens.<sup>114</sup>

If you, the reader, have just finished reading the above review of compounds shown to inhibit the NF- $\kappa$ B pathway you’ll notice the above list of commonly occurring PAIN-ful natural products are well represented in the NF- $\kappa$ B literature. In fact, nearly all of the molecules shown to be anti-inflammatory are PAINs. Suggesting perhaps that the NF- $\kappa$ B pathway is particularly susceptible to the effect of these molecules.

So the question begged, is whether it is fruitless to consider any PAIN containing molecule for discovery of novel therapeutic indices or for the discovery of probe compounds. Perhaps not, take artemisinin (**1-28**) which has more than a hundred suggested biological targets<sup>115</sup> but has nevertheless won the Nobel Prize in Medicine for its clinical ability to treat malaria.<sup>116</sup> There has even been a successful, if truly heroic, SAR campaign around **1-28** to yield a second generation peroxide malaria treatment OZ439 (**1-29**).<sup>117</sup> Another such success story is

of rohitukine (**1-30**) which, despite containing a reactive enol moiety as well as phenolic groups known to be disruptive to cell membranes, was elaborated by medicinal chemists to flavopiridol (**1-31**) an FDA approved treatment for acute myelogenous leukemia.<sup>118</sup>

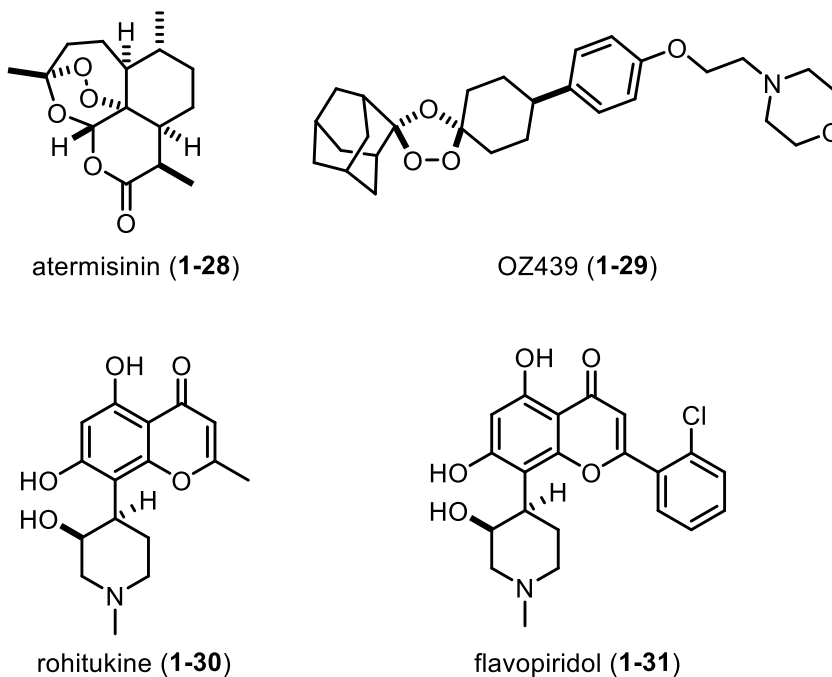


**Figure 1.12-** Successful examples of overcoming apparent PAINs to advance natural products to specific and active pharmaceuticals.

How are we, the scientific community, then to know whether a literature report of an isolated natural product, that contains a PAIN moiety is worth the effort to target for synthesis and study? How are we, chemical biologists, supposed to be able to glean from a 20<sup>th</sup> century report of low micromolar activity of a molecule that contains a PAIN moiety if it is a valuable molecule to include as a positive control in our assays? Well, recently two separate groups concurrently reported on a systematic analysis of putative PAIN-moiety containing molecules.<sup>114,119</sup>

In these, nearly identical, reports the authors computationally analyzed data from publicly available PubChem and PAINS Alert databases. They then looked for 1) if compounds flagged as being PAINs are statistically more likely to cause PAIN and 2) what motifs if any are

routinely flagged as PAINs without displaying appreciable Pan Assay INterference. In their analysis they found that the median hit rate for compounds excluded from screening libraries for PAIN structural alerts is 4 per 100 assays conducted, compared to 2-3 per 100 assays for compounds lacking PAIN alerts. 75% of PAIN alert compounds were active in fewer than 7 assays per 100 conducted compared to fewer than 5 per 100 for non-PAIN alert compounds. These results are statistically significant, certainly but if the expected hit rate is on the order of 3 'hits' in 100 assays and PAIN molecules are providing 1 additional false positive on average is that practically relevant.

When the authors examined specifically Michael acceptors the results were quite striking. They found that in a database of 463 Michael acceptors across 1.5% had been identified as a hit in a luciferase assay, 0.8% had been identified as a hit in a  $\beta$ -lactamase assay, and 2.2% had been identified as hits in an assay with a fluorescent tag read out. Across all assays they identified Michael acceptors generated a 2.1% hit rate. So why do Michael acceptors have a bad reputation as a PAIN alert? Perhaps it is because in the same analysis they found that 16 of 483 PAIN alert Michael acceptors are active in >10% of all primary screens they are reported in suggesting that when a Michael accepting compound is promiscuous it is quite promiscuous.

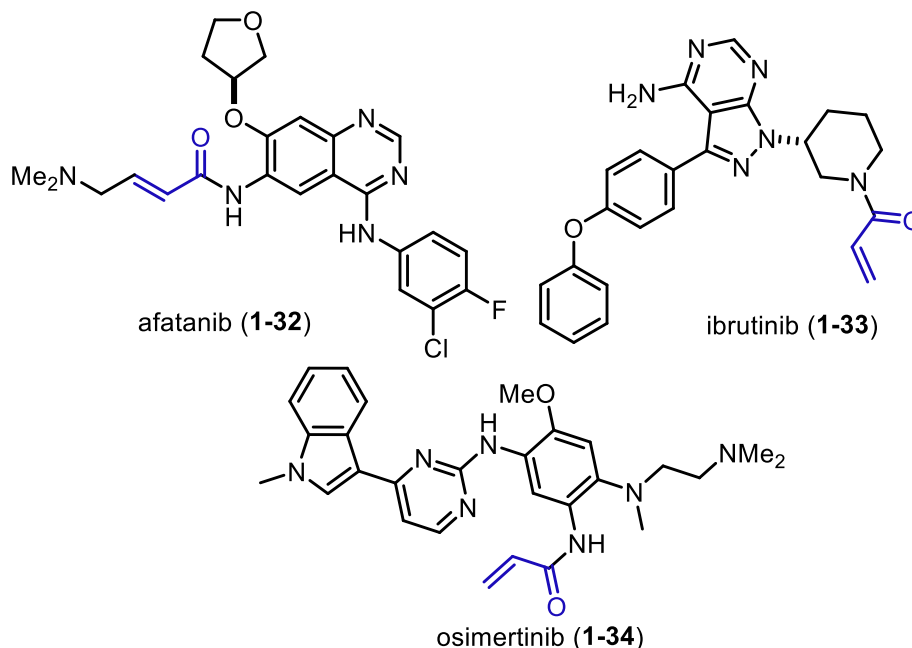


**Figure 1.13-** Michael acceptors in recently approved pharmaceuticals.

Recently, Michael accepting covalent inhibitors have been validated as a viable approach for the development of therapeutics with the approval of afatanib (**1-32**), ibrutinib (**1-33**), and osimertinib (**1-34**) which were developed to modify specific cysteines on specific proteins (Figure 1.13). The challenge then, it seems, is to identify when a Michael acceptor is too promiscuous for utility and when it is slow to react enough that it can be targeted at a specific cysteine residue.

This challenge is heightened when the kinetics of covalently labeling an enone are considered. Independent of the effect of thermodynamics on observing Michael additions, this is a bimolecular reaction, identical concentrations of both enone and nucleophile are necessary to efficiently compare the rates of reactions from two different reports of the reactivity of enones.<sup>120</sup> Generally, however, it can be said that rate of thiol additions are as follows enals > enones > acrylates > acrylamide > acrylic acids. Outside of these dimensions, electronics and sterics can play an outsized role in the reactivity of any given Michael acceptor.

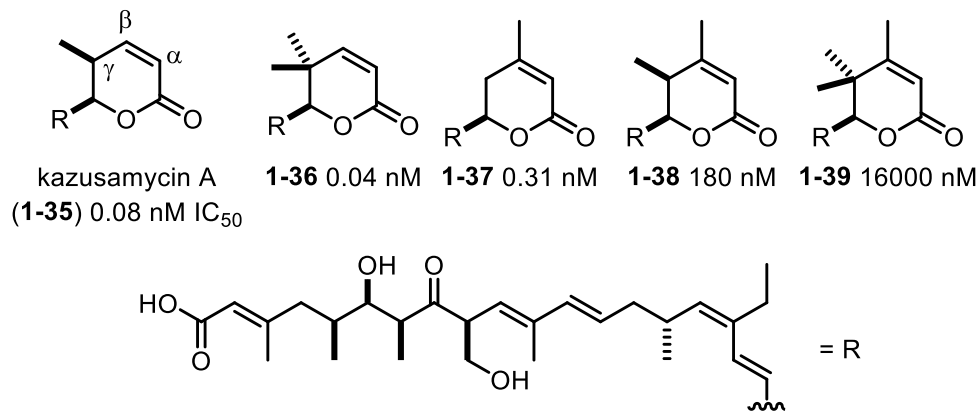


**Figure 1.14-** Kazusamycin A (**1-35**) and related analogs with their reported IC<sub>50</sub> values against HPAC cells.

The natural product,  $\alpha,\beta$  unsaturated lactone kozusamycin A (**1-35**) displays quite potent activity against HPAC cells, 0.08 nM, suggestive of specific activity (Figure 1.14). When the steric bulk around the enone at the  $\gamma$  position is increased the molecule, **1-36** is more potent against HPAC cells, 0.04 nM, perhaps as a result of less off-target activity. However, there is a limit to this observation, a  $\beta$  methyl substituent with no, **1-37**, one **1-38**, or two **1-39**  $\gamma$  methyl groups trends towards less activity against HPAC cells (0.31, 180, 16000 nM respectively).<sup>121</sup> This is likely a result of the enone losing affinity for and/or reactivity towards its cellular targets.

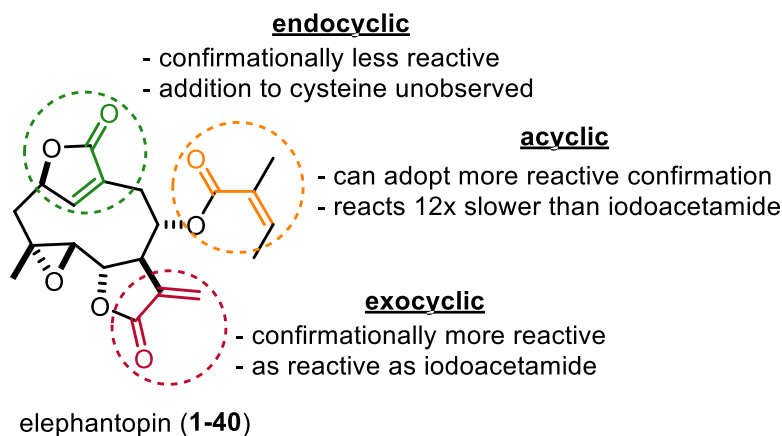


**Figure 1.15-** Elephantopin (**1-40**) possesses 3 electronically similar, but conformationally distinct Michael acceptors providing a case study in the consequences of enone conformation on reactivity.

The orientation of the enone is also pertinent to its reactivity. Consider the general schemes highlighted in Figure 1.11. In a Michael addition such as Figure 1.11A the approaching thiol nucleophile is activating the carbonyl enhancing its electrophilicity. One might expect that in complicated molecular scaffold the ability to conform to an architecture like **1-22** would relate to the rate of Michael additions. This can, indeed, be observed in literature report of Michael additions on sesquiterpene lactones (Figure 1.15). Researchers studying the addition of cysteine to elephantopin (**1-40**) have shown that the exocyclic Michael acceptor (red) reacts with cysteine at a rate equivalent to iodoacetamide, the a cyclic Michael acceptor (orange) reacts 12 times slower with cysteine than the exocyclic Michael acceptor and they did not observe addition to the endocyclic Michael acceptor at all in the time scale of their NMR studies.<sup>122</sup> This corroborates the hypothesis that conformation is relevant to reactivity. The exocyclic Michael acceptor (red) is locked in a more reactive conformation, the acyclic Michael acceptor (orange) can transiently adopt a more reactive conformation, and the endocyclic Michael acceptor (green) is locked in a less reactive conformation.

**These results are of critical importance to our work.** As described above any number of PAINs have been shown to bind or inhibit the NF- $\kappa$ B pathway. Even more complex natural product scaffolds than BAY-11-7082 (**1-14**) have been observed to bind and inhibit NF- $\kappa$ B subunits. For example, parthenolide (**1-41**)<sup>123</sup> and *ent*-kaurene diterpenoids such as ericalyxin B (**1-42**)<sup>124</sup> have been shown to bind specific cysteines in NF- $\kappa$ B (Figure 1.16). It should be noted that each of these molecules bears an exocyclic Michael acceptor (red) similar to the exocyclic Michael acceptor in **1-40**. Specific rate measurements have not, to my knowledge been done, but it would not surprise me if these structurally similar enones were similarly reactive towards iodoacetamide as well, which is to say completely unselective. It should be noted however that



**1-42** also possesses an endocyclic Michael acceptor (green) as well. The relative reactivities and the importance of these Michael acceptors to specific protein targets **have not been elucidated**.<sup>120</sup> Limited studies in the area of ericalyxin **1-41** and similar *ent*-kaurene biological activities have been towards their general cytotoxicity and limited research has suggested that **reducing more reactive exocyclic Michael acceptors reduces the general cytotoxicity of these molecules but they retain specific activity**.<sup>125</sup> Additionally, prodrug strategies have been developed to mask reactive Michael acceptors as tertiary amides which can, slowly in biological systems, revert to the reactive enones. This tends to improve the drug like properties of otherwise over reactive molecules.<sup>126</sup>

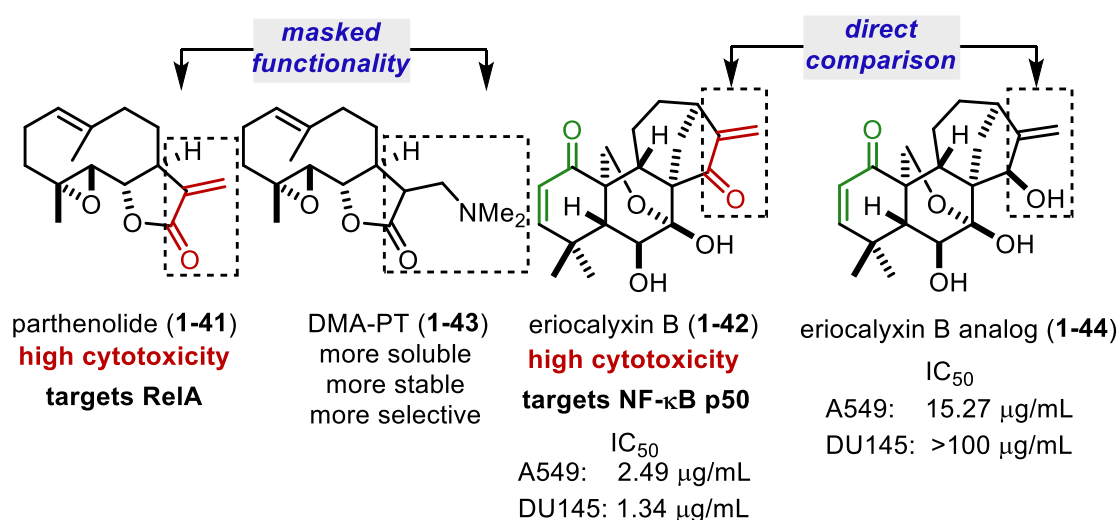


**Figure 1.16-** Strategies for handling overly reactive exocyclic Michael acceptors (red).

It is our opinion that these observations warrant further study to help set the record straight in the natural product literature around the bioactivity of these terpene natural products. We hope that with synthetic access to these molecules we can differentiate between pan assay inhibition and selective, likely irreversible, inhibitory activities of these endocyclic Michael acceptors.

In the following chapters you will read about our efforts towards the synthesis of pharbinilic acid, a putative NF- $\kappa$ B pathway inhibitor, our discovery of a gibberellin bearing an endocyclic Michael acceptor with a high selectivity profile against cancer derived cell lines and a unique phenotypic activity against the NF- $\kappa$ B pathway, our synthesis of a common intermediate to more than 600 *ent*-kaurene diterpenoids, to enable the direct comparison of Michael acceptor reactivity and selectivity, and the development of a synthetic method to take advantage of Michael acceptors to promote specific aldol reactions for the purpose of synthesizing diterpene alkaloids.

## Bibliography

1. Sen, R.; Baltimore, D. *Cell* **1986**, *46*, 705.
2. Zhang, Q.; Lenardo, M. J.; Baltimore, D. *Cell* **2017**, *168*, 37.
3. Hayden, M. S.; Ghosh, S. *Genes Dev.* **2012**, *26*, 203.
4. Smale, S. T. *Immunol. Rev.* **2012**, *246*, 193.
5. Isoda K.; Roth, S.; Nusslein-Volhard, C. *Genes Dev.* **1992**, *6*, 619.
6. Zhong, H.; May, M. J.; Jimi, E.; Ghosh, S. *Mol. Cell* **2002**, *9*, 625.
7. Hoffmann, A.; Natoli, G.; Ghosh, G. *Oncogene* **2006**, *25*, 6706.
8. Espinosa, L.; Bigas, A.; Mulero, M. C. *Br. J. Cancer* **2014**, *111*, 1688.
9. Lin, L.; DeMartino, G. N.; Greene, W. C. *Cell* **1998**, *92*, 819.
10. Gilmore, T. D. *Oncogene* **2006**, *25*, 6680.
11. Sun, S. C.; Ley, S. C. *Trends Immunol.* **2008**, *29*, 469.
12. Sriskantharajah, S.; et al. *Nat. Immunol.* **2009**, *10*, 38.
13. Yang, H. T.; et al. *Mol. Cell. Biol.* **2012**, *32*, 3438.
14. Israel, A. *Cold Spring Harb. Perspect. Biol.* **2010**, *2*, a000158.
15. Sun, S.-C. *Nat. Rev. Immun.* **2017**, *17*, 545.
16. Wang, V. Y.; Huang, W.; Asagiri, M.; Spann, N.; Hoffmann, A.; Glass, C.; Ghosh, G. *Cell Rep.* **2012**, *2*, 824.
17. Wang, V. Y.-F.; Li, Y.; Kim, D.; Zhong, X.; Du, Q.; Ghassemian, M.; Ghosh, G. *Mol. Cell* **2017**, *67*, 484.
18. Lamberti, C.; Lin, K. M.; Yamamoto, Y.; Verma, U.; Verma, I. M.; Byers, S.; Gaynor, R. B. *J. Biol. Chem.* **2001**, *276*, 42276.
19. Huang, W. C.; Ju, T. K.; Hung, M. C.; Chen, C. C. *Mol. Cell* **2007**, *26*, 75.
20. Anest, V.; Hanson, J. L.; Cogswell, P. C.; Steinbrecher, K. A.; Strahl, B. D.; Baldwin, A. S. *Nature* **2003**, *423*, 659.
21. Yamamoto, Y.; Verma, U. N.; Prajapati, S.; Kwak, Y. T.; Gaynor, R. B. *Nature* **2003**, *423*, 655.
22. Fernandez-Majada, V.; Aguilera, C.; Villanueva, A.; Vilardell, F.; Robert-Moreno, A.; Aytes, A.; Real, F. X.; Capella, G.; Mayo, M. W.; Espinosa, L.; Bigas, A. *Proc. Natl. Acad. Sci. USA* **2007**, *104*, 276.
23. Hoberg, J. E.; Yeung, F.; Mayo, M. W. *Mol. Cell* **2004**, *16*, 245.
24. Park, K. J.; Krishnan, V.; O'Malley, B. W.; Yamamoto, Y.; Gaynor, R. B. *Mol. Cell* **2005**, *18*, 71.
25. Tu, Z.; Prajapati, S.; Park, K. J.; Kelly, N. J.; Yamamoto, Y.; Gaynor, R. B. *J. Biol. Chem.* **2006**, *281*, 6699.
26. Shiah, H. S.; Gao, W.; Baker, D. C.; Cheng, Y. C. *Mol. Cancer Ther.* **2006**, *5*, 2484.
27. Hirata, Y.; Maeda, S.; Ohmae, T.; Shibata, W.; Yanai, A.; Ogura, K.; Yoshida, H.; Kawabe, T.; Omata, M. *Infect Immun.* **2006**, *74*, 1452.
28. Furuya, K.; Ozaki, T.; Hanamoto, T.; Hosoda, M.; Hayashi, S.; Barker, P. A.; Takano, K.; Matsumoto, M.; Nakagawara, A. *J. Biol. Chem.* **2007**, *282*, 18365.
29. Luo, J. L.; Tan, W.; Ricono, J. M.; Korchynskyi, O.; Zhang, M.; Gonias, S. L.; Cheresch, D. A.; Karin, M. *Nature* **2007**, *446*, 690.
30. Huang, W.-C.; Hung, M.-C. *J. Biomed. Sci.* **2013**, *20*, 1.

31. Lu, Y. C.; Yeh, W. C.; Ohashi, P. S. *Cytokine* **2008**; *42*, 145.
32. Coope, H. J.; et al. *EMBO J.* **2002**, *15*, 5375.
33. Liao, G.; Zhang, M.; Harhaj, E. W.; Sun, S. C. *J. Biol. Chem.* **2004**, *279*, 26243.
34. Razani, B.; et al. *Sci. Signal.* **2010**, *3*, ra41.
35. Wang N.; Liang, H.; Zen, K. *Front. Immunol.* **2014**, *5*, 614.
36. Sica, A.; Mantovani, A. *J. Clin. Invest.* **2012**, *122*, 787.
37. Mosser, D. M. *J. Leukoc. Biol.* **2003**; *73*, 209.
38. Zhu, J.; Yamane, H.; Paul, W. E. *Annu. Rev. Immunol.* **2010**; *28*, 445.
39. Oh, H.; Ghosh, S. *Immunol. Rev.* **2013**, *252*, 41.
40. Yu, J.; Wang, Y.; Yan, F.; Zhang, P.; Li, H.; Zhao, H.; et al. *J. Immunol.* **2014**, *193*, 2574.
41. Stohl, W. *Expert Rev. Clin. Immunol.* <http://dx.doi.org/10.1080/1744666X.2017.1291343>, **2017**.
42. Pannicke, U.; Baumann, B.; Fuchs, S.; Henneke, P.; Rensing-Ehl, A.; Rizzi, M.; Janda, A.; Hese, K.; Schlesier, M.; Holzmann, K.; et al. *N. Engl. J. Med.* **2013**, *369*, 2504.
43. Chen, K.; Coonrod, E. M.; Kuma'novics, A.; Franks, Z. F.; Durtschi, J. D.; Margraf, R. L.; Wu, W.; Heikal, N. M.; Augustine, N. H.; Ridge, P. G.; et al. *Am. J. Hum. Genet.* **2013**, *93*, 812.
44. Willmann, K. L.; Klaver, S.; Dogu, F.; Santos-Valente, E.; Garncarz, W.; Bilic, I.; Mace, E.; Salzer, E.; Conde, C. D.; Sic, H.; et al. *Nat. Commun.* **2014**, *5*, 5360.
45. Mooster, J. L.; Le Bras, S.; Massaad, M. J.; Jabara, H.; Yoon, J.; Galand, C.; Heesters, B. A.; Burton, O. T.; Mattoo, H.; Manis, J.; Geha, R. S. *J. Exp. Med.* **2015**, *212*, 185.
46. Fuchs-Telem, D.; Sarig, O.; van Steensel, M. A.; Isakov, O.; Israeli, S.; Nousbeck, J.; Richard, K.; Winnepeninckx, V.; Vernooij, M.; Shomron, N.; et al. *Am. J. Hum. Genet.* **2012**, *91*, 163.
47. Simmonds, R. E.; Foxwell, B. M. *Rheumatology* **2008**; *47*, 584.
48. Noort, A. R.; Tak, P. P.; Tas, S. W. *Arthritis Res. Ther.* **2015**, *17*, 15.
49. Wei, F.; Chang, Y.; Wei, W. **2015**, *76*, 537.
50. Hussman J. P.; Beecham, A. H.; Schmidt, M.; Martin, E. R.; McCauley, J. L.; Vance, J. M.; et al. *Genes Immun.* **2016**, *17*, 305.
51. International Multiple Sclerosis Genetics, C Genetics, Consortium, Beecham A. H.; Patsopoulos N. A.; Xifara, D. K.; Davis, M. F.; et al. *Nat. Genet.* **2013**, *45*, 1353.
52. Mitterski, B.; Bohringer, S.; Klein, W.; Sindern, E.; Haupts, M.; Schimrigk, S.; et al. *Genes Immun.* **2002**, *3*, 211.
53. Brambilla, R.; Dvorianchikova, G.; Barakat, D.; Ivanov, D.; Bethea, J. R.; Shestopalov, V. I. *J. Neuroinflammation* **2012**, *9*, 213.
54. Brambilla, R.; Persaud, T.; Hu, X.; Karmally, S.; Shestopalov, V. I.; Dvorianchikova, G.; et al. *J. Immunol.* **2009**, *182*, 2628.
55. Rogler, G.; Brand, K.; Vogl, D.; Page, S.; Hofmeister, R.; Andus, T.; et al. *Gastroenterology* **1998**, *115*, 357.
56. Schreiber, S.; Nikolaus, S.; Hampe, J. *Gut* **1998**, *42*, 477.
57. Neurath, M. F.; Pettersson, S.; Meyer zum Buschenfelde, K. H.; Strober, W. *Nat. Med.* **1996**, *2*, 998.

58. Fichtner-Feigl, S.; Fuss, I. J.; Preiss, J. C.; Strober, W.; Kitani, A. *J. Clin. Invest.* **2005**, *115*, 3057.
59. Greten, F. R.; Eckmann, L.; Greten, T. F.; Park, J. M.; Li, Z. W.; Egan, L. J.; et al. *Cell* **2004**, *118*, 285.
60. Choudhary, S.; et al. *Endocrinology* **2011**, *152*, 3622.
61. Starkey, J. M.; et al. *Diabetes* **2006**, *55*, 1252.
62. Sheng, L.; et al. *Nat. Med.* **2012**, *18*, 943.
63. Ben-Neriah, Y.; Karin, M. *Nat. Immunol.* **2011**, *12*, 715.
64. Xia, L.; Tan, S.; Zhou, Y.; Lin, J.; Wang, H.; Oyang, L.; Tian, Y.; Liu, L.; Su, M.; Wang, H.; Cao, D.; Liao, Q. *Onco. Targ. Ther.* **2018**, *11*, 2063..
65. He, K.-L.; Ting, A. T. *Mol. Cell. Biol.* **2002**, *22*, 6034.
66. Wang, D.J.; Ratnam, N.M.; Byrd, J.C.; Guttridge, D.C. *Cell Rep.* **2014**, *9*, 90.
67. Huang, S.; Pettaway, C.A.; Uehara, H.; Bucana, C.D.; Fidler, I.J. *Oncogene* **2001**, *20*, 4188.
68. Wu, Y.; Deng, J.; Rychahou, P.G.; Qiu, S.; Evers, B.M.; Zhou, B.P. *Cancer Cell* **2009**, *15*, 416.
69. Mosialos G. *Semin. Cancer Biol.* **1997**, *8*, 121.
70. Migliazza, A.; Lombardi, L.; Rocchi, M.; Trecca, D.; Chang, C. C.; Antonacci, R.; Fracchiolla, N. S.; Ciana, P.; Maiolo, A. T.; Neri, A. *Blood* **1994**, *84*, 3850.
71. Neri, A.; Chang, C. C.; Lombardi, L.; Salina, M.; Corradini, P.; Maiolo, A. T.; Chaganti, R. S.; Dalla-Favera, R. *Cell* **1991**, *67*, 1075.
72. Yu, Q.; Geng, Y.; Sicinski, P. *Nature* **2001**, *411*, 1017.
73. Sau, A.; Lau, R.; Cabrita, M. A.; et al. *Cell Stem Cell.* **2016**, *19*, 52.
74. Walther W.; Kobelt, D.; Bauer, L.; Aumann, J.; Stein, U. *Int. J. Oncol.* **2015**, *47*, 2276.
75. Mukhopadhyay, T.; Roth, J. A.; Maxwell, S. A. *Oncogene* **1995**, *11*, 999.
76. Son, D. S.; Kabir, S. M.; Dong, Y.; Lee, E.; Adunyah, S. E. *J. Inflamm. (Lond).* **2013**, *10*, 25.
77. Neri, A.; Fracchiolla, N. S.; Roscetti, E.; Garatti, S.; Trecca, D.; Boletini, A.; Perletti, L.; Baldini, L.; Maiolo, A. T.; Berti, E. *Blood* **1995**, *86*, 3160.
78. Zhang, J.; Jia, L.; Lin, W.; et al. *J. Virol.* **2017**, *91*, e02168.
79. Ammirante, M.; Luo, J.-L.; Grivennikov, S.; Nedospasov, S.; Karin, M. *Nature*, **2010**, *464*, 302.
80. Kim, S. H.; Ezhilarasan, R.; Phillips, E.; et al. *Cancer Cell.* **2016**, *29*, 201.
81. Baud, V.; Karin, M. *Nat. Rev. Drug Discov.* **2009**, *8*, 33.
82. Nandakumar, V.; Singh, T.; Katiyar, S. K. *Cancer Lett.* **2008**, *269*, 378.
83. Rahman, I.; Biswas, S. K.; Kirkham, P. A. *Biochem. Pharmacol.* **2006**, *72*, 1439.
84. Sethi, G.; Sung, B.; Aggarwal, B. B. *Exp. Biol. Med.* **2008**, *233*, 21.
85. Kuper, H.; Adami, H. O.; Trichopoulos, D. *J. Intern. Med.* **2000**, *248*, 171.
86. Lin, Y.; Bai, L.; Chen, W.; Xu, S. *Expert Opin. Ther. Targets* **2010**, *14*, 45.
87. Garcia, M. G.; Alaniz, L.; Lopes, E. C.; et al. *Leuk. Res.* **2005**, *29*, 1425.
88. Hideshima, T.; Chauhan, D.; Kiziltepe, T.; et al. *Blood* **2009**, *113*, 5228.
89. Yang, J.; Amiri, K. I.; Burke, J. R.; et al. *Clin. Cancer Res.* **2006**, *12*, 950.
90. Choo, M. K.; Sakurai, H.; Kim, D. H.; Saiki, I. *Oncol. Rep.* **2008**, *19*, 595.
91. Ravaut, A.; Cerny, T.; Terret, C.; et al. *Eur. J. Cancer* **2005**, *41*, 702.

92. Shen, H. M.; Tergaonkar, V. *Apoptosis* **2009**, *14*, 348.
93. Dingli, D.; Rajkumar, S. V. *Oncology* **2009**, *23*, 407.
94. Gasparian, A. V.; Guryanova, O. A.; Chebotaev, D. V.; et al. *Cell Cycle* **2009**, *8*, 1559.
95. Cardoso, F.; Durbecq, V.; Laes, J. F.; et al. *Mol. Cancer Ther.* **2006**, *5*, 3042.
96. Sloss, C. M.; Wang, F.; Liu, R.; et al. *Clin. Cancer Res.* **2008**, *14*, 5116.
97. Lynch, T. J.; Fenton, D.; Hirsh, V.; et al. *J. Thorac. Oncol.* **2009**, *4*, 1002.
98. Nakajima, S.; Kato, H.; Takahashi, S.; Johno, H.; Kitamura, M. *FEBS Lett.* **2011**, *585*, 2249.
99. Hideshima, T.; Ikeda, H.; Chauhan, D.; Okawa, Y.; Raje, N.; Podar, K.; Mitsiades, C.; Munshi, N. C.; Richardson, P. G.; Carrasco, R. D.; et al. *Blood* **2009**, *114*, 1046.
100. Bruno, P. A.; Morriss-Andrews, A.; Henderson, A. R.; Brooks, C. L.; Mapp, A. K. *Angew. Chem. Int. Ed. Engl.* **2016**, *55*, 14997.
101. Mabuchi, S.; Ohmichi, M.; Nishio, Y.; et al. *J. Biol. Chem.* **2004**, *279*, 23477.
102. Gaurnier-Hausser, A.; Patel, R.; Baldwin, A. S.; May, M. J.; Mason, N. J. *Clin. Cancer Res.* **2011**, *17*, 4661.
103. Lau, J. L.; Dunn, M. K. *Bioorg. Med. Chem.* **2018**, *26*, 2700.
104. Lee, C. T.; Seol, J. Y.; Lee, S. Y.; et al. *Lung Cancer* **2003**, *41*, 199.
105. Uetsuka, H.; Haisa, M.; Kimura, M.; et al. *Exp. Cell Res.* **2003**, *289*, 27.
106. Baell, J. B.; Holloway, G. A. *J. Med. Chem.* **2010**, *53*, 2719.
107. Baell, J. B. *J. Nat. Prod.* **2016**, *79*, 616.
108. Mereles, D.; Hunstein, W. *Int. J. Mol. Sci.* **2011**, *12*, 5592.
109. Baggstrom, M. Q.; Qi, Y.; Koczywas, M.; Argiris, A.; Johnson, E. A.; Millward, M. J.; Murphy, S. C.; Erlichman, C.; Rudin, C. M.; Govindan, R.; Mayo Phase, C.; California, C. J. *Thorac. Oncol.* **2011**, *6*, 1757.
110. Priyadarsini, K. I. *Curr. Pharm. Des.* **2013**, *19*, 2093.
111. Schneider, C.; Gordon, O. N.; Edwards, R. L.; Luis, P. B. *J. Agric. Food Chem.* **2015**, *63*, 7606.
112. Marcu, M. G.; Jung, Y. J.; Lee, S.; Chung, E. J.; Lee, M. J.; Trepel, J.; Neckers, L. *Med. Chem.* **2006**, *2*, 169.
113. Ingolfsson, H. I.; Thakur, P.; Herold, K. F.; Hobart, E. A.; Ramsey, N. B.; Periole, X.; de Jong, D. H.; Zwama, M.; Yilmaz, D.; Hall, K.; Maretzky, T.; Hemmings, H. C., Jr.; Blobel, C.; Marrink, S. J.; Kocer, A.; Sack, J. T.; Andersen, O. S. *ACS Chem. Biol.* **2014**, *9*, 1788.
114. Jasial, S.; Hu, Y.; Bajorath, J. *J. Med. Chem.* **2017**, *60*, 3879.
115. Wang, J.; Zhang, C.-J.; Chia, W. N.; Loh, C. C. Y.; Li, Z.; Lee, Y. M.; He, Y.; Yuan, L.-X.; Lim, T. K.; Liu, M.; Liew C. X.; Lee, Y. Q.; Zhang, J.; Lu, N.; Lim, C. T.; Hua, Z.-C.; Shen, H.-M.; Tan, K. S. W.; Lin, Q. *Nat. Commun.* **2015**, *6*, 1011110.1038/ncomms10111.
116. *Chem. Eng. News* **2015**, *93*, 7.
117. Charman, S. A.; Arbe-Barnes, S.; Bathurst, I. C.; Brun, R.; Campbell, M.; Charman, W. N.; Chiu, F. C.; Chollet, J.; Craft, J. C.; Creek, D. J.; Dong, Y.; Matile, H.; Maurer, M.; Morizzi, J.; Nguyen, T.; Papastogiannidis, P.; Scheurer, C.; Shackleford, D. M.; Sriraghavan, K.; Stingelin, L.; Tang, Y.; Urwyler, H.; Wang, X.; White, K. L.; Wittlin, S.; Zhou, L.; Vennerstrom, J. L. *Proc. Natl. Acad. Sci. U. S. A.* **2011**, *108*, 4400.

118. Jain, S. K.; Bharate, S. B.; Vishwakarma, R. A. *Mini-Rev. Med. Chem.* **2012**, *12*, 632.
119. Capuzzi, S. J.; Muratov, E. N.; Tropsha, A. *J. Chem. Inf. Model.* **2017**, *57*, 417.
120. Jackson, P. A.; Widen, J. C.; Harki, D. A.; Brummond, K. M. *J. Med. Chem.* **2017**, *60*, 839.
121. Ando, R.; Amano, Y.; Nakamura, H.; Arai, N.; Kuwajima I. *Bioorg. Med. Chem. Lett.* **2006**, *16*, 3315.
122. Kupchan, S. M.; Fessler, D. C.; Eakin, M. A.; Giacobbe, T. J. *Science* **1970**, *168*, 376.
123. (a) Kwok, B. H.; Koh, B.; Ndubuisi, M. I.; Eloffsson, M.; Crews, C. M. *Chem. Biol.* **2001**; *8*:759.
124. Kong, L.-M.; Deng, X.; Zuo, Z.-L.; Sun, H.-D.; Zhao, Q.-S.; Li, Y. *Oncotarget* **2014**, *5*, 11354.
125. Zhao, Y.; Niu, X.-M.; Qian, L.-P.; Liu, Z.-Y.; Zhao, Q.-S.; Sun, H.-D. *Eur. J. Med. Chem.* **2007**, *42*, 494.
126. (a) Woods, J. R.; Mo, H. P.; Bieberich, A. A.; Alavanja, T.; Colby, D. A. *Med. Chem. Comm.* **2013**, *4*, 27. (b) Amslinger, S. *Chem. Med. Chem.* **2010**, *5*, 351.

## Chapter 2 Gibberellins as Inhibitors of the NF- $\kappa$ B Pathway

### Chapter 2.1 Introduction

#### Chapter 2.1.1 Gibberellic acid (**2-1**) isolation and biosynthesis

Gibberellic acid (GA<sub>3</sub>, **2-1**, Figure 2.1) is among the most well studied and characterized terpenes. Its roots go back to the early 1800's, in 1809 a semiliterate farmer, Konishi, dictated a book on farming and described a disease prevalent in rice farming. He described a disease in which a single plant grows much taller, thinner and faster than its neighbors which he named bakanae or "foolish seedling."<sup>1</sup> From that time forward significant effort was undertaken in identifying the cause of this disease. It was not, however, until 1929 when Kurosawa found that only the extract from the growth media of a disease-causing fungus was necessary for causing the disease phenotype.<sup>2</sup> This caused researchers to start searching for a small molecule that was responsible for the disease and in 1938 Yabuta and Sumaki isolated two crystalline compounds both of which could cause the disease phenotype.<sup>3</sup> It was not until the 1950's that researchers in the US and Britain joined the field of gibberellin research.<sup>4</sup> The application of cutting edge crystallographic techniques were finally able to confirm some of the competing structural hypotheses by X-ray chromatography.<sup>5</sup> The field of study of gibberellins have flourished ever since owing to their ability to promote plant growth (*vide infra*).



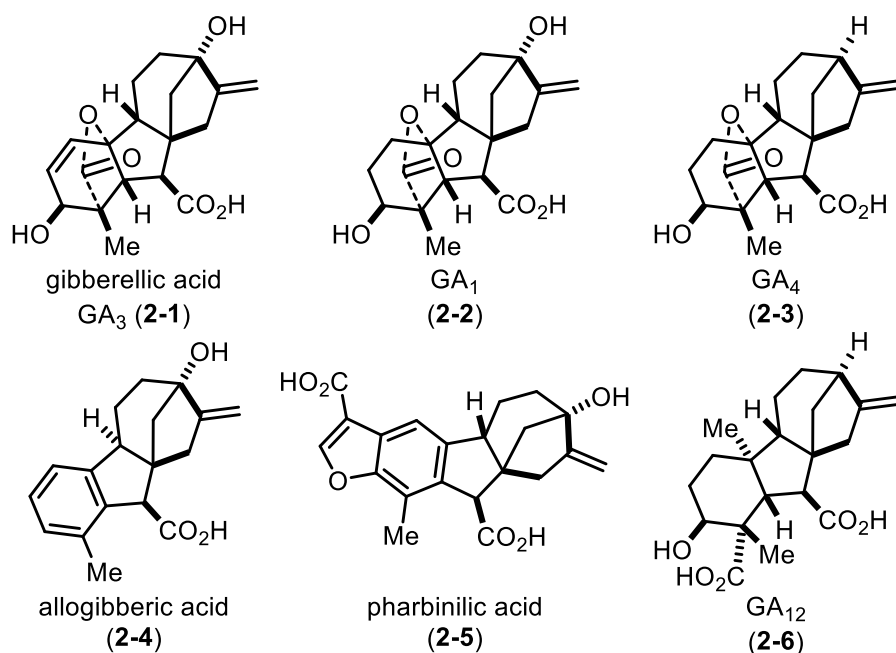


**Figure 2.1-** Selected gibberellin diterpenoids.

Though originally isolated from the extract of fungi, gibberellins are synthesized by essentially all higher plants. Though at least 136 gibberellins have been isolated from plants only a select few appear to be active as growth hormones, the most prevalent being GA<sub>1</sub> (2-2), GA<sub>4</sub> (2-3) and GA<sub>3</sub> (2-1).<sup>6</sup> The rest appear to be biosynthetic precursors and are typically isolated in much higher concentrations than the active hormones themselves.

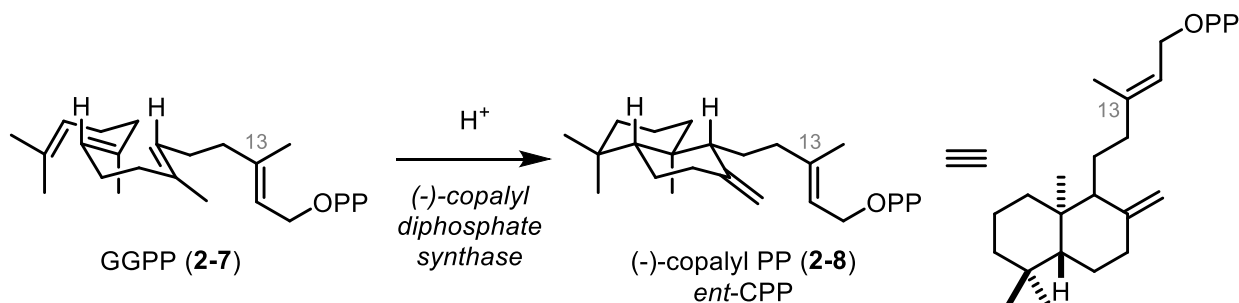


**Figure 2.2-** The first step in gibberellin biosynthesis is the conversion of GGPP (2-7) to *ent*-CPP (2-8).

Like most diterpenoids, the gibberellin diterpenoids are biosynthetically derived from the linear C<sub>20</sub> geranylgeranyl pyrophosphate (2-7, GGPP) whereupon first GGPP (2-7) is cyclized to afford a bicyclic intermediate, *ent*-copalyl pyrophosphate (*ent*-CPP, 2-8) (Figure 2.2).<sup>7</sup> These

intermediates can then differentially derivatized by oxidations, reductions, cyclizations, acetylations, and glycosylations to furnish a variety of structurally unique diterpenoids.

The same enzyme that promotes the formation of *ent*-CPP (**3-7**), (-)-copalyl diphosphate synthase, also referred to as *ent*-kaurene synthase, can promote the subsequent functionalization to *ent*-kaurene (**2-10**) via a similar cationic rearrangement (Figure 2.3).<sup>8</sup> This core structure is then subjected to a series of subsequent oxidations by *ent*-kaurenoic acid oxidase, first to *ent*-kaurenoic acid (**2-11**) then to *ent*-7 $\alpha$ -hydroxykaurenoic acid (**2-12**). Oxidation of this alcohol proceeds with ring contraction to **2-13** which is oxidized once more to GA<sub>12</sub> (**2-6**) which is the progenitor of all other gibberellins.<sup>6</sup> In the biosynthesis of gibberellic acid (**2-1**) and similar gibberellins the first step is oxidation at C<sub>13</sub> by, the creatively named, gibberellic acid 13-oxidase providing GA<sub>53</sub> (**2-14**). One remarkable step in the biosynthesis of **2-1** is the loss of C<sub>20</sub> which proceeds by oxidation and loss of C<sub>20</sub> as carbon dioxide ultimately yielding GA<sub>20</sub> (**2-16**).<sup>9</sup> Finally, gibberellic acid 3-oxidase oxidizes **2-16** to an olefin providing GA<sub>5</sub> (**2-17**) and then one more oxidation yields gibberellic acid (**2-1**).

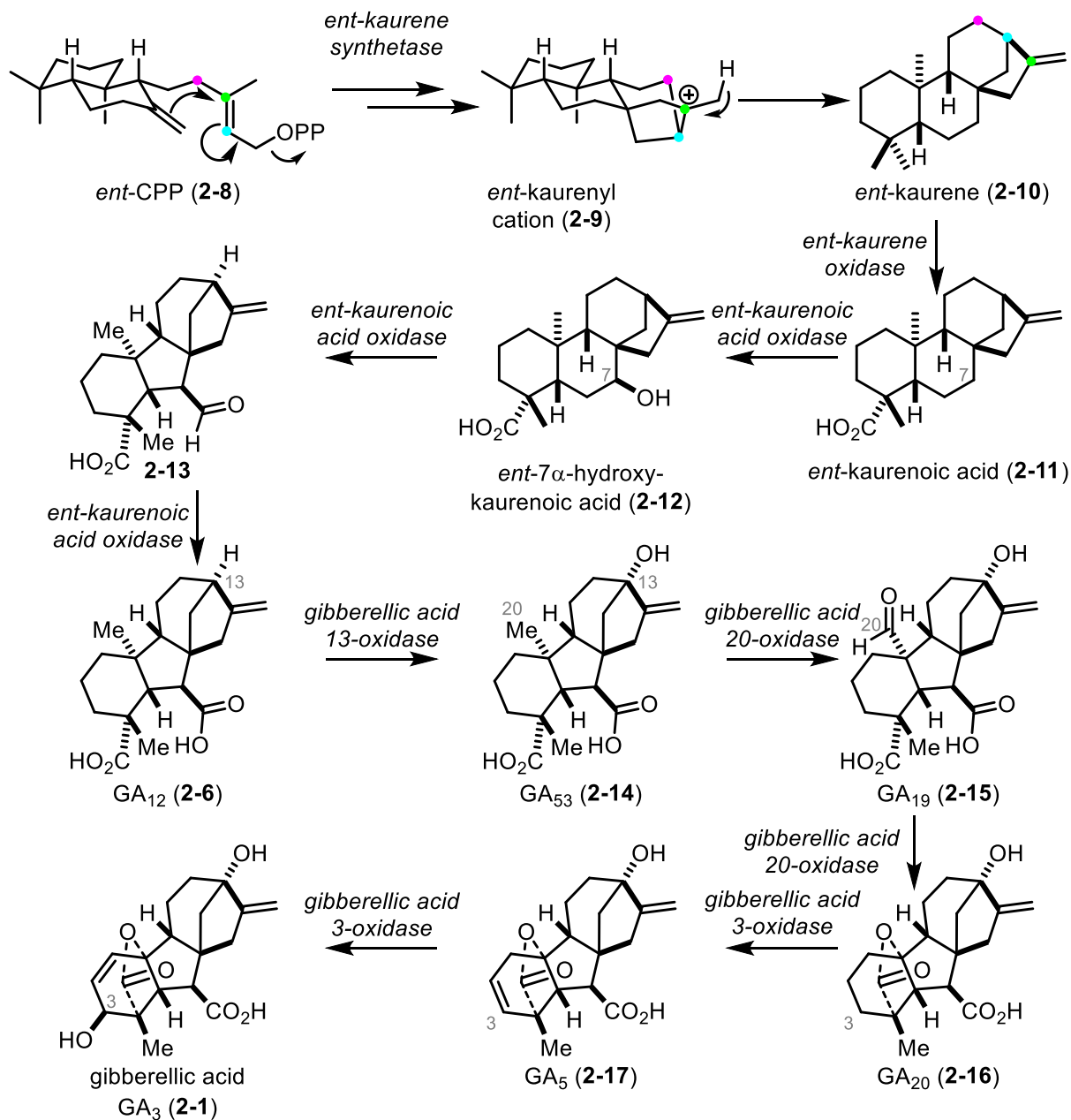


**Figure 2.3-** The biosynthesis of gibberellic acid (**2-1**) from *ent*-karene (**2-10**) and  $\text{GA}_{12}$  (**2-6**).

### Chapter 2.1.2 Gibberellic acid (**2-1**) synthesis

Synthetic interest in gibberellic acid (**2-1**) began as soon as its structure was elucidated but it was not until 1978 that the synthesis was completed, as a single enantiomer by Corey and coworkers.<sup>10</sup> This synthesis relied on an oxidative dearomatization to form **2-19** followed by a Diels Alder to **2-20**. The most challenging sequence of steps involves closing the highly strained

C/D ring. Corey and coworkers manage this task by a titanium mediated radical ring closure to form **2-22**. Oxidatively opening the B ring cyclohexene followed by aldol condensation and olefination lead to a second Diels Alder precursor **2-23**. The Diels Alder did close the A ring to **2-24**. Until this point the sequence had been racemic but Corey and coworkers were able to couple the C<sub>13</sub> hydroxyl group to an amino acid to enable a stereo-resolution which yielded a single enantiomer which they elaborated to **2-1** in a total of 14 steps from **2-24**. Though an impressive undertaking, 40 steps relying on a stereo-resolution that loses half of the mass is the most efficient way to gain access to **2-1**.

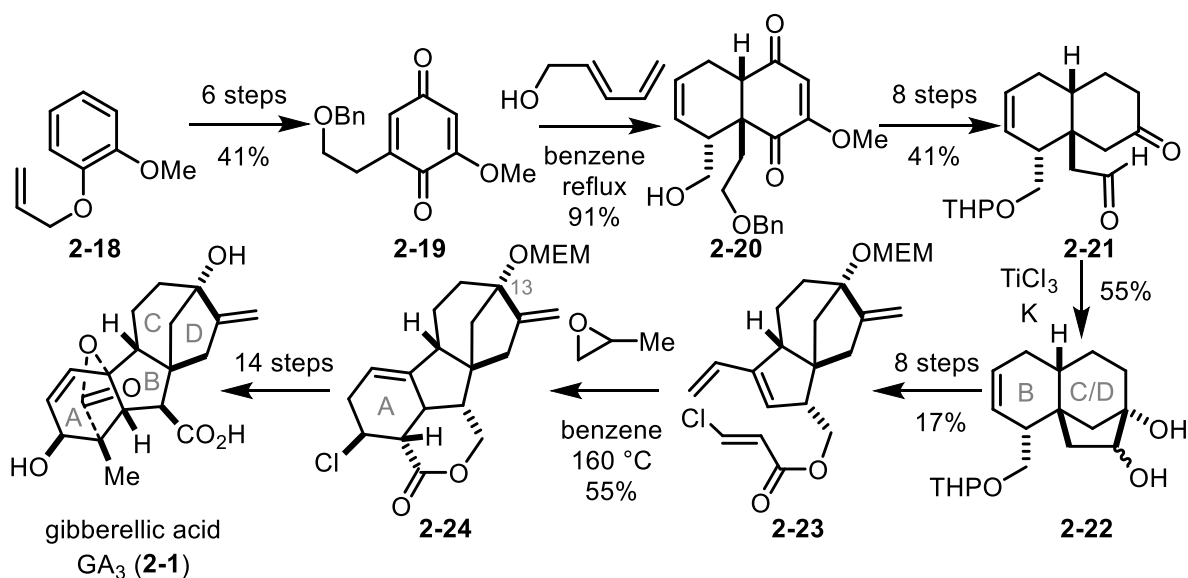


**Figure 2.4-** Highlights from Corey's 1978 synthesis of gibberellic acid (**2-1**).

Though gibberellic acid (**2-1**) has been synthesized since, by Yamada,<sup>11</sup> Mander,<sup>12</sup> and twice by Corey,<sup>13</sup> none of these synthetic approaches, the shortest being 31 steps, have improved upon the original to the point of allowing for easy synthetic access to **2-1**. In large part this is due to the challenge of constructing and working with the C/D ring bicycle. In particular, the incredible strain inherent in the cis-boat configuration provides a strong thermodynamic driving force that enables a Wagner-Meerwein rearrangement in which the C/D ring olefin can react with even mild electrophiles, such as Lewis or Bronstead acids (Figure 2.5).<sup>10</sup> Furthermore it has been

shown that even in neutral water the bridging A ring bicycle can eliminate to form gibberellenic acid (**2-26**).<sup>14</sup> In more acidic media, presumably upon eliminating water from the A ring of gibberellenic acid (**2-26**), the A ring can decarboxylate and aromatize to provide allogibberic acid (**2-4**) and H<sub>9</sub>-*epi*-allogibberic acid (**2-27**). These products form in a mixture favoring **2-4**, likely due to the release of ring strain in the C/D ring.<sup>15</sup> Taken together these side reactions prompted E.J. Corey to label it as a “singularly diabolical placement and density of functionality.”<sup>16</sup>

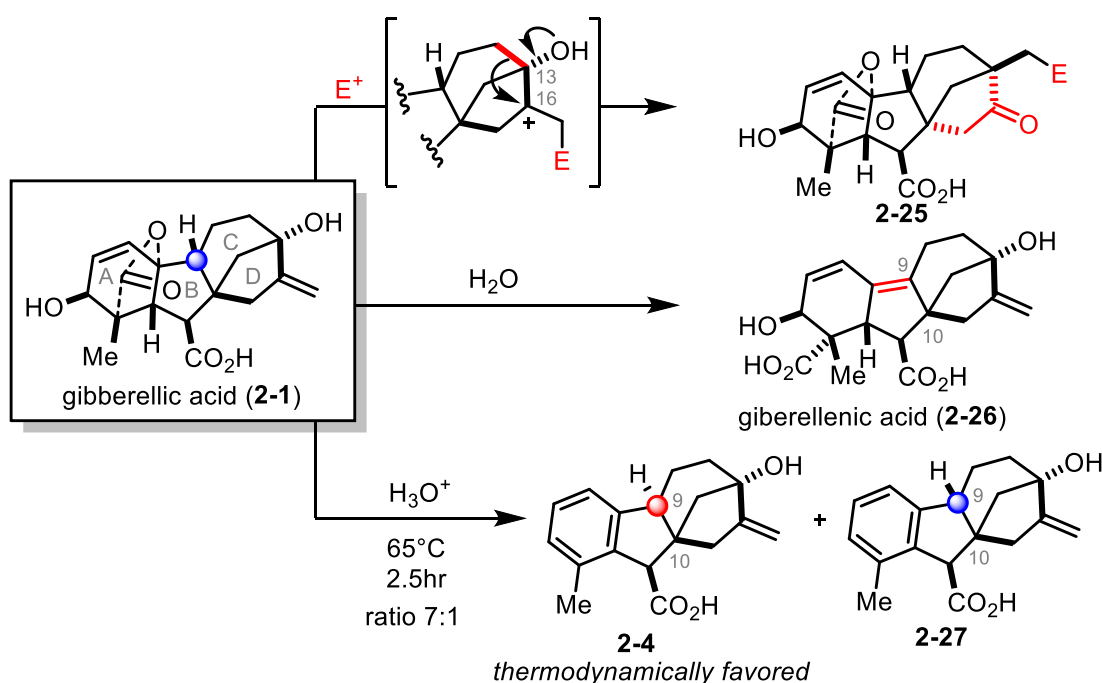


**Figure 2.5-** Side reactions from gibberellic acid (**2-1**) include Wagner Meerwein rearrangements, eliminations, and aromatizations.

Gibberellic acid (**2-1**), despite these challenges inherent in its synthesis, is a valuable target. This is due to its myriad of biological activities (*vide infra*), chief among those is its ability to act as a plant growth hormone and promote healthy plant growth. Especially with the rise of organic farming practices access to **2-1** and related gibberellins is of paramount interest to the agricultural community. Shu and coworkers first addressed this challenge in a scalable way in 1959.<sup>17</sup> They showed that in a mixture of glucose and galactose that they could produce **2-1** at

concentrations of  $880 \text{ mgL}^{-1}$  on bench top scale but more importantly  $650 \text{ mgL}^{-1}$  in a 1000 gallon reactor. This represented a production of  $11.8 \text{ kg h}^{-1}$  a feat that synthetic methods would struggle to match. This initial entreaty is hardly a unique occurrence, in 1986 Lonsane and Kumar reported a solid state fermentation process that could produce **2-1** for half the cost of liquid fermentation at a rate of  $150 \text{ m}^3 \text{ y}^{-1}$ .<sup>18</sup> In 1997 Barrios-Gonzalez and coworkers reported that by using low density polyurethane as a support they could increase the efficiency of the procedure developed by Losane and Kumar by increasing the extraction efficiency from the solid state growth medium.<sup>19</sup> In 2000 Escamillia and coworkers used modern bioreactors and computationally driven multivariant analysis to more than triple the efficiency of existing methods, up to  $3.9 \text{ gL}^{-1}$ .<sup>20</sup> More modern efforts take a green chemistry approach and show how food waste can be used as feedstock in bioreactors to produce **2-1** including coffee husks,<sup>21</sup> and citric pulp.<sup>22</sup> With all these advancements in the production of gibberellic acid by fermentation it is available in bulk for \$180/kg.

### Chapter 2.1.3 Gibberellic acid (**2-1**) biological activity

Historically, commercially, and most famously gibberellins function as plant growth hormones. The first and most obvious of its activities are the way that it promotes stem elongation. From the very first report in 1809 farmers characterized gibberellins by the spindly growth of affected rice plants, called bakanae.<sup>1</sup> The next 150 years of phenotypic study of the effects of gibberellins took place in Japan and are nicely highlighted in a review by Yamake and Stowe.<sup>23</sup> It has long been known that gibberellins promote growth in plants afflicted by dwarfism.<sup>24</sup> This is likely due both to the ability of gibberellins to promote cell division<sup>25</sup> and also their ability to promote cell elongation in plant stems.<sup>26</sup> In plant physiology there is a factor that promotes stem growth, auxin, and it was long been debated the interplay between auxin and

the gibberellins. In 2001 Reid and coworkers put the controversy to bed by identifying that auxin effects cell elongation by promoting gibberellin biosynthetic pathways.<sup>27</sup>

The second most well studied physiological effect of gibberellins are in their role in seed germination. Application of gibberellins to plant seeds accelerate the germination even in seeds that typically require photactivation.<sup>28</sup> In cereal crops, such as rice, wheat, and barley, germination is chiefly controlled and associated with production and secretion of  $\alpha$ -amylase which hydrolyzes macromolecules in the seed aleurone providing nutrients for the growing seedling. Even in 1940 researchers had determined that gibberellins induced the production and secretion of  $\alpha$ -amylase in barley seeds.<sup>29</sup> In 1976 researcher showed that gibberellins increase the amount of mRNA transcripts of  $\alpha$ -amylase.<sup>30</sup> It was not until 1995 that researchers were able to elucidate that gibberellins regulate the expression of MYB a transcription factor that binds the  $\alpha$ -amylase gene promoter region and promotes the transcription of  $\alpha$ -amylase.<sup>31</sup> Of course together these observed biological effects beg the question how gibberellins control the transcription of particular genes.

At first it was postulated that gibberellins might bind a G protein coupled receptor (GPCR) and as a result control for the expression of genes.<sup>32</sup> This hypothesis is preceded in part due to the inability of bioactive gibberellins to passively cross the cell membrane. However more recent data sheds doubt on whether plants have any GPCRs at all.<sup>33</sup> A more attractive hypothesis presented itself with the discovery of a nuclear receptor *GID1* that binds and is activated by gibberellins.<sup>34</sup> Subsequent X-ray crystallography provides structural evidence that upon binding physiologically active gibberellins *GID1* closes around the small molecule with a flexible N-terminus acting as a lid.<sup>35</sup> The effect of this conformational change is to allow *GID1* to bind a family of proteins that contain DELLA domains resulting in their polyubiquitinylation

and degradation (Figure 2.6).<sup>36</sup> Focus on the biological activity has turned, therefore, to the activity of DELLA proteins. Among the best characterized activity of DELLA proteins are as co-transcriptional regulators and they've been found to both promote and repress a wide variety of gene expression though a two second sound bite would be that DELLA proteins inhibit cell and plant growth.<sup>37</sup> A non-transcriptional affect of DELLA has also been observed as an inhibitor of microtubule assembly, which also contributes to their net anti-cell proliferative effects.<sup>38</sup>

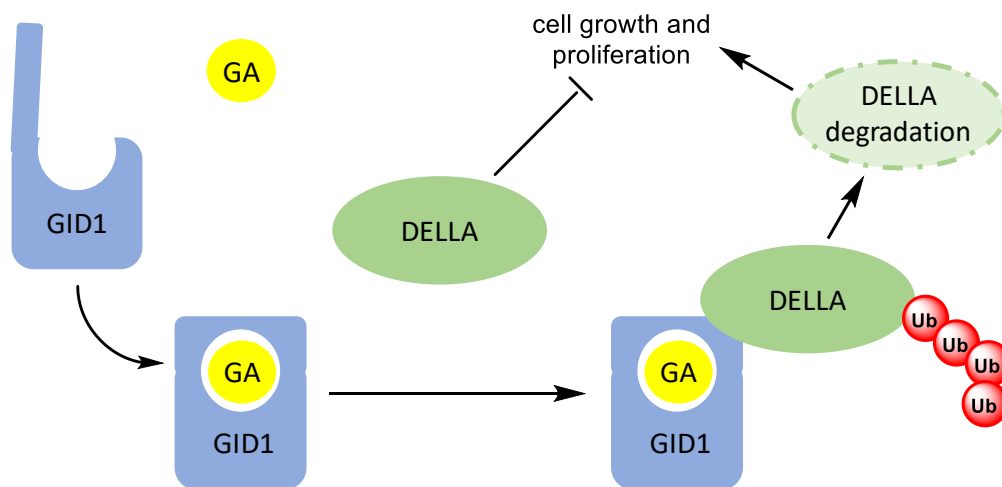


**Figure 2.6-** Bioactive gibberellins bind the nuclear receptor GID1, which induces a conformational change, which allows GID1 to recruit and promote the degradation of DELLA proteins.

In animals, gibberellins are often thought of as being safe. Even in long term exposure experiments rats don't have significant negative trends. Though one experiment from the mid 90's indicated the potential for an increase in cancer incidence.<sup>39</sup> Longitudinal studies conducted later show no increase in cancer and mild, non-statistically significant changes in oxidative stress response factors.<sup>40</sup> Additional research on teratogenicity in frog embryos show that prolonged exposure to **2-1** at concentrations of  $1.3 \text{ gL}^{-1}$  can cause 10% increase in incidents of birth defects.<sup>41</sup>

Some efforts have been undertaken in the area of cancer research. Researchers at Yunan University in China have synthesized a small library of gibberellins that they demonstrated have



activity against a variety of cancer derived cell lines.<sup>42</sup> In particular GA-13315 (**2-28**) was shown to have 2.9  $\mu\text{M}$   $\text{IC}_{50}$  against HT29 cells, as well as inhibiting topoisomerase I at 8  $\mu\text{g}/\text{mL}$ . It should be noted that despite possessing both a more reactive exo-cyclic, and a less reactive endo-cyclic Michael acceptor, this molecule was somewhat selective killing all tested cell lines at 40-60  $\mu\text{M}$ . This 20-fold selectivity was enough to convince the researchers to conduct studies in mouse xenografts in which they showed that **2-28** reduced A549 tumor size at  $19 \pm 7.6 \mu\text{M}$  over 3 days.<sup>43</sup> They also showed that this reduction in size was a result of mitochondrial apoptosis and that this was characterized by a decrease in cellular concentration of Bcl-2, a pro-survival protein, controlled by NF- $\kappa\text{B}$ , that inhibits apoptosis.

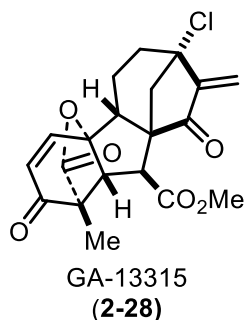


**Figure 2.7-** Structure of GA-13315 (**2-28**).

Of particular inspiration to us is the research conducted by Koehler and coworkers that showed that gibberellins might serve as selective binders and inhibitors of NF- $\kappa\text{B}$ .<sup>44</sup> They identified that commercial gibberellic acid (**2-1**) bound to p50 of NF- $\kappa\text{B}$  by small molecule microarray (SMM) and confirmed this initial hit by surface plasmon resonance (SPR). However, these results were somewhat inconsistent, in particular when they HPLC purified **2-1** they found that the activity of **2-1** in their SPR and inhibition assays was remarkably reduced. When they investigated further they identified that allogibberic acid (**2-4**) was a significant contaminant in commercial gibberellic acid (**2-1**) and that **2-4** is a significantly more potent binder of NF- $\kappa\text{B}$  p50 as determined by SPR.

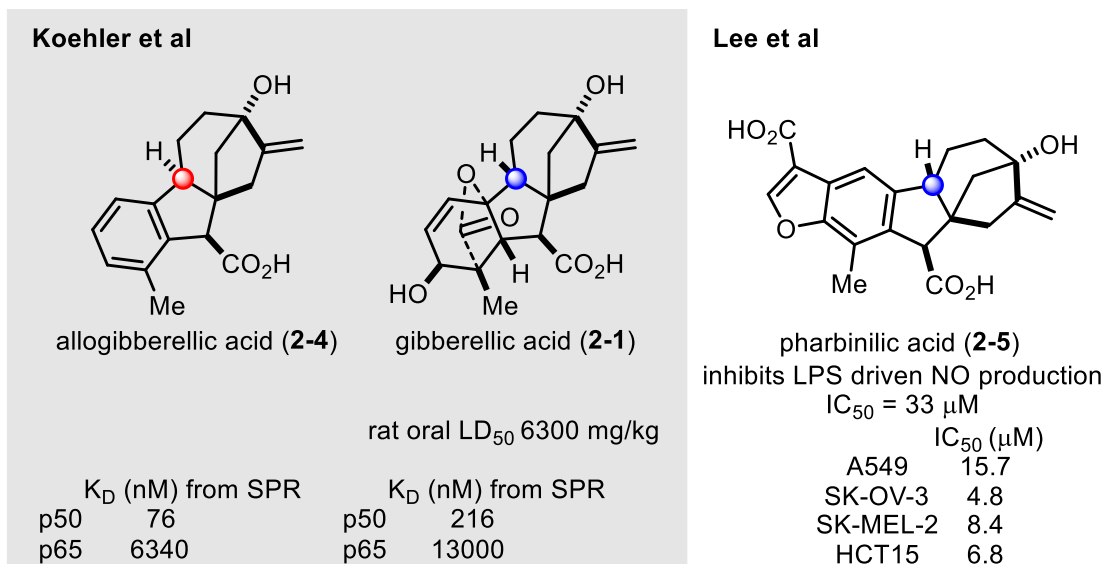


**Figure 2.8-** Known biological activity of select gibberellins.

#### Chapter 2.1.4 Pharbinilic acid (**2-5**) isolation and biological activity

Pharbinilic acid was isolated shortly before I began my thesis work from the seeds of Morning Glories.<sup>45</sup> From 2 kg of dried seeds they isolated 6 mg of **2-5**. This was of significance to the gibberellin academic community because pharbinilic acid (**2-5**) is likely intentionally produced by plants and to date the only other isolated aromatic gibberellins are thought to be degradation products of other gibberellins. Though its physiological purpose remains unknown the isolation chemists tested it against a variety of cell lines and found modest activity against several of them. Additionally, they looked to see if **2-5** inhibited LPS driven inflammatory signaling and showed that it did. Taken together, these two physiological activities, as well as its structural homology to **2-4**, a known direct binder of NF-κB indicated to us that pharbinilic acid (**2-5**) might be a binder and inhibitor of the NF-κB pathway.

Chapter 2.2 Synthesis and biological evaluation of pharbinilic acid (**2-5**)

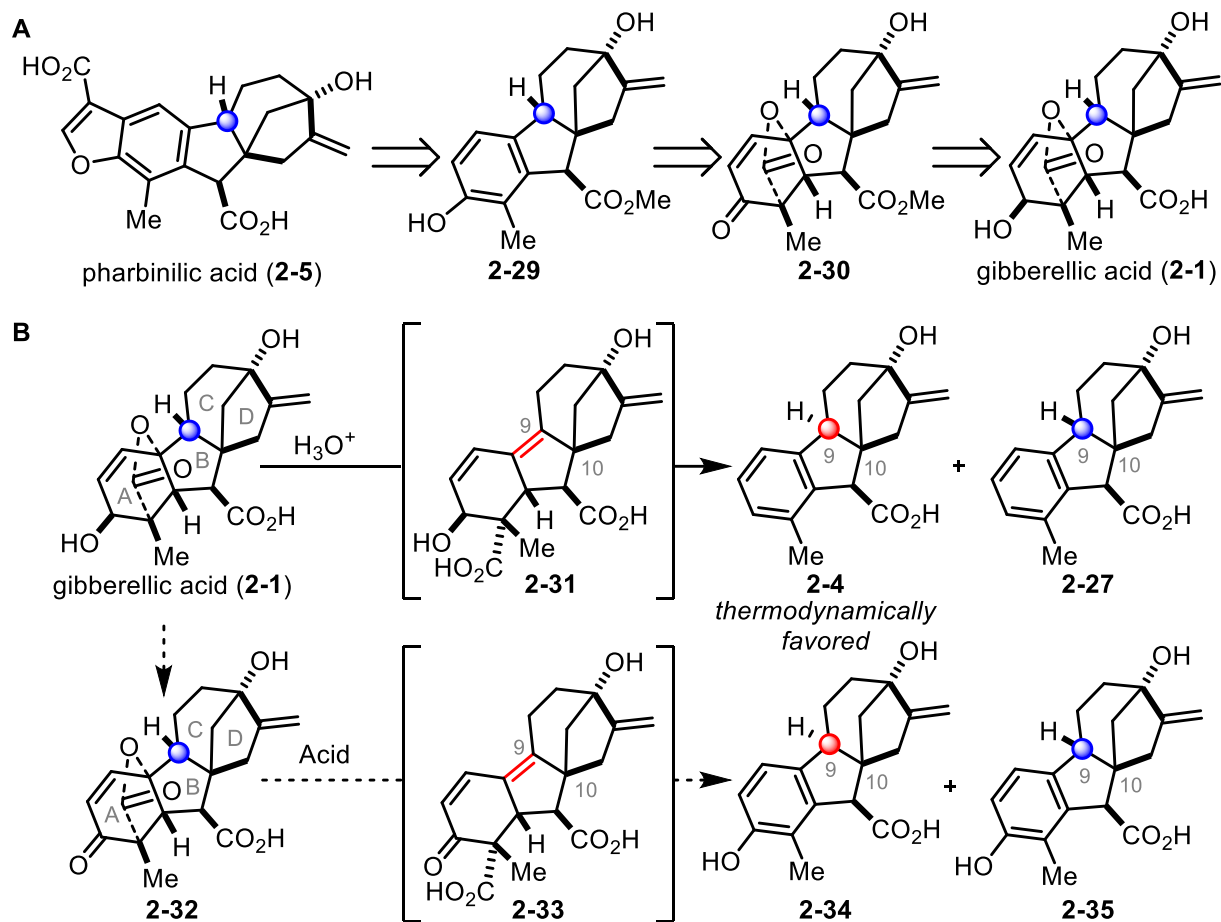


**Figure 2.9- A.** Retrosynthetic analysis of pharbinilic acid (**2-5**). **B.** Initial synthetic strategy.

In light of our interest in studying and inhibiting the NF- $\kappa$ B pathway and the limited global supply of pharbinilic acid (**2-5**) we chose to target pharbinilic acid (**2-5**) for synthesis and study (Figure 2.9A). We thought that if we could disconnect the furan ring of pharbinilic acid it would take us back to an aromatized intermediate **2-29**. Key precedent from Hergenrother and coworkers showed that gibberellic acid (**2-1**) could be treated with Bronstead acids at intermediately elevated temperatures which provide allogibberic acid (**2-4**) and *epi*-9H-allogibberic acid (**2-27**).<sup>15</sup> We hypothesized that if we first oxidized the A ring of **2-1** we could conduct a similar acid promoted aromatization decarboxylation sequence which would provide oxidized allogibberic acids **2-34** and **2-35**.

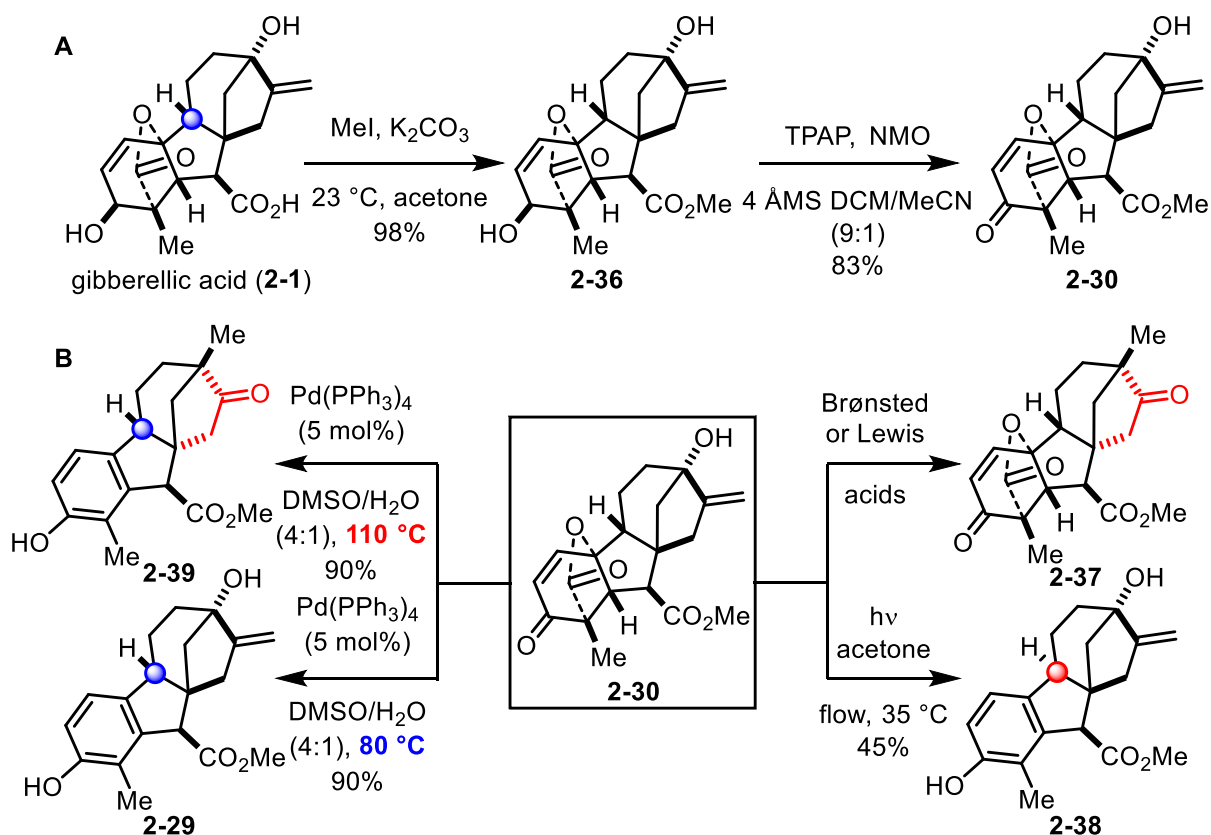


**Figure 2.10-** A. Synthesis of key intermediate **2-30**. B. Efforts towards promoting an aromatization of **2-30** to **2-29**.

For solubility and ease of purification we began our synthesis by methyl esterifying to **2-36**. Next we had to oxidize the A ring to enone **2-30** (Figure 2.10A). This was not a trivial transformation, significant side products were observed with IBX and activated DMSO based oxidations. Manganese dioxide provide poor and inconsistent yields of **2-30**. Dess-Martin periodinane worked well but the expense and risk of preparing the reagent on scale caused us to switch to a catalytic Griffith-Ley oxidation. Next we tried our key disconnections strategy. However, no matter which Lewis or Bronstead acid we tried we were unable to observe any aromatized product. Instead, we did occasionally observed C/D ring epimerization product **2-37**. We then turned to reactions reported without spectral information from the 1970s that suggested that oxidized gibberellins could be aromatized in low (3-15%) yields.<sup>46</sup> We were able to optimize this transformation in flow all the way to 45% yield however the product was the undesired H9-

epimer **2-38**. Next we reimagined this transformation using a transition metal catalyzed approach. We thought that palladium might undergo oxidative addition into the allylic A ring lactone. This intermediate would be unable to undergo a syn 1,2-beta-hydride elimination to form a gibberellenic acid like intermediate, perhaps avoiding a thermodynamic protonation that would lead to epimerization at H9. While our initial results yielded the desired aromatic A-ring and avoided H9 epimerization it proceeded with Wagner-Meerwein rearrangement of the C/D ring **2-39**. However, by reducing the temperature to 80 °C we were able to suppress this thermal rearrangement providing the desired intermediate **2-29**.

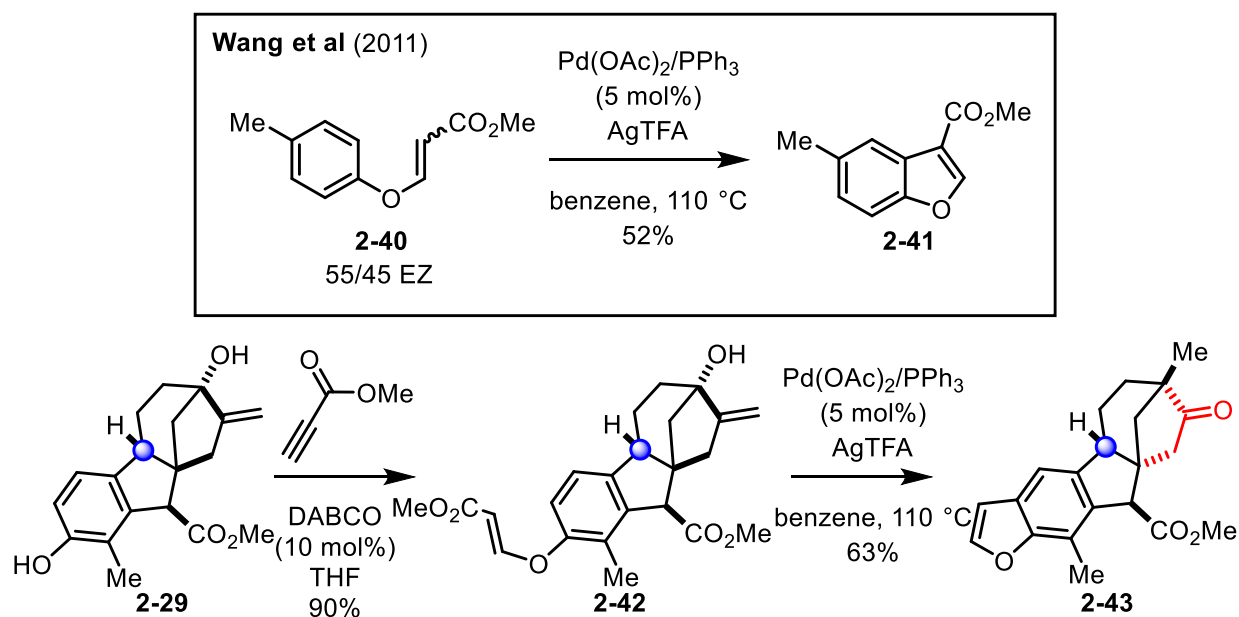


**Figure 2.11-** Key precedent by Wang and coworkers inspired and attempted oxidative coupling of **2-42**.

We had hoped to take advantage of recent precedent involving an oxidative Mizoroki-Heck coupling (Figure 2.11).<sup>47</sup> However when we constructed substrate **2-42** we found that not only did the reaction conditions epimerize the C/D ring but the furan ring closed with decarboxylation, perhaps upon hydrolysis of the methyl ester by advantageous water. Several solvents, silver sources and palladium conditions were evaluated and whenever the benzofuran

ring was closed it closed only with decarboxylation. Additionally, no conditions could be found that avoided the C/D ring epimerization.

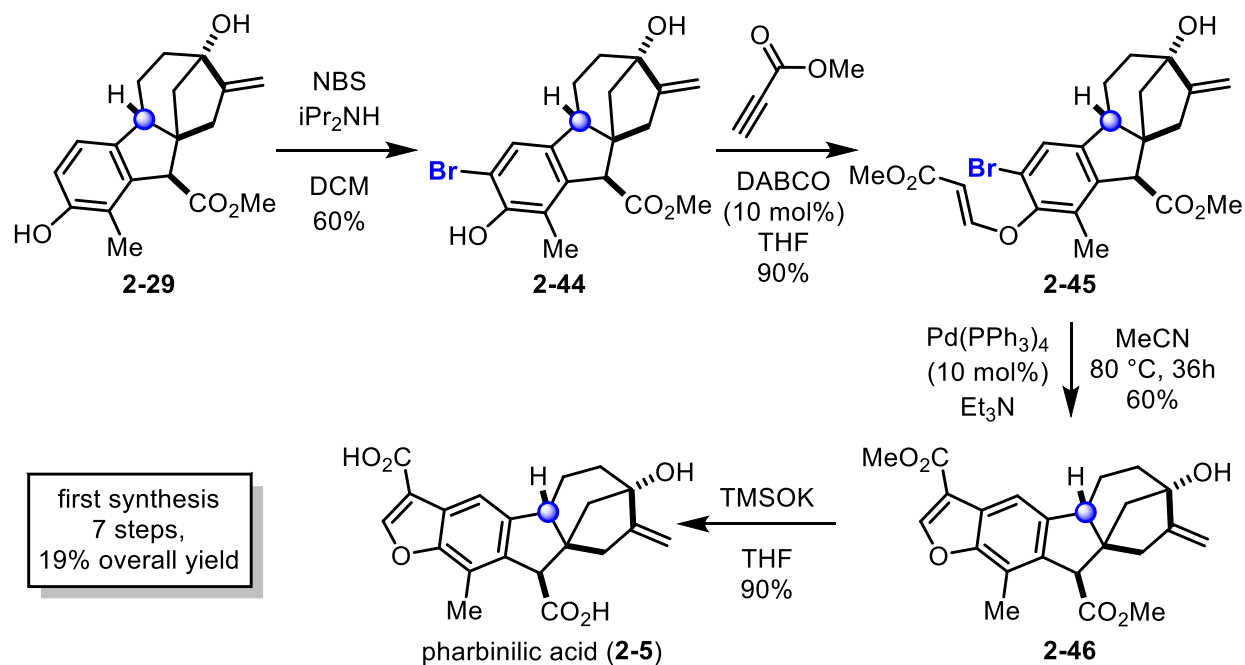


**Figure 2.12-** The completion of the total synthesis of pharbinilic acid (2-5).

This forced us to reevaluate our synthetic strategy (Figure 2.12). We had originally wanted to avoid pre-functionalizing the A ring phenol because we had feared that any electrophilic aromatic substitution would also rearrange the C/D ring. Fortunately, we found conditions that provided the desired bromo-phenol 2-44 as the major product, though the remaining mass balance was C/D ring epimerization and doubly brominated A ring phenol. Despite the challenging nature of what might be described as a 5-endo trig cyclization we were able to treat 2-45 under palladium catalyzed conditions that provided 2-46 in good yield. Finally, we were able to saponify bismethyl ester 2-46 with trimethoxysilane to provide pharbinilic acid (2-5) in 7 total steps and 19% overall yield.

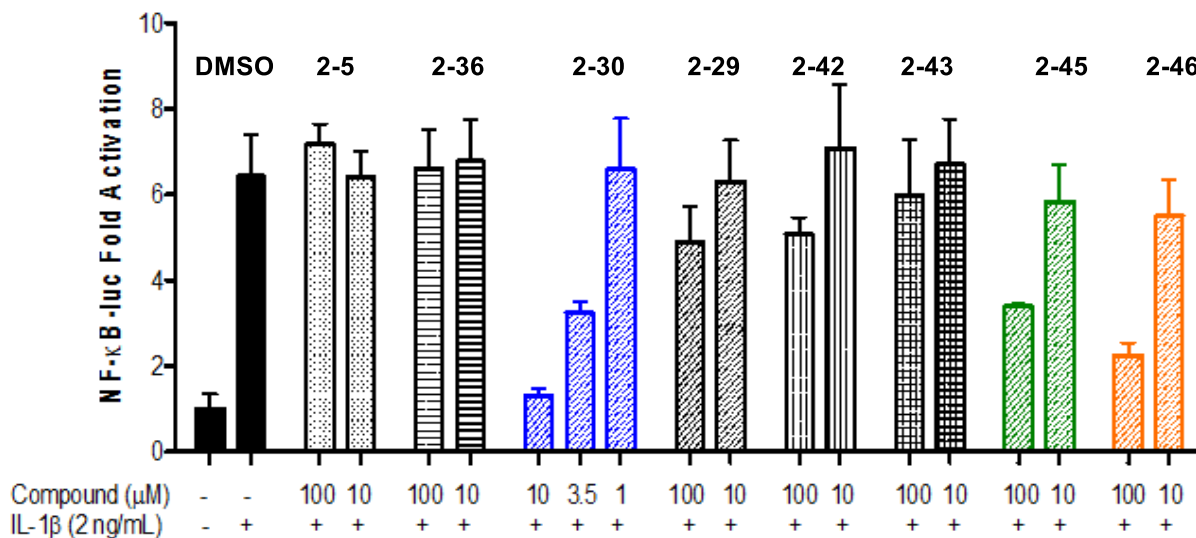


**Figure 2.13-** Initial biological evaluation of synthetic gibberellins as inhibitors of the NF-κB pathway as determined by a Luciferase reporter gene assay.

Owing to our interest in pharbinilic acid (**2-5**) as an NF-κB pathway inhibitor we decided to analyze our synthetic **2-5** and all synthetic gibberellins as NF-κB pathway inhibitors. To test this, we developed a Luciferase reporter gene assay in which HeLa cells were transiently transfected with a plasmid that contained a Luciferase gene driven by six NF-κB response elements (Figure 2.13). Though we observed no activity against the NF-κB pathway by **2-5**, perhaps due to poor cell permeability, the bismethyl ester **2-46** did exhibit some pathway inhibition, as did aryl bromide **2-45**. However, enone **2-30** showed remarkable activity against the pathway. We were, initially, nervous about **2-30** as it contained an enone which we thought might be a pan assay interfering compound (PAINS, see Chapter 1.2).<sup>48</sup> So we followed up on this reporter assay hit by looking at the ability of **2-30** to inhibit the transcription of NF-κB controlled genes. We were pleased to see by qT-PCR that enone **2-30** specifically inhibited the transcription of NF-κB controlled gene expression, specifically MIP3α.

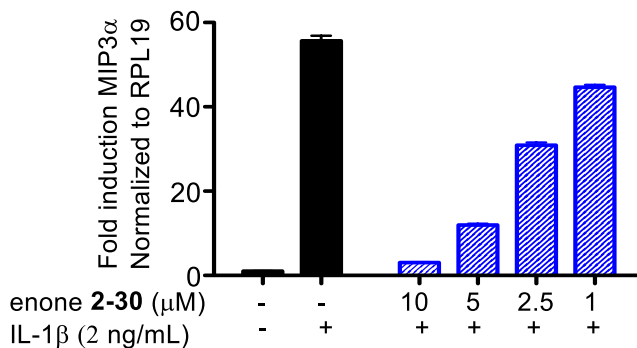


**Figure 2.14-** Quantitative PCR analysis of NF-κB controlled gene MIP3α shows that **2-30** inhibits NF-κB driven transcription.

We were pleased to publish our efforts towards the synthesis of pharbinilic acid (**2-5**) as well as our initial biological evaluations and discovery of a new NF-κB pathway inhibitor **2-30** in 2015.<sup>49</sup> Since the time of publication we have been studying the mechanism of action of enone **2-30** and related synthetic gibberellins, details of which are to follow.

## Chapter 2.3 Evaluation of gibberellins as NF-κB pathway inhibitors

### Chapter 2.3.1 Structure Activity Relationship (SAR) studies—synthesis and NF-κB pathway inhibition

Excited by the initial results around enone **2-30**, we were first interested in what structural elements are key to the activity of **2-30**. In order to better accommodate the throughput of identifying the inhibition against the NF-κB pathway we switched from our initial assay design of transiently transfected HeLa cells stimulated by IL-1β to stably transfected HEK-293T cells stimulated by TNFα. Additionally these experiments were conducted at the Koch Integrative Cancer Research Institute at MIT. First, we thought that an easy point of differentiation would be the B ring carboxylic acid, so we esterified or formed a peptide bond with a small collection of alcohols and amines (Figure 2.15). We found that none of these coupled molecules were active but just like **2-36** is inactive and **2-30** is we thought that by



oxidizing the A ring alcohol to an electrophilic enone we might recover the activity. Though that was true we observed less activity in all cases than with the methyl ester and also less selectivity as observed by some level of toxicity at concentrations about 50  $\mu\text{M}$ . An important set of molecules are terminal alkynes **2-53-56** as these will allow for further biotinylation and analysis by pulldown studies (*vide infra*).

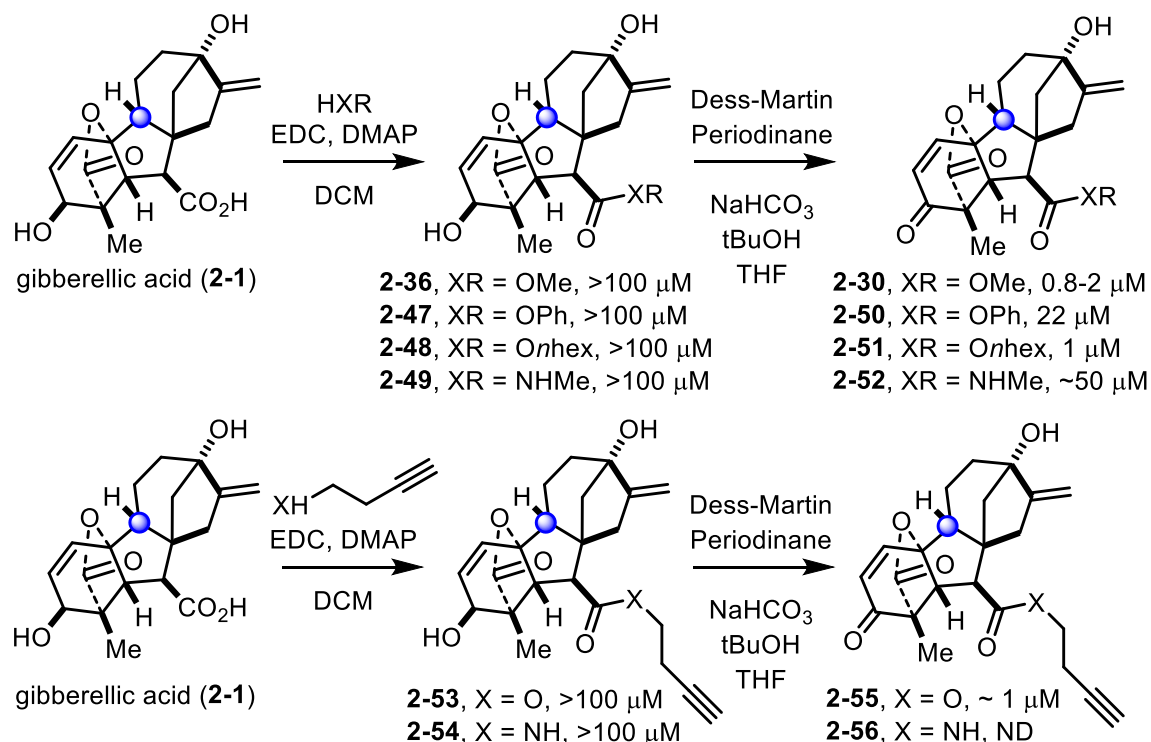


**Figure 2.15-** SAR studies around functionalizing the B ring carboxylic acid.  $\text{IC}_{50}$  against TNF $\alpha$  stimulated HEK293T cells stably transfected with an NF- $\kappa$ B driven luciferase gene.

Our next area of SAR exploration took advantage of our ability to very selectively form 9 $\beta$ -H aromatic gibberellins. This was especially true in light of the work of Koehler and coworkers who indicated that allogibberellic acid would be a good binder and inhibitor of the NF- $\kappa$ B pathway. In our initial studies on IL-1 $\beta$  stimulated transiently transfected HeLa cells we observed no pathway inhibition by 9 $\alpha$ -H allogibberellic acid (**2-4**). We thought there might be something about the difference between the two assays and that the commercial allogibberic acid used by Koehler and coworkers may have been contaminated by 9 $\beta$ -H allogibberellic acid (**2-27**).

We found that by triflating and proto-demetallating **2-29** we could form 9 $\beta$ -H allogibberellins and directly compare their activities to the more readily accessible 9 $\alpha$ -H allogibberellins.

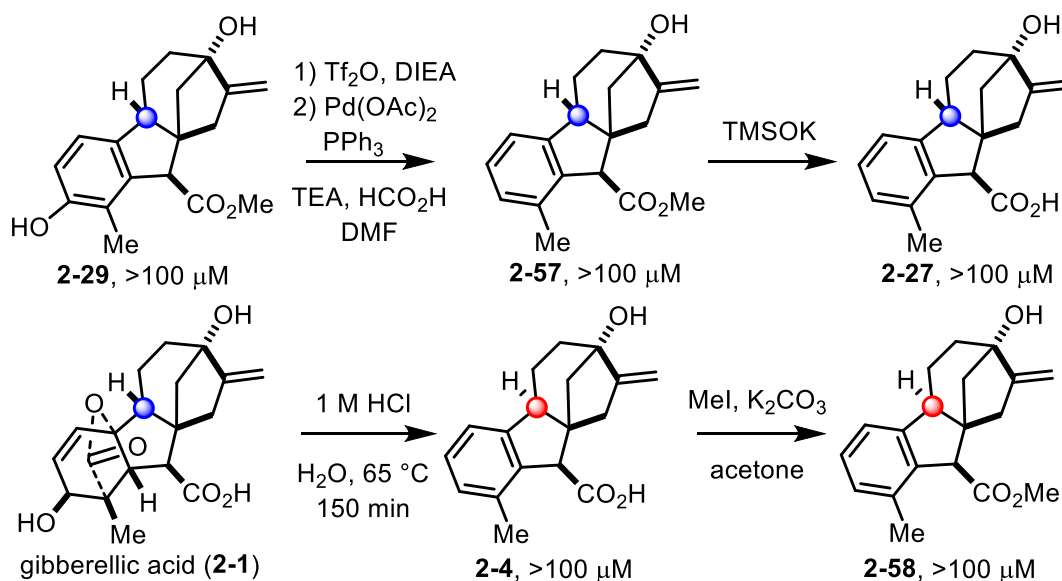


**Figure 2.16-** SAR studies around the H9 epimeric state in allogibberellins.  $\text{IC}_{50}$  against TNF $\alpha$  stimulated HEK293T cells stably transfected with an NF- $\kappa$ B driven luciferase gene.

Another possibility and opportunity with regards to studying the NF- $\kappa$ B pathway inhibition is that the C/D ring epimer of the gibberellins might possess unique activities. While non-electrophilic allogibberellins, regardless of H9 epimerism, **2-59-62**, were not found to be active, the 9 $\beta$ -H epimer was found to be active when it bears a C/D ring Michael acceptor (Figure 2.17).

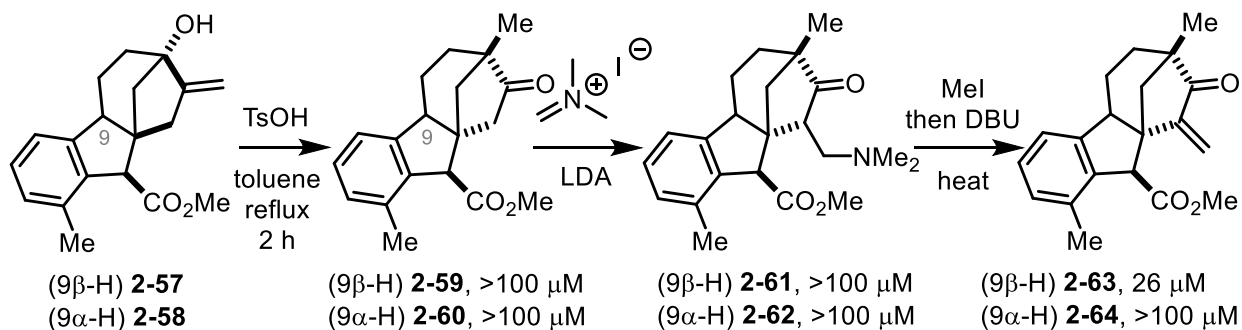


**Figure 2.17-** SAR studies around the H9 epimeric state in C/D ring epimerized allogibberellins.  $\text{IC}_{50}$  against TNF $\alpha$  stimulated HEK293T cells stably transfected with an NF- $\kappa$ B driven luciferase gene.

With the indication that a C/D ring enone might provide activity in our NF- $\kappa$ B luciferase assay we also constructed the unpimerized C/D ring allogibberellins (Figure 2.18). Riley oxidations could provide epimeric alcohols one of which would cyclize to form a new lactone the other of which we could oxidize to a new C/D ring enone which we found to be active in our pathway though the 9 $\beta$ -H epimer was found to be more active.

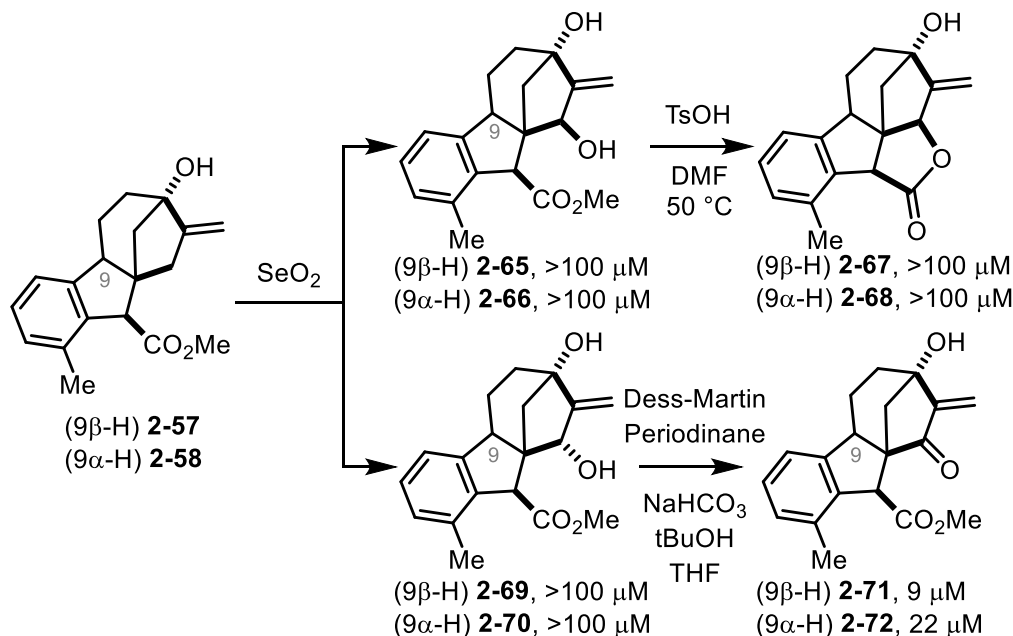


**Figure 2.18-** SAR studies around the H9 epimeric state in native C/D ring allogibberellins. IC<sub>50</sub> against TNF $\alpha$  stimulated HEK293T cells stably transfected with an NF- $\kappa$ B driven luciferase gene.

Excited about this potential we constructed C/D ring enones from phenol **2-29** as well as **2-30** (Figure 2.19). Of particular interest was the difference in activities between **2-76** and **2-30**. Though possessing nearly identical structural features to each other **2-76** was found to be less active perhaps because the C/D ring enone is more reactive and less selective functionally lowering the cellular concentration of **2-76**. This is also interesting in contrast to the biological activities reported of GA-13315 (**2-28**) which also possesses both an endocyclic A ring enone and an exocyclic C/D ring enone and is shown to be quite active against cancer both in cultured cells and in xenografts.

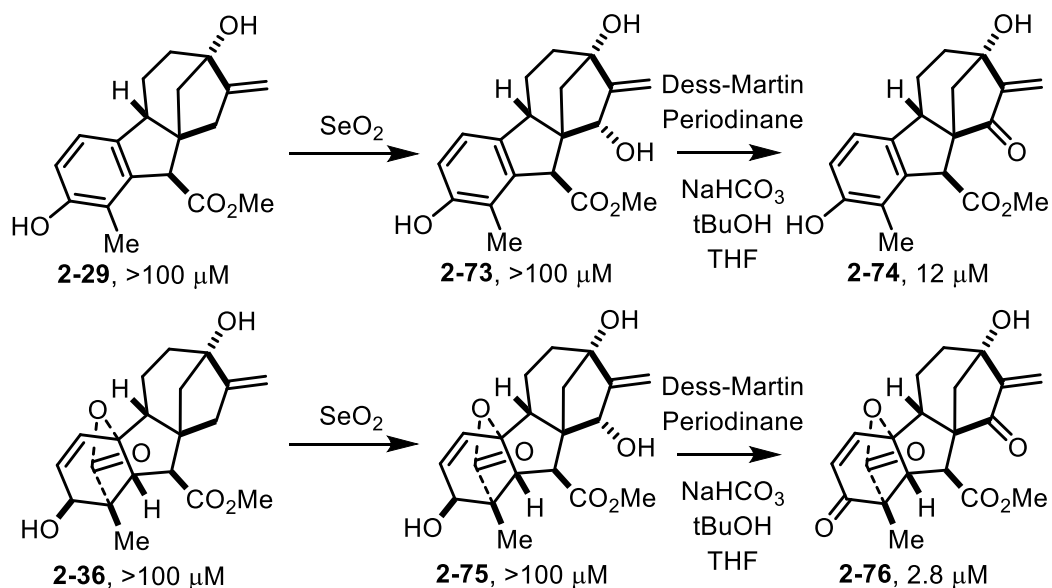


**Figure 2.19-** SAR studies around the native C/D ring enones.  $\text{IC}_{50}$  against  $\text{TNF}\alpha$  stimulated HEK293T cells stably transfected with an NF- $\kappa\text{B}$  driven luciferase gene.

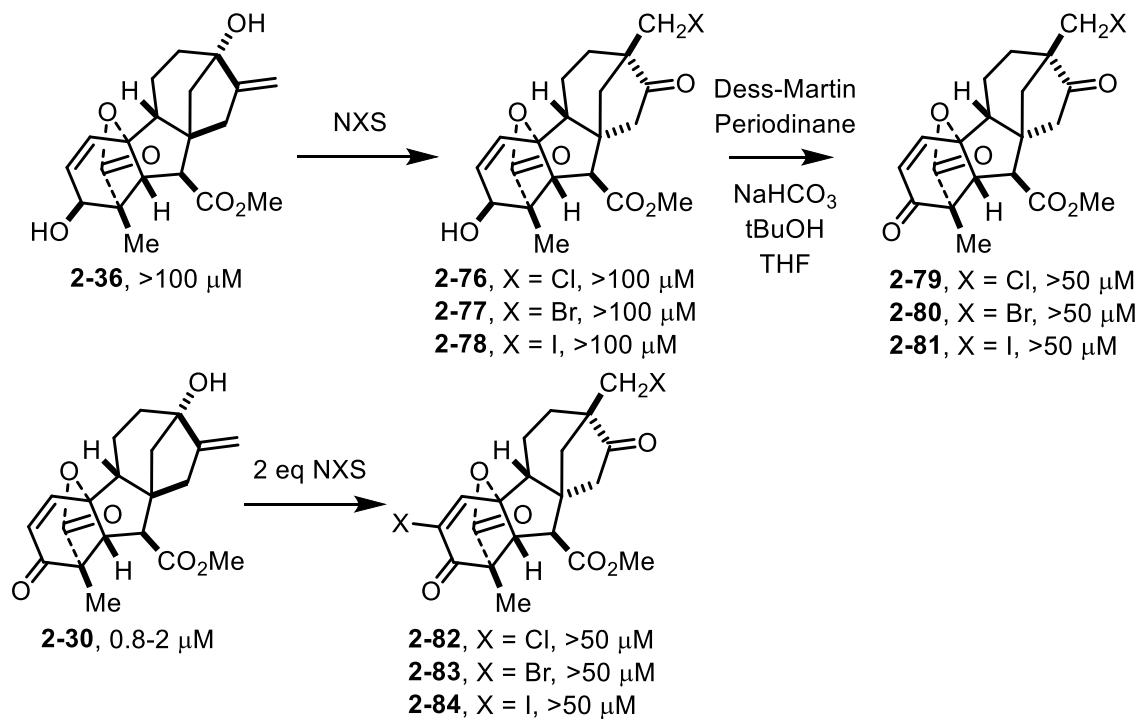
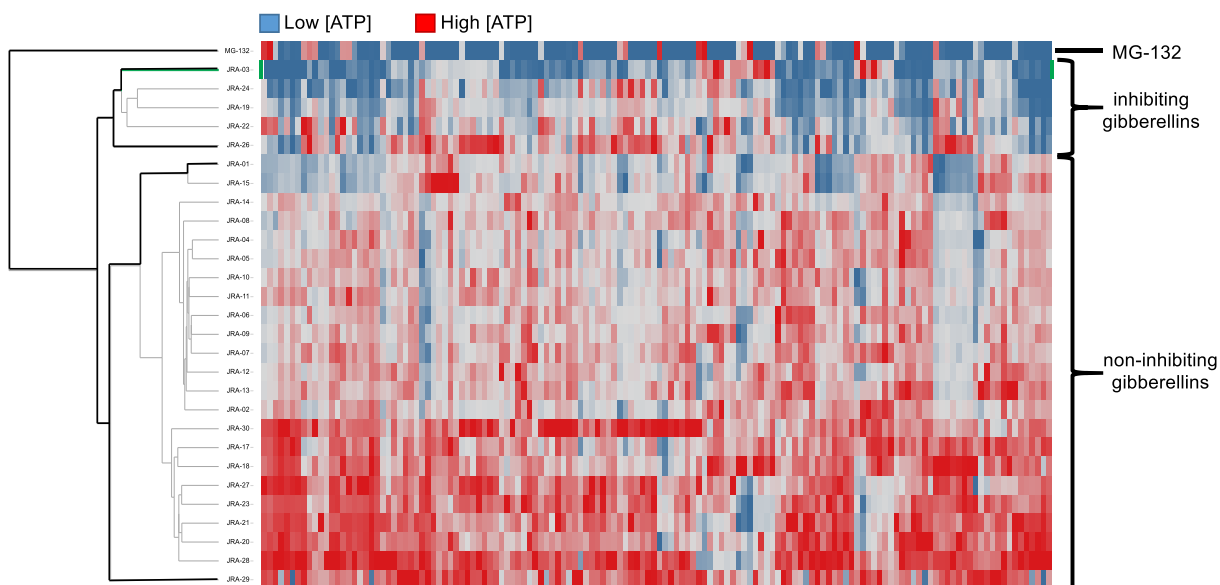


**Figure 2.20-** SAR studies around epimerizing the C/D ring juncture with halogen electrophiles.  $\text{IC}_{50}$  against  $\text{TNF}\alpha$  stimulated HEK293T cells stably transfected with an NF- $\kappa\text{B}$  driven luciferase gene.

Epimerization of the C/D ring juncture using electrophilic halogenating reagents can provide unique gibberellins with and without an A ring enone (Figure 2.20). It seems that C/D ring epimerization in this manner did not provide for a more active analog to **2-30**.

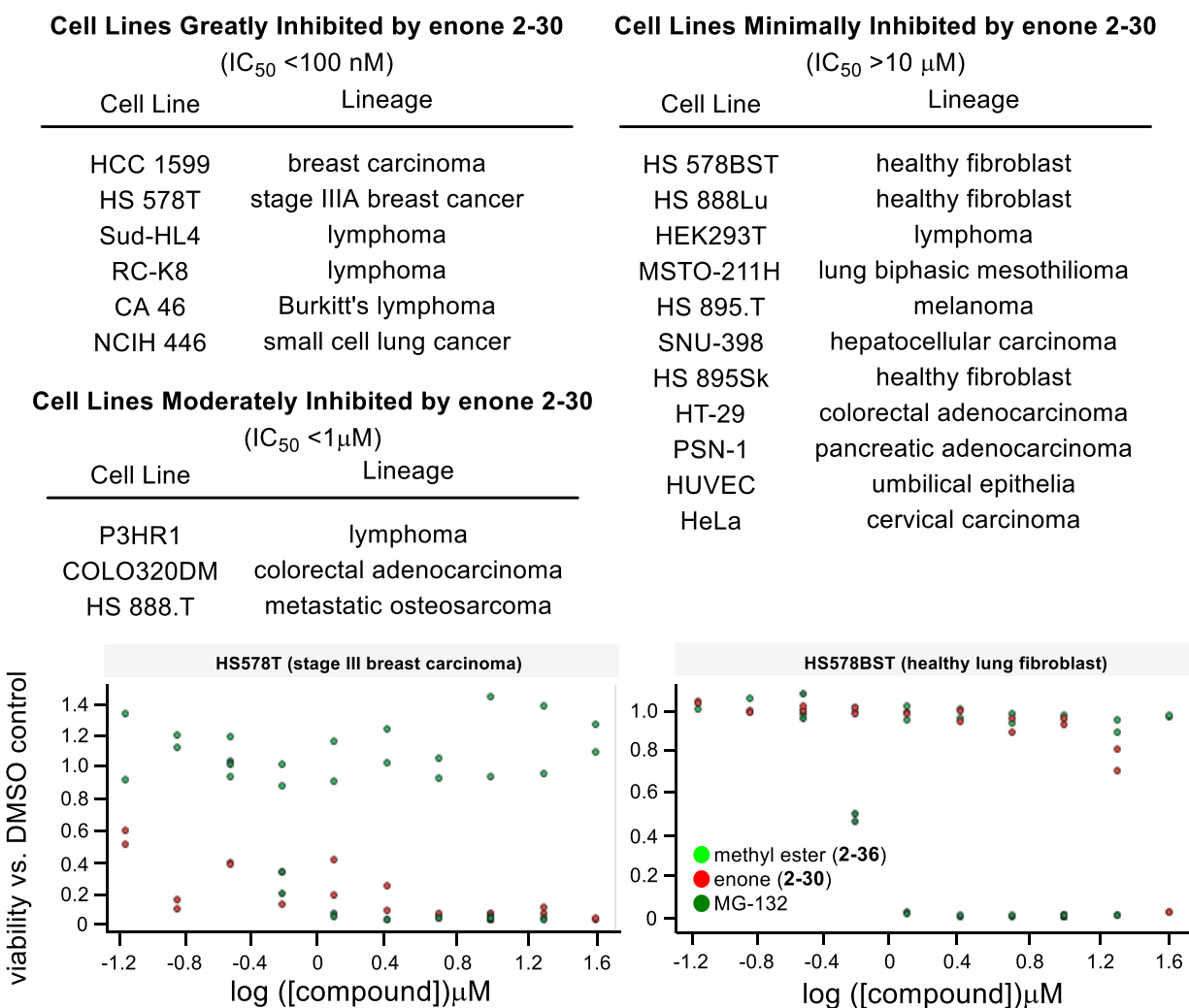
### Chapter 2.3.2 Structure Activity Relationship (SAR) studies—HTS Cell Titre Glo

After assessing whether or not our synthetic gibberellins were inhibitors of the NF- $\kappa$ B pathway. We were interested in whether pathway inhibition would have any therapeutic relevance, so we conducted a high throughput screen (HTS) Cell Titre Glo cell viability in a wide variety of cancer and non-cancer derived cell lines. 28 different cell lines were assayed against full dilution curves of 29 different synthetic gibberellins, duplicate curves per plate, duplicate plates per day, duplicate days. A hierarchical clustering of all of the data against the assay positive control, MG-132, showed a clustering of all NF- $\kappa$ B inhibiting gibberellins both with each other and with the positive control (Figure 2.21).



**Figure 2.21-** Hierarchical clustering of HTS Cell Titre Glo cell viability assays cluster NF- $\kappa$ B inhibiting gibberellins and the positive control MG-132.

Analysis of individual results show that gibberellins that possess a C/D ring enone are typically cytotoxic against all assayed cell lines. Interestingly, enone **2-30** was quite specific with thousand fold selectivity for cells derived from a stage III breast carcinoma against healthy fibroblast derived cells (Figure 2.22). In fact, enone **2-30** was found to be quite toxic to a wide variety of inflammatory cancer derived cell line but was not generally toxic to non-cancer derived cells and some non-inflammatory cancer derived cell lines. These results provoked our interest in the molecular mechanism of action (MoA) of enone **2-30** in cells.

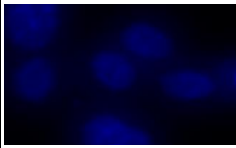
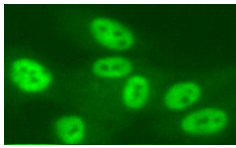
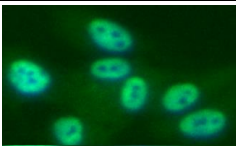
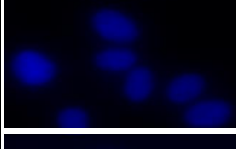
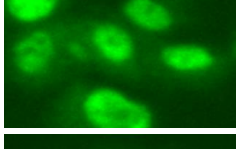
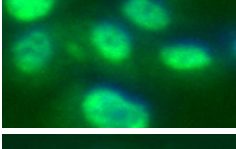
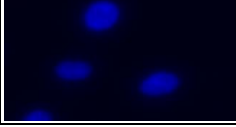
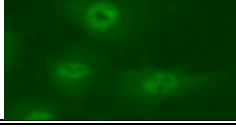
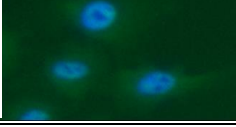


**Figure 2.22-** Enone **2-30** selectively kills cell lines derived from inflammatory cancers or lymphoma as determined by a HTS Cell Titre Glo cell viability assay. It is, however, inactive against non-cancer derived cell lines as well as non-inflammatory cell lines.

### Chapter 2.3.3 NF- $\kappa$ B nuclear translocation studies—highlighting a potential MoA

As describe in chapter 1 the NF- $\kappa$ B pathway is tightly regulated by controlling the cellular compartmentalization of transcriptionally active NF- $\kappa$ B. In particular the pathway is characterized by the phosphorylation, ubiquitinylation, and proteolytic degradation of an inhibitory complex (I $\kappa$ B) that keeps transcriptionally active NF- $\kappa$ B subunits locked in the cytoplasm. Upon degradation a nuclear localization signal on transcriptionally active NF- $\kappa$ B is revealed and the proteins are actively transported to the nucleus where they can then bind DNA and control for the expression of target genes. Thus, identifying whether NF- $\kappa$ B family members are being nuclearly translocated can help identify if a pathway inhibitor is acting upstream of I $\kappa$ B phosphorylation or downstream.

We first used an immunohistochemical staining approach to look for the location of RelA in HUVEC cells by fluorescent microscopy (Figure 2.23). As a negative control we used **2-36**, which, though bearing nearly complete structural homology to active inhibitor **2-30**, does not inhibit the NF- $\kappa$ B pathway. We did not have a small molecule that inhibited nuclear translocation of RelA but in the absence of stimulation by TNF $\alpha$ , NF- $\kappa$ B is not translocated into the nucleus and thus serves as a serviceable positive control. In this assay we see that enone **2-30** does not significantly inhibit the nuclear translocation of RelA at 10  $\mu$ M, a concentration  $\sim$ 10x the IC<sub>50</sub> in a luciferase assay.

compound	IC <sub>50</sub> (μM)	Hoechst	αRelA-AF488	merged
<b>2-36</b>	>100			
<b>2-30</b>	0.8-2.0			
uninduced (positive control)	-			

**Figure 2.23-** Immunohistochemical staining of HUVEC cells. Cells in treatment rows were induced with TNF $\alpha$ . Compounds were dosed at 10  $\mu$ M.

However, these initial histochemistry experiments, conducted at the Koch Cancer Research Institute at MIT, were valuable for informing initial hypotheses they did not provide complete information. In particular, fluorescent microscopy provides a top down look at cells and it can be difficult to see if a protein is actually within the nucleus or if it is instead outside the nucleus at the nuclear membrane. Confocal microscopy would give a more compelling look at compartmentalization. Additionally, these initial experiments only looked at RelA when two additionally transcriptionally active NF- $\kappa$ B subunits exist, namely RelB and c-Rel. It would still be possible that our molecules were acting by preventing the translocation of one of these other subunits.

To address these concerns, we conducted additional microscopy experiments (Figure 2.24). This time we looked at all three transcriptionally active subunits by confocal microscopy. These imaging experiments, conducted in the Molecular Imaging Laboratory in the Biomedical Science Research Building at the University of Michigan, were conducted on Hek-293T cells in the absence or presence of stimulation by IL-1 $\beta$ . Again, we used **2-36** as a negative control at 50  $\mu$ M, along with DMSO as a vehicle control. Once again, we observed no inhibition of



translocation in any of the three transcriptionally active NF- $\kappa$ B subunits in the presence of 10  $\mu$ M **2-30**.

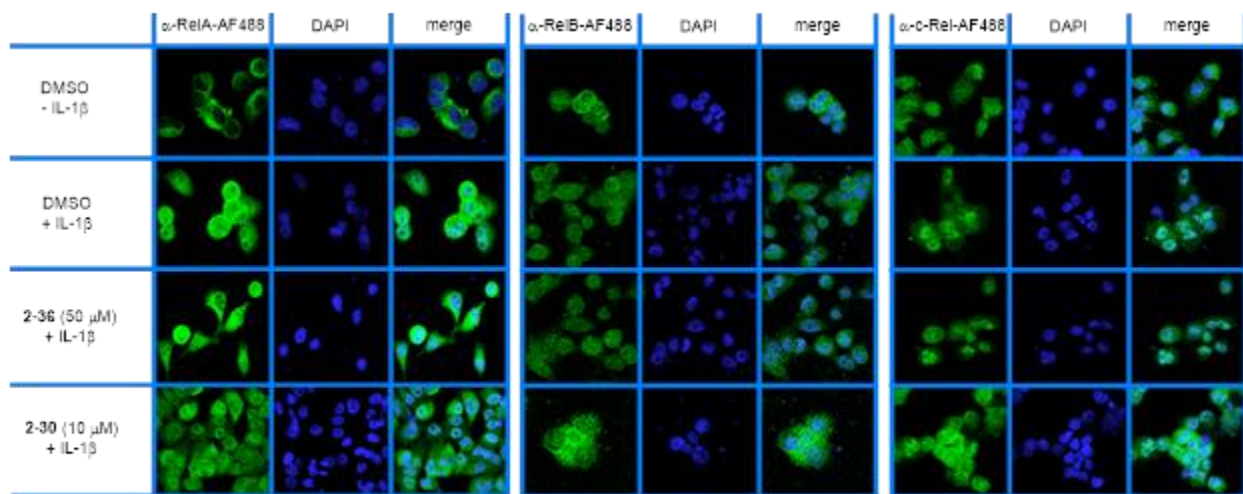


**Figure 2.24-** Immunohistochemical staining and confocal microscopy of Hek-293T cells upon treatment with DMSO, **2-36**, or **2-30** in the presence or absence of induction by IL-1 $\beta$ .

In the course of these experiments we also looked at the fate of the kinases that are responsible for phosphorylating I $\kappa$ B and activating transcriptionally active NF- $\kappa$ B for translocation, namely IKK $\alpha$  and IKK $\beta$  (Figure 2.25). If I'm being honest, we included these images in our experimental plan because we expected that they would stay in the cytoplasm and provide us with a nice assay control. We were surprised, however, to see that upon inducing NF- $\kappa$ B pathway activity with IL-1 $\beta$ , we found that both IKK $\alpha$  and IKK $\beta$ . We later did our job and looked in the literature for reports of IKK activity in the nucleus and saw a limited series of articles that demonstrated a nuclear role of IKKs phosphorylating and deactivating NF- $\kappa$ B inhibitory complexes (for details see chapter 1.1.2). This was of particular interest when we noticed that our active NF- $\kappa$ B pathway inhibitor, enone **2-30**, did inhibit the nuclear translocation of IKK $\alpha$  and IKK $\beta$ . This suggested perhaps a novel MoA for our small molecule inhibitors.

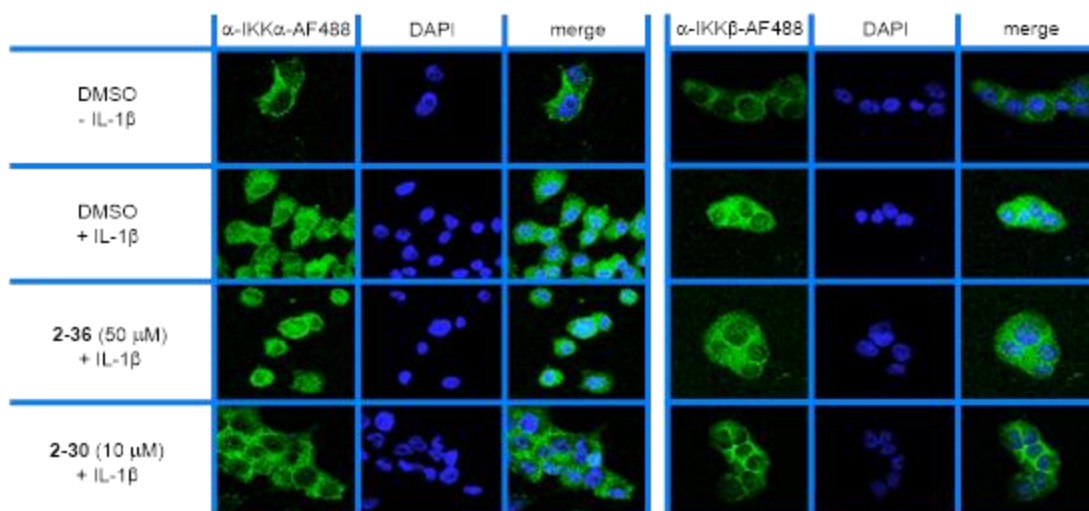
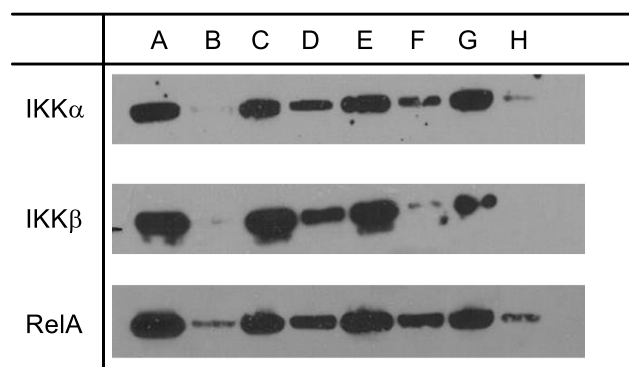


**Figure 2.25-** Immunohistochemical staining and confocal microscopy of Hek-293T in the presence or absence of NF- $\kappa$ B pathway induction by IL-1 $\beta$ .

These images are all snapshots, to take a population level look at the nuclear translocation of NF- $\kappa$ B pathway components we fractionated the nuclear and cytosolic fractions of Hek-293T cells and analyzed them for NF- $\kappa$ B pathway members by Western blotting (Figure 2.26). This analysis confirmed the results suggested by the microscopy. Enone **2-30**, even at 10x its IC<sub>50</sub>, did not significantly inhibit the translocation of transcriptionally active NF- $\kappa$ B subunits. Instead it prevented the nuclear translocation of the IKK kinases. These results prompted us to conduct pulldown experiments to attempt to identify the cellular target of enone **2-30**.



conditions: A- Cytosol, DMSO, -IL-1 $\beta$   
 B- Nucleus, DMSO, -IL-1 $\beta$   
 C- Cytosol, DMSO, +IL-1 $\beta$   
 D- Nucleus, DMSO, +IL-1 $\beta$   
 E- Cytosol, 15  $\mu$ M GAmE (**2-36**), +IL-1 $\beta$   
 F- Nucleus, 15  $\mu$ M GAmE (**2-36**), +IL-1 $\beta$   
 G- Cytosol, 15  $\mu$ M kGAmE (**2-30**), +IL-1 $\beta$   
 H- Nucleus, 15  $\mu$ M kGAmE (**2-30**), +IL-1 $\beta$

**Figure 2.26-** Hek-293T cells in the absence or presence of induction by IL-1 $\beta$  and the absence or presence of treatment with **2-36** or **2-30** were fractioned and analyzed by Western blotting for the presence of pathway members.

#### Chapter 2.3.4 Pulldown studies and proteomics

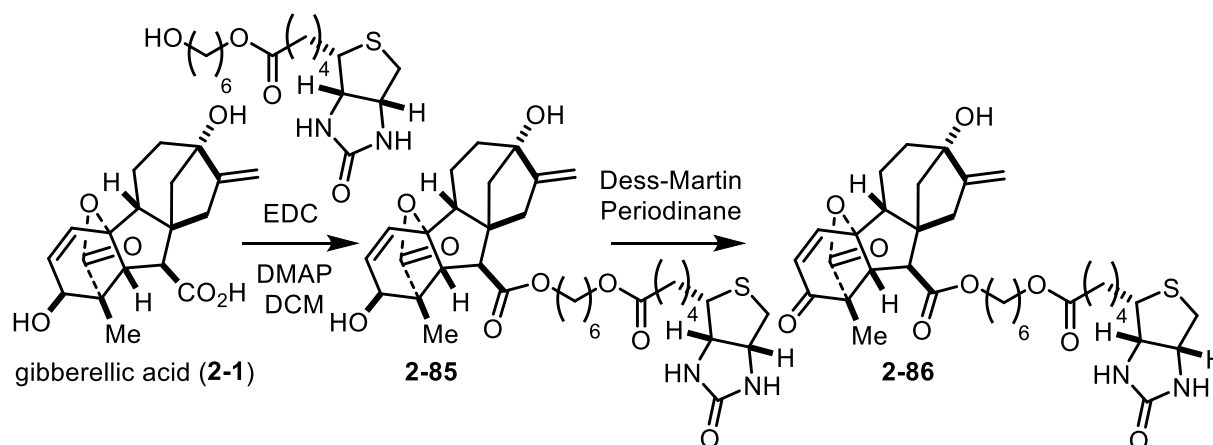


**Figure 2.27-** Synthesis of the first generation of pulldown probe molecules.

We first envisioned conducting pulldown experiments with biotinylated compounds **2-85**, which we expect would not bind the target and **2-86** which we had hoped would (Figure 2.27). When we ran the pulldowns with 5 and 1  $\mu$ M of **2-85** and **2-86** we first looked for total protein (Figure 2.28). We observed, as expected, no significant protein in the lanes with **2-85** but were

somewhat surprised to see such an unclean profile with **2-86** though it was somewhat promising to see relatively few protein bands at 1  $\mu$ M.

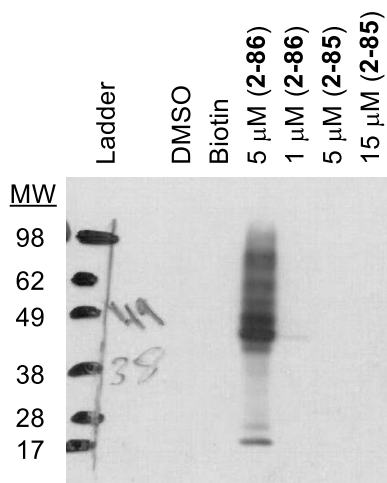


**Figure 2.28-** Silver stained protein gel of Hek-293T Nutravadin pulldowns using biotinylated analogs of **2-36** and **2-30**.

When we took our Nutravadin pulldown and analyzed it by Western blotting we were able to observe RelA, RelB, cRel, IKK $\alpha$ , and IKK $\beta$  (Figure 2.29). We did not observe p50 or p52. These pulldowns were conducted with relatively low concentration of salt in the wash steps. So it's possible that we are merely pulling down the NF- $\kappa$ B family members as a part of a larger complex. The silver staining is relatively unclean, so it is also possible that we are tagging every protein present in sufficient concentrations with a nucleophilic cysteine. This seems unlikely for **2-30**, as it is incredibly selective in the HTS viability screen, but we did see an increase in activity and selectivity when we changed the B ring ester identity.

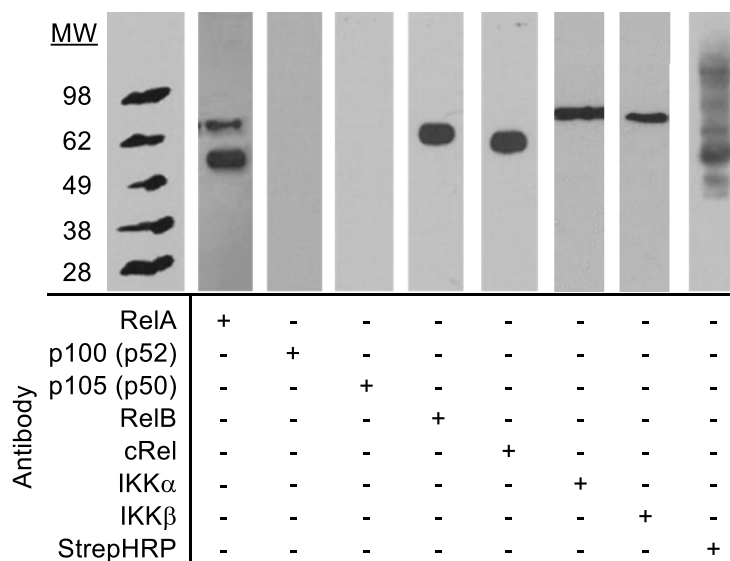


**Figure 2.29-** Western blotting of Hek-293T cells pulled down with 5  $\mu$ M **2-86**.

Taken together these data suggested we needed to employ an alternative strategy in which 1) we use more stringent wash conditions to be sure of target identity and 2) we conduct a competition experiment by pretreating cells with **2-30** before adding **2-86**, the loss of signal when compared to treatment with **2-86** alone would provide insight into selectivity. Finally, we wanted to conduct our pulldown experiments in a relatively unbiased manner, so we thought that a proteomic analysis would provide the most accurate and fruitful means of acquiring target ID.

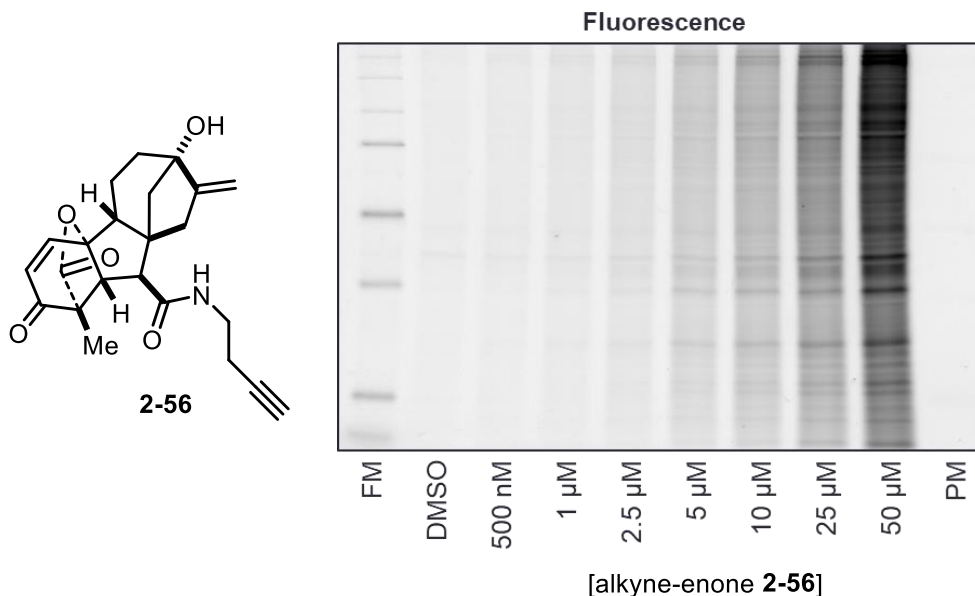


**Figure 2.30-** Treatment of Hek-293T cell lysates with alkyne **2-56** followed by clicking onto a fluorescent azide and running on a gel.

So we switched to a probe that did not contain a labile ester allowing for more stringent washing conditions, 6M urea. First, we checked to look for an appropriate concentration to use our probe at (Figure 2.30). We determined that 1  $\mu\text{M}$  **2-56** would be the optimal concentration. The fluorescent profile indicated to us that **2-56** was not selective so when conducted our pulldown experiments, we did so with or without pretreatment with **2-30** and we analyzed for the presence of members of the NF- $\kappa\text{B}$  pathway. The analysis was conducted by Dr. Kyle Cole in the Weerapana lab and the experiment was conducted by stable isotopic labeling of amino acids in cell culture (SILAC) mass spec proteomics (Figure 2.31). These results showed no specific activity against RelA, RelB, cRel, p50, or p52. Unfortunately, the total counts for IKK $\alpha$  and IKK $\beta$  were low and there was significant error at the low end of the spectra. That being said, IKK $\alpha$  was significantly competed away by pretreatment with IKK $\alpha$ . This supports the hypothesis that inhibition of nuclear translocation of IKK $\alpha$  is a result of direct, specific covalent binding.

### Initial Mass Spec Proteomics: NFkB

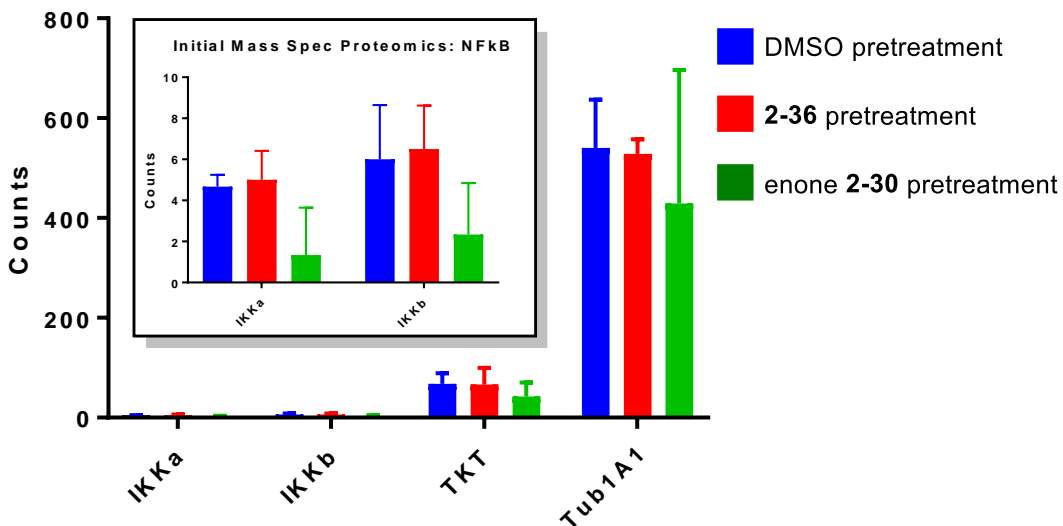


**Figure 2.31-** Results of SILAC mass spectrometry competition pulldown experiments in which Hek-293T are pretreated with 10  $\mu$ M of a synthetic gibberellin, or DMSO, before being pulled down with **2-56**.

One additional advantage of a mass spec proteomic approach like this is that it is unbiased allowing us to analyze other potential targets. To do so we looked for proteins that were successfully competed away in 2 different triplicate pulldowns (Figure 2.32). This analysis highlighted relatively few potential targets for **2-30**. Arguably the most interesting of which were the members of TCP-1 Ring Complex (TRiC) a chaperonin<sup>50</sup> most well characterized for folding actin and tubulin<sup>51</sup> but which has also been shown to fold the pro-leukemia oncogenic fusion protein AML1-ETO<sup>52</sup>. We did attempt to validate TRiC as a target and looked to see if enone **2-30** inhibited the folding and assembly of actin filaments, in collaboration with the Verhey lab at the University of Michigan, however we were unable to observe any inhibition of tubule or filament assembly in Hek-293T or HS578T cells.

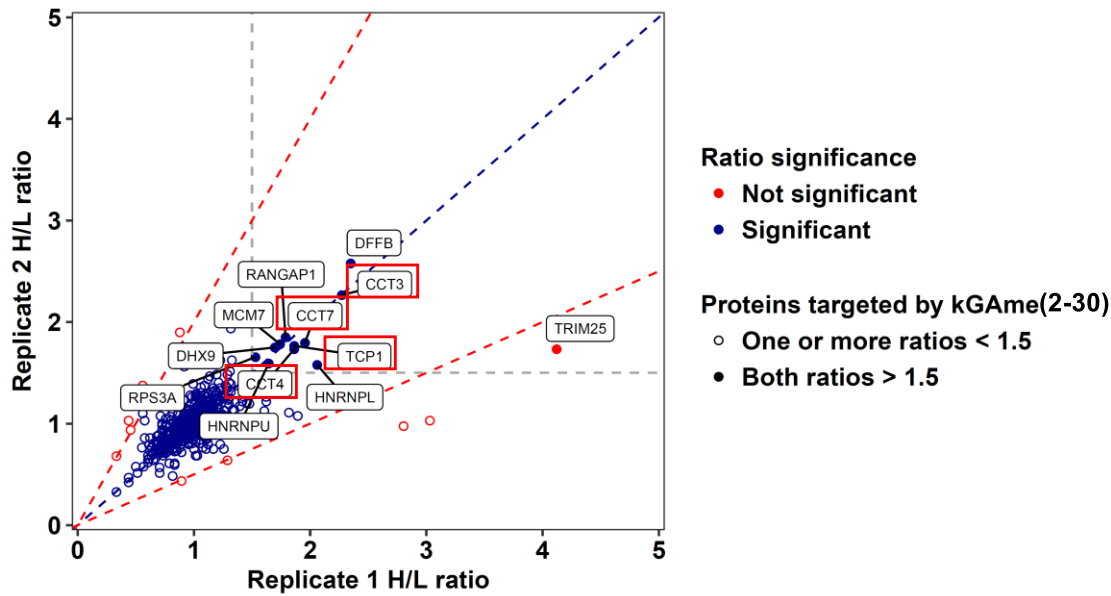


**Figure 2.32-** Results of SILAC mass spectrometry competition pulldown experiments in which Hek-293T are pretreated with 10  $\mu$ M of **2-30**, or DMSO, before being pulled down with **2-56**. Proteins highlighted in red are members of the TRiC chaperonin.

#### Chapter 2.4 Conclusions and mechanistic hypothesis

In light of these data we can see trends in the activity of enone **2-30**. It 1) inhibits the NF- $\kappa$ B pathway  $IC_{50} = 0.8 - 2 \mu$ M, 2) is cytotoxic towards many inflammatory cell lines, particularly lymphoma and breast cancers  $IC_{50} < 100$  nM, 3) Directly and specifically binds  $IKK\alpha$ , may specifically bind  $IKK\beta$ , 4) does not inhibit the activity of  $IKK\alpha$  and  $IKK\beta$ , as RelA, RelB, and c-Rel are still translocated to the nucleus, and 5) inhibits the nuclear translocation of  $IKK\alpha$  and  $IKK\beta$ . As  $IKK\alpha$  and  $IKK\beta$ , upon translocation to the nucleus, help activate intentionally silenced genes, we have created a unifying hypothesis for the mechanism of action of **2-30** (Figure 2.33). We believe that by preventing the nuclear translocation of  $IKK\alpha$  we are preventing the activity of the NF- $\kappa$ B pathway, decreasing the transcription of pro-survival proteins and ultimately leading to apoptosis in cancer derived cell lines.



## Bibliography Chapter 2

1. Konishi, T. A.; Nogyo-yowa, Part I., Subsection Nawashiro, Section Kome, Edo (Tokyo) Publisher unknown (1828). Reprinted in Takimoto, S.; Nippon Keizai Taiten, **1929**, 29, 549.
2. Kurosawa, E. *Trans. Natl. Hist. Soc. Formosa* **1926**, 16, 213.
3. Yabuta, T.; and Sumiki, Y. *J. Agr. Chem. Soc. Japan* **1938**, 14, 1526.
4. (a) Borrow, A.; Brian, P. W.; Chester, V. E.; Curtis, P. J.; Hemming, H. G.; Henehan, C.; Jeffreys, E. G.; Lloyd, P. B.; Nixon, I. S.; Norris, G. L. F.; Radley, M. *J. Sci. Food Agr.* **1955**, 6, 340. (b) Mitchell, J. E.; Angel, C. R. *Phytopathology*, **1950**, 40, 872.
5. Grove, J. F. *Q. Rev.* **1961**, 15, 56.
6. Hedden, P.; Thomas S. G. *Biochem. J.* **2012**, 444, 11.
7. Toyomasu, T.; Sassa, T. *Diterpenes in Comprehensive Natural Products II. Chemistry and Biology*. Mander, L.; Liu, H.-W., Eds.; Newnes: 2010; Vol. 1.
8. Dewick, P.M. *Medicinal Natural Products. A Biosynthetic Approach*; Wiley, 2008.
9. Hedden, P. *Physiol. Plant.* **1997**, 101, 709.
10. (a) Corey, E. J.; Danheiser, R. L.; Chandrasekaran, S.; Siret, P.; Keck, G. E.; Gras, J. L. *J. Am. Chem. Soc.* **1978**, 100, 8031. (b) Corey, E. J.; Danheiser, R. L.; Chandrasekaran, S.; Keck, G. E.; Gopalan, B.; Larsen, S. D.; Siret, P.; Gras, J. L. *J. Am. Chem. Soc.* **1978**, 100, 8034.
11. Nagaoka, H.; Shimano, M.; Yamada, Y. *Tet. Lett.* **1989**, 30, 971.
12. Hook, J. M.; Mander, L. N.; Urech, R. *J. Am. Chem. Soc.* **1980**, 102, 6628.
13. (a) Corey, E. J.; Munroe, J. E. *J. Am. Chem. Soc.* **1982**, 104, 6129. (b) Corey, E. J.; Guzman-Perez, A.; Loh, T.-P. *J. Am. Chem. Soc.* **1994**, 116, 3611.
14. (a) Pryce, R.J. *J. Chem. Soc., Perkin Trans.* **1974**, 1179. (b) Salaman, S. R.; Derwish, G. A. W.; Al-Salih, S. S. *Spectrochim. Acta.* **1986**, 405.
15. Huigens III, R. W.; Morrison K. C.; Hicklin R. W.; Flood Jr, T. A.; Richter, M. F.; Hergenrother, P. J. *Nat. Chem.* **2013**, 195.
16. Strategies and Tactics in Organic Synthesis, ed. T. Lindenberg, The total synthesis of gibberellic acid R. L. Danheiser, Academic Press Inc., **1994**, vol. 1, pp. 21–70.
17. Darken, M. A.; Jensen, A. L.; Shu, P. *Appl. Microbiol.* **1959**, 7, 301.
18. Kumar, P. K. R.; Lonsane, B. K. *Biotech. and Bioeng.* **1987**, 30, 267.
19. Tomasini, A.; Fajardo, C.; Barrios-González, J. *World J. of Microbiol. and Biotech.* **1997**, 13, 203.
20. Escamilla S, E. M.; Dendooven, L.; Magaña, I. P.; Parra S, R.; De la Torre, M. *J. Biotech.* **2000**, 76, 147.
21. Machado, C. M. M.; Soccol, C. R.; de Oliveira, B. H.; Pandey, A. *Appl. Biochem. Biotechnol.* **2002**, 102, 179.
22. de Oliveira, J.; Rodrigues, C.; Vandenberghe, L. P. S.; Câmara, M. C.; Libardi, N.; Soccol, C. R. *Biomed. Res. Int.* **2017**, Article ID 5191046
23. Stowe R. B.; Yamake, T. *Annu. Rev. Plant Physiol.* **1957**, 8, 181.

24. (a) Brian, P. W.; Elson, G. W.; Hemming, H. G.; Radley, M. J. *Sci. Food Agric.* **1954**, *5*, 602. (b) Brian P. W.; Hemming, H. G. *Physiol. Plant* **1955**, *8*, 669.
25. Sachs, R. M. Stem elongation. *Annu. Rev. Plant Physiol.* **1965**, *16*, 73.
26. Cosgrove, D. J.; Sovonick-Dunford, S. A. *Plant Physiol.* **1989**, *89*, 184.
27. Ross, J. J.; O'Neill, D. P.; Wolbang, C. M.; Symons, G. M.; Reid J. B. *J. Plant Growth Regul.* **2001**, *20*, 349.
28. Kamiya, Y.; Garcia-Martinez, J. L. *Curr. Opin. Plant. Biol.* **1999**, *2*, 398.
29. Hayashi, T. *J. Agric. Chem. Soc. Japan* **1940**, *16*, 531.
30. Higgins, T. J. V.; Zwar, J. A.; Jacobsen, J. V. *Nature* **1976**, *260*, 166.
31. Gubler, F.; Kalla, R.; Roberts, J. K.; Jacobsen, J. V. *Plant Cell* **1995**, *7*, 1879.
32. Ueguchi-Tanaka, M.; Fujisawa, Y.; Kobayashi, M.; Ashikari, M.; Iwasaki, Y.; Kitano, H.; Matsuoka, M. *Proc. Natl. Acad. Sci. USA* **2000**, *97*, 11638.
33. Taddese, B.; Upton, G. J. G.; Bailey, G. R.; Jordan, S. R. D.; Abdulla, N. Y.; Reeves, P. J.; Reynolds, C. A. *Plant Physiol.* **2014**, *164*, 287.
34. Ueguchi-Tanaka, M.; Ashikari, M.; Nakajima, M.; Itoh, H.; Katoh, E.; Kobayashi, M.; Chow, T. Y.; Hsing, Y. I.; Kitano, H.; Yamaguchi, I.; Matsuoka, M. *Nature* **2005**, *437*, 693.
35. Shimada, A.; Ueguchi-Tanaka, M.; Nakatsu, T.; Nakajima, M.; Naoe, Y.; Ohmiya, H.; Kato, H.; Matsuoka, M. *Nature* **2008**, *456*, 520.
36. Griffiths, J.; Murase, K.; Rieu, I.; Zentella, R.; Zhang, Z. L.; Powers, S. J.; Gong, F.; Phillips, A. L.; Hedden, P.; Sun, T. P.; Thomas, S. G. *Plant Cell* **2006**, *18*, 3399.
37. Zentella, R.; Zhang, Z. L.; Park, M.; Thomas, S. G.; Endo, A.; Murase, K.; Fleet, C. M.; Jikumaru, Y.; Nambara, E.; Kamiya, Y.; Sun, T. P. *Plant Cell* **2007**, *19*, 3037.
38. Locascio, A.; Blazquez, M. A.; Alabadi, D. *Curr. Biol.* **2013**, *23*, 804.
39. El-Mofty, M. M.; Sakr, S. A.; Rizk, A. M.; Moussa, E. A. *Nutrition and Cancer* **1994**, *21*, 183.
40. Celik, I.; Tuluce, Y.; Isik, I. *Journal of Enzyme Inhibition and Medicinal Chemistry* **2007**, *22*, 219.
41. Boğa, A.; Binokay, S.; Sertdemir, Y. *Turk. J. Biol.* **2009**, *33*, 181.
42. Chen, J.; Sun, Z.; Zhang, Y.; Zeng, X.; Qing, C.; Liu, J.; Li, L.; Zhang, H. *Bioorg. Med. Chem. Lett.* **2009**, *19*, 5496.
43. Xie, L.; Chen, Y.; Chen, J.; Zhang, H.; Liao, Y.; Zhou, Y.; Zhou, L.; Qing, C. *Cell. Mol. Bio. Lett.* **2019**, *24*, 6.
44. Koehler, A. N. *Methods for modulating NF-κB using gibberellins, U.S. Pat.*, 2009/005938, **2009**
45. Kim, K. H.; Choi, S. U.; Son, M. W.; Choi, S. Z.; Clardy, J.; Lee, K. R. *J. Nat. Prod.* **2013**, *76*, 1376.
46. (a) Adam, G.; Voight, B. *Tett. Lett.* **1971**, 4601. (b) Gurvich, I. A.; Kobrina, N. S.; Serebryakov, E. P.; Kucherov, V. F. *Tetrahedron* **1972**, 5901. (c) Serebyrakov, E. P.; Kobrina, N. S.; Kucherov, V. F. *Tetrahedron* **1971**, 3819. (d) Adam, G. *Tetrahedron* **1973**, 3177.
47. Li, C.; Zhang, Y.; Li, P.; Wang, L. *J. Org. Chem.* **2011**, 4692.

48. (a) Baell, J. B.; Holloway, G. A. *J. Med. Chem.* **2010**, *53*, 2719. (b) Baell, J. B.; Ferrins, L.; Falk, H.; Nikolakopoulos, G. *Aust. J. Chem.* **2013**, *66*, 1483. (c) Baell, J.; Walters, M. A. *Nature* **2014**, *60*, 1620.
49. Annand, J. R.; Bruno, P. A.; Mapp, A. K.; Schindler, C. S. *Chem. Commun.* **2015**, *51*, 8990.
50. Rüßmann, F.; Stemp, M. J.; Mönkemeyer, L.; Etchells, S. A.; Bracher, A.; Hartl, F. U. *PNAS* **2012**, *109*, 21208.
51. Llorca, O.; Martín-Benito, J.; Ritco-Vonsovici, M.; Grantham, J.; Hynes, G. M.; Willison, K. R.; Carrascosa, J. L.; Valpuesta, J. M. *EMBO J* **2000**, *19*, 5971.
52. Roh, S.-H.; Kasembeli, M.; Galaz-Montoya, J. G.; Trnka, M.; Lau, W. C.-Y.; Burlingame, A.; Chiu, W.; Tweardy, D. J. *J. Biol. Chem.* **2016**, *291*, 4732.

## Chapter 3 Efforts Towards the Unified Synthesis of the *ent*-Kaurene Diterpenoids

### Chapter 3.1 Introduction

#### Chapter 3.1.1 *ent*-Kaurene history and biosynthesis

The *ent*-kaurene family of natural products belongs within the larger family of terpene and terpenoid natural products, which are characterized by being built up from five carbon isoprene units.<sup>1</sup> Specifically, the *ent*-kaurenes are diterpenoids, which are characterized by being made up of four isoprene units.<sup>2</sup> The parent kaurene structure (**3-1**), as defined by IUPAC, is tetracyclic and contains a characteristic 6-6-[3,2,1]bicyclic fused ring system.<sup>3</sup> However, the vast majority of isolated kaurene natural products belong to the *ent*-kaurene subclass in which every kaurene stereocenter is inverted (**3-2**) (Figure 3.1).<sup>4</sup>

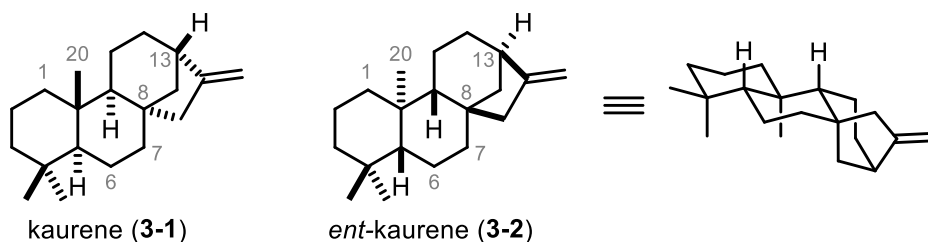


**Figure 3.1-** Parent structures for the kaurene diterpenoids.

More than 600 members of this class of natural products have been isolated from tropical plants of the genus *Isodon*, a family of more than 150 flowering plants primarily found in tropical and sub-tropical Asia. *Isodon lamiaceae* are traditional Chinese medicinal herbs and have been used to treat cancer and diseases associated with inflammation for centuries.<sup>5</sup> *ent*-Kaurene diterpenoids have been found to be as much as 1.5% of the dry weight of these plants and have been studied for more than a century. 1910 investigations of the bitter principles of

‘enmei-so,’ a household folk treatment for gastrointestinal disorders sourced from *Isodon japonicus* and *Ilex trichocarpa*. identified enmein (**3-3**) as one of the first known bioactive *ent*-kaurene diterpenoids.<sup>6</sup> Though the structure of enmein (**3-3**) was not elucidated until 1966 (Figure 3.2).<sup>7</sup> Modern work on more than 36 *Isodon* species have identified more than 600 *ent*-kaurenes that have been studied to gain insight into their biosynthesis and myriad of biological properties.<sup>4</sup>

Additional early work beginning in 1901 in South America identified *Stevia rebaudiana* as having characteristically sweet leaves.<sup>8</sup> In 1908 was isolated as a compound making up 20% of the dry weight of the leaves.<sup>9</sup> It was not until 1931 that the sweet tasting compound was purified and characterized as a triglycoside named stevioside (**3-5**) enzymatic hydrolysis of which provided the diterpenoid steviol (**3-4**).<sup>10</sup> Finally in the 1950s the structures of stevioside (**3-5**) and steviol (**3-4**) were unambiguously assigned (Figure 3.2).<sup>11</sup>

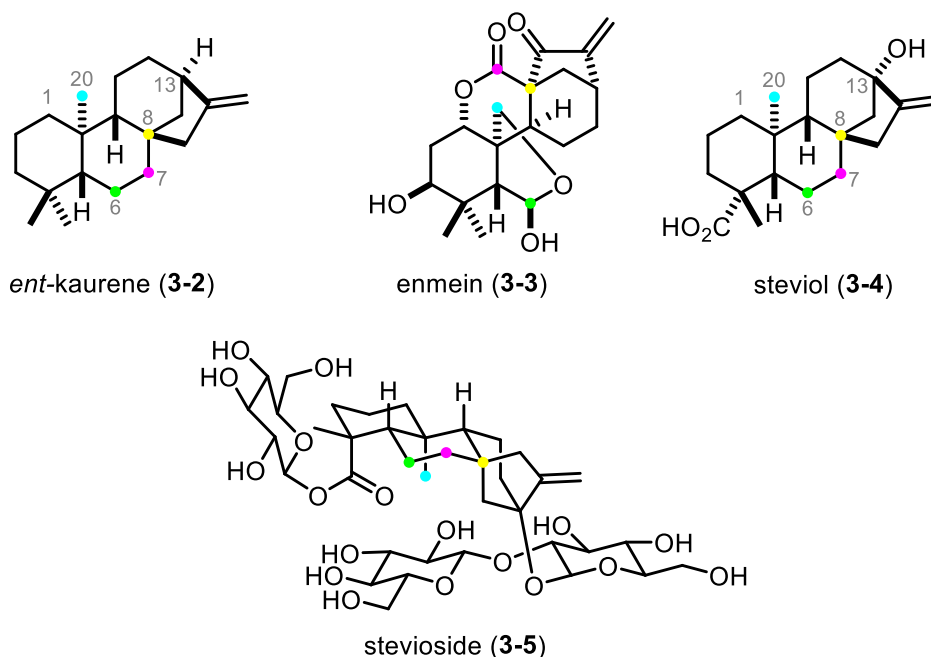


**Figure 3.2-** Some of the earliest studied *ent*-kaurene diterpenoids.

Like most diterpenoids, the *ent*-kaurene diterpenoids are biosynthetically derived from the linear C<sub>20</sub> geranylgeranyl pyrophosphate (**3-6**, GGPP) whereupon first GGPP (**3-6**) is cyclized to afford a bicyclic intermediate, copalyl pyrophosphate (CPP, **3-7**) or *ent*-copalyl pyrophosphate (*ent*-CPP, **3-8**) (Figure 3.3).<sup>12</sup> These intermediates can then differentially derivatized by oxidations, reductions, cyclizations, acetylations, and glycosylations to furnish a variety of structurally unique diterpenoids.

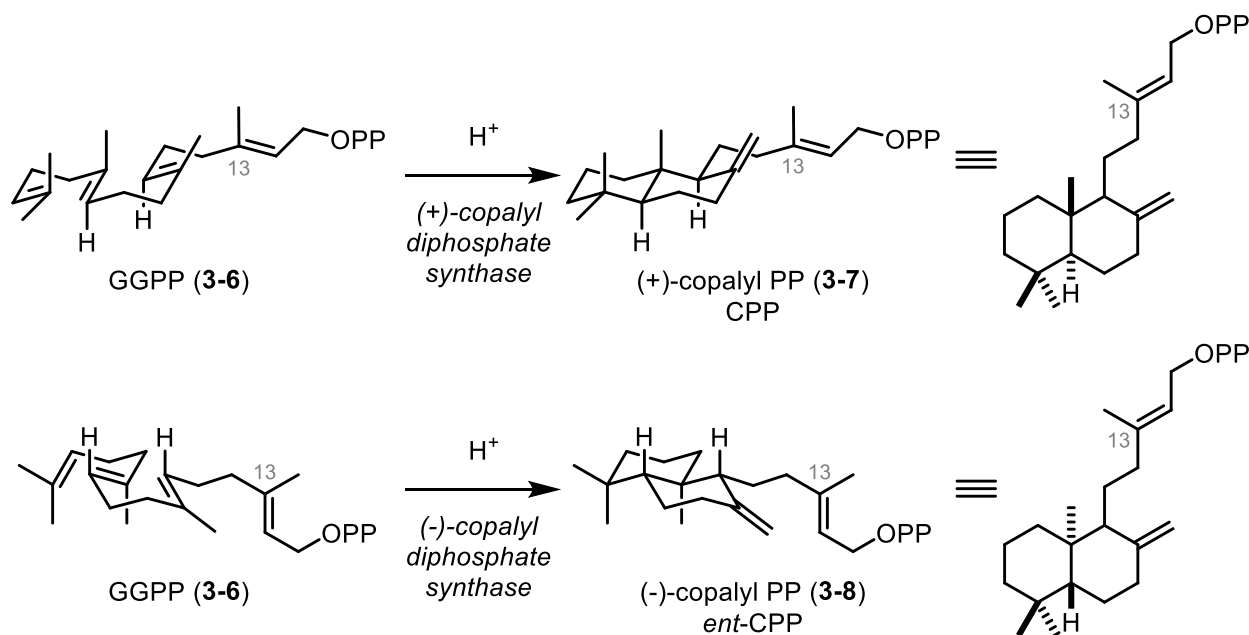


**Figure 3.3-** The first step in kaurene biosynthesis is the conversion of GGPP (**3-6**) to CPP (**3-7**) or *ent*-CPP (**3-8**).

The same enzyme that promotes the formation of *ent*-CPP (**3-7**), (-)-copalyl diphosphate also referred to as *ent*-kaurene synthase, can promote the subsequent functionalization to the *ent*-kaurene core structure (**3-2**). First loss of the pyrophosphate leads to formation of tertiary carbocation **3-9**. This could be captured by the terminal olefin to generate the *ent*-beyenranyl cation (**3-10**), so named for its intermediacy towards the *ent*-beyerene family of diterpenoids. This cation, **3-10**, can then undergo a Wagner-Meerwein rearrangement to form a new *ent*-kaurenyl cation (**3-11**) which upon elimination furnishes the *ent*-kaurene core structure (**3-2**) (Figure 3-

4A).<sup>13</sup> This core structure is then subjected to a series of subsequent oxidations, and often acetylations or glycosylations such as in the biosynthesis of steviol (3-4) (Figure 3-4B).<sup>14</sup>

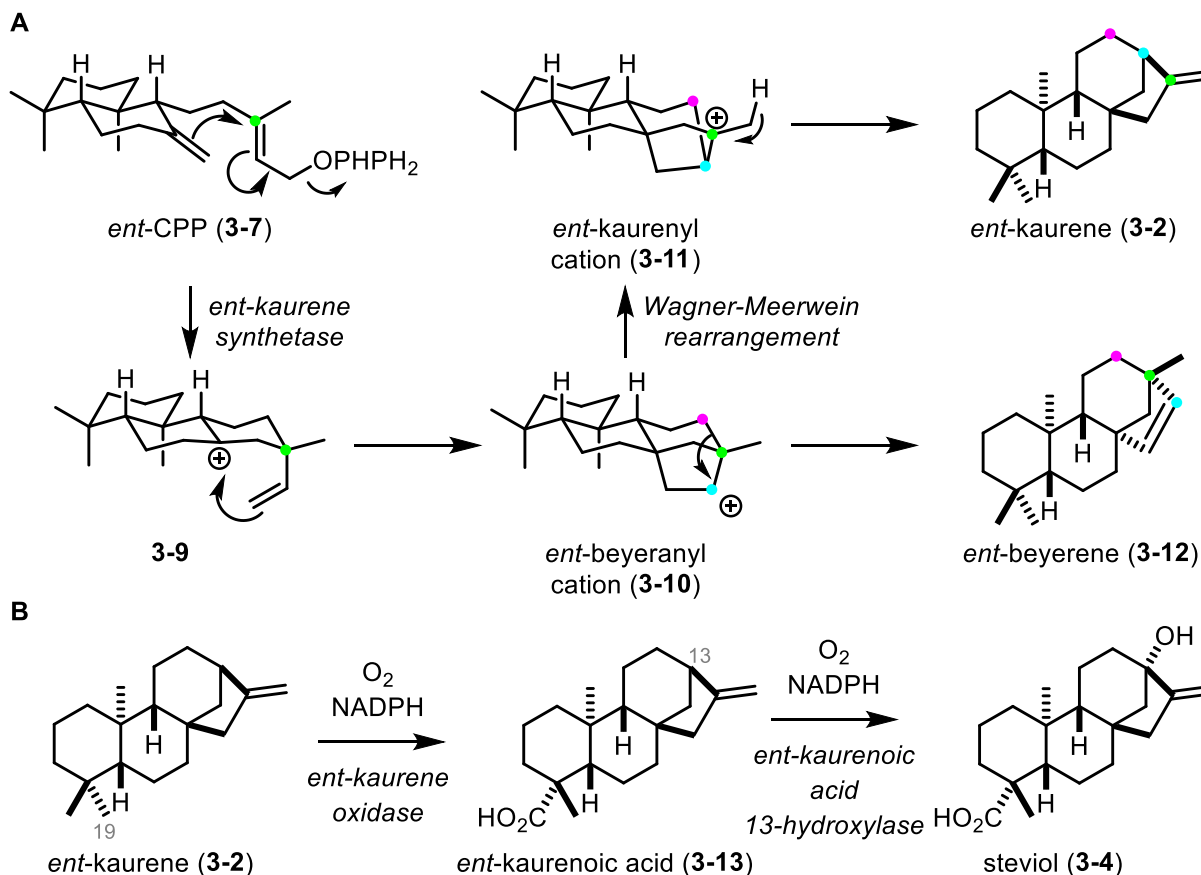


**Figure 3.4- A.** The formation of *ent*-kaurene (3-2) from *ent*-CPP (3-7). **B.** The formation of steviol (3-4) by oxidative functionalization of *ent*-kaurene (3-2).

### Chapter 3.1.2 Selected biological activities of *ent*-kaurene diterpenoids

Even from the very beginning, researchers have been interested in the biologically relevant activities of the *ent*-kaurenes (eg. enmein (3-3) and steviol (3-4) *vide supra*). Interestingly, the plants that produce *ent*-kaurenes such as ‘dangling cao,’ or *Isodon rubescens*, as well as *Isodon ternifolia*, *Isodon lophanthoids*, *Isodon megathyrsus* and *Isodon eriocalyx* have been used in traditional folk medicine for centuries to treat diseases related to inflammation, as well as infections and cancer.<sup>4</sup> Gratifyingly, the *ent*-kaurenes that are isolated from these

medicinally relevant plants have since been characterized as having biological activity relevant to those traditional medicinal uses.

Early studies towards the medicinal effects of *Isodon* plants were focused on ethanolic extracts of *Isodon japonicus* and *Isodon trichocarpa* which were found to inhibit the growth of Gram-positive bacteria.<sup>15</sup> Researchers identified an active component of that mixture to be enmein (**3-3**) while, notably, dihydroenmein (**3-15**) was found to be inactive.<sup>16</sup> Further research identified several *ent*-kaurenes that had activity against Gram positive bacteria including isodonal (**3-14**), nodosin (**3-16**), oridonin (**3-17**). Although the researchers note that the exocyclic Michael acceptors found on the fused C/D rings are essential for activity, which is corroborated by the lack of activity of dihydroenmein (**3-15**) and shikokianidin (**3-18**) (Figure 3.5).<sup>17</sup> Additionally the major component of *Isodon eriocalyx*, eriocalyxin B (**3-19**), has been shown to have potent activity against Gram positive bacteria that the authors describe as being related to the exocyclic Michael acceptor as well as the C6-OH group which might serve to activate the C15-carbonyl for nucleophilic attack through hydrogen bonding (Figure 3.5).<sup>18</sup> It should be noted here that Gram positive bacteria have a well-documented susceptibility to electrophilic interventions.<sup>19</sup>



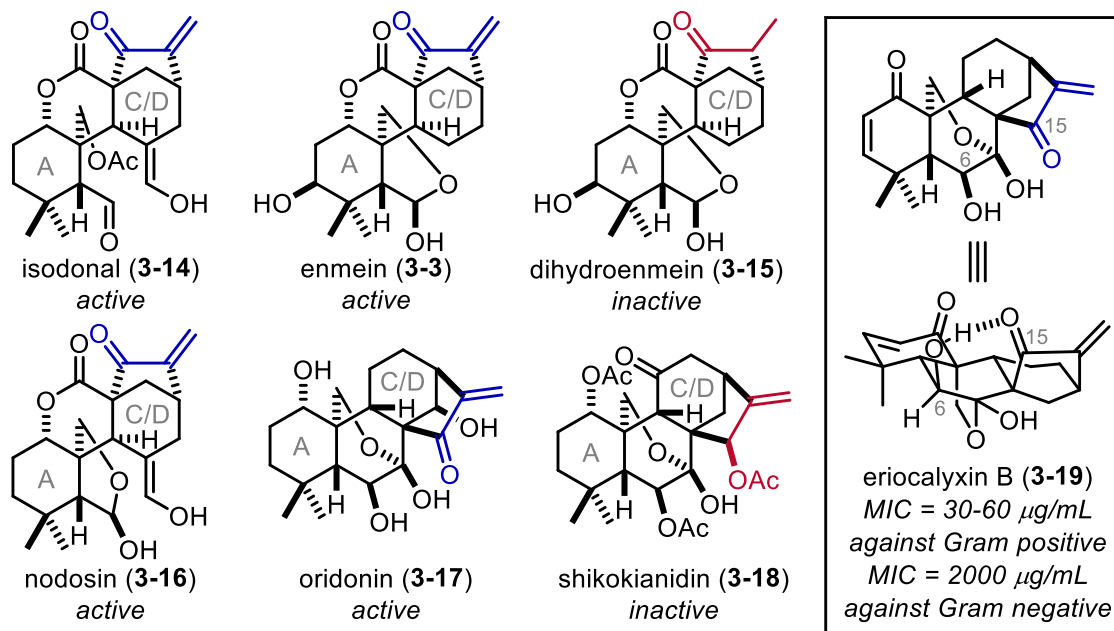


**Figure 3.5-** *ent*-Kaurene diterpenoids that bear an exocyclic Michael acceptor (blue) are also found to be active against Gram positive bacteria. Those that contain a reduced Michael acceptor (red) are found to be inactive against Gram positive bacteria. Eriocalyxin B (3-19) is exceptionally potent against Gram positive bacteria due to an activating hydrogen bonding interaction between the C<sub>6</sub>-hydroxyl and the C<sub>15</sub>-carbonyl.

Just as many *ent*-kaurenes display activity against bacteria, so to do they exhibit activity against cancers. The earliest work in this area was the 1960's and early 1970's in which enmein (3-3) and oridonin (3-17) were found to have significant activity against ascites in mouse tumor models.<sup>20</sup> Though there does seem to be a structure activity relationship in the anti-tumor properties of the *ent*-kaurenes thus far the most significant predictor of activity is the presence or absence of exocyclic Michael acceptors. While some sources suggest that these molecules have relatively low toxicity,<sup>4,5</sup> other sources show general activity of these molecules against a wide variety of cell types<sup>21</sup> and work conducted in our laboratory suggests that exocyclic Michael acceptors of this type display broad toxicity against all mammalian cells (see Chapter 1.2 and 2.3 for a discussion of Michael acceptors and their specificity in the gibberellin diterpenoids). However, despite this general activity, the existence of structure activity relationships do suggest that specific interactions between *ent*-kaurenes and biological macromolecules are responsible

for observed biological effects including against telomerase, p53, phosphatidylinositol-3-kinase (PI3K)/protein kinase B (AKT), epidermal growth factor receptor (EGFR) signaling, AMP-activated protein kinase, and the NF- $\kappa$ B pathway.

One key motif amongst tumor cell lines is the ability to endlessly replicate. Most healthy cells, however, have a limited capacity to self-replicate in part due to degradation of the protective ends of chromosomes, telomeres.<sup>22</sup> The ribonuclear protein telomerase provides cells the ability to protect their telomeric integrity and thus avoid irreversible cell cycle arrest. It is unsurprising therefore that telomerase activity has been found in almost all cancer cell lines.<sup>23</sup> Eriocalyxin B (**3-19**) was found to inhibit 86.7% of telomerase activity at 1  $\mu$ M.<sup>5</sup> Additionally, treatment with oridonin (**3-17**) was found to upregulate the expression of HP1 beta, a protein which reduces the ability of telomerase to associate with telomeres.<sup>24</sup> These inhibitory activities may contribute to the known antitumor properties of eriocalyxin B (**3-19**) and oridonin (**3-17**).

Another feature of tumor cell lines is the ability to suppress or avoid pro-apoptotic signaling. Apoptosis is a mechanism for programmed cell death in which the mitochondrial outer membrane is permeabilized and caspases are released into the cytoplasm irreversibly triggering cell death. One feature that promotes apoptosis is the presence of reactive oxygen species (ROS) such as hydroxyl radicals, nitric oxide, peroxides, and singlet oxygen. Activation of the tumor suppressor protein pathway p53 can result in an increase in ROS which has been shown to induce apoptosis.<sup>25</sup> In HepG2 cells, derived from human hepatoma, treatment with oridonin (**3-17**) leads to p53 activation and ROS mediated apoptosis.<sup>26</sup> Additionally, eriocalyxin B (**3-19**) was shown in pancreatic adenocarcinoma cells to activate p53 and thus cell cycle arrest, apoptosis and limit proliferation.<sup>27</sup> These p53 activatory effects might contribute to the anti-tumor effects of eriocalyxin B (**3-19**) and oridonin (**3-17**).

The PI3K/AKT pathway is found to be upregulated in many cancers and has been linked to the resistance of tumors to available chemotherapies.<sup>28</sup> It has been postulated that suppressing AKT activity might serve as a proapoptotic intervention in tumor cells, either alone or in combination with existing therapies. Oridonin (**3-17**) was shown to inhibit AKT signaling and promote apoptosis in HeLa cells.<sup>29</sup> Structurally related excisanin (**3-20**) was shown to inhibit AKT signaling and promote apoptosis *in vivo* as well as *in vitro*. It promotes apoptosis in both MDA-MB453 breast cancer cells as well as Hep3B hepatocarcinoma derived cells. Notably excisanin (**3-20**) has even been shown to reduce Hep3B tumor size in mouse xenografts.<sup>30</sup>

Epithelial cells can become cancerous upon acquiring activating mutations in the EGFR signaling pathway. Over expression of EGFR is found in 80% of head and neck squamous cell carcinoma (HNSCC).<sup>31</sup> Oridonin (**3-17**) has been shown to be proapoptotic in squamous cell derived Hep-2 cells. Indeed in those cells treatment with oridonin (**3-17**) has reduced the EGFR induced phosphorylation while leaving protein concentrations unaffected suggesting that it may be acting on the pathway as an inhibitor.<sup>32</sup>

Additionally, many *ent*-kaurene diterpenoids were found to inhibit the NF- $\kappa$ B pathway. As discussed previously (*vide supra*, Chapter 1.1.4) NF- $\kappa$ B not only drives inflammation but also has been shown to play a role in all stages of cancer development and is found to be constitutively active in many different inflammatory cancer cell types.<sup>33</sup> Inflexinol (**3-21**), kamebakaurin (**3-22**), and ericalyxin B (**3-19**) have all been shown to directly and irreversibly bind the NF- $\kappa$ B subunits themselves.<sup>34,35</sup> Inflexinol (**3-21**) was shown to inhibit NF- $\kappa$ B translocation. Eriocalyxin B (**3-19**) was shown to bind in the DNA binding domain of NF- $\kappa$ B and thereby prevent NF- $\kappa$ B from binding DNA.<sup>36</sup>

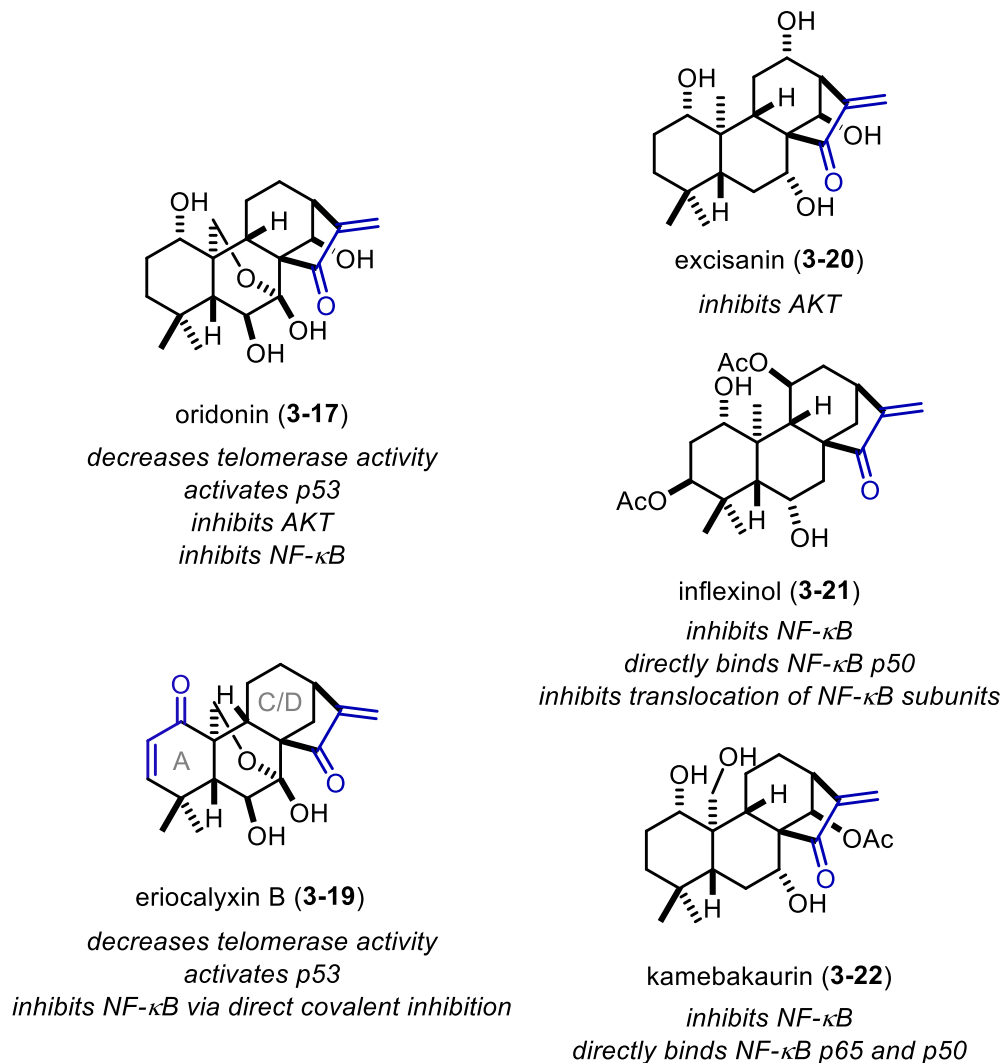


**Figure 3.6-** Several *ent*-kaurene diterpenoids have well studied biological activities against oncogenic pathways.

What is notable about the structure of these bioactive *ent*-kaurenes is that they all contain Michael acceptors (Figure 3.6). However, some limited studies have been done on isolated eriocalyxin B (**3-19**) that have demonstrated that eriocalyxin B (**3-19**) and other derivatives that contain very reactive exocyclic C/D ring Michael acceptors are quite generally toxic in a variety of different mammalian cell lines derived from cancers (Figure 3.7). The researchers were also able to reduce the exocyclic Michael acceptor while retaining the less reactive endocyclic A ring Michael acceptor to generate analog **3-29**. While the researchers note that such a reduction costs

significant and broad spectrum activity against the cell lines tested, we note that it *retains activity against select cancer cell lines* (Figure 3.8).<sup>21</sup> This suggests that the reduced analog **3-29** might be more selective and more specific to a subset of pathways important to only malignant mammalian cells rather than the broad spectrum of activities that have been ascribed to its parent ericalyxin B (**3-19**).

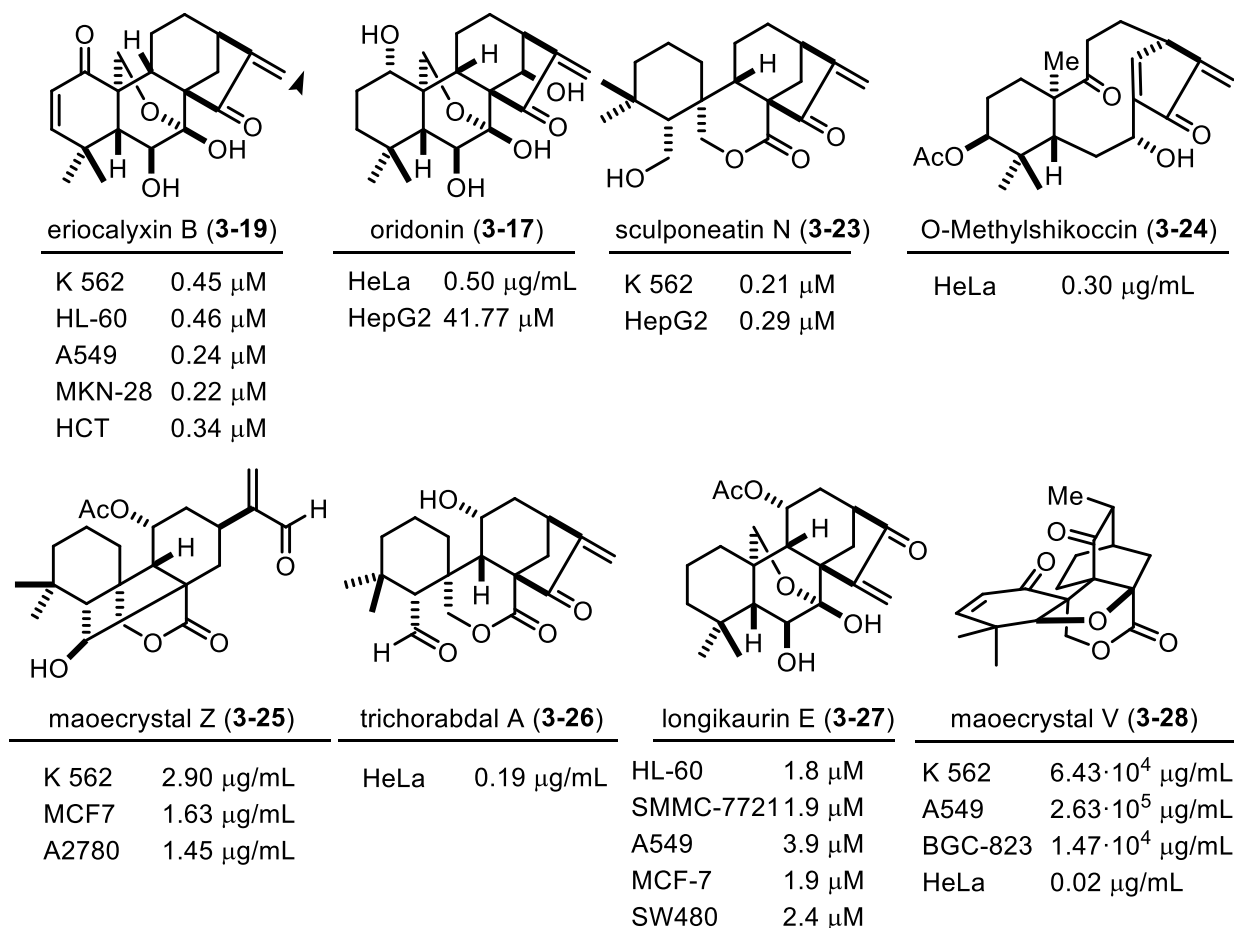


**Figure 3.7-** *ent*-Kaurene diterpenoids that bear exocyclic Michael acceptors are found to be generally cytotoxic towards cancer derived cell lines.

It is this underexplored area of research that would most benefit from forward, general total syntheses that would allow for complete control of the presence of reactive Michael acceptors to assess which of the myriad of reported activities of these molecules are due to

specific interactions with biological macromolecules and which are merely a byproduct of the susceptibility to said macromolecules towards electrophilic stress.

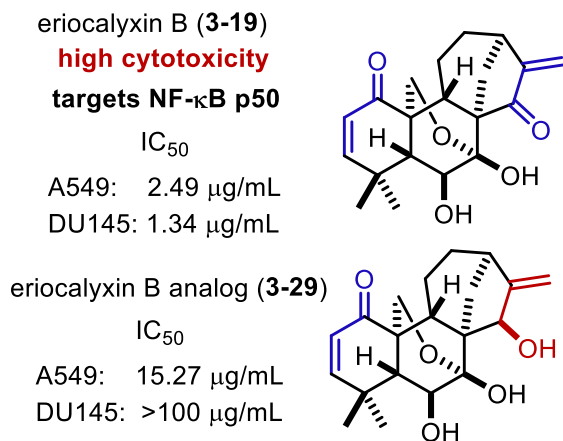


**Figure 3.8-** Published medicinal chemistry indicates that ablating reactive exocyclic Michael acceptors enhances selectivity.

### Chapter 3.1.3 *ent*-Kaurene classifications

As of 2006 over 600 *ent*-kaurene diterpenoids had been isolated.<sup>37</sup> These natural products are generally classified into 5 major classes which are distinguished by their oxidation patterns (Figure 3.9) and alternative connectivity patterns through the tetracyclic core (Figure 3.10).

However, some notable *ent*-kaurene diterpenoids are challenging to classify, the most famous of which is maeocrystal V (**3-28**) which bears a unique 6,7-*seco-ent*-kaurene skeleton (Figure 3.10).

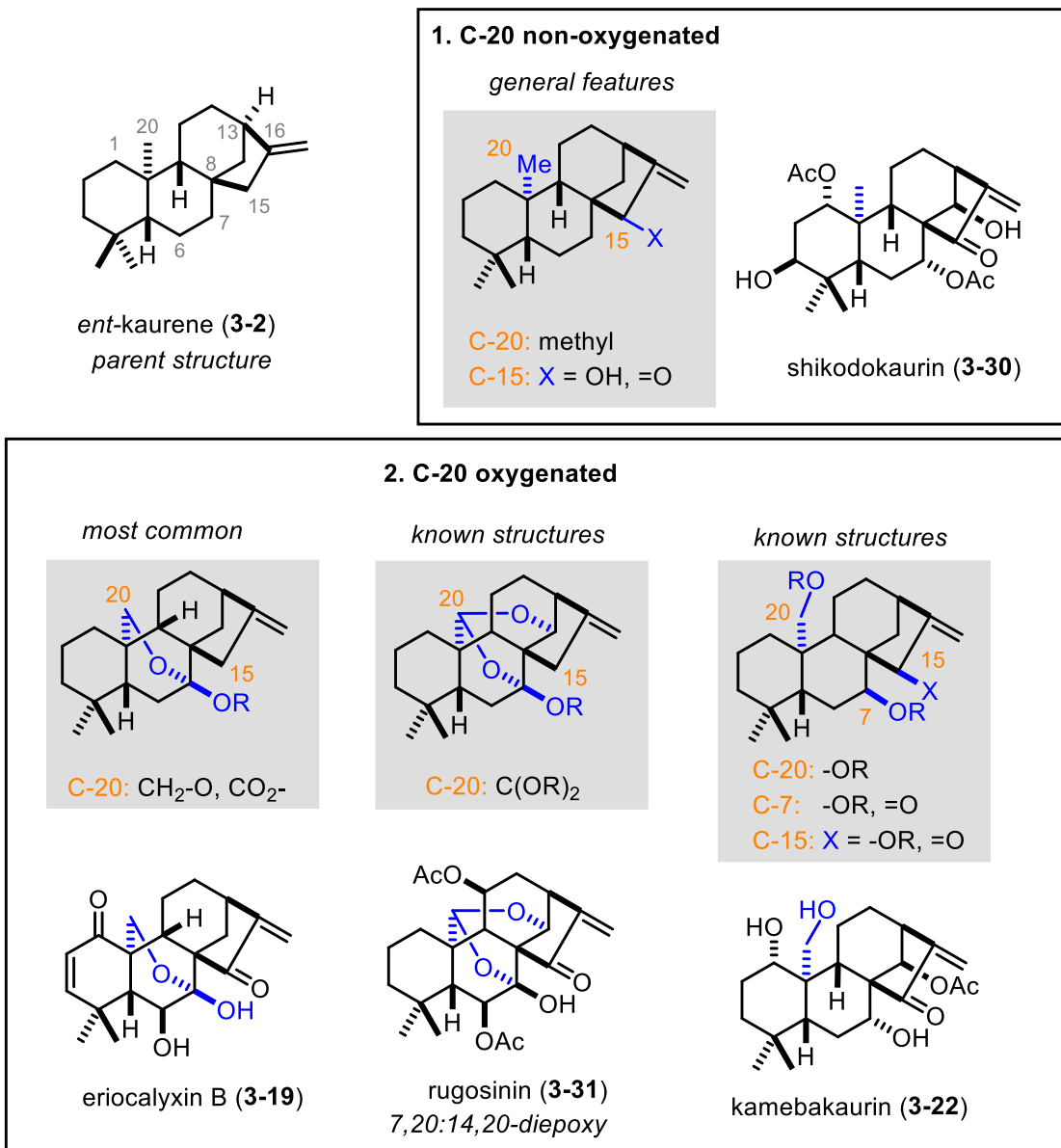


**Figure 3.9-** Two major classifications of *ent*-kaurene diterpenoids pertain to their oxidation pattern at C<sub>20</sub>.

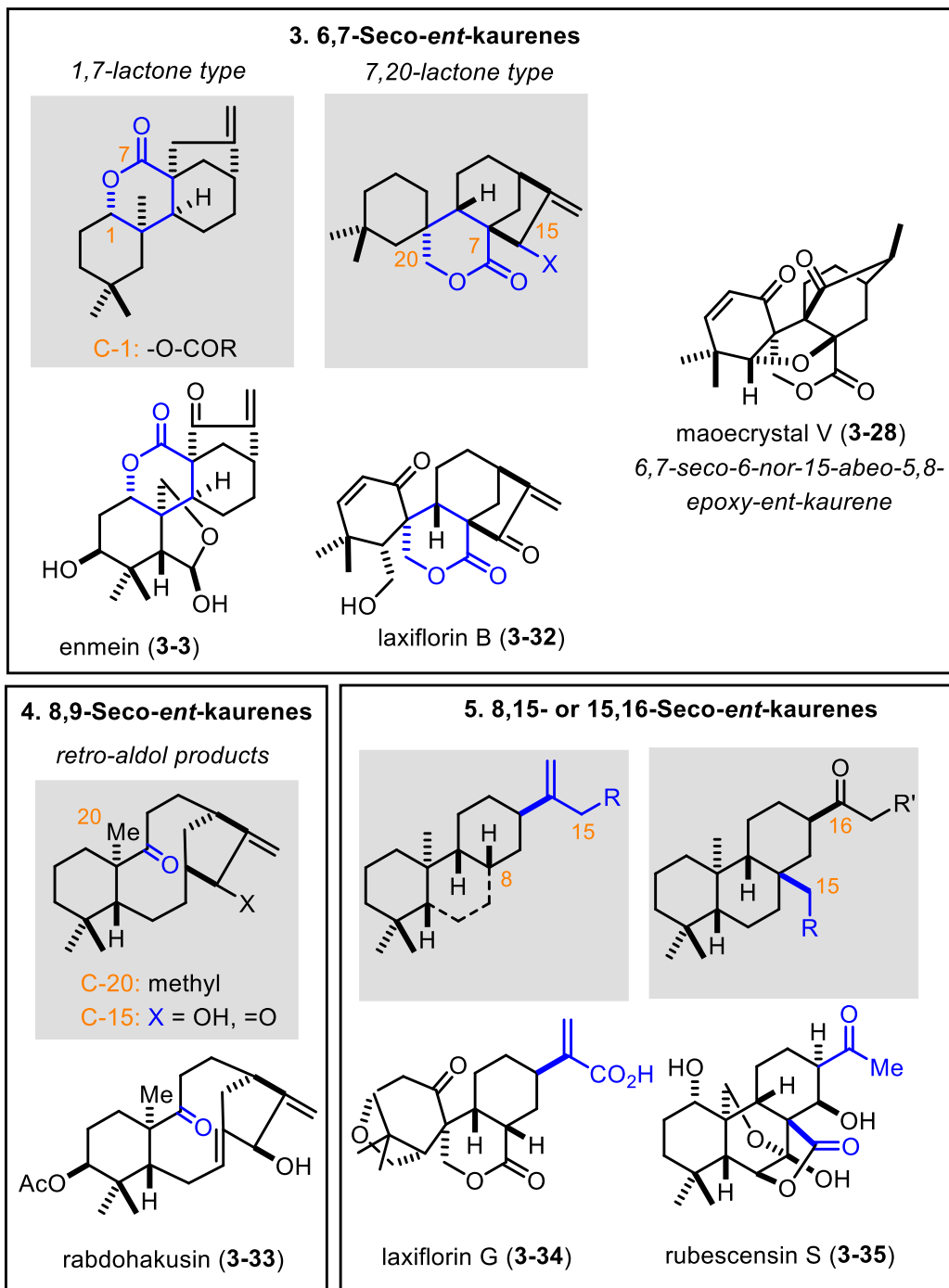


**Figure 3.10-** Three major classification of *ent*-kaurene diterpenoids that pertain to the disconnections across the tetracyclic core structure.



### Chapter 3.1.4 Selected syntheses towards the *ent*-kaurene diterpenoids

Among the earliest syntheses of the kaurene diterpenoids were the syntheses of kaurene (**3-1**), enmein (**3-3**), and steviol (**3-5**), perhaps unsurprisingly. Ireland and coworkers conducted the first synthesis of kaurene (**3-1**), racemically, in 1966 (Figure 3.11).<sup>38</sup> His synthesis is reminiscent of early steroid syntheses in that he begins with tetralone **3-36** which he elaborates via a series that includes a Robinson annulation to a tricyclic framework **3-37**.<sup>39</sup> **3-37** is then subjected to a series of reductions, including a Birch reduction to provide a more saturated tricycle **3-38**. Then a series of oxidation state manipulations and pericyclic rearrangements installs the missing two carbons to form the C/D ring bridge which is closed by an aldol reaction. This provides **3-40** which is oxidized, methenylated and reduced to form the final racemic kaurene (**3-41**).

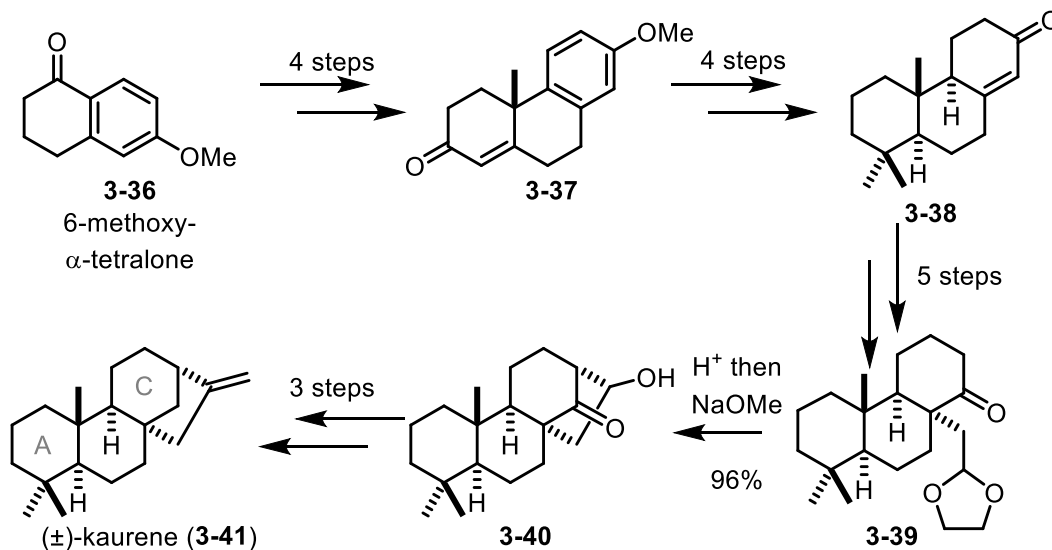


**Figure 3.11-** Highlights from Ireland's 1966 synthesis of kaurene.

In 1972 Fujita and coworkers completed the first synthesis of enmein (**3-3**) which at the time was among the most well studied *ent*-kaurene diterpenoid (Figure 3.12).<sup>40</sup> Their synthesis began with an advanced tricyclic intermediate **3-42** not unlike **3-37**. Like in Ireland's synthesis of kaurene (**3-41**), this intermediate was transformed in a series that include a Birch reduction of

the C ring fragment to C ring ketone **3-43**. This was transformed in 11 steps to tetracycle **3-44** which was accessible from degradation of isolated enmein (**3-3**). Several redox manipulations were required to install the C<sub>6</sub>-C<sub>20</sub> hemiacetal and the C<sub>1</sub>-C<sub>7</sub> lactone **3-46**. And several more were required to furnish the correct oxidation states on the ethyl bridge of the C/D ring [2,3,1]-bicyclic, to yield enmein (**3-3**) in 42 steps from **3-42**. While certainly elegant for its time this synthesis does illustrate the challenges in rapidly assembling an unfunctionalized tricyclic ring system and then attempting to install the necessary functionality to access more challenging synthetic targets.

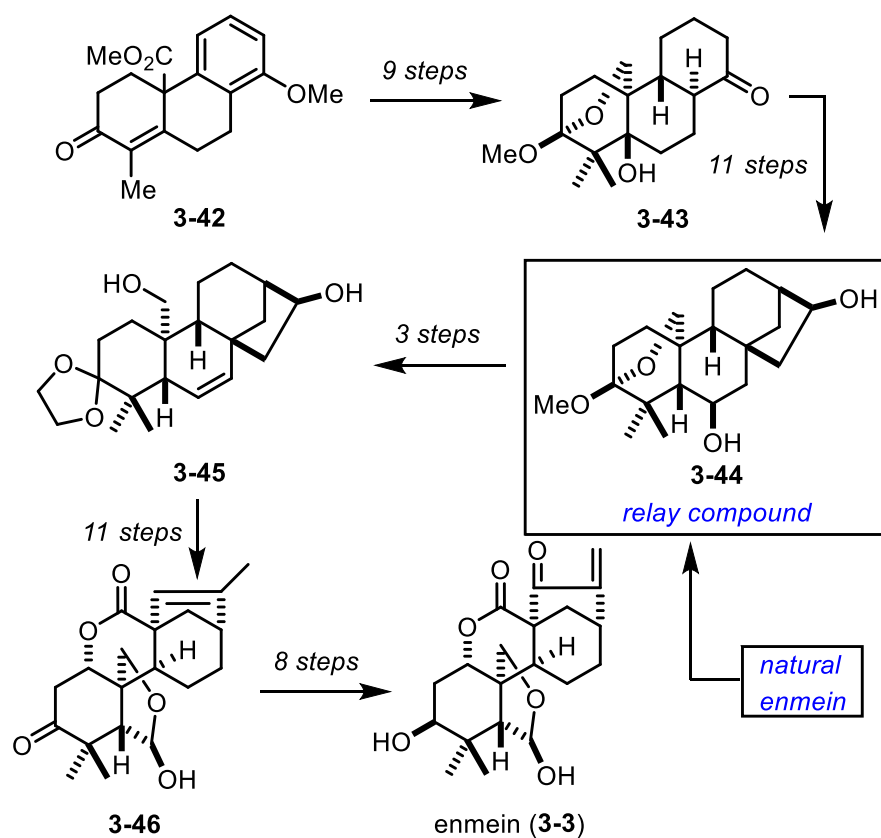


**Figure 3.12-** Highlights from Fujita's 1972 relay synthesis of enmein (**3-3**).

Ziegler and coworkers completed the racemic synthesis of steviol methyl ester (**3-52**) in 1977 (Figure 3.13).<sup>41</sup> They also quickly assembled a tricyclic aromatic core by first coupling the A-ring and C-ring systems (not shown) and then constructing the center B-ring system in 6 steps

to form **3-47**, which they had to dearomatize, oxidatively open to a dicarbonyl, and condense to a cyclopentene ring **3-50**. This enal **3-50** underwent a photochemical [2+2] and then ring expansion to install the appropriate C/D ring and furnish steviol methyl ester (**3-52**). While this approach does highlight an innovative and successful way to form the challenging C/D ring system it does so in quite low yields and is somewhat specific to compounds bearing C<sub>13</sub> oxidation.

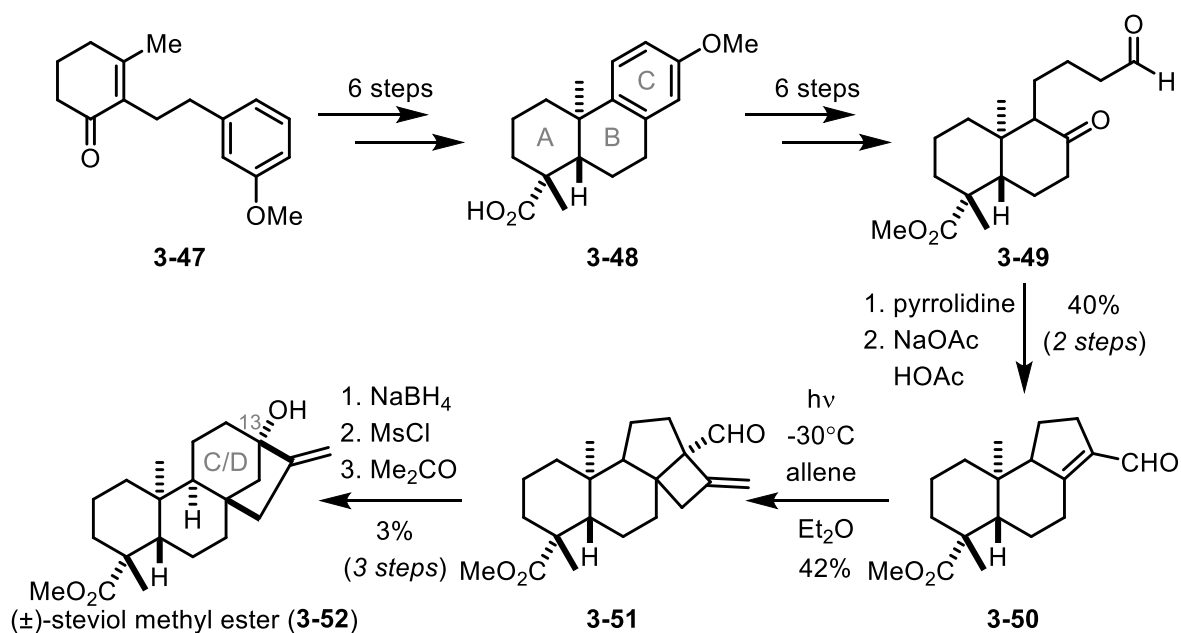


**Figure 3.13-** Highlights from Ziegler's 1977 racemic synthesis of steviol methyl ester (**3-52**).

In contrast, in their racemic 1998 synthesis of isosteviol (**3-53**), Snider and coworkers turned to a biomimetic strategy (Figure 3.14).<sup>42</sup> This relied on constructing the highly unsaturated  $\beta$ -keto ester **3-53**. This was subjected to a radical, oxidative cyclization which in one step assembled tetracycle **3-54** Which could be transformed to isosteviol (**3-55**) in only 6 transformations. This approach elegantly demonstrated how biomimetic approaches could efficiently form the kaurene core structure however the lack of regio-control and enantioselectivity outside of the context of an enzyme active site does limit this approach generally.

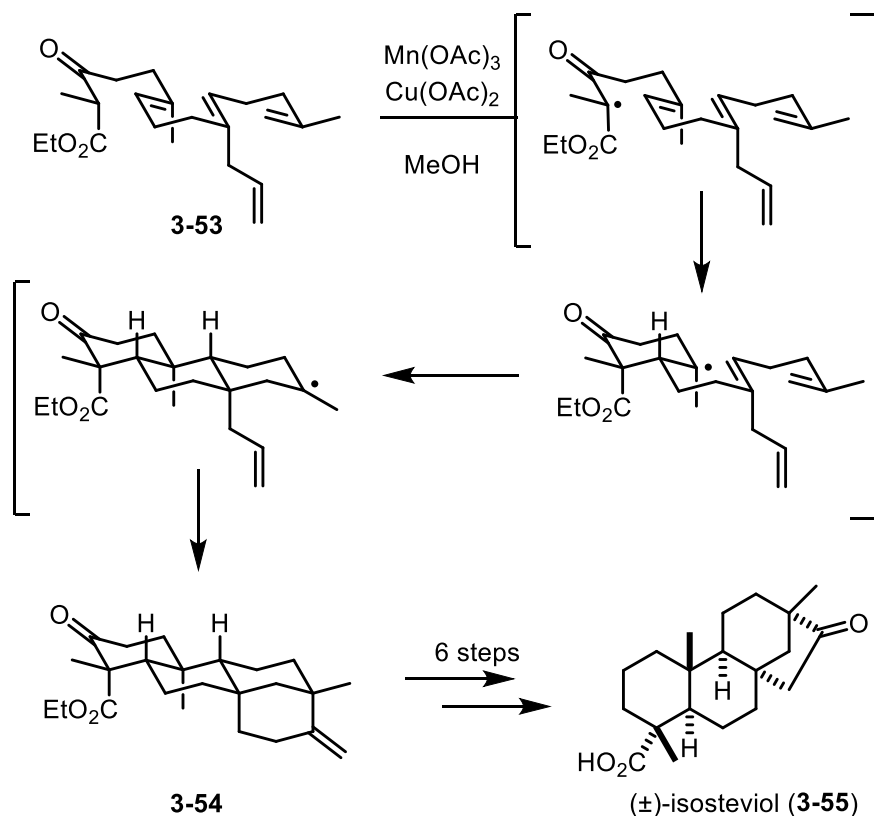


**Figure 3.14-** Highlights from Snider's 1998 racemic synthesis of isosteviol (**3-55**).

In 2013, Baran and coworkers took advantage of all the prior art in the area of steviol (**3-5**) synthesis to take enantioenriched epoxide **3-56** forward to steviol (**3-5**) in 15 steps as a single enantiomer (Figure 3.15).<sup>43</sup> They combined the pseudo biomimetic cyclization of Snider's synthesis, to provide **3-57**, with the well-established dearomative approaches of Ireland, Fujita, Ziegler, and others to form **3-58**. Here they used a photochemical [2+2] followed by a retro-Dieckman/Dieckman cyclization to form [2,2,2] bicycle **3-61**. Which had been previously demonstrated to undergo a zinc promoted rearrangement to the desired [2,3,1] bicycle **3-62**.<sup>44</sup> This late stage intermediate could be efficiently converted to the natural product in 3 steps. Though very efficient and enantioselective, this route again necessitates oxidation at C<sub>13</sub> to form the C/D ring juncture and is thus limited to steviol-type products.

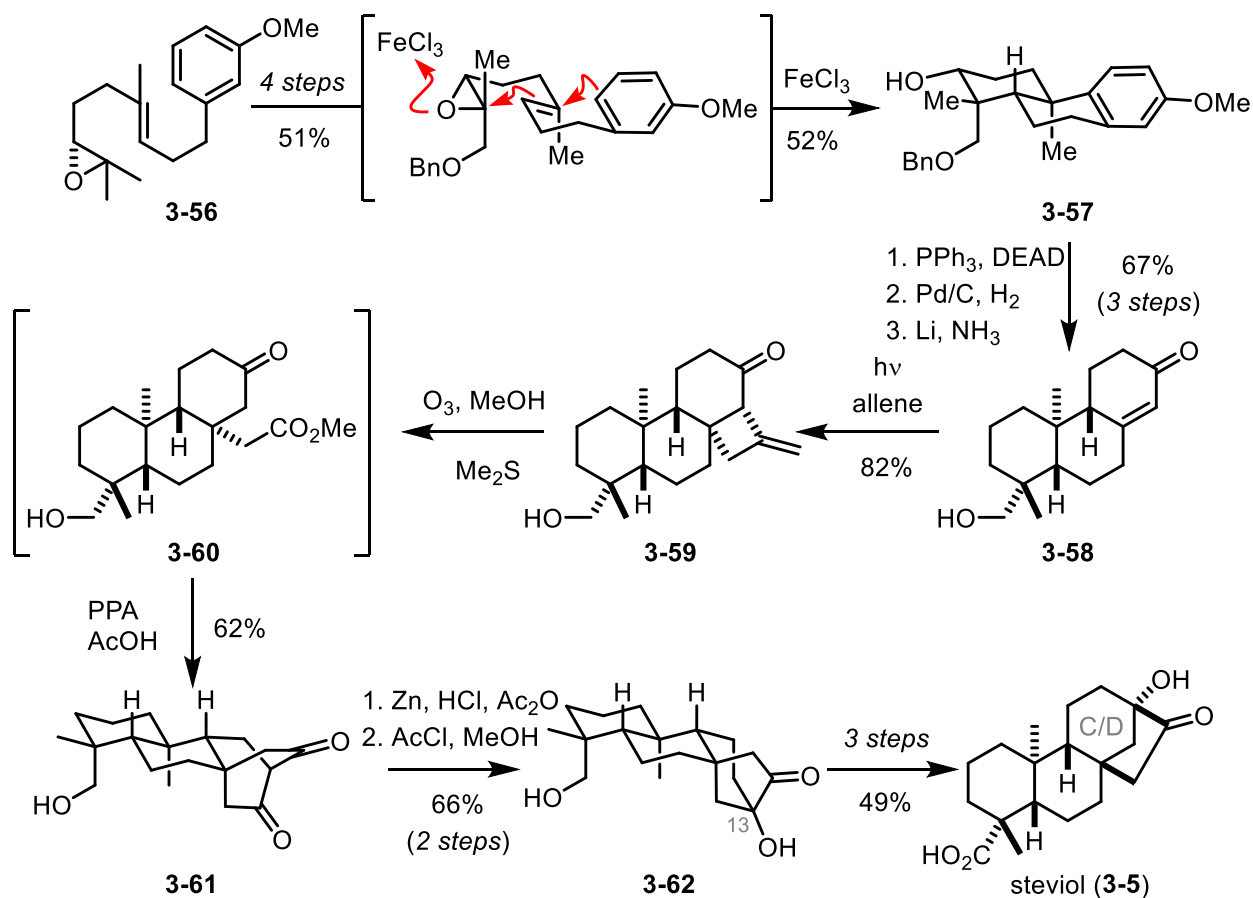


**Figure 3.15-** Highlights from Baran's 2013 enantioselective synthesis of steviol (**3-5**).

These strategies together nicely highlight what had by the early 2000s been the state of the art. Rapidly constructing the tricyclic core of the *ent*-kaurene diterpene target and then functionalizing it by constructing the bicycle toward the end of the synthesis. Unfortunately, these strategies were highly targeted. The divergence points of these strategies were in the construction of the tricycle, often racemically, and converting simple tricycles to complex target structures involved lengthy step counts and exhaustive redox manipulations. An exception to this trend was the 1986 racemic synthesis of 15-Desoxy-effusin (**3-69**) by Mander and coworkers (Figure 3.16).<sup>45</sup> They began with aromatic acid **3-63** and constructed the C/D ring first providing [2,3,1] bicycle **3-65** in 7 steps. Then they constructed the A ring carbocycle **3-67** in 14 synthetic

transformations which still required 11 steps to form 15-desoxy-effusin (**3-69**) relying on a key and clever oxidative C<sub>6</sub>-C<sub>7</sub> bond cleavage from hemiacetal **3-68**.

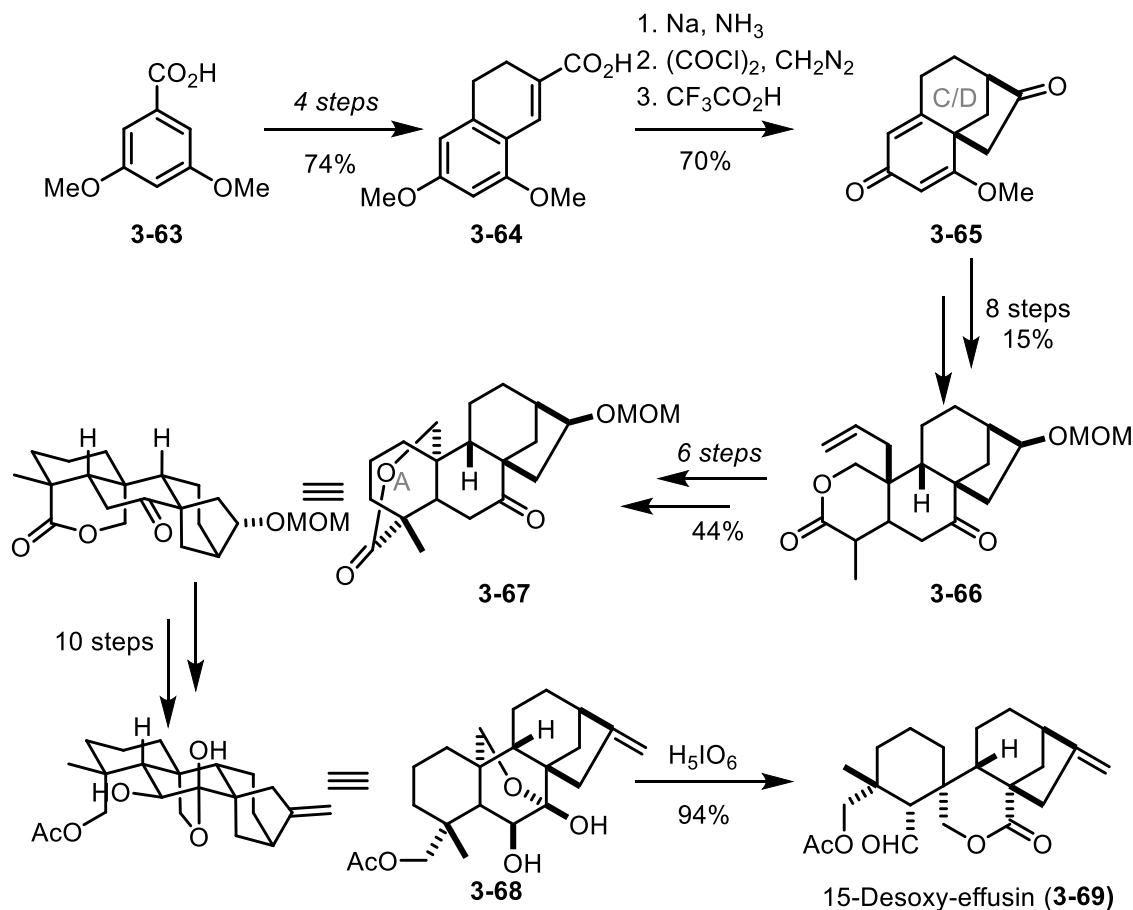


**Figure 3.16-** Highlights from Mander's 1986 racemic synthesis of 15-Desoxy-effusin (**3-69**).

These works perhaps presaged many modern approaches which rely on first constructing key portions of the target *ent*-kaurenes and then appending the rest of the molecule in as efficient a manner as possible. These have even yielded quite diversifiable synthetic efforts perhaps most notably by Riesman and coworkers.

The synthetic efforts of Riesman and coworkers are notable in that they begin with the rapid construction of a common core structure (Figure 3.17).<sup>46</sup> **3-78** is formed by an SN-2 type alkylation of enantio-enriched lactone **3-73** and chiral iodide **3-77**. Lactone **3-73** is formed via (-)- $\gamma$ -cyclogeraniol (**3-3-71**), which is accessible in 7 steps via a previously reported route from

methyl heptenone **3-70**.<sup>47</sup> (-)- $\gamma$ -Cyclogeraniol (**3-71**) is protected and oxidized to epoxide **3-72**. This epoxide is directly converted to lactone **3-73** via a titanocene mediated single electron reduction of the epoxide to form a tertiary radical which undergoes a Michael addition and subsequent lactonization. The chiral iodide **3-77** is formed using a chiral auxiliary based strategy. pentenoic acid **3-74** is coupled to pseudoephedrine, alkylated to form the key stereocenter in **3-76**. This intermediate is then reduced and iodinated to furnish the electrophilic primary iodide **3-77**.

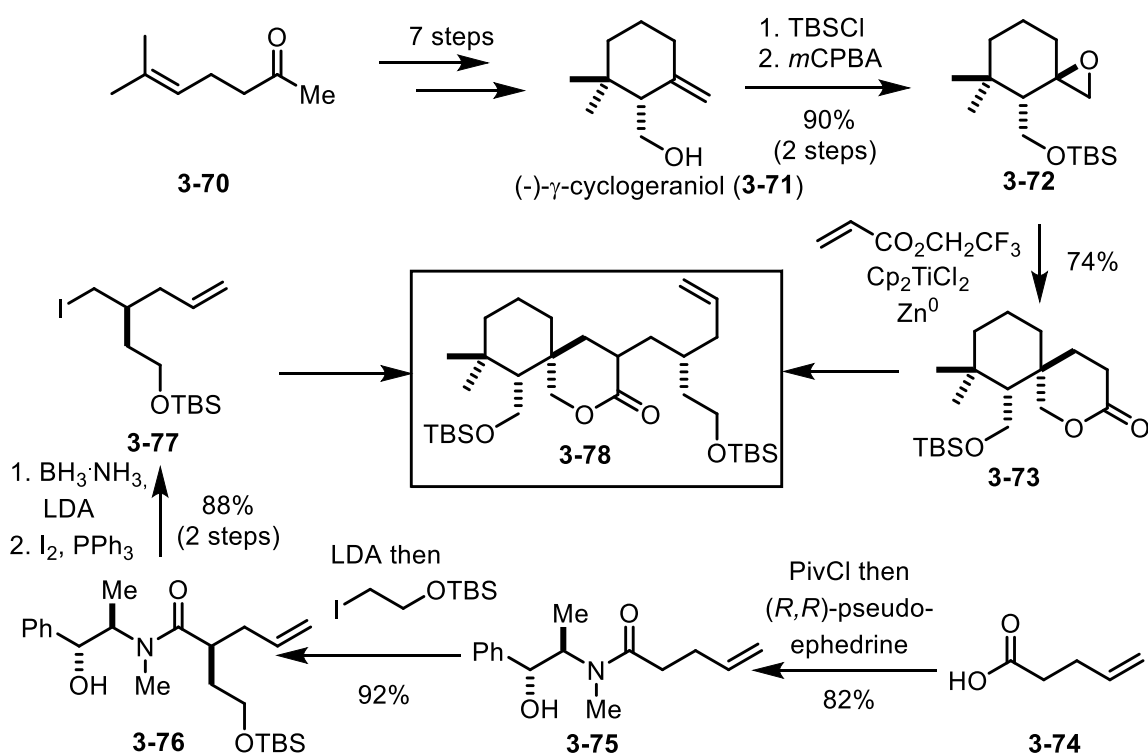


**Figure 3.17**- Synthetic route towards the Riesman group's common intermediate to select *ent*-kaurene diterpenoids **3-78**.

The hallmark of the Riesman syntheses from common intermediate **3-78** is the  $\text{SmI}_2$  induced cyclization cascades (Figure 3.18). Towards maeocrystal Z (**3-25**) the Riesman group fully deprotected and oxidized **3-78** to dialdehyde **3-79**.<sup>46</sup> This is then subjected to  $\text{SmI}_2$  which presumably first closes the C-ring and then closes the cyclopentane ring to form **3-80**. Tetracycle

**3-80** is converted to diacetate **3-81** which impressively can be selectively deacetylated to provide maeocrystal Z (**3-25**).

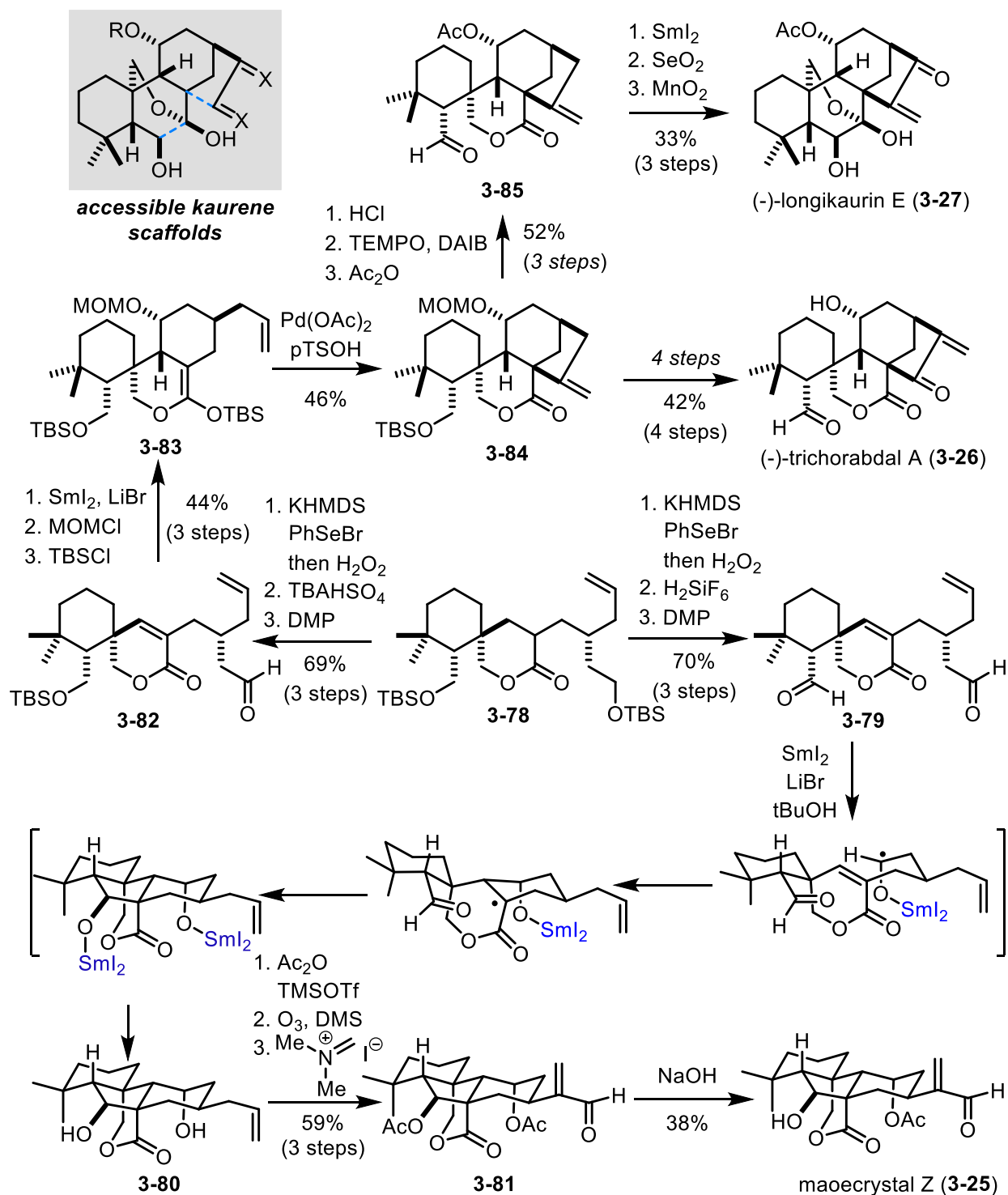


**Figure 3.18-** Intermediate **3-78** is converted to maeocrystal Z (**3-25**) as well as (-)-trichorabdal A (**3-26**) and (-)-longikaurin E (**3-27**).



The Riesman group was also able to convert common intermediate **3-78** towards (-)-logikaurin E (**3-27**) and (-)-trichorabdal A (**3-26**).<sup>48</sup> The strategy employs a mono TBS-deprotection and oxidation to **3-82** followed by a SmI<sub>2</sub> promoted cyclization and protection to form silyl ketal ether **3-82**. This is poised to undergo an enolate Heck cyclization to close the C/D-ring to form tetracycle **3-84**. This tetracyclic lactone **3-84** can be converted with four simple functional group manipulations to provide (-)-trichoribdal A (**3-26**). Tetracyclic lactone **3-84** can also be deprotected and oxidized to aldehyde **3-85**. This aldehyde is poised to undergo another SmI<sub>2</sub> promoted reductive cyclization which is oxidized to (-)-longikaurin E (**3-27**).

This body of work is quite impressive particularly as it highlights the ability of modern synthetic techniques to provide for rapid, convergent asymmetric access to highly functionalized intermediates which bear the necessary oxidation to be rapidly transformed into a variety of bioactive *ent*-kaurene diterpenoids. Though the approach is somewhat limited to less functionalized A-rings and C<sub>11</sub>-oxidations. Though in principal it would be possible to modify the synthetic approach to include other oxidatively differentiated starting materials, rendering them asymmetrically and efficiently is not trivial to realize. This is unfortunate because many of the more biologically interesting *ent*-kaurenes, such as eriocalyxin B (**3-19**) and laxiflorin B (**3-32**), are not accessible via this strategy.

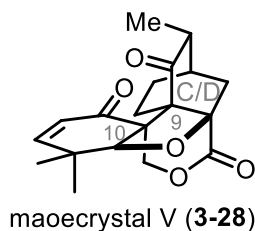
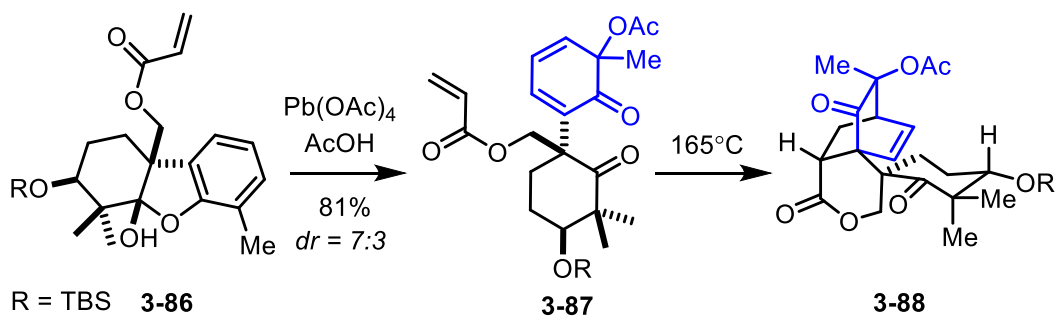


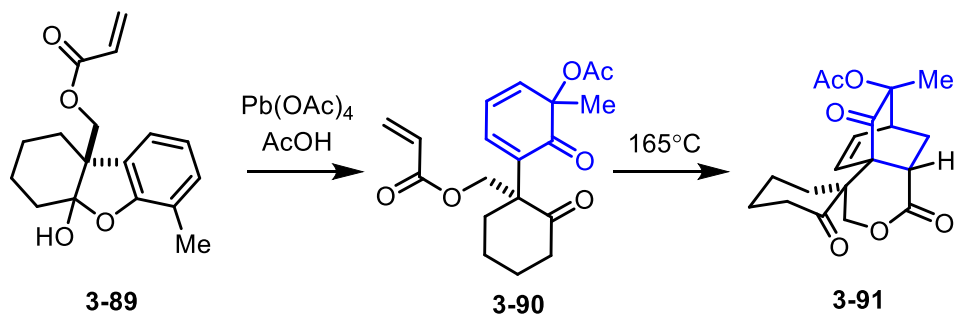
**Figure 3.19-** Structural features of maoecrystal V (**3-28**).

Any discussion of modern synthetic approaches towards *ent*-kaurene diterpenoids would be lacking if they did not discuss the synthetic efforts towards maoecrystal V (**3-28**). This *ent*-kaurene was structurally confirmed only in 2004 and is one of the most structurally unique kaurenes isolated to date. Additionally, very early, material limited, biological studies on isolated maoecrystal V (**3-28**) identified that it was an extraordinarily active molecule against cancer derived cell lines however they could not conduct extensive studies, nor even duplicate their original results, as they did not have sufficient quantities of **3-28**.<sup>49</sup> It is unsurprising, therefore, that synthetic access reported thus far to this natural product has been very focused and isolated seeing as **3-28** is both structurally unique and required significant material throughput to verify initial promising biological studies.

**P.S. Baran (2009)**



**Z. Yang (2009)**



**A. Zakarian (2011)**

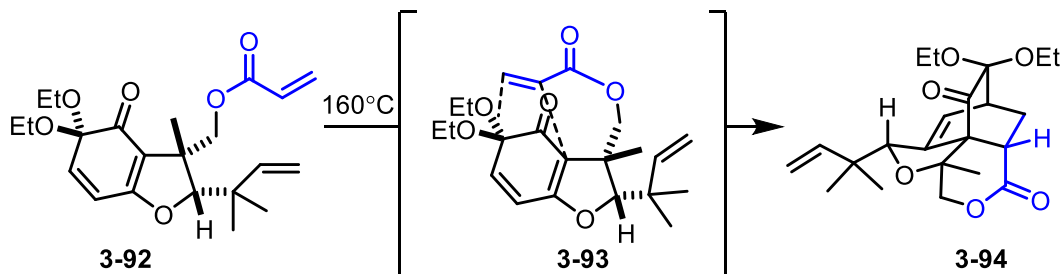


**Figure 3.20-** Key disconnections by Baran,<sup>50</sup> Yang,<sup>51</sup> and Zakarian<sup>52</sup> in early studies towards maoecrystal V (**3-28**) take advantage of oxidative dearomatization-Diels-Alder sequences.

The two chief structural challenges towards maoecrystal V (**3-28**) are the vicinal quaternary stereocenters between C<sub>9</sub> and C<sub>10</sub> as well as the bridged C/D [2.2.2] bicycle. (Figure 3.19) It is unsurprising that many of the approaches focus on a Diels-Alder reaction to address both of those challenges. The strategies typically will either rely on an oxidative dearomatization strategy for providing the Diels-Alder substrate (Figure 3.20) or the generation of a stable enolate to provide for the Diels-Alder substrate (Figure 3.21). Both of these approaches are quite efficient but any route that relies on a Diels-Alder reaction to close the C/D ring concomitantly

with forming the C<sub>9</sub> stereocenter will only provide access to a limited scope of kaurenes that contain that closed C/D ring moiety.

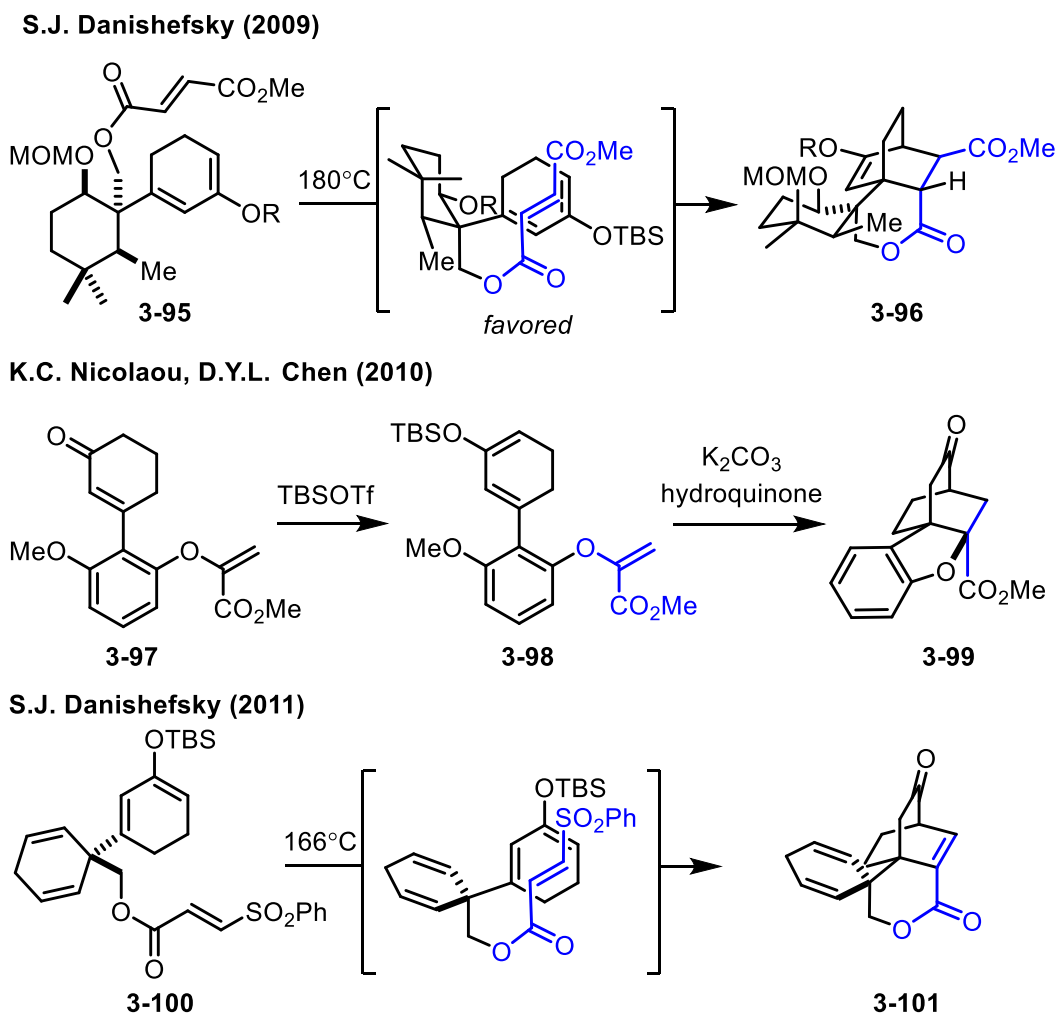


**Figure 3.21-** Key disconnections by Danishefsky<sup>53</sup> along with Nicolaou and Chen<sup>54</sup> in early studies towards maeocrystal V (**3-28**) take advantage of generating an enolate diene for a Diels-Alder reaction.

One particularly inspirational approach to maeocrystal V (**3-28Z**) was conducted in 2014 by Thomson and coworkers (Figure 3.22).<sup>55</sup> Relying on an enantioenriched epoxide **3-102** the researchers directly append the C-Ring as an aromatic subunit to form ether **3-103**. This is set up to do a challenging 6-exo-trig Mizoroki-Heck cyclization which proceeds with isomerization of the resultant olefin to the more thermodynamically stable distal position in tricycle **3-104**. After

oxidative dearomatization and selective reduction of the resultant enone ketone **3-105** is deprotonated and protected to form a diene which is immediately subjected to a Diels-Alder reaction with nitroethylene to provide bicycle **3-106**. This must then be subjected to a variety of functional group manipulations including the reduction of a ketone via an intermediate dithiane to form **3-108** which is then oxidized both allylically to enone **3-109** and also to form a lactone as the final step in the synthetic sequence to maoecystal V (**3-28**). Though this route did not deliver sufficient quantities of **3-28** to support or reject the initial biological findings, this route did take an inspirational approach as the two ring systems were initially brought together to build the central ring systems. However, the choice of a Diels-Alder reaction, while efficient towards the formation of **3-28**, limits the ability to extend this route towards other *ent*-kaurenes.

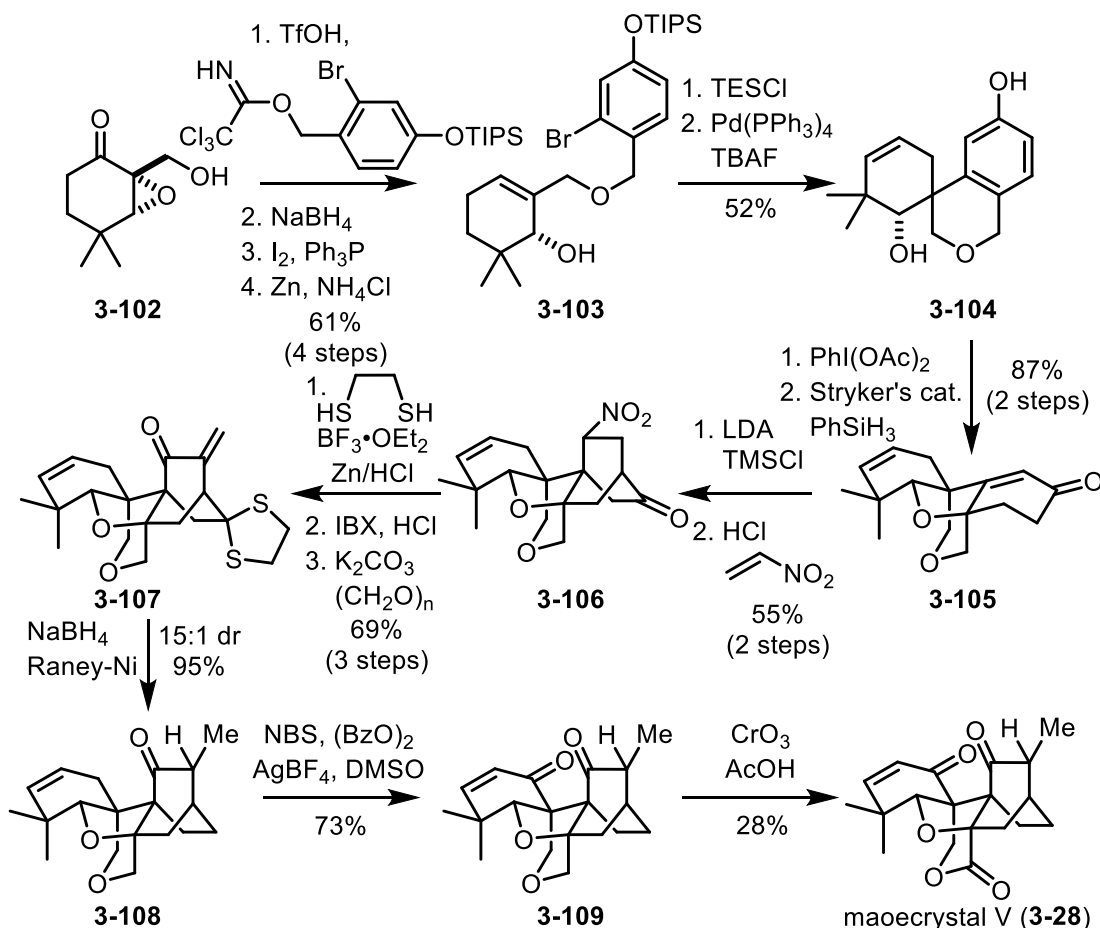


**Figure 3.22-** Highlights from Thomson's 2014 enantioselective synthesis of maoecrystal V (**3-28**).

No discussion of maoecrystal V (**3-28**) syntheses could be considered complete without mentioning the 2016 enantioselective synthesis by Baran and coworkers (Figure 3.23).<sup>56</sup> The synthesis begins with an enantioselective Michael addition onto cyclohexenone to form ketone **3-110**. This is then oxidized to alpha-keto acetate **3-111** which undergoes an intramolecular allylation to form [3,2,1] bicycle **3-112**. After the tertiary alcohol is protected and the acetate is oxidized to a ketone the A-ring of maoecrystal V (**3-28**) is added via a Grignard addition. This provides **3-113** which is subjected to acidic conditions without further purification which promotes a Wagner-Meerwein type rearrangement to the desired [2,2,2] bicycle in **3-114**. Upon alkylation to **3-115** the in situ formed acetal is rearranged to **3-116** which without purification is

captured by cyanide and hydrolyzed to form the central lactone in **3-117**. This can be converted to maoecrystal V (**3-28**) by epoxidation, epoxide opening and oxidation.

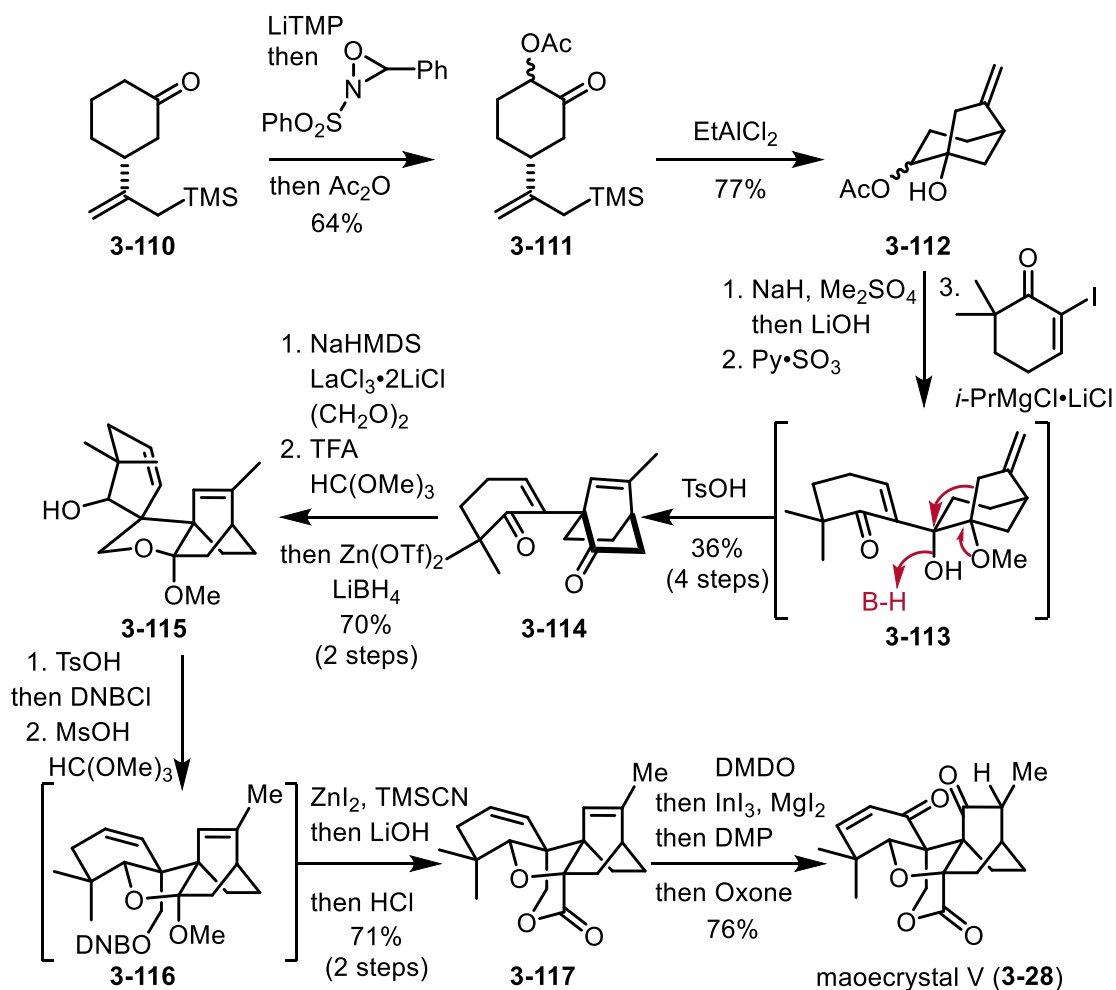


**Figure 3.23-** Highlights from Baran's 2016 enantioselective synthesis of maoecrystal V (**3-28**).

Notably, this sequence provided sufficient material, 80 mg, to conduct exhaustive biological evaluations. In these experiments the researchers failed to reproduce the promising biological activities that were disclosed upon isolation. This led Baran and researchers to conclude that either the initial experiments were done with error or that the initial biological evaluations had missed a particularly active impurity. Either way this information is of value to a community of scientists studying these natural products and could only be realized by the efforts of total synthesis. Of personal interest, maoecrystal V (**3-28**) does contain an A-ring Michael

acceptor. This provides evidence that *ent*-kaurenes that have a sterically congested A-ring enone are likely less generally reactive and have more specific biological activity than their analogs that contain a more reactive, less selective exocyclic C/D-ring Michael acceptor.

## Chapter 3.2 Retrosynthetic analysis for a unified approach to the *ent*-kaurene diterpenoids

### Chapter 3.2.1 Eriocalyxin B as a retrosynthetic target

Eriocalyxin B (**3-19**) is among the most well studied *ent*-kaurene diterpenoids. Perhaps the wealth of biological studies on **3-19** is a result of its biological abundance, in *Isodon eriocalyx* *ent*-kaurene diterpenoids make up 1.5% of the dry weight of the leaves of mature plants of which eriocalyxin B (**3-19**) is a major component.<sup>57</sup> This abundance, along with promising biological activities (*vide infra*), has prompted isolation chemists and chemical retailers to make this material commercially available, accelerating the pace of research into **3-19**.<sup>58</sup>

We became interested in eriocalyxin B (**3-19**) owing to its ability to inhibit or modulate the NF- $\kappa$ B pathway. Leizer and coworkers demonstrated that eriocalyxin B (**3-19**) inhibits the NF- $\kappa$ B pathway in ovarian cancer stem cells (OCSCs).<sup>59</sup> They showed that the inhibition of NF- $\kappa$ B in OCSCs led to a decrease in the production of pro-carcinogenic inflammatory cytokines as well as a reduction in pro-survival protein, XIAB. Together they show that **3-19** inhibits cell growth at 0.5  $\mu$ M. Zhao and coworkers found that **3-19** significantly inhibited the NF- $\kappa$ B pathway in four different lymphoma derived cell lines; SU-DHL-4, Namalwa, H9, and Jurkat cells.<sup>60</sup> They show that **3-19**, at 1.5  $\mu$ M, inhibits the phosphorylation of I $\kappa$ B, modestly inhibits the nuclear translocation of RelA(p65), and inhibits the ability of RelA to bind DNA. The result of these effects was found to be a significant decrease in pro-survival proteins, Bcl-2 and Bcl-xL.



This led to an increase in apoptosis and lymphoma cell death. Several different groups have shown that, though ericalyxin B (**3-19**) does inhibit nuclear translocation of RelA at concentrations significantly higher than the  $IC_{50}$  against the pathway, at lower concentrations they find no inhibition of nuclear translocation.<sup>36,61</sup> Instead they show that **3-19** prevents NF- $\kappa$ B from binding DNA. They even identify the specific cysteine, Cys62, that **3-19** covalently modifies to prevent p50 from binding DNA. With well identified, moderately specific activity against NF- $\kappa$ B synthetic access to ericalyxin B (**3-19**) would provide us the ability to more specifically interrogate the structural features of **3-19** that are required for reactivity.

In addition to furthering our research interests in NF- $\kappa$ B pathway inhibition and study, ericalyxin B (**3-19**) has a variety of other published biological activities. **3-19** shows activity against JAK2/STAT3 signaling in SW1116 colon cancer cells and the researchers link that inhibitory activity to cancer proliferation, migration, invasion, and angiogenesis.<sup>62</sup> Additionally, **3-19** has been identified as a covalent modifier of Cys712 on STAT3 and was shown to inhibit STAT3 signaling, inducing apoptosis in a variety of STAT-dependent cancer cell lines including A549 and MDA-MB-453 cells.<sup>63</sup> Eriocalyxin B (**3-19**) has been shown to enhance the proapoptotic effects of established chemotherapeutics, for example it enhances the effect of gembaticine in pancreatic cancer.<sup>64</sup> In other studies, **3-19** promoted p53 activity in pancreatic adenocarcinoma derived cell lines causing cell cycle arrest and promoting apoptosis.<sup>65</sup> Eriocalyxin B (**3-19**) and related diterpenoids were shown to inhibit telomerase activity at concentrations as low as 10 nM and exhibited cytotoxicity with  $IC_{50}$ s below 1  $\mu$ M in K562, HL-60, MKN, and A549 cells.<sup>66</sup>

Taken together, these biological activities warrant consideration for targeting for synthesis. **3-19** contains two separate enones. The bulk of the biological studies indicate that

ericalyxin B (**3-19**) works by covalently modifying cysteines on biological macromolecules. However, these studies also suggest that **3-19** is not very specific limiting its utility as a biological probe or chemotherapeutic candidate. Synthetic access would provide a platform for diversification and structure activity relationship (SAR) studies that enable hypothesis driven study rather than material availability driven study. Towards this end we designed our synthesis to target both **3-19** specifically and enable detailed access and SAR to identify new, specific inhibitors.

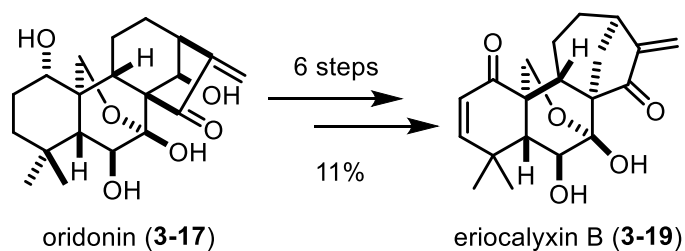


**Figure 3.24-** 1990 semi-synthesis of ericalyxin B (**3-19**) from oridonin (**3-17**).

Some synthetic efforts towards ericalyxin B (**3-19**) have been disclosed. Before we began our synthetic efforts ericalyxin B (**3-19**) had been synthesized via a semi-synthesis from oridonin that has been isolated from natural sources which neither provided enough quantity of material to enable further study nor allowed for significant structural diversification (Figure 3.24).<sup>67</sup> While our synthetic efforts were underway a racemic, though quite scalable, synthesis of **3-19** was disclosed (Figure 3.25).<sup>68</sup> While this certainly could provide sufficient quantities of **3-19** for testing it is very targeted and does not enable additional synthetic access to the *ent*-kaurene diterpenoids. As such it still seemed valuable to continue the synthetic efforts described herein.

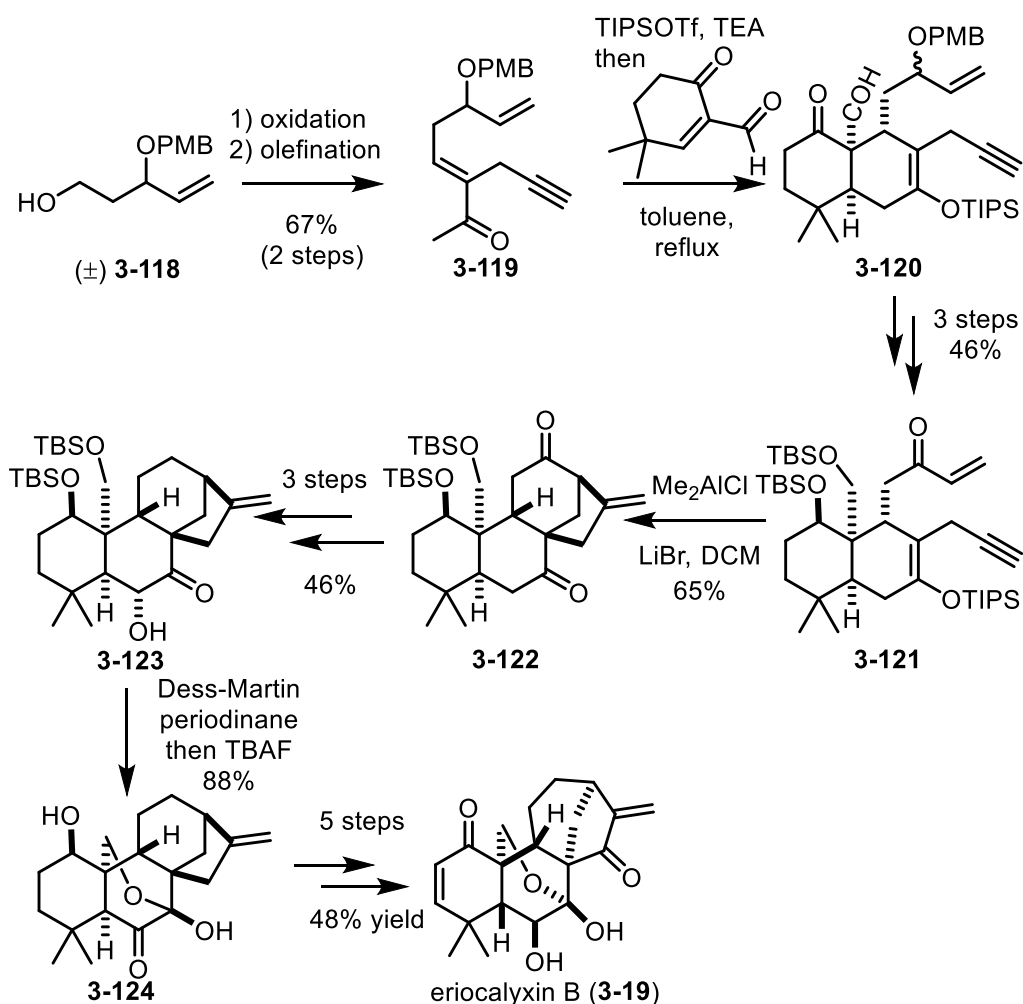
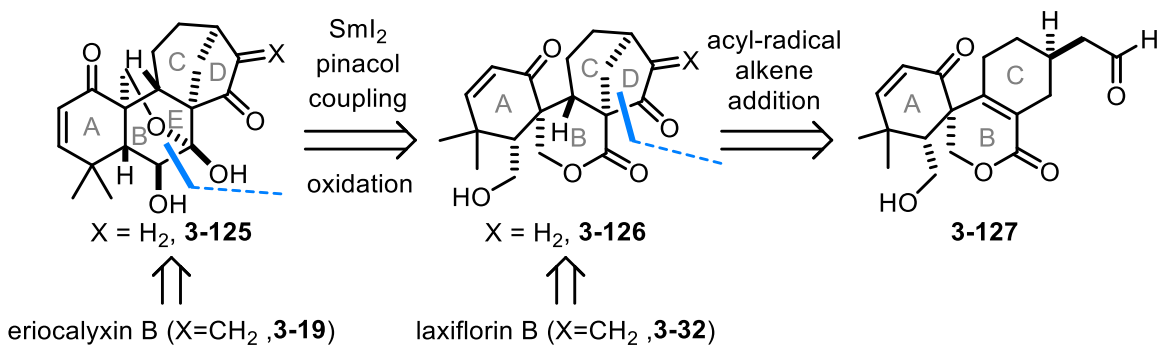


Figure 3.25- Lee group's 2018 synthesis of ericalyxin B (3-19).

Chapter 3.2.2 Retrosynthetic analysis highlights a common intermediate to the *ent*-kaurene diterpenoids

When considering synthetic approaches to **3-19** we wanted to be able to install the C/D ring Michael acceptor last, providing a natural access to analogs with and without that structural feature. It has been well demonstrated that the B/E ring cyclic core can be constructed by a pinacol coupling mediated by samarium diiodide.<sup>46,48</sup> This would provide the carbocyclic core common to the laxiflorins (**3-119**), particularly laxiflorin B (**3-32**). It is expected that the C/D

ring could be disconnected relying on either an acyl radical alkene addition, or a reductive aldol reaction.<sup>69,70</sup>



**Figure 3.26-** Retrosynthetic analysis of eriocalyxin B (**3-19**) provides spirocyclic lactone **3-120**.

This proposed intermediate, **3-127**, we contend is a useful synthetic intermediate not just for eriocalyxin B (**3-19**) and laxiflorin B (**3-32**) but instead all *ent*-kaurenes bearing the oxidation state of **3-127**. One set of products could be envisioned being derived from laxiflorin B (**3-32**) or its unmethenylated precursor, **3-126** (Figure 3.27). We envisioned that **3-126** or **3-32** could be converted via a lumiketone rearrangement to the neolaxiflorins A (**3-128**) and B (**3-129**). pinacol coupling via  $\text{SmI}_2$  would provide eriocalyxin B (**3-19**) or maoecrystal C (**3-130**) which differ only in the oxidation state of the C/D ring. Eriocalyxin B (**3-19**) could be converted to maoecrystal P (**3-131**) by first oxidizing the B/E ring secondary alcohol to a ketone and then allowing for the isomerization of the  $\text{C}_{20}$  oxidation to form an A ring bicycle via an oxa-Michael addition. These products are of biological interest because they differ significantly in the reactivity of their Michael acceptors. Especially maoecrystal P (**3-131**) which contains a masked A ring enone.

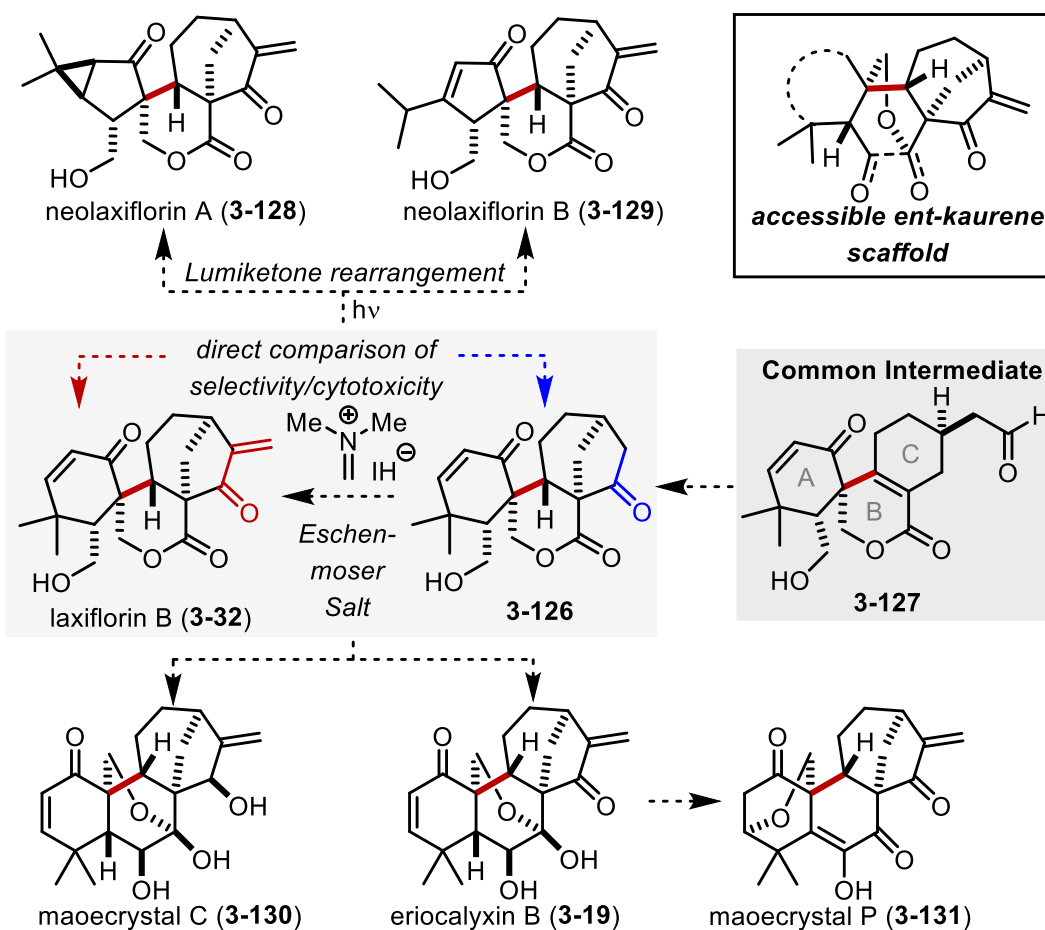


**Figure 3.27-** Common intermediate **3-127** could be converted to laxiflorin B (**3-32**) and thus to a wide variety of *ent*-kaurene diterpenoids bearing a common scaffold.

Additionally, a common intermediate such as **3-127** would be advantageous because it allows for facile access to 8-15 seco *ent*-kaurenes (Figure 3.28). An oxa-Michael addition followed by a methenylation would provide laxiflorin G (**3-34**) which is a reduction away from laxiflorin F (**3-132**). While both of these molecules contain a masked A-ring enone, **3-34** has a more reactive electrophilic acrylic acid moiety. A macrolactonization with the A ring and C<sub>15</sub> could provide access to the terfenolides such as terfenolide A (**3-133**). This can also provide access to some unique laxiflorins such as laxiflorin P (**3-134**) which would be the product of a pinacol type coupling, as discussed above and once again contains a masked A ring enone and a very reactive enal moiety.

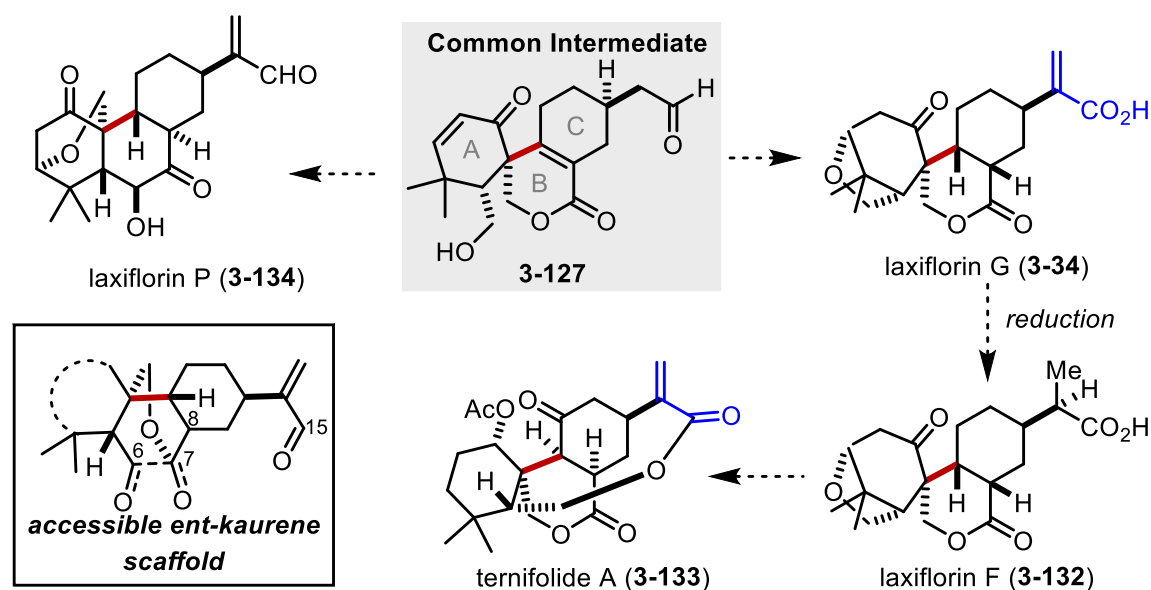


**Figure 3.28-** Common intermediate **3-127** could be converted *ent*-kaurene diterpenoids that lack the connectivity of the C/D ring with and without attachment between C<sub>6</sub> and C<sub>7</sub>.

Having established the ability of a common intermediate such as **3-127** to be translated to a variety of interesting targets, we turned towards the synthesis of **3-127**. An ideal synthesis is one in which a fully elaborated A ring fragment was combined with a fully elaborated C ring fragment constructing both the ester of the B ring lactone and the C<sub>10</sub>-C<sub>9</sub> bond, shown in red (Figure 3.29). This would allow for not only **3-135** and **3-136** to be combined but, in principal, A ring and C ring fragments bearing alternative oxidation patterns, such as at C<sub>19</sub> or C<sub>14</sub> could be subjected to the same coupling conditions and provide access to an even more diverse set of *ent*-kaurene diterpenoids. It seemed apparent that the first key step of the synthesis would be forging this key C—C bond.

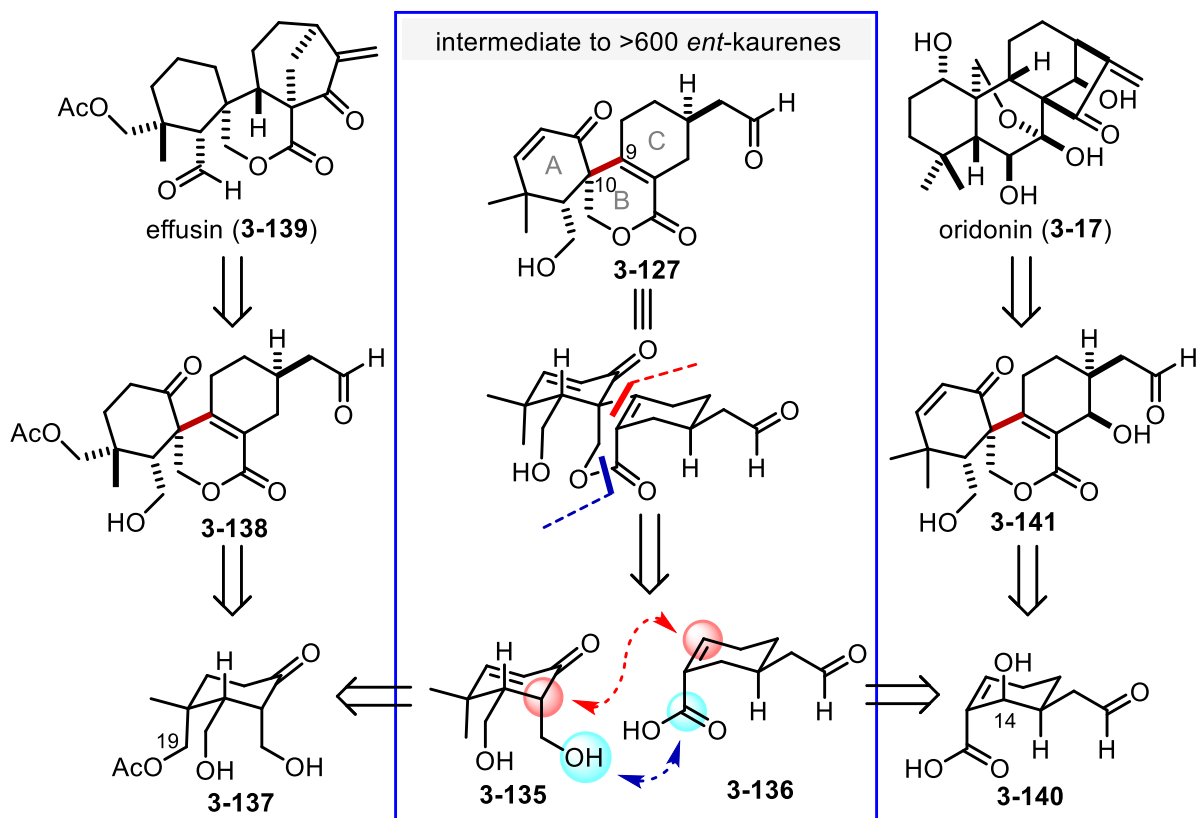


**Figure 3.29-** A convergent strategy to **3-127** would allow for extension of the initial synthetic efforts to additional *ent*-kaurenes depending on the oxidation state of precursors used.

### Chapter 3.2.3 Model system studies towards synthesizing a common intermediate to the *ent*-kaurene diterpenoids

Our first concept was that a photochemical [2+2] cycloaddition could be undertaken to form a highly substituted cyclobutene such as **3-142** (Figure 3.30). We imagined that a diene such as **3-144** and a cyclic enone such as **3-145** could come together. Then **3-146** could undergo an elimination, fragmentation and lactonization which could in one step provide the common intermediate **3-127**. This approach posed two significant challenges. First, [2+2] cycloadditions to form fully substituted cyclobutanes were unknown at the time of our investigation and second, the fragmentation conditions could induce alternative products including retro-[2+2]. In model system studies we found that both challenges were significant obstacles. We could overcome the challenge of making highly substituted cyclobutanes by careful analysis of solvents and the use

of flow reactors. In flow, and only in flow, **3-148** and **3-149** could be combined to form **3-150** and **3-148** and **3-152** could be combined to form **3-153** both in synthetically useful yields. However, all attempts to fragment the cyclobutanes yielded only retro [2+2] and we could not promote the desired cyclobutene fragmentation. This prompted us to consider alternative approaches to form the key bond in **3-127**.

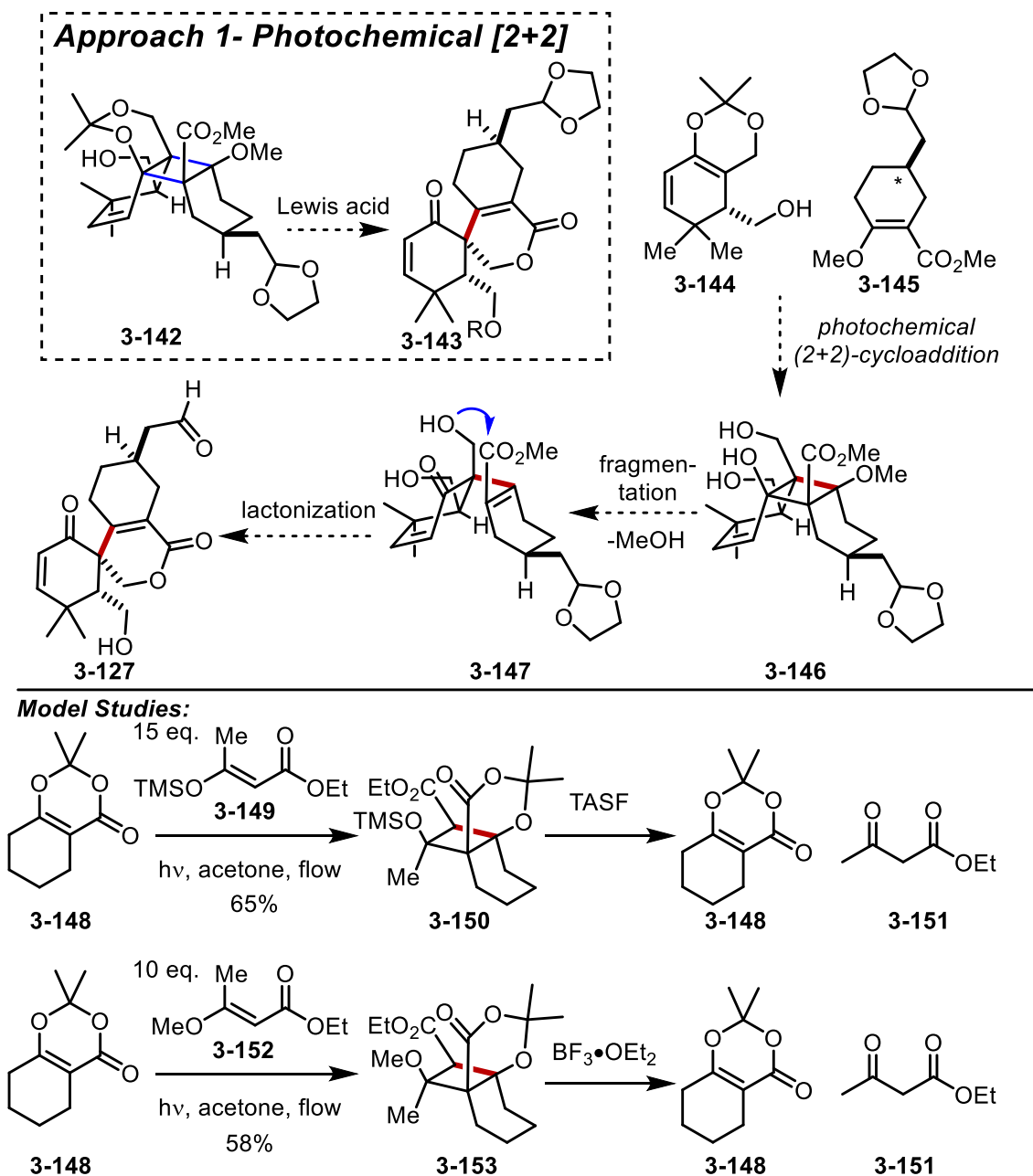


**Figure 3.30-** The first approach towards a common intermediate to the *ent*-kaurene diterpenoids.



Our second approach is one in which we envisioned taking an ester such as **3-154** and then generating an enolate which might undergo a Michael addition/elimination cascade to form common intermediate **3-143** (Figure 3.31). However, this approach does suffer from a potential  $E_{1CB}$  elimination mode in which the enolate that is formed simply eliminates the ester as a leaving group. This is what is observed in model system studies such as the conversion of ester **3-155** to **3-156**. When we tried to carry out an intermolecular Michael addition, we found that if there was an oxygen in the beta position, which would be necessary to form a B ring lactone, it only reacted by  $E_{1CB}$  elimination to form **3-156**. We thought that such an elimination would be impossible if we had a  $\beta$ -keto ester such as **3-157**. However, we could not identify conditions in which an enolate generated from **3-157** would engage an electrophile such as **3-158** in a Michael addition. These experiments highlighted to us the importance of both stable, and reactive coupling partners if we intended to carry out a reaction manifold such as this.

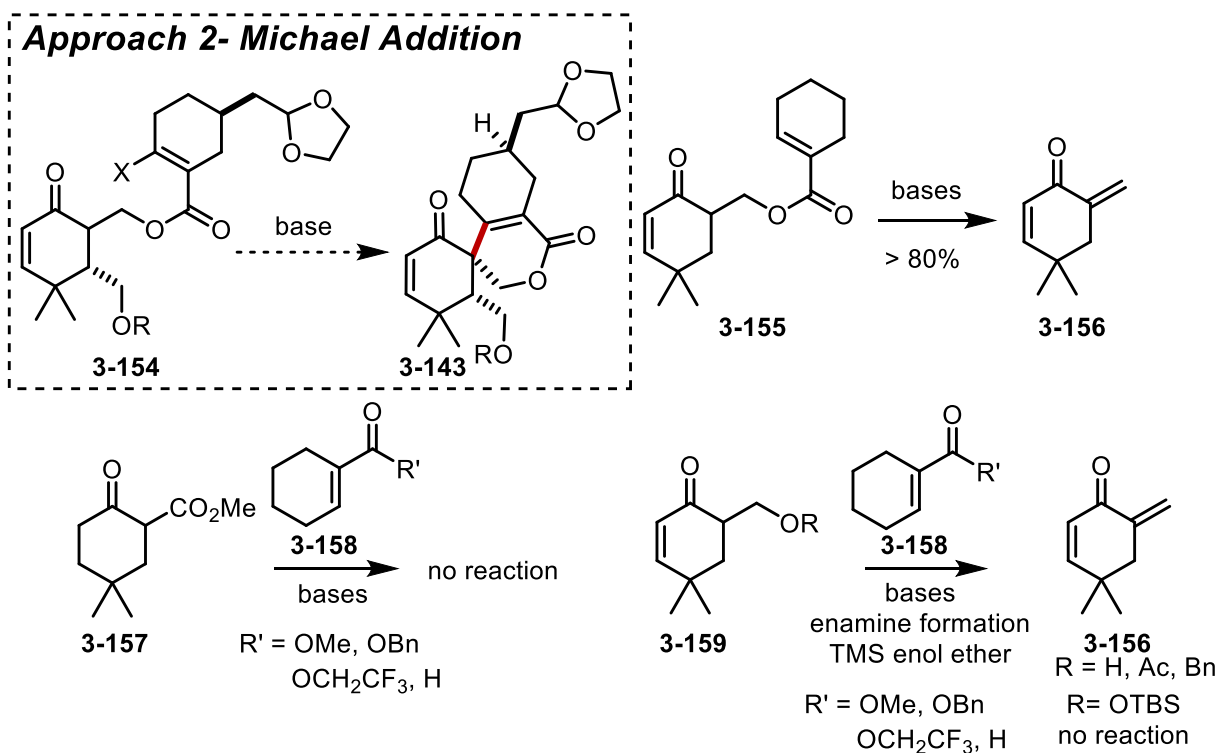


**Figure 3.31-** The second approach towards a common intermediate to the *ent*-kaurene diterpenoids.

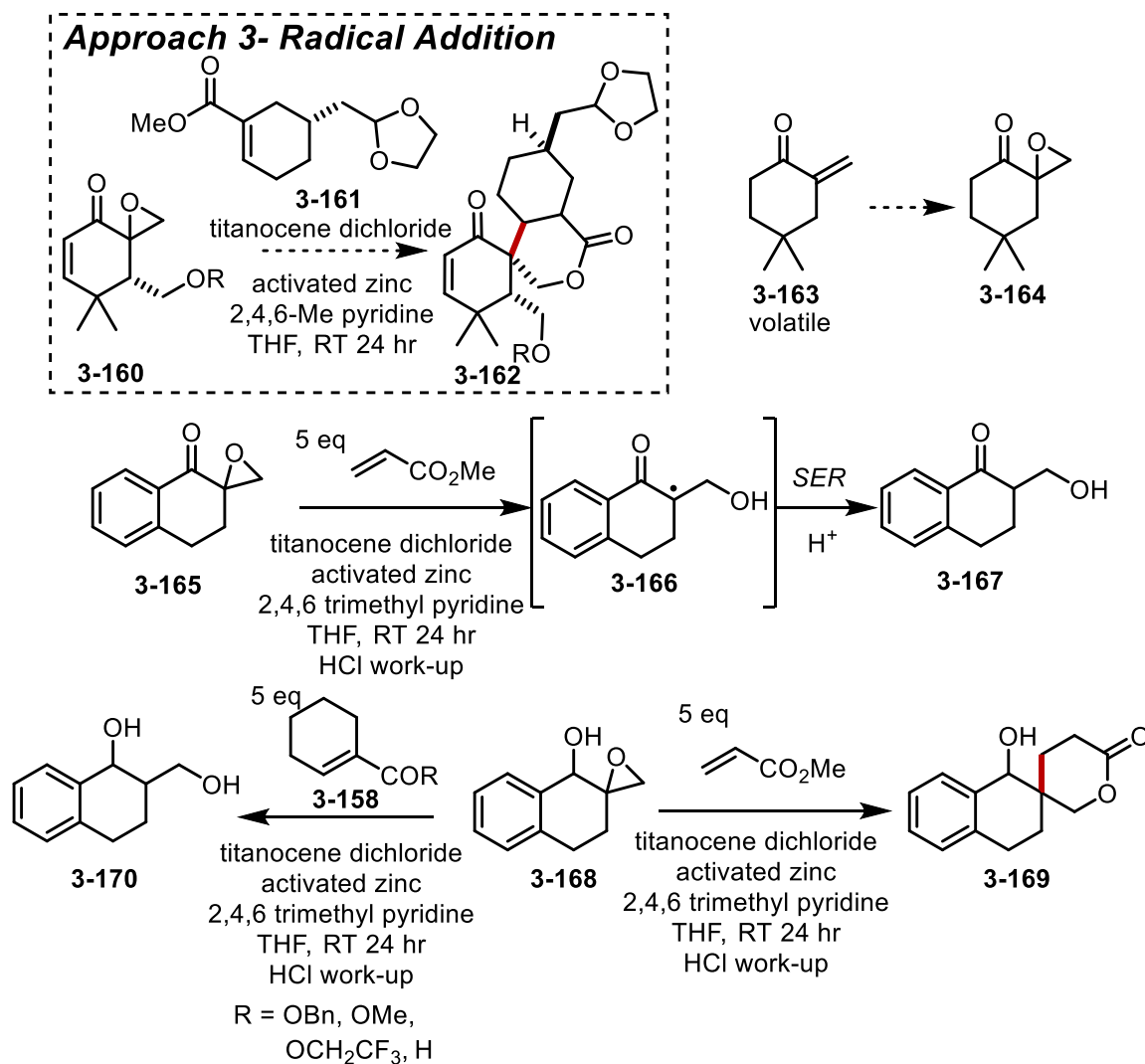


**Figure 3.32-** The third approach towards a common intermediate to the *ent*-kaurene diterpenoids.

In our third approach we hoped that a nucleophilic radical, generated by the single electron reduction (SER) of an epoxide like **3-160** could react intermolecularly with an enone such as **3-161** and then subsequent lactonization would form common intermediate **3-162** (Figure 3.32).<sup>46,71</sup> We initially hoped to use a model system epoxide **3-164**, but we encountered volatility problems that prompted us to redesign our model system studies to utilize keto epoxide **3-165**. Unfortunately, upon subjection to titanocene-mediated SER the tertiary radical **3-166** was not reactive enough to productively interact with methyl acrylate and instead underwent a second SER to an enolate which upon protonation led to epoxide reduction product **3-167**. In response,

we hoped that by reducing the ketone to an alcohol, **3-168**, we would be able to avoid this over reduction problem. Gratifyingly, when **3-168** was subjected to titanocene it did efficiently react with methyl acrylate to form desired lactone **3-169**. However, when we switched to an electrophile, **3-158**, that was more analogous to our desired electrophile, **3-161**, we found no desired Michael addition product. Instead the only isolable product was over reduction product **3-170**. Taken together these approaches highlight the inherent challenges with constructing this bond via a Michael addition. Either in a single electron process or a two-electron process, Michael acceptors such as **3-158** are too unreactive to outcompete side reactions. These results prompted us to totally rethink our strategy.

Our fourth strategy involved a 6-exo-trig cyclization via a Mizoroki-Heck reaction (Figure **3.33**). A vinyl halogen, or pseudo-halogen, such as **3-171**, could be a substrate for an intramolecular Mizoroki-Heck reaction would provide common intermediate **3-172**. This approach was not without complications, The A ring product is less oxidized than originally planned, though this would provide simpler access to more A ring functionalization present in the *ent*-kaurene diterpenoids. Additionally, 6-exo-trig cyclizations from Mizoroki-Heck reactions are rare as are Heck reactions with beta-carbonyls which can chelate transition metals after oxidative addition preventing the complex from undergoing productive migratory insertion. Finally, the allylic ester is a suitable electrophile for oxidative addition providing an alternative reaction pathway that proceeds through a palladium-allyl species that would provide a diene product rather than the desired Heck product.

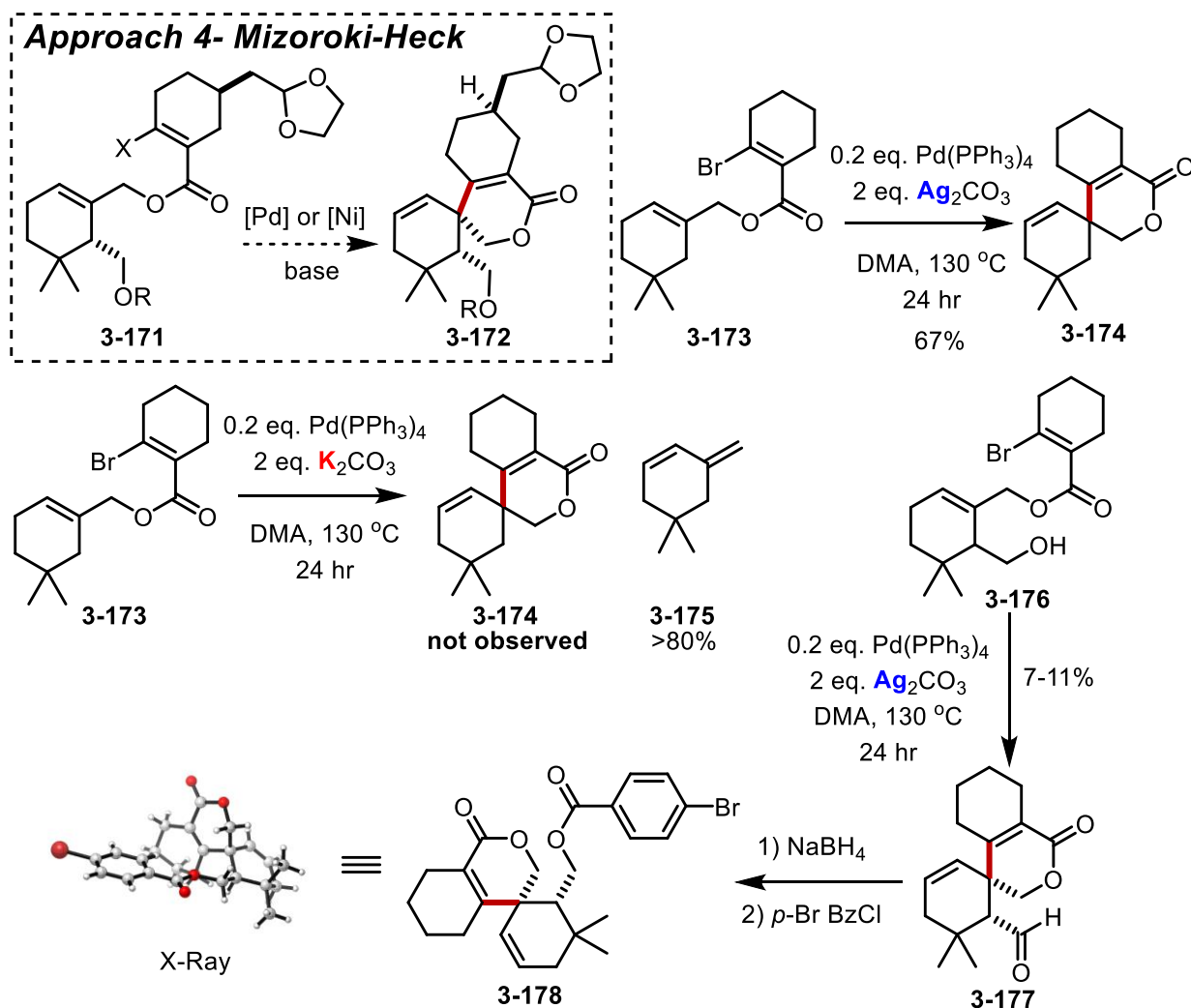


**Figure 3.33-** The fourth approach towards the *ent*-kaurene diterpenoids successfully provides the desired product.

Despite these potential pitfalls, we constructed a vinyl bromide model system **3-173** which we subjected to palladium tetrakis and potassium carbonate. Unfortunately, we saw exclusive formation of the volatile diene, **3-175**, rather than the desired **3-174**. We hoped that a Lewis acid would be capable of promoting the desired oxidative addition and silver salts are well precedented to promote oxidative addition.<sup>72</sup> We found that by switching to silver carbonate under otherwise identical conditions that we efficiently observed **3-174**. We knew that the addition of steric bulk around the sites of reactivity could impact our system and additionally we needed this transformation to be highly diastereoselective. Fortunately, we found that **3-176** was

converted to **3-177** which was derivatized to **3-178**, crystallized and the relative configuration unambiguously determined to be the desired configuration.

### Chapter 3.3 The synthesis of a common intermediate towards the *ent*-kaurene diterpenoids

#### Chapter 3.3.1 Synthesis of the A ring fragment

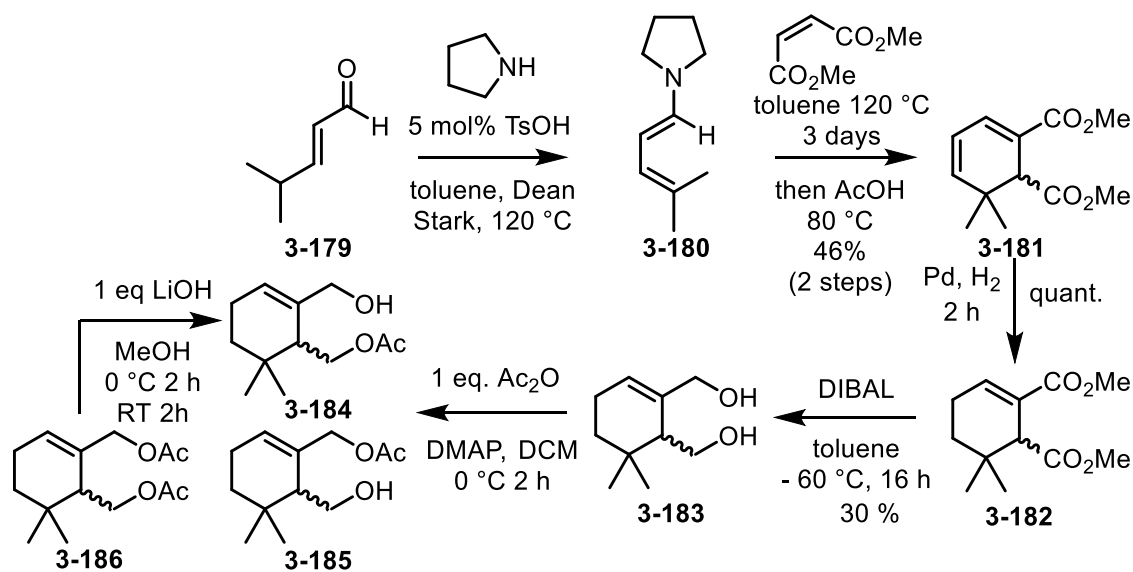


**Figure 3.34-** First approach to A ring fragment **3-184**.

In order to both synthesize and study the conversion of **3-171** to **3-172** we needed to construct an A ring fragment that we could link to a C ring fragment via an esterification. Our first approach was based on a published approach to **3-183** that proceeds via a Diels-Alder reaction.<sup>73</sup> Aldehyde **3-179** is converted to an enamine diene to give **3-180**. Unfortunately, this diene, though quite electronically activated, is sterically encumbered to efficiently promote a Diels-Alder reaction with dimethyl malonate. The effect of which is a sluggish reaction even at 120 °C to form **3-181**. This meant that it was unlikely to succumb to an enantioselective Diels Alder reaction as they almost exclusively require lower temperatures to maintain high

enantiomeric excesses.<sup>74</sup> Selective hydrogenation of **3-181** followed by a careful reduction to **3-183** provided a platform with which to explore protecting group strategies. The challenge here was selectively installing a protecting group. Using one equivalent acetic anhydride we could observe a combined 60% yield of a 2:1:2 ratio of desired **3-184** to undesired **3-185**, to doubly protected **3-186**. The bis acetate **3-186** could be somewhat selectively deacetylated to **3-184** providing **3-184** and **3-185** in a 2:1 ratio with 50% conversion. The lack of enantiomeric excess and the challenge in selectively diversifying the diol **3-183** to a monoprotected acetate **3-184** led us to consider alternative approaches.

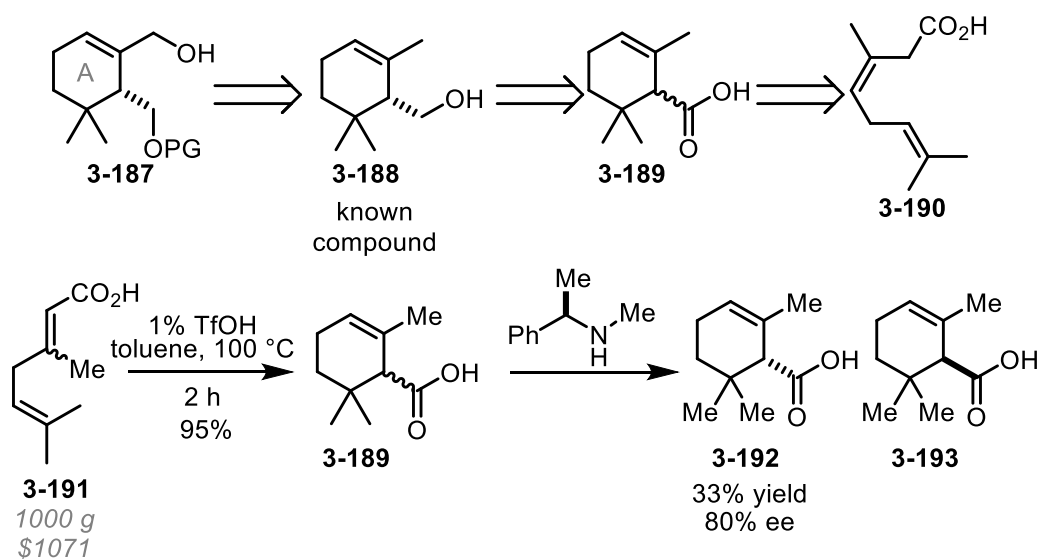


**Figure 3.35-** Second approach to A ring fragment **3-187**.

Our next series of strategies relied on the intermediacy of chiral cyclogeraniol (**3-188**). In our first attempts we took geranic acid (**3-191**) which can be purchased on scale as a mixture of E/Z isomers. We found that catalytic triflic acid could efficiently promote the cyclization to racemic cyclogeranic acid (**3-189**). We then thought that we could take advantage of the availability of **3-189** to promote a chiral resolution to **3-192**.<sup>75</sup> However, in our hands we found that we could isolate at best 33% yield and 80% ee of **3-192**. This rather moderate enantiomeric excess prompted us to explore an alternative strategy.

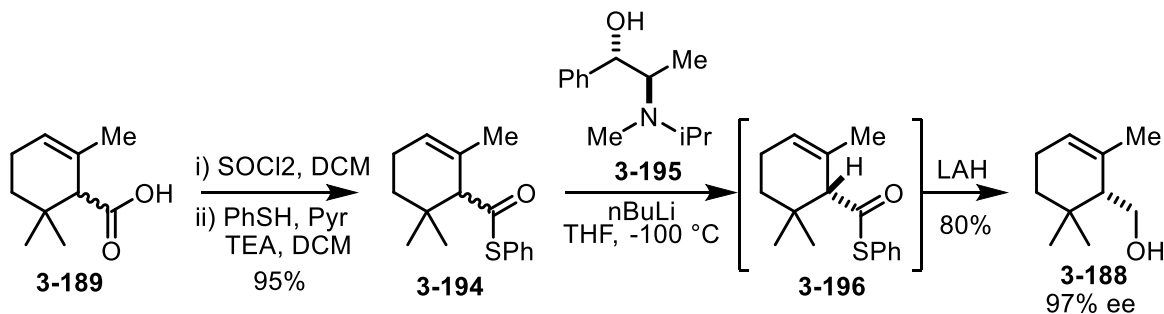


**Figure 3.36-** Successful synthesis of intermediate **3-188**.

We were able to approach the problem of synthesizing **3-188** in high enantiomeric excess. We found that by preparing the thiophenyl ester of cyclogeranic acid **3-194** we could take advantage of an enantioselective protonation strategy to achieve high %ees (Figure 3-36).<sup>76</sup> At -100 °C we formed a stable enolate of **3-194** which could be protonated by N-isopropyl ephedrine (**3-195**) with excellent facial selectivity. chiral thioester **3-196** is reduced in situ to provide desired chiral cyclogeraniol **3-188**.

The next challenge was to oxidize the allylic methyl group to provide **3-187**. Our first strategy was to engage that methyl group in a direct C—H oxidation (Figure 3.37). We first wanted to try a Suarez oxidation to form an allylic iodide **3-199**.<sup>77</sup> This strategy was unsuccessful and so we attempted a Hartwig silylation oxidation sequence which was originally optimized for 1,3 C—H abstraction oxidation sequences.<sup>78</sup> In our case there are no hydrogen atoms on the 3-position so we hoped that the methodology could be extended to a 1,4 C—H abstraction. This ultimately failed to provide **3-200**. Next we hoped that we could perhaps overcome latent selectivity in a Riley-type allylic oxidation.<sup>79</sup> We did observe the desired product **3-202** in an inseparable mixture of oxidation products but in low yield. Finally we employed an approach developed by White and coworkers to use Mn porphyrins to selectively do C—H aminations instead of aziridations.<sup>80</sup> Unfortunately, we were again trying to push the method to a 1,4

functionalization and so did not observe **3-204** and instead we did detect azirane **3-205**. These failures prompted us to attempt an alternative strategy.

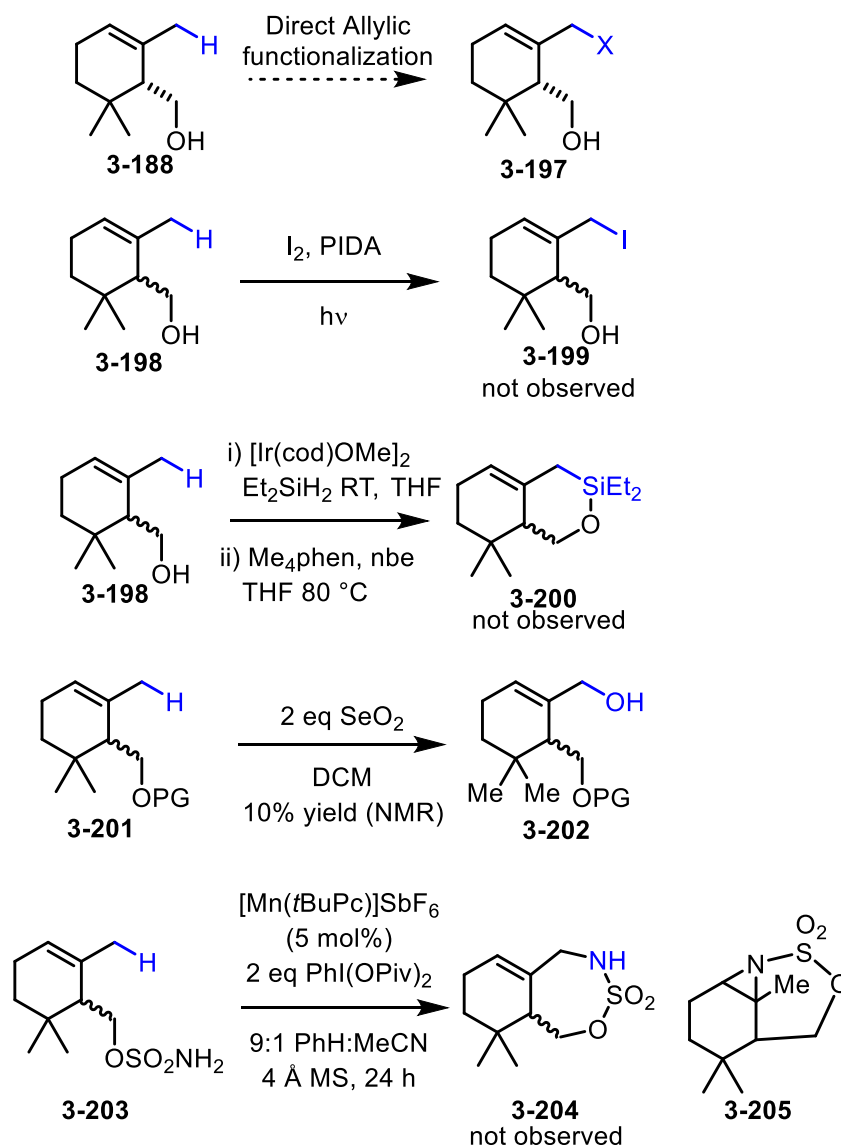


**Figure 3.37-** Attempts to do a directed C-H oxidation towards **3-197**.

Our next strategy relied on first oxidizing the olefin in **3-206** then engaging in a kinetic ring opening to **3-208** and finally attempting to promote a transposition to **3-209** (Figure 3.38). We saw some success in epoxidizing **3-210** and opening the epoxide with a bulky base, LiTMP, to **3-211** in a highly diastereoselective sequence. We then employed a known gold cation catalyzed rearrangement but were disappointed to see very low conversion to **3-213**.<sup>81</sup>



Additionally, when we reisolated **3-211** we saw that it had become distereomerically enriched. So we hypothesized that if we could invert the stereochemistry of the intermediate acetate such as by a Mitsunobu to **3-214**, we would be able to promote the rearrangement in higher yield. Even though the Mitsunobu provided an inseparable 1:1 mixture of acetate **3-214** and desired  $S_N2'$  product **3-213**, we could transform the crude mixture directly to the desired **3-213** using the same method. Though this did provide us with highly enantioenriched **3-213** it relied on two moderately yielding transformations and the LiTMP epoxide opening was completely intolerable of other protecting group strategies. Together these limitations compelled us to continue exploring alternative strategies.

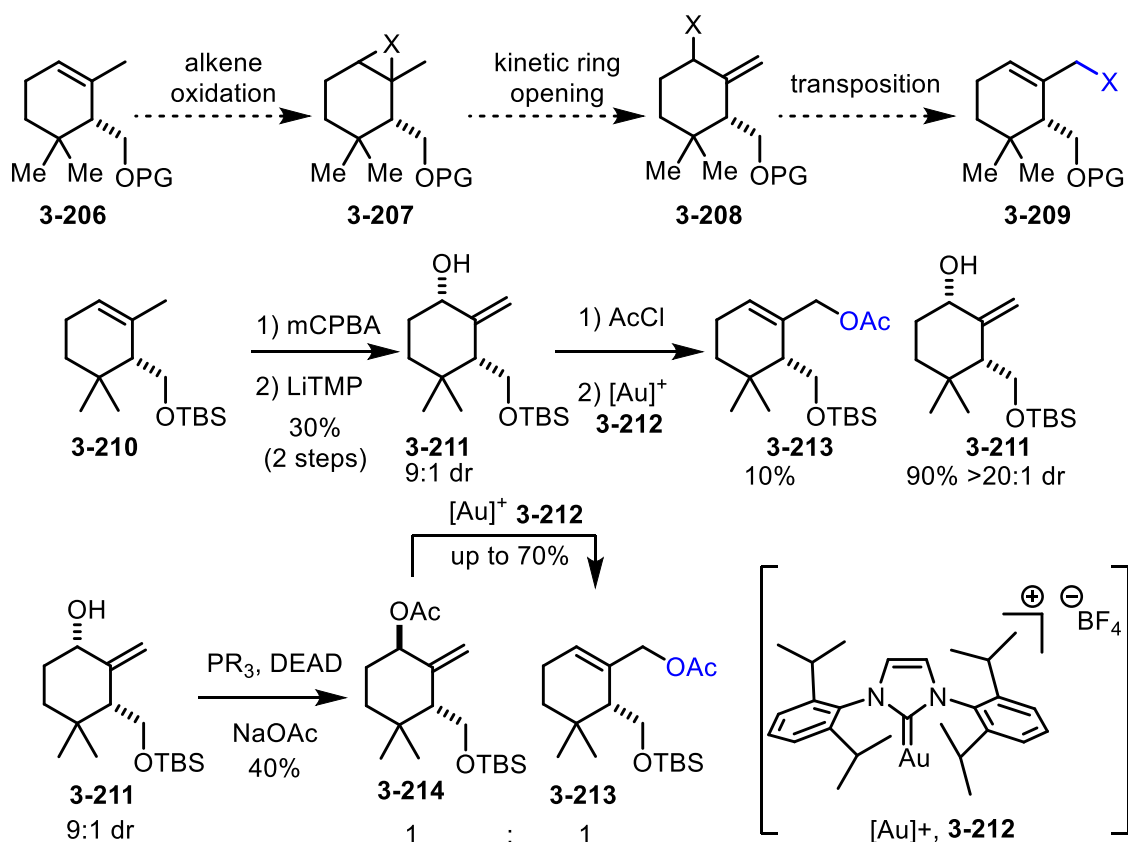


**Figure 3.38-** Initial results via an olefin oxidation, isomerization strategy towards **3-209**.

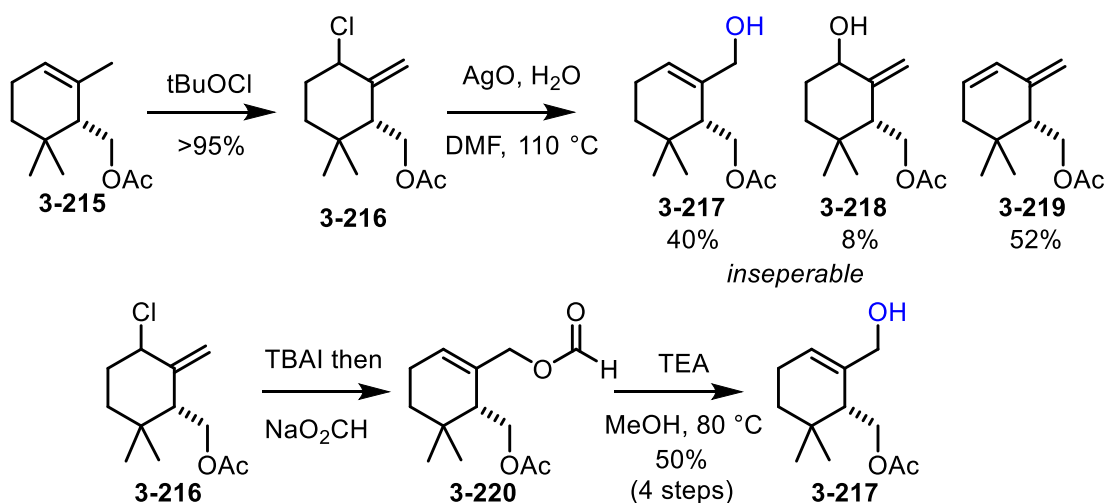


**Figure 3.39-** Current strategy towards A ring fragment **3-217**.

We found that by chlorinating **3-215** we could achieve a kinetic olefinic product without resorting to strong, bulky bases (Figure 3.39).<sup>82</sup> This allowed for a more efficient, less protecting group sensitive approach. We were able to promote a silver (I) oxide directed  $\text{S}_{\text{N}}2'$  of  $\text{OH}$ . However, the selectivity of this approach was suspect. Especially as **3-217** and **3-218** are inseparable. This could be overcome by an  $\text{S}_{\text{N}}2'$  reaction with iodide which is not isolated but instead substituted with sodium formate. Primary formate **3-220** could be selectively methanolized at elevated temperatures. This allowed gram scale access to **3-217** in 97% ee with 36% yield from geranic acid (**3-191**).

### Chapter 3.3.2 Synthesis of the C ring fragment

Our successful strategy towards **3-224** relies on forming symmetrical ketone **3-222**.<sup>83</sup> This was achieved by taking monoacetal **3-221** and subjecting it to an HWE olefination which provides a mixture of olefin isomers which can be immediately hydrogenated. The ester is reduced, and the acetal is hydrolyzed. It should be noted that the alcohol here is incredibly water-soluble necessitating washing with saturated sodium sulfate in order to successfully extract it.

Finally, a TBS protection yields **3-222** in 65% yield over five steps requiring only one purification on a one mole scale in a single pass.

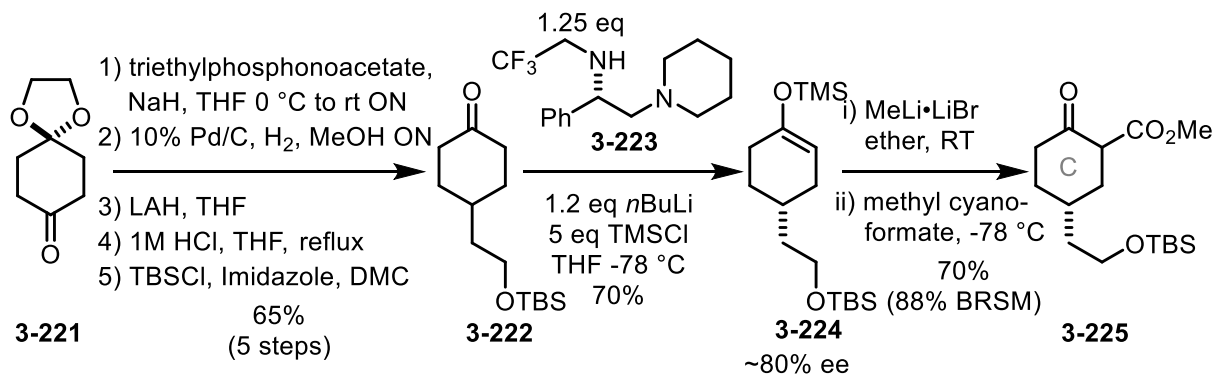


**Figure 3.40-** Current strategy towards C ring fragment **3-225**.

This symmetric ketone **3-222** was subjected to a desymmetrizing deprotonation using a chiral lithium amide generated from Koga's amine **3-223**.<sup>84</sup> We tried to directly convert the in situ generated chiral lithium enolate to **3-225** in a single step but unfortunately it proceeded with limited yield. We found that by isolating and purifying a TMS enol ether **3-224** we could then transmetallate to a lithium enolate which could be captured by Mander's reagent though it does require the addition of HMPA which can provide **3-225**. It should be noted that this transformation is very sensitive to the quality of MeLi used. It works best with Acros methyl lithium, lithium bromide conjugate. Additionally, we explored alternative protecting group strategies and found that carbonyl based protecting groups were nucleophilically deprotected by methyl lithium. Benzyl-type protecting groups were eliminated off by methyl lithium over the course of the transformation of **3-224** to **3-225**. Additionally, the enantiomeric excess of **3-225** could only be provided at 9:1 er, or 80% ee. Taken together these highlight just how important the modification to the A ring route (*vide supra*) were to provide high %ees and broad protecting group compatibilities. Another challenge that needed to be overcome was the determination of the %ee. No conditions could be uncovered that could determine the %ee by chiral HPLC, chiral GC, or chiral SFC. We found success using a two step procedure in which first we deprotected the TBS group to **3-226** and then we formed a Mosher ester, **3-228**, and analyzed the %ee by NMR (Figure 3.41).

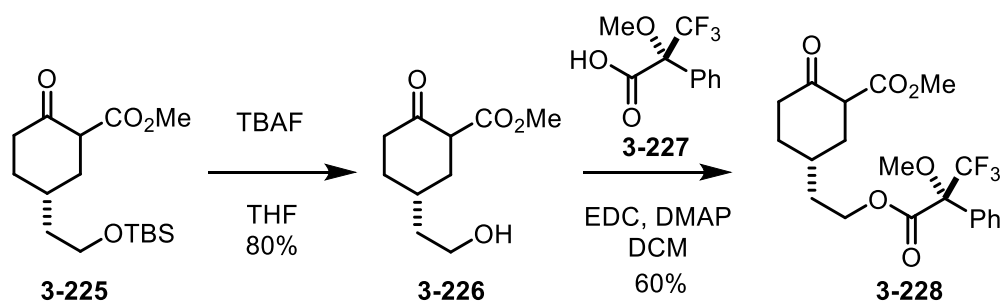


**Figure 3.41-** Methodology required to determine the enantiomeric excess of **3-225**.

Chapter 3.3.3 Combining the A ring and C ring fragments towards a common intermediate to the *ent*-kaurenes

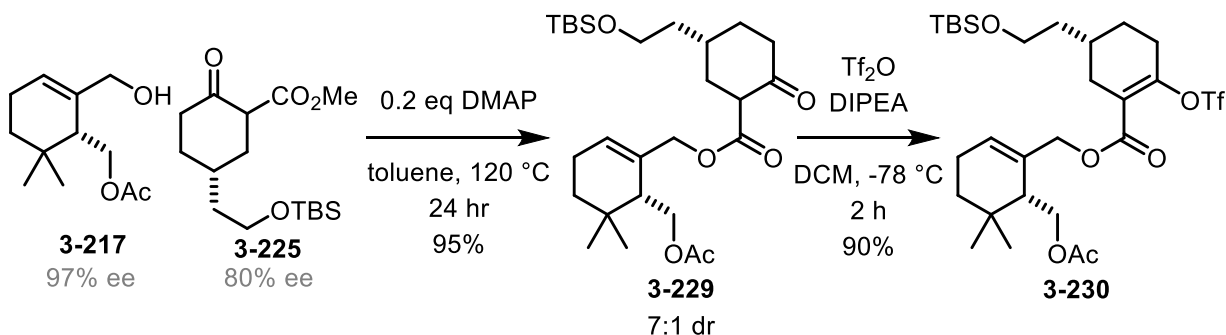


**Figure 3.42-** The synthesis of Mizoroki-Heck substrate **3-230**.

Gratifyingly the first of two key bonds towards a common intermediate to the *ent*-kaurene diterpenoids was relatively straightforward. A ring fragment **3-217** and C ring fragment **3-225** were combined via a DMAP promoted transesterification reaction which is both high yielding and selective for the methyl beta-keto ester over the A ring acetate. Then transester **3-229** was smoothly converted to vinyl triflate and Mizoroki-Heck substrate **3-230**. At this point all that remained towards a common intermediate was the discovery and development of an intramolecular 6-exo trig Mizoroki-Heck reaction.

A Mizorkoi-Heck reaction on a substrate such as **3-230** could provide a myriad of products (Figure 3.42). If the transition metal catalyst inserted into the allylic ester to generate a metal allyl species, we would expect to observe a diene **3-237**. If the desired oxidative addition occurs a metal hydride or proton source could provide a net proto-demetalated product **3-236**. Additionally, at elevated temperatures even mild Lewis acids such as potassium or silver cations could deprotect a silyl ether protecting group which could return a desilylated substrate **3-235**. Even if the desired C—C bond is formed this reaction proceeds via an intermediate metal

hydride species which is capable of transposing olefinic products which could provide with either **3-231** or transposed olefin **3-232** and if these products are desilated the reaction could additionally provide **3-233** or **3-234**. These challenges loomed large as we continue to optimize this transformation.

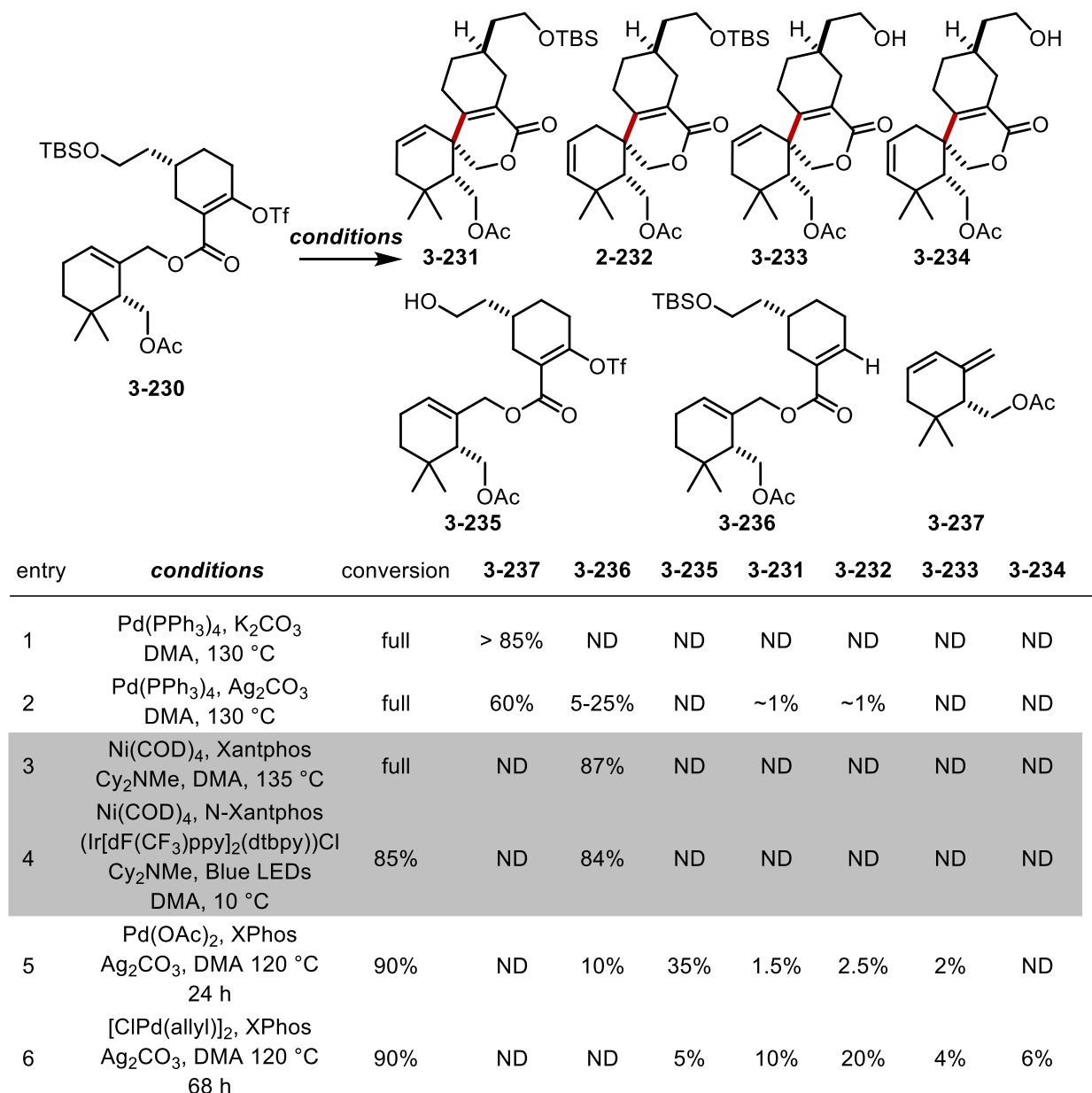


**Figure 3.43-** Current efforts towards the optimization of a Mizoroki-Heck reaction towards **3-231** and **3-232**.

We worked in concert with the Merck Process Chemistry catalysis group to conduct HTE on this reaction screening over 800 different reaction condition combinations. We evaluated 48 separate ligands in palladium catalyzed processes with Pd(OAc)<sub>2</sub> and a variety of combinations of bases, temperatures and solvents. Additionally, we explored the idea that a nickel catalyzed

Mizoroki-Heck reaction either with heat or in the presence of a photocatalyst would promote the reaction as well and were disappointed to find only efficient proto-demetalation to **3-236**. We took the best ligands from our screen at Merck and evaluated different sources of palladium hypothesizing that insitu generated silver acetate might be detrimental to the reaction. We found both PdCl<sub>2</sub> and [ClPd(allyl)] dimer out performed Pd(OAc)<sub>2</sub>. Under the optimal reaction conditions (entry 6, Figure 3.42) we have observed on 50 mg scale up to 87% yield of combined desired Heck products though more typical yields are 30-40% as represented in Figure 3.42.

Current work continues 1) better optimize this Mizorkoi-Heck reaction as we 2) work towards elaborating the common intermediates which we prepare in a combined 12% yield in 11 longest linear steps.

### Bibliography-Chapter 3

1. Chinou, I. *Curr. Med. Chem.* **2005**, *12*, 1295.
2. Kataev, V.E.; Khaybullin, R.N.; Sharipova, R.R.; Strobykina, I.Y. *Rev. J. Chem.* **2011**, *1*, 93.
3. Giles, P.M., Jr. *Pure Appl. Chem* **1999**, *71*, 587.
4. Riehl, P.S.; DePorre, Y.C.; Armaly, A.M.; Grosio, E.J.; Schindler C.S. *Tetrahedron* **2015**, *71*, 6629.
5. Sun, H.-D.; Huang, S.-X.; Han, Q.-B. *Nat. Prod. Rep.* **2006**, *23*, 673.
6. Yagi, S.J. *Kyoto Med. Soc.* **1910**, *7*, 30.
7. (a) Kubota, T.; Matsuura, T.; Tsutsui, T.; Uyeo, S.; Irie, H.; Numata, A.; Fujita, T.; Suzuki, T. *Tetrahedron* **1966**, *22*, 1659. (b) Iiatata, Y.; Natsume, M. *Tetrahedron* **1964**, *20*, 1257.
8. *Stevia – the genus stevia*. Douglas Kinghorn, A., Ed.; CRC: 1992.
9. Hanson, J.R.; De Oliveira, B.H. *Nat. Prod. Rep.* **1993**, *10*, 301.
10. (a) Bridel, M.; Lavieille, R. *J. Pharm. Chim.* **1931**, *14*, 99; (b) Bridel, M.; Lavieille, R. *J. Pharm. Chim.* **1931**, *14*, 369.
11. (a) Mosettig, E.; Nes, W.R. *J. Org. Chem.* **1955**, *20*, 884; (b) Wood, H. B.; Allerton, R.; Diehl, H.W.; Fletcher, H.G. *J. Org. Chem.* **1955**, *20*, 875; (c) Mosettig, E.; Beglinger, U.; Dolder, F.; Lichti, H.; Quitt, P.; Waters, J.A. *J. Am. Chem. Soc.* **1963**, *85*, 2305.
12. Toyomasu, T.; Sassa, T. *Diterpenes in Comprehensive Natural Products II. Chemistry and Biology*. Mander, L., Liu, H.-W., Eds.; Newnes: 2010; Vol. 1.
13. Dewick, P.M. *Medicinal Natural Products. A Biosynthetic Approach*; Wiley, 2008.
14. MacMillan, J.; Beale, M.H. *Diterpene Biosynthesis in Comprehensive Natural Product Chemistry*; Cane, D. E., Ed.; Pergamon: 2000.
15. Tanabe, S.; Nishikawa, H. *Jpn. J. Bact.* **1954**, *9*, 475.
16. Arai, T.; Koyama, Y.; Suenaga, T.; Morita, T. *J. Antibiotics Ser. A* **1963**, *16*, 132.
17. Kubo, I.; Taniguchi, M.; Satomura, Y., Kubota, T. *Agric. Biol. Chem.* **1974**, *38*, 1261.
18. Sun, H.D.; Xu, Y.L.; Jiang, B. *Diterpenoids from Isodon Species*; Science: Beijing, China, 2001.
19. Huyen, N. T. T.; Eiamphungporn, W.; Mäder, U.; Liebeke, M.; Lalk, M.; Hecker, M.; Helmann, J. D.; Antelmann, H. *Molecular Microbiology* **2009**, *71*, 876.
20. (a) Arai, T.; Koyama, Y.; Suenaga, T.; Kaji, H. *Chemotherapy* **1961**, *9*, 404. (b) Fujita, E.; Nagao, Y.; Kaneko, K.; Nakazawa, S.; Kuroda, H. *Chem. Pharm. Bull.* **1976**, *24*, 2118.
21. Zhao, Y.; Niu, X.-M.; Qian, L.-P.; Liu, Z.-Y.; Zhao, Q.-S.; Sun, H.-D. *Eur. J. Med. Chem.* **2007**, *42*, 494.
22. Shay, J. S.; Zou, Y.; Hiyama, E.; Wright, W.E. *Human Mol. Genetics* **2001**, *10*, 677.
23. Blackburn, E. *Mol. Cancer Res.* **2005**, *3*, 477.
24. Wang, H.; Ye, Y.; Pan, S.-Y.; Zhu, G.-Y.; Li, Y.-W.; Fong, D.W.F.; Yu, Z.-L. *Phytomedicine* **2011**, *18*, 163.
25. (a) Ma, Y.-C.; Ke, Y.; Zi, X.; Shi, X.J.; Liu, H.-M. *Curr. Cancer Drug Targets* **2013**, *13*, 611. (b) Simon, A.; Haj-Yehia, A.; Levi-Schaffer, F. *Apoptosis* **2000**, *5*, 415.

26. Jian, H.; Lijun, W.; Tashiro, S.; Onodero, S.; Ikejima, T. *J. Pharm. Sci.* **2008**, *107*, 370.
27. Li, L.; Yue, G.G.L.; Lau, C.B.S.; Sun, H.; Fung, K.P.; Leung, P.C.; Han, Q.; Leung, P.S. *Tox. Appl. Pharmacol.* **2012**, *262*, 80.
28. (a) Porta C.; Paglino C.; Mosca A. *Front. Oncol.* **2014**, *4*, 64. (b) Huang, W.C.; Hung M.C. *J. Formos. Med. Assoc.* **2009**, *108*, 180.
29. Hu, H.; Yang, Y.; Xu, X.; Shen, H.; Shu, Y.; Ren, Z.; Li, X.; Shen, H.; Zeng, H. *Acta Pharmacol. Sin* **2007**, *1* 1819.
30. Deng, R.; Tang, J.; Xia, L.-P.; Li, D.-D.; Zhou, W.-J.; Wang, L.-L.; Feng, G.-K.; Zeng, Y.-X.; Gao, Y.-H.; Zhu, X.-F. *Mol. Cancer Ther.* **2009**, *8*, 873.
31. Yewale, C.; Baradia, D.; Vhora, I.; Patil, S.; Misra, A. *Biomaterials* **2013**, *34*, 8690.
32. Kang, N.; Zhang, J.-H.; Qiu, F.; Tashiro, S.; Onodera, S.; Ikejima, T. *Cancer Letters* **2010**, *294*, 147.
33. Karin, M. *Cold Spring Harb. Perspect. Biol.* **2009**, *1*, a000141.
34. Leung, C.-H.; Grill, S.P.; Lam, W.; Gao, W.; Sun, H.-D.; Cheng, Y.-C. *Mol. Pharmacol.* **2006**, *70*, 1946.
35. Ban, O. J.; Oh, J. H.; Hwang, B. J.; Moon, D. C.; Jeong, H.-S.; Lee, S.; Kim, S.; Lee, H.; Kim, K.-B.; Han, S. B.; Hong, J. T. *Mol. Cancer Ther.* **2009**, *53*, 1613.
36. Kong, L.-M.; Deng, X.; Zuo, Z.-L.; Sun, H.-D.; Li, Y. *Oncotarget* **2014**, *5*, 11354.
37. Fujita, E.; Node, M. *Fortschritte der Chemie organischer Naturstoffe/Progress in the Chemistry of Organic Natural Products*; Springer, 1984.
38. Church, R. F.; Ireland, R. E.; Marshall, J. A. *J. Org. Chem.* **1966**, *31*, 2526.
39. (a) Stork, G.; Meisels, A.; Davies, J.E. *J. Am. Chem. Soc.* **1963**, *85*, 3419. (b) Stork, G. J. *Am. Chem. Soc.* **1947**, *69*, 576.
40. (a) Fujita, E.; Shibuya, M.; Nakamura, S.; Okada, Y.; Fujita, T. *J. Chem. Soc. Chem. Commun.* **1972**, 1107. (b) Fujita, E.; Shibuya, M.; Nakamura, S.; Okada, Y.; Fujita, T. *J. Chem. Soc. Chem. Commun.* **1974**, 165.
41. Ziegler, F. E.; Kloek, J. A. *Tetrahedron* **1977**, *33*, 373.
42. Snider, B. B.; Kiselgof, J. Y.; Foxman, B. M. *J. Org. Chem.* **1998**, *63*, 7945.
43. Cherney, E. C.; Green, J. C.; Baran, P. S. *Angew. Chem. Int. Ed.* **2013**, *52*, 9019.
44. Mori, K.; Matsui, M. *Tetrahedron* **1968**, *24*, 3095.
45. (a) Kenny, M. J.; Mander, L. N.; Sethi, S. P. *Tetrahedron Lett.* **1986**, *27*, 3923. (b) Kenny, M. J.; Mander, L. N.; Sethi, S. P. *Tetrahedron Lett.* **1986**, *27*, 3927.
46. Cha, J. Y.; Yeoman, J. T. S.; Reisman, S. E. *J. Am. Chem. Soc.* **2011**, *133*, 14964.
47. (a) Fehr, C.; Galindo J. *Helv. Chim. Acta.* **1995**, *78*, 539. (b) Tanimoto, H.; Oritani, T. *Tetrahedron* **1997**, *53*, 3527.
48. Yeoman, J. T. S.; Mak, V. W.; Reisman, S. E. *J. Am. Chem. Soc.* **2013**, *135*, 11764.
49. Li, S.-H.; Wang, J.; Niu, X.-M.; Shen, Y.-H.; Zhang, H. J.; Sun, H.-D.; Li, M.-L.; Tian, Q.-E.; Lu, Y.; Cao, P.; Zheng, Q.-T. *Org. Lett.* **2004**, *6*, 4327.
50. Krawczuk, P. J.; Schöne, N.; Baran, P. S. *Org. Lett.* **2009**, *11*, 4774.
51. Gong, J.; Lin, G.; Li, C. C.; Yang, Z. *Org. Lett.* **2009**, *11*, 4770.
52. Gu, Z.; Zakarian, A. *Org. Lett.* **2011**, *13*, 1080.
53. (a) Peng, F.; Yu, M.; Danishefsky, S. J. *Tetrahedron Lett.* **2009**, *50*, 6586. (b) Peng, F.; Danishefsky, S. J. *Tetrahedron Lett.* **2011**, *52*, 2104.



54. Nicolaou, K. C.; Dong, L.; Deng, L. J.; Talbot, A. C.; Chen, D. Y. K. *Chem. Commun.* **2010**, 70.
55. Zheng, C.; Dubovyk, I.; Lazarski, K. E.; Thomson, R. J. *J. Am. Chem. Soc.* **2014**, *136*, 17750.
56. Cernijenko, A.; Risgaard, R.; Baran, P. S. *J. Am. Chem. Soc.* **2016**, *138*, 9425.
57. Du, G.; Gong, H.-Y.; Feng, K.-N.; Chen, Q.-Q.; Yang, Y.-L.; Fu, X.-L.; Lu, S.; Zeng, Y. *Phytochemistry* **2019**, *158*, 96.
58. As of July 30, 2019 a SciFinder search for vendors of ericalyxin B (**3-19**) indicates that it can be purchased from multiple vendors: 5 mg for ~\$950. Additionally online vendors indicate they would prepare bulk quantities on demand, presumably at some significant expense.
59. Leizer, A. L.; Alvero, A. B.; Fu, H. H.; Holmberg, J. C.; Cheng, Y.-C.; Silasi, D.-A.; Rutherford, T.; Mor, G. *American Journal of Reproductive Immunology* **2011**, *65*, 438.
60. Zhang, Y.-W.; Jiang, X.-X.; Chen, Q.-S.; Shi, W.-Y.; Wang, L.; Sun, H.-D.; Shen, Z.-X.; Chen, Z.; Chen, S.-J.; Zhao, W.-L. *Experimental Hematology* **2010**, *38*, 191.
61. Leung, C.-H.; Grill, S. P.; Lam, W.; Gao, W.; Sun, H.-D.; Cheng, Y.-C. *Mol. Pharmacol.* **2006**, *70*, 1946.
62. Lu, Y.-M.; Chen, W.; Zhu, J.-S.; Chen, W.-X.; Chen, N.-W. *Mol. Med. Rep.* **2016**, *13*, 2235.
63. Yu, X.; He, L.; Cao, P.; Yu, Q. *PLOS ONE* **2015**, *10*, e0128406.
64. Li, L.; Zhao, S. L.; Yue, G. G. L.; Wong, T. P.; Pu, J. X.; Sun, H. D.; Fung, K. P.; Leung, P. C.; Han, Q. B.; Lau, C. B. S.; et al. *Phytomedicine* **2018**, *44*, 56.
65. Li, L.; Yue, G. G. L.; Lau, C. B. S.; Sun, H.; Fung, K. P.; Leung, P. C.; Han, Q.; Leung, P. S. *Toxicology and Applied Pharmacology* **2012**, *262*, 80.
66. Yang, Y.; Sun, H.; Zhou, Y.; Ji, S.; Li, M. *Nat. Prod. Res.* **2009**, *23*, 1007.
67. Zhou, W.; Cheng, Y. *Huaxue Xuebao* **1990**, *48*, 1185.
68. Zhu, L.; Ma, W.; Zhang, M.; Lee, M. M.-L.; Wong, W.-Y.; Chan, B. D.; Yang, Q.; Wong, W.-T.; Tai, W. C.-S.; Lee, C.-S. *Nat. Commun.* **2018**, *9*, 1.
69. (a) Mathvink, R.; Boger, D. *J. Org. Chem.* **1992**, *57*, 1429. (b) Dudley, G.; Tan, D.; Kim, G.; Tanski, J.; Danishevsky, S. *Tet. Lett.* **2001**, *42*, 6789.
70. (a) Taylor, S. J.; Duffey, M. O.; Morken, J. P. *J. Am. Chem. Soc.* **2000**, *122*, 4528. (b) Zhao, C.-X.; Duffey, M. O.; Taylor, S. J.; Morken, J. P. *Org. Lett.* **2001**, *3*, 1829. (c) Lam, H. W.; Murray, G. J.; Firth, J. D. *Org. Lett.* **2005**, *7*, 5743. (d) Lumby, R. J.; Joensuu, P. M.; Lam, H. W. *Tetrahedron* **2008**, *64*, 7729. (e) Doi, T.; Fukuyama, T.; Minamino, S.; Ryu, I. *Synlett.* **2006**, *18*, 3013. (f) Kiyooka, S.; Shimizu, A.; Torii, S. *Tet. Lett.* **1998**, *39*, 5237.
71. Morcillo, S. P.; Miguel, D.; Campaña, A. G.; Cienfuegos, L. A.; Justicia, J. Cuerva, J. M. *Org. Chem. Front.* **2014**, 15.
72. *The Mizoroki-Heck Reaction*. Oestreich, M., Ed.; John Wiley & Sons: 2009.
73. Snowden, R. L.; Linder, S. M. *Helv. Chim. Acta.* **1988**, *71*, 1587.
74. *Enantioselective Chemical Synthesis: Methods, Logic and Practice*. Corey, E. J.; Kürti, L., Ed.; Direct Book Publishing: 2010.
75. Oritani, T.; Yamashita, K. *Agric. Biol. Chem.* **1987**, 1271.
76. Fehr, C.; Galindo, J. *Angew. Chem.* **1994**, 1967.

77. de Armas, P.; Carrow, R.; Concepción, J.I.; Fransisco, C.G.; Hernández, R.; Suárez, E. *Tet. Lett.* **1985**, 2493.
78. Li, B.; Driess, M.; Hartwig, J.F. *J. Am. Chem. Soc.* **2014**, 6586.
79. Mlochowski, J.; Wójtowicz-Mlochowska, H. *Molecules* **2015**, 10205.
80. Paradine, S.P.; Griffin, J.R.; Zhao, J.; Petronico, A.L.; Miller, S.M.; White, M.C. *Nat. Chem.* **2015**, 987.
81. Marion, N.; Gealageas, R.; Nolan, S.P. *Org. Lett.* **2007**, 2653.
82. Nakamura, E.; Aoki, S.; Sekiya, K.; Oshino, H.; Kuwajima, I. *J. Am. Chem. Soc.* **1987**, 8056.
83. Ito, S.; Tosaka, A.; Hanada, K.; Shibuya, M.; Ogasawara, K.; Iwabuchi, Y. *Tetrahedron: Asymmetry* **2008**, 19, 176.
84. Aoki K.; Tomioka, K.; Noguchi, H.; Koga, K. *Tetrahedron* **1997**, 13641.

## Chapter 4 Lewis Base-Catalyzed Reductive Aldol Reaction to Access Quaternary Carbons

### Chapter 4.1 Introduction

Toxicity is known to be the leading cause for drug candidates failing clinical trials.<sup>1</sup> Recent studies suggest that compounds of higher complexity, as measured by the saturation and presence of sp<sup>3</sup>-hybridized quaternary carbon centers, have fewer off-target effects, show less toxicity, and have a greater success rate in the clinic.<sup>2</sup> However, synthetic access to molecules with increased complexity requires successful methods for the construction of quaternary carbon centers.<sup>3</sup> Despite recent advances, synthetic challenges in the formation of quaternary carbon centers still exist, and prove even more difficult when the desired quaternary carbons are chiral.<sup>3a</sup> Additionally, quaternary carbon centers in acyclic molecules and molecular fragments remain challenging to access.<sup>3b,c, 4</sup> Furthermore, most of the methods currently available for the construction of quaternary carbons rely on metal-based catalysts, and the development of alternative catalytic systems was recently described as a future challenge.<sup>3b</sup> Here we describe a method for the diastereoselective construction of  $\beta$ -hydroxyl lactones and lactams bearing  $\alpha$ -quaternary carbon centers that relies on simple, electronically differentiated phosphine oxides as Lewis base catalysts that enables access to structural motifs prevalent in many biologically relevant target structures.<sup>5, 6</sup>

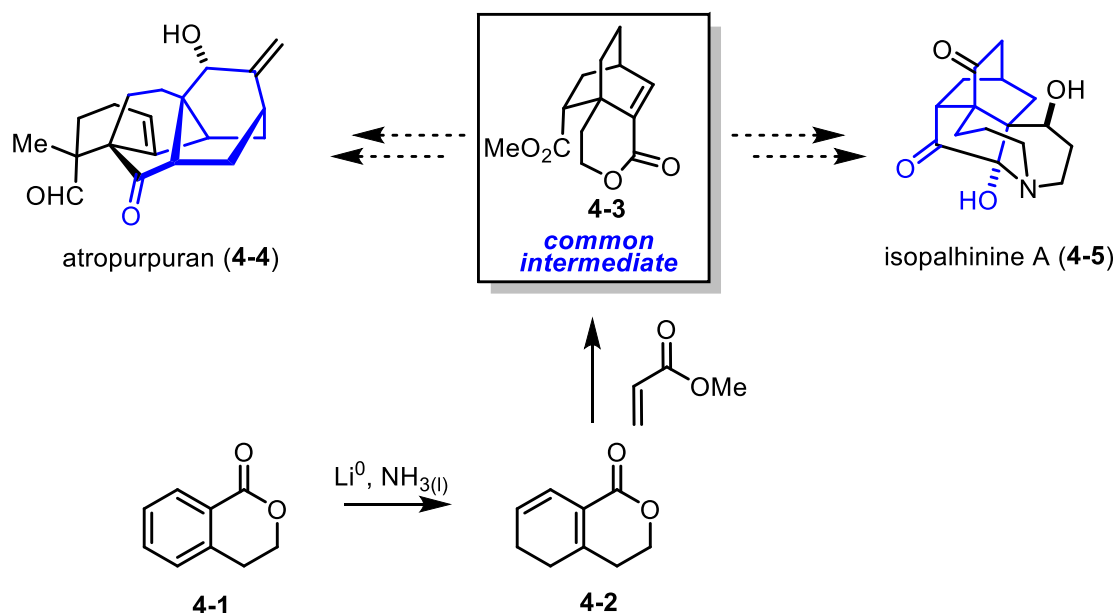


**Figure 4.1-** Synthetic strategies towards atropurpuran (**4-4**) and isopalhinine A (**4-5**) rely on common core structure and common intermediate **4-3**.

In fact, this methodology was inspired by a synthetic challenge presented by ongoing synthetic work in our lab (Figure 4.1). We identified a common core structural motif in both atropurpuran (**4-4**) as well as isopalhinine A (**4-5**) and hypothesized that rapid assembly of that core structure would enable efficient access to both molecules. Tetralone **4-1** could undergo Birch reduction and isomerization to diene **4-2** which can be subject to a Diels-Alder reaction to form **4-3** which we believed could be prepared in bulk and diversified to both natural products.

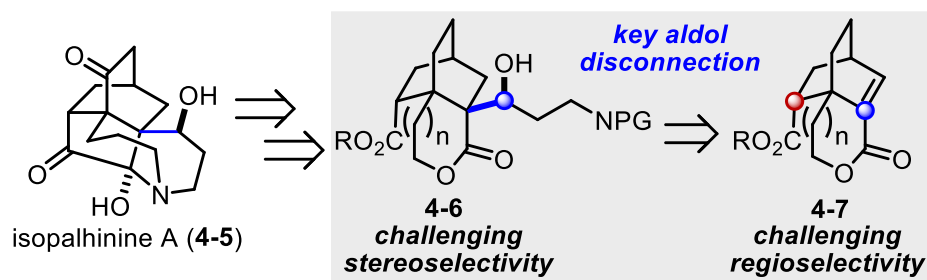


**Figure 4.2-** A retrosynthetic analysis of isopalhinine A (**4-5**) reveals a challenging aldol disconnection to provide **4-6** from **4-7**.

When considering a retrosynthetic analysis of isopalhinine A (**4-5**) towards the common core structure **4-7** a key aldol disconnection is highlighted (Figure 4.2). This aldol reaction would

suffer from two distinct selectivity challenges. The first is a regioselectivity challenge; with two carbonyls in the molecule, both esters both in nearly identical steric environments, selecting for one over the other in a traditional aldol reaction we expect would be hard. There is also a steric challenge with one and only one stereoisomer of the product  $\beta$ -hydroxy lactone desirable for completion of the natural product it was not immediately clear that this reaction could proceed with complete steric control.

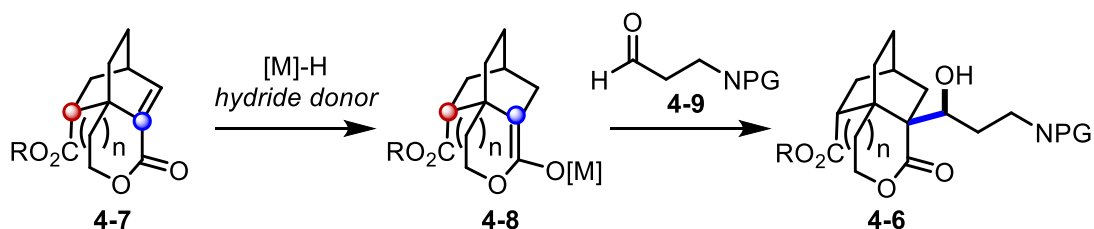


**Figure 4.3-** A reductive aldol reaction would provide regioselectivity towards the formation of **4-6**.

A reductive aldol approach seemed particularly desirable, as it would permit a select Michael acceptor such as **4-7** to react in the presence of enolizable functional groups (Figure 4.3). Several successful protocols for transition metal-catalyzed reductive aldol reactions for  $\alpha,\beta$ -unsaturated carbonyl compounds **4-10** have been described that rely on Rh,<sup>7</sup> Ir,<sup>8</sup> Cu,<sup>9</sup> Co,<sup>10</sup> Ru,<sup>11</sup> or Pd<sup>12</sup> in combination with boranes, silanes or hydrogen gas as suitable reductants. Unfortunately, methods for converting  $\alpha,\alpha$ -disubstituted (**4-11**),<sup>13</sup> or  $\alpha,\alpha,\beta$ -tri- (**4-12**)<sup>14</sup> and tetra- (**4-13**) substituted enones to the reductive aldol products bearing  $\alpha$ -quaternary carbons are less common (Figure 4.4).<sup>15</sup>

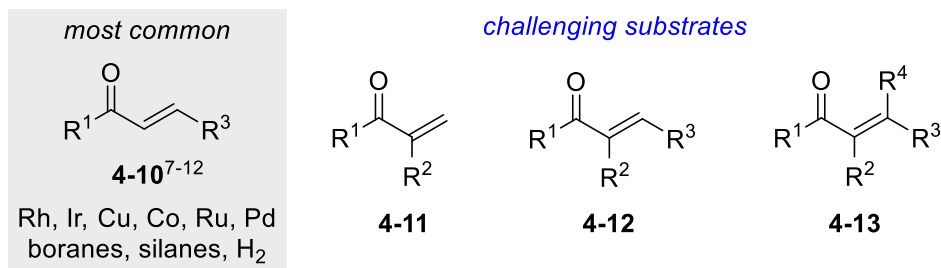


**Figure 4.4-** Literature precedents highlight underexplored substrates for a reductive aldol methodology.

An inherent challenge to enones **4-11-13** relates to the identification of potent catalyst systems that 1) exhibit high levels of chemoselectivity for 1,4-reduction, 2) activate both the resulting enolate nucleophile and aldehyde electrophile for aldol addition while 3) minimizing competing reduction of the aldehyde electrophile. Denmark's pioneering work has established Lewis bases as a powerful class of catalysts capable of enhancing enolate nucleophilicity in asymmetric aldol reactions.<sup>16</sup> Recently, Nakajima has shown that Lewis bases, such as triphenyl phosphine oxide (TPPO, **4-23**) and hexamethyl phosphoramide (HMPA, **4-24**), are able to promote reductive aldol reactions of  $\alpha,\beta$ -disubstituted enones **4-10**, though  $\alpha,\alpha$ -disubstituted (**4-11**) and  $\alpha,\alpha,\beta$ -trisubstituted (**4-12**) enones still remain elusive as substrates.<sup>17</sup> We postulated that the reactivity of these Lewis base catalysts can be tuned to the specific electronic and steric requirements inherent to highly functionalized enones **4-11-13**, to enable both, *in situ* conjugate reduction and activation of the resulting enolate for a subsequent aldol reaction.

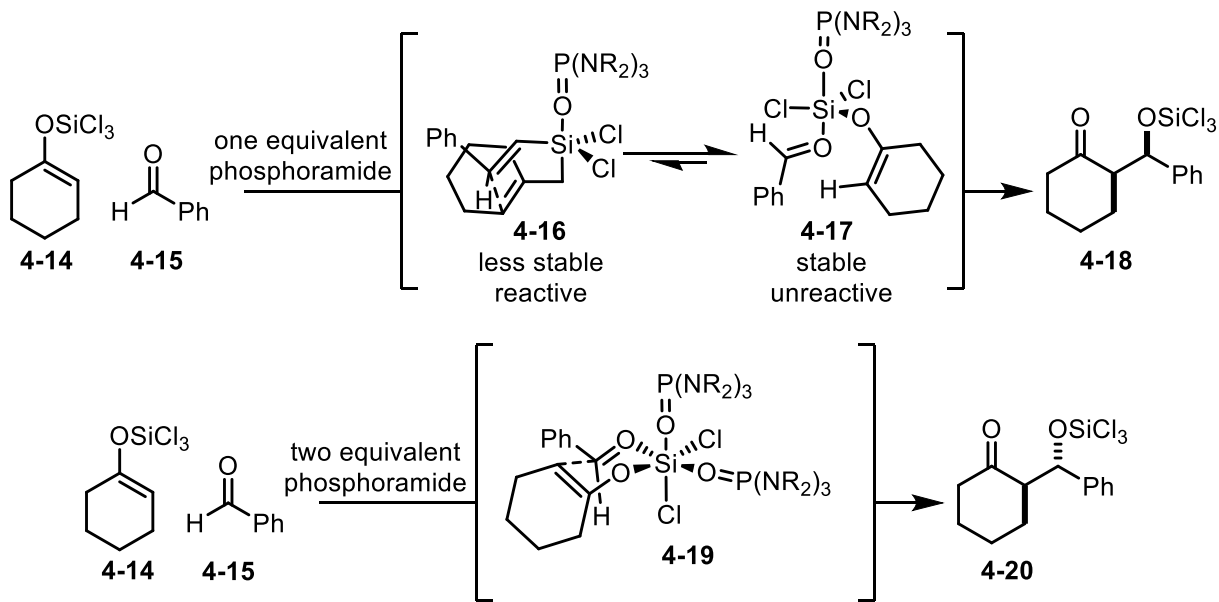


**Figure 4.5-** Denmark's proposed transition states account for stereodivergent outcomes based upon relative equivalencies of silenol ether **4-14** and phosphoramidate.

What is particularly promising about the extant literature on phosphine oxide mediated reductive aldol reactions is that they highlighted the potential to solve the second challenge presented by the transformation of **4-7** to **4-6**. Denmark and coworkers have shown that chiral phosphine oxides can affect the configuration about trichlorosilane and allow aldol reactions of trichlorosilenol ethers to proceed either through a boat-like transition state or a chair-like transition state (Figure 4.5).<sup>16,18c</sup> They present a case study of the reaction of stable enolate analog **4-14** with benzaldehyde **4-15** which in the presence of one or fewer equivalents of a phosphoramidate Lewis base provides a syn disposed product **4-18** while with two or more equivalents of phosphoramidate they observe anti disposed product **4-20**. A chair-like Zimmerman Traxler transition state **4-19** would suggest that the observed product should be **4-20** but Denmark and coworkers suggest that a pentavalent silyl complex would form a structure **4-17** in which no chair-like transition state could be stably formed. Instead they suggest that this

pentavalent silyl complex would form a reactive boat-like complex **4-16** which would be more stable than any reactive chair complex.

Taken together this suggests that if we could develop a new method that relied on a Lewis basic phosphine oxide to promote a silane reduction of an  $\alpha,\alpha,\beta$ -trisubstituted enone we could (1) provide for a method to synthesis quaternary stereocenters concomitantly with creating a C—C bond, allowing for the synthesis of less toxic molecules with more  $sp^3$  character. We would (2) address a significant gap in currently available methodology for conducting reductive aldol reactions on substrates more analogous to complex drug-like and natural product-like scaffolds. And we would (3) enable the synthetic efforts towards isopalhinine A (**4-5**).

#### Chapter 4.2 Reaction optimization and diastereoselectivity

Aryl phosphine oxide derivatives seemed like an excellent starting point for optimization as we postulated that the reactivity of these Lewis base catalysts can be tuned to the specific electronic and steric requirements inherent to highly functionalized enones **4-11-13**. Aryl phosphine oxide derivatives allow for facile electronic differentiation of the aryl substituents to probe our hypothesis. We began our study by attempting to react lactone **4-21**, bearing an exocyclic Michael acceptor, with benzaldehyde as an electrophile and TPPO (**4-23**) or HMPA (**4-24**) as Lewis base catalyst with  $\text{HSiCl}_3$  as the reductant. These initial attempts proved quite promising and resulted in the formation of the reductive aldol product **4-22** in 43% and 45% yield, respectively (entries 1 and 2, Figure 4.6).





entry	R	yield (%)	entry	R	yield (%)
1		<b>4-23</b> 43	6		<b>4-28</b> 39
2		<b>4-24</b> 45	7		<b>4-29</b> 37
3		<b>4-25</b> 0	8		<b>4-30</b> 71
4		<b>4-26</b> 49	9		<b>4-31: R = H</b> 18
5		<b>4-27</b> 23	10		<b>4-32: R = OMe</b> 9

**Conditions:** Reactions were ran in 0.25 M DCM at 30 °C for 48 hours with 1.2 equivalents of benzaldehyde.

**Figure 4.6-** Optimization of the triaryl phosphine oxide Lewis base catalyst.

Although both catalysts produced **4-22** in similar yields, the reaction profiles differed dramatically. Unreacted starting material (**4-21**) was recovered when employing TPPO (**4-23**), but **4-21** was consumed with HMPA (**4-24**), forming both 1,4-reduced lactone and benzyl alcohol as side products. These results suggest that HMPA (**4-24**) is a potent catalyst for initial conjugate reduction but is either too sterically encumbering to fully promote subsequent aldol addition, or so aelectronically activating it allows for competitive direct reduction of the bezaldehyde electrophile, or both. In comparison, TPPO (**4-23**) is not Lewis basic enough to complete the initial conjugate reduction reaction thus resulting in the reisolation of starting material **4-21**. Unfortunately, when we attempted to overcome this lack of reactivity by the

addition of more **4-23** we observed no significant effect. When we tried to enhance reactivity by adding more trichlorosilane we saw over reduction of benzaldehyde. When we elongated reaction times we did not see improved conversions, presumably because of nonproductive consumption of trichlorosilane.

When we attempted to overcome the challenges associated the use of HMPA, through analogs **4-24** and **4-25**, which we hypothesized would decrease steric bulk in the aldol addition, we observed no reaction or no improved yield of the desired reductive aldol product **4-22** (entries 3 and 4, Table 1). This perhaps supports the hypothesis that HMPA is not an effective catalyst because it is promoting indiscriminate reduction of benzaldehyde to benzyl alcohol. As a result, subsequent catalyst optimization centered on electronic differentiation of triaryl phosphine oxides to increase their reactivity in the initial 1,4-reduction.

An advantage of triarylphosphine oxides is that the aromatic rings can be decorated with electron donating or withdrawing groups which effect the Lewis basicity of these catalysts. Lewis bases **4-27**, **4-31** and **4-32**, bearing electron-donating substituents in the *ortho*-position, formed lactone **4-22** in low yields. Perhaps this is the effect of an increased steric bulk decreasing the rate of an aldol addition. *Para*-methyl triarylphosphine oxide **4-28** showed a reaction profile similar to TPPO (**4-23**) and resulted in the formation of **4-22** in 39% yield together with reisolated starting material (entry 6, Table 1). In comparison, the corresponding Lewis base **4-29** bearing a dimethylamine moiety in the *para*-position showed low solubility in dichloromethane and resulted in inconsistent yields of **4-22** (entry 7, Table 1). However, *para*-methoxy triarylphosphine **4-30** led to formation of product **4-21** in 71% yield with minor competing reduction (entry 8, Table 1) and was identified as the optimal Lewis base catalyst.

Subsequent reaction optimization focused on the silane reductant. It was found that 2.5 equivalents of trichlorosilane were optimal, while increased amounts resulted in diminished yields of the desired reductive aldol products due to competing reduction side-products. Additionally, 20 mol% catalyst loadings proved superior with minimal reduction of the aldehyde electrophile (<10%), while stoichiometric quantities of Lewis base **4-30** resulted in diminished yields of **11** in 28%. Notably, the diastereomeric ratio of aldol product **4-21** remained constant despite changes in catalyst loading.<sup>18</sup>

An aside, though the trichlorosilane in theory needs only 1 equivalent to promote this reaction, we used 2.5 equivalents of trichlorosilane. This observation is likely a result of nonproductive consumption of trichlorosilane. The reagent turned the septa used to seal the flask brittle and grey after the reaction was complete the septa did occasionally have to be cut away from the flask. With repeated use of the reagent the tygon tubing connecting the flasks to a Schlenk line were discolored by the reagent as well. When we scaled this reaction we found that sometimes changing the amount of trichlorosilane could be beneficial. We also saw mixed results with a slow addition protocol in which trichlorosilane was added to the reaction over the course of hours as a solution in dichloromethane. Though required for excellent yields and selectivities described herein, this reagent proved to be a troublesome one.

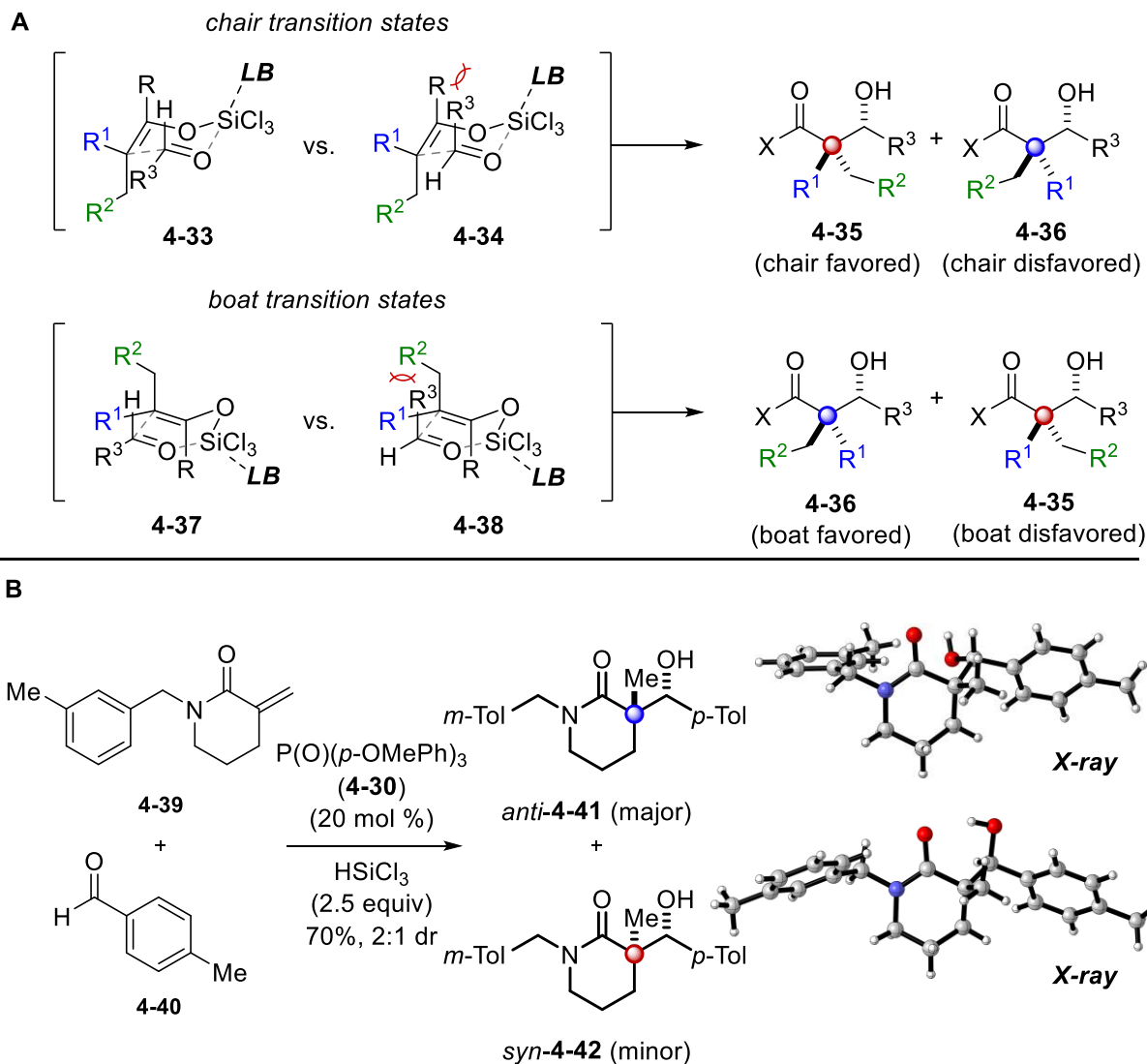


**Figure 4.7- A.** Two possible closed transition state models exist, a chair-like transition state and a boat-like transition state. **B.** The stereochemical outcome of our reductive aldol as determined by X-ray crystallography.

Transition state models similar to those proposed by Denmark for phosphoramidate-catalyzed aldol reactions of pre-formed trichlorosilyl enolates can justify the stereochemical outcome observed in the reductive aldol reaction.<sup>19</sup> Stereochemical models are consistent with a boat transition state **4-37** resulting in the major diastereomer **4-36** with both the  $\text{CH}_2\text{R}^2$  and hydroxyl substituent being anti to one another. The minor diastereomer with the  $\text{CH}_2\text{R}^2$  and hydroxyl group being syn to one another could be formed either via the less favorable boat

transition state **4-38** or by a chair transition state **4-33** (Figure 4.7A). The relative configuration of both diastereomeric products of lactam **4-39** and tolualdehyde **4-40** was confirmed using x-ray analysis to result in the formation of lactam anti-**4-41** as the major diastereomer and syn-**4-42** as the minor diastereomer in combined 70% yield (Figure 4.7B). This supports the Denmark hypothesis that such a reaction would proceed via a boat-like transition state.

### Chapter 4.3 Substrate scope and derivitization

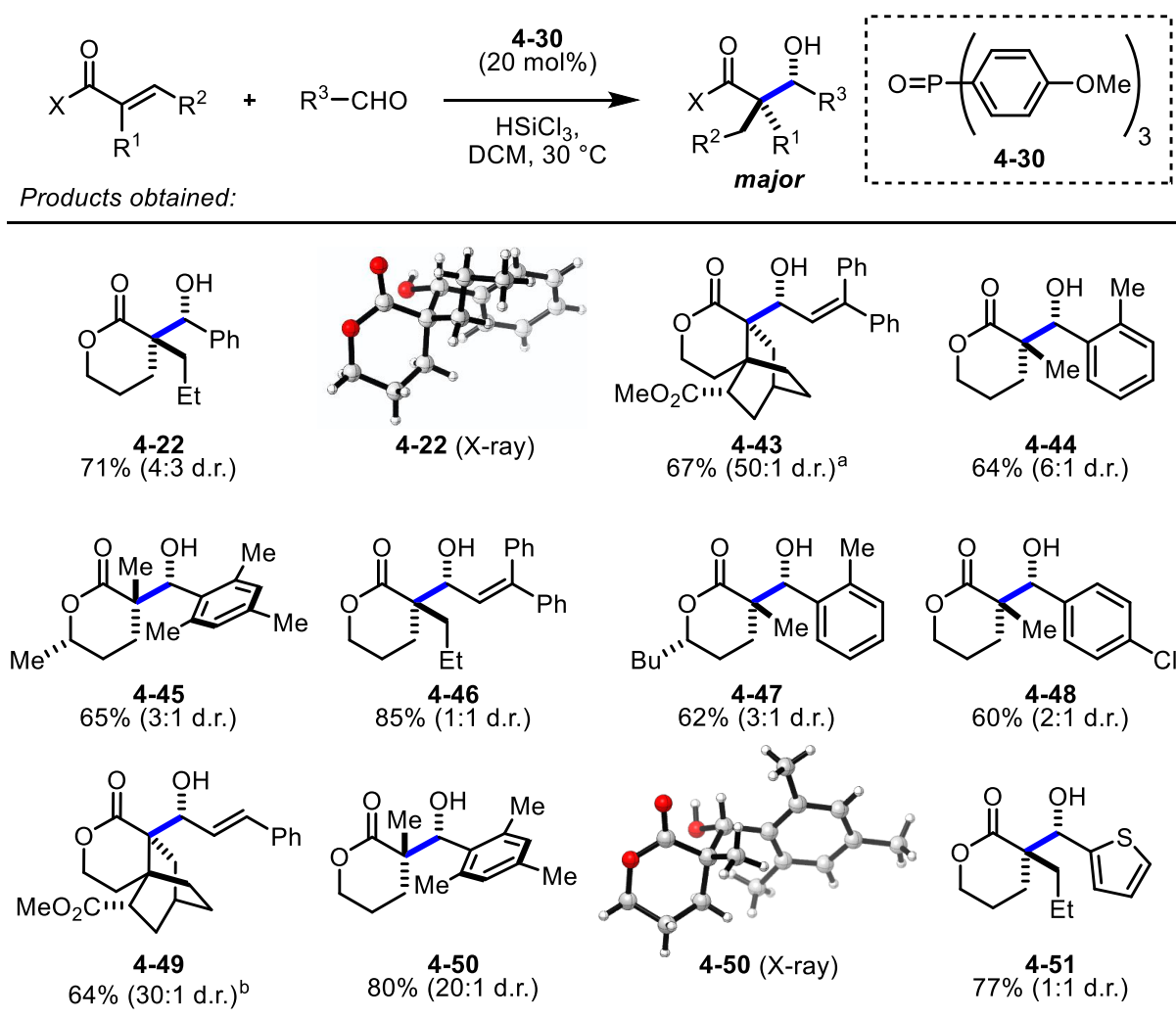
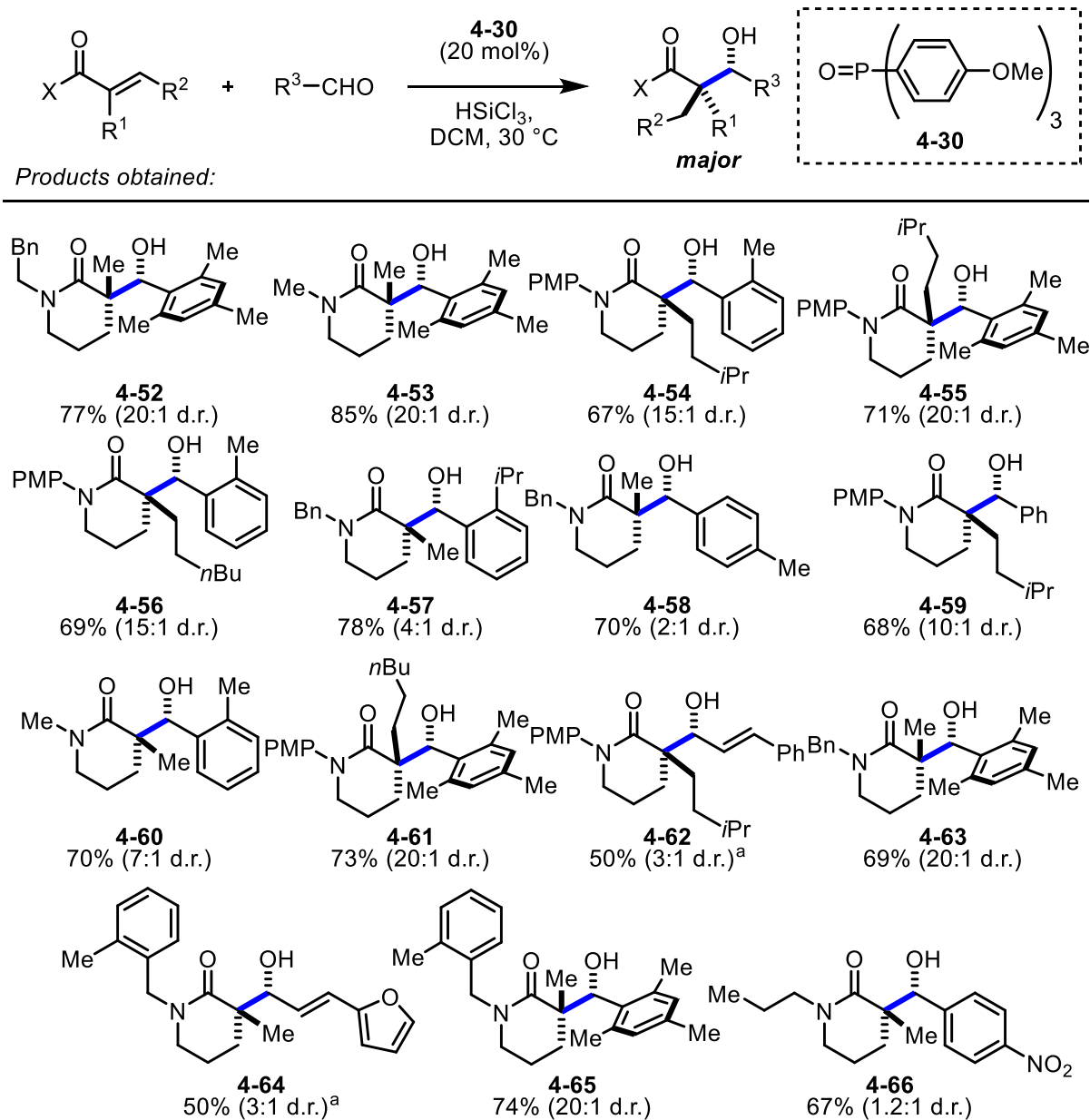


**Figure 4.8-** Substrate scope for lactone Michael acceptors and aryl or vinyl aldehydes.

First we assessed the reaction scope on a variety of  $\alpha,\alpha$ -di- and  $\alpha,\alpha,\beta$ -tri-substituted lactone enones (Figure 4.8). We then investigated the reaction scope on  $\alpha,\alpha$ -di- and  $\alpha,\alpha,\beta$ -tri-substituted lactam enones (Figure 4.9). The conditions developed proved efficient affording yields and diastereomeric ratios up to 85% and 50:1, respectively. For 6-membered monocyclic lactones and lactams, the *anti*-product was favored with diastereomeric ratios up to 20:1 d.r., increasing with both aldehyde and alkene bulk. Importantly, sterically encumbered tricyclic lactones resulted in the formation of the corresponding  $\beta$ -hydroxylactones **4-43** and **4-49** in up to 67% yield and 50:1 d.r. (Figure 4.8). It should be noted that these lactones are analogous to the desired synthetic intermediate **4-7** for the synthesis of isopalhinine A (**4-5**) *N*-alkyl- or *N*-aryl-substituted lactams proved efficient under the optimized reaction conditions and resulted in up to 85% yield and 20:1 d.r. of the desired reductive aldol products. Notably, lactams bearing removable para-methoxyphenyl (PMP) or benzyl protecting groups afforded high yields and good to excellent diastereomeric ratios of the desired  $\beta$ -hydroxylactams though unsubstituted lactams were not tolerated, presumably due to the acidic N—H bond. Aryl aldehydes with varying substitution are viable electrophiles, and increased hindrance on the aromatic moieties lead to higher diastereomeric ratios. Aldehydes conjugated to heterocycles including furan and thiophene were tolerated well as electrophiles rendering yields up to 77%. Initial efforts to extend the substrate scope to unsaturated aldehydes, such as cinnamaldehyde, proved challenging due to the formation of competing aldol condensation products. However, conducting the reaction in toluene under otherwise identical conditions attenuated this competing self-condensation and resulted in good yields of the respective  $\beta$ -hydroxylactone and -lactam adducts.



**Conditions:** Michael acceptor (1 mmol), aldehyde (1.5 mmol), *p*OMe-TPPO (**4-30**, 20 mol%), HSiCl<sub>3</sub> (2.5 equiv.), in dichloromethane (0.25 M) at 30°C for 48h; a) in toluene (0.25M)

**Figure 4.9-** Substrate scope for lactam Michael acceptors and aryl or vinyl aldehydes.

Aliphatic aldehydes were initially problematic. At first, we didn't know if the reaction of otherwise reactive enones, such as **4-67**, and aliphatic aldehydes failed because the aldehydes were electronically mismatched for reactivity or if it was a function of the acidic alpha proton. Either way when we ran the reaction under optimized conditions with an aliphatic aldehyde

bearing an acidic alpha proton, **4-68**, we returned only reduced lactones and lactams, **4-69** (Figure 4.10). Interestingly, when we ran these same reactions with aliphatic aldehyde bearing acidic alpha deuterons, **4-70**, we saw deuterium incorporation in the alpha position of our reduced substrates, **4-71**. This suggested that our inability to tolerate aliphatic aldehydes was a function of their acidity.

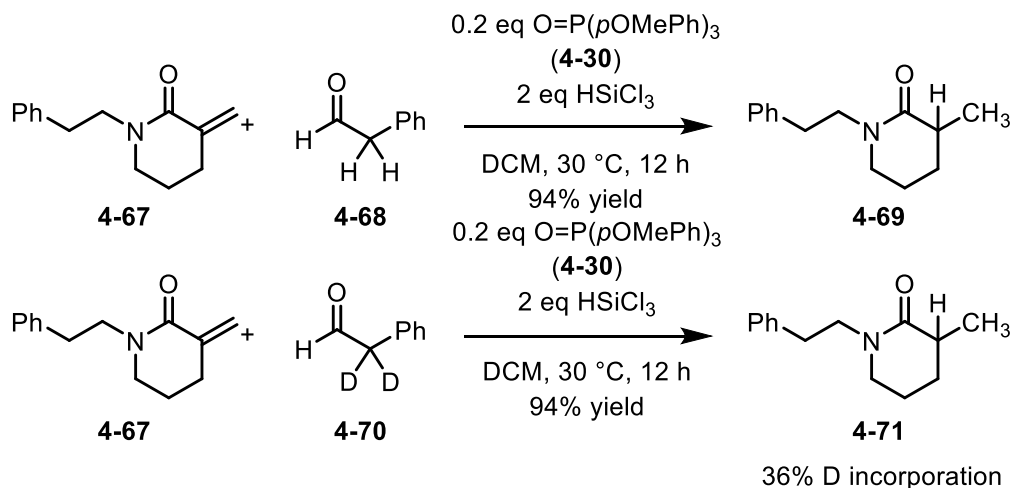
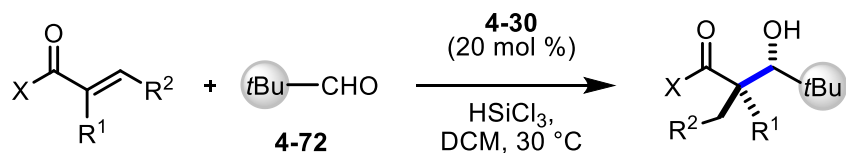


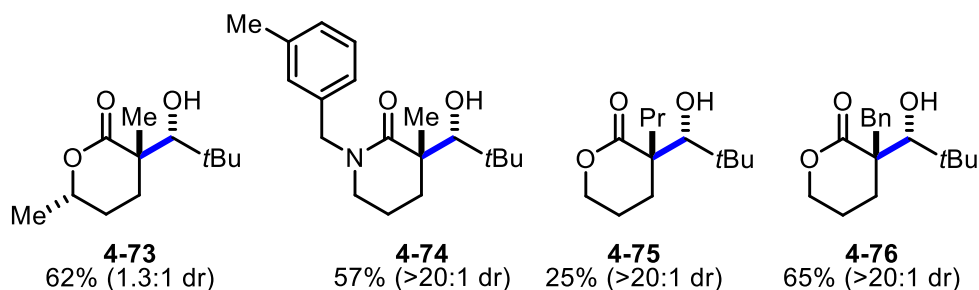
**Figure 4.10-** Deuterium incorporation experiments highlight the challenges with aliphatic aldehyde electrophiles.

If it were only a problem of acidity, we would expect that aliphatic aldehydes that lacked an acidic alpha proton, such as pivaldehyde **4-72**, would be well tolerated under our optimized reaction conditions. We found this hypothesis to be true (Figure 4.11). Our optimized reaction conditions were found to be successful with  $\alpha,\alpha$ -di- and  $\alpha,\alpha,\beta$ -tri-substituted lactone enones. Lactams reacted well with pivaldehyde. Unsurprisingly given the steric bulk of **4-72**, the reactions proceeded in very high d.r. and gratifyingly in good yields.





Products obtained:

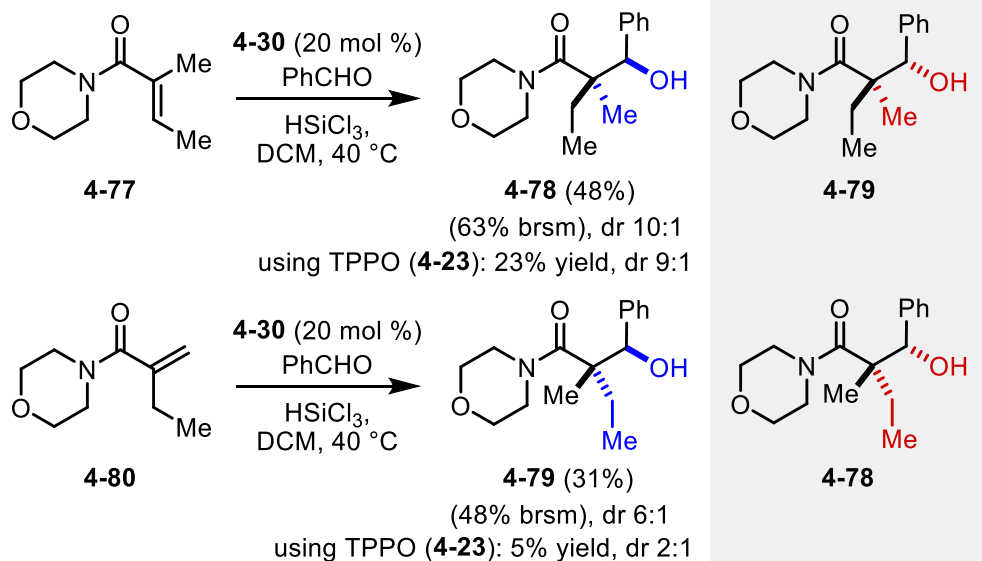


**Conditions:** Michael acceptor (1 mmol), aldehyde (1.5 mmol), *p*MeO-TPPO (**4-30**, 20 mol %), HSiCl<sub>3</sub> (2.0 equiv), in dichloromethane (0.2 M) at 30 °C for 48 h.

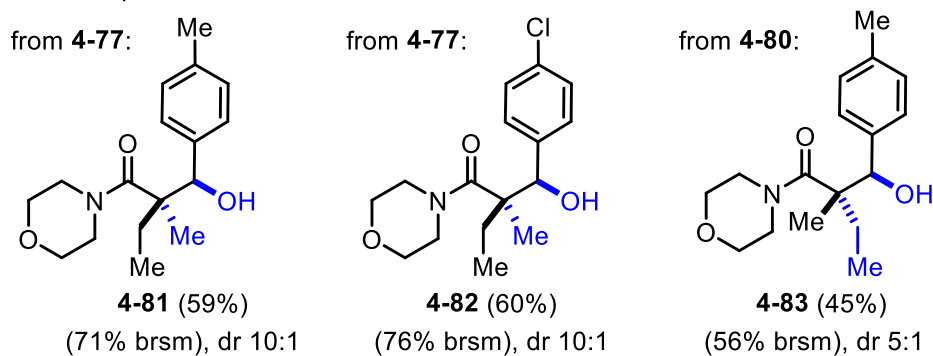
**Figure 4.11-** Substrate scope of lactones and lactams with pivalaldehyde **4-72**.

We tried some acyclic esters and amides without much success. We hypothesized that this discrepancy was due to a conformational requirement where the beta position of the enone needs to be in close proximity to the carbonyl in order for the conjugate reduction to occur. If this were the explanation we would expect that conformationally constrained acyclic substrates, such as morpholine amides would be tolerated and we were pleased to find that to be true (Figure 4.12). Morpholine amides are important synthetic alternatives to Weinreb amides characterized by their ease of use.<sup>21</sup> This reaction was successful with  $\alpha,\alpha$ -di- and  $\alpha,\alpha,\beta$ -tri-substituted morpholine acrylamides (**4-80** and **4-77**, respectively). The products of this reaction are stereodivergent with existing (Ipc)<sub>2</sub>BH mediated methodologies.<sup>22</sup>

**A** Reaction of morpholine amides:



**B** Selected products:



**Conditions:** Michael acceptor (1 mmol), aldehyde (1.5 mmol), *p*MeO-TPPO (**4-30**, 20 mol %), HSiCl<sub>3</sub> (2.5 equiv), in dichloromethane (0.25 M) at 30 °C for 96 h.

**Figure 4.12-** Results of the reductive aldol reaction of morpholine amides.

Finally, we demonstrated that the products of our reductive aldol methodology could be converted into versatile building blocks bearing a stereogenic quaternary carbon core (Figure 4.13). We can deprotect benzyl lactam **4-63** to form substituted piperidine **4-84** in excellent yield over two steps. Additionally, we could take lactone **4-22** to an acyclic triol **4-85** via a lithium aluminum hydride reduction in 74% yield. Most importantly, protected amine **4-86**, which is formed using our methodology in 66% yield, as a single diastereomer on multi-gram scale, can

be protected and hydrogenated to yield **4-87**, the desired intermediate towards isopalhinine A (**4-5**).

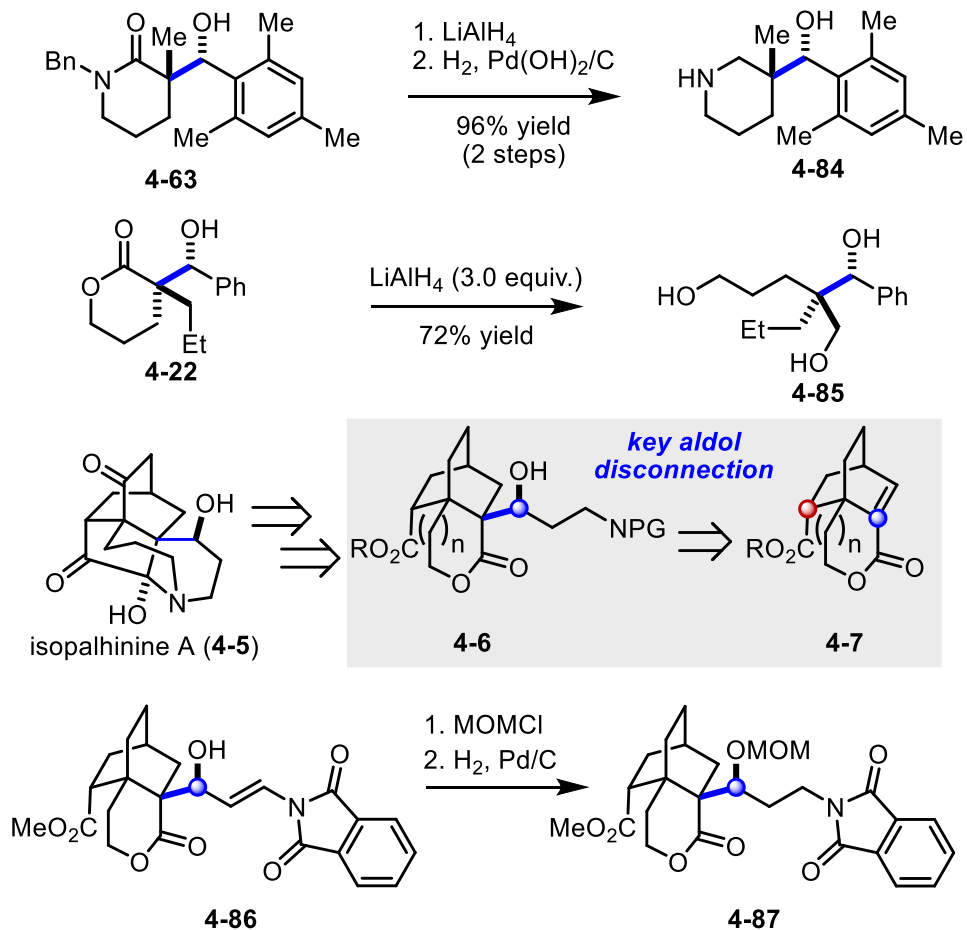


**Figure 4.13-** Derivatization of reductive aldol products leads to useful synthetic building blocks bearing all carbon quaternary stereocenters.

I am grateful to report that this methodology has been published and that this methodology is currently being applied by my coworkers towards the synthesis of isopalhinine A (**4-5**).<sup>23</sup>

## Bibliography

1. Kramer, J. A.; Sagartz, J. E.; Morris, D. L. *Nat. Rev. Drug Discovery* **2007**, *6*, 636-649.
2. Lovering, F. *Med. Chem. Comm.* **2013**, *4*, 515-519.
3. (a) Liu, Y.; Han, S.-J.; Liu, W.-B.; Stoltz, B. M. *Acc. Chem. Res.* **2015**, *48*, 740-751. (b) Quasdorf, K. W.; Overman, L. E. *Nature* **2014**, *516*, 181-191. (c) Prakash, J.; Marek, I. *Chem. Commun.* **2011**, *47*, 4593-4623. (d) Murphy, J. J.; Bastida, D.; Paria, S.; Fagnoni, M.; Melchiorre, P. *Nature* **2016**, *532*, 218-222.
4. For a recent example, see: Minko, Y.; Pasco, M.; Lercher, L.; Botoshansky, M.; Marek, I. *Nature* **2012**, *490*, 522-526.
5. For selected examples, see: (a) *acochlearine*: Meriçi, A. H.; Süzgeç, S.; Bitiş, L.; Meriçli, F.; Özçelik, H.; Zapp, J.; Becker, H. *Pharmazie* **2006**, *61*, 483-485. (b) *pseudolaric acid B*: Zhou, B. N.; Ying, B. P.; Song, G. Q.; Chen, Z. X.; Han, J.; Yan, Y. F. *Planta Med* **1983**, *47*, 35-38. (c) *scholarisine A*: Cai, X.-H.; Tan, Q.-G.; Liu, Y.-P.; Feng, T.; Du, Z.-Z.; Li, W.-Q.; Luo, X.-D. *Org. Lett.* **2008**, *10*, 577-580.
6. For additional recent examples, see: (a) Holmbo, S. D.; Godfrey, N. A.; Hirner, J. J.; Pronin, S. V. *J. Am. Chem. Soc.* **2016**, *138*, 12316-12319. (b) Huang, C.-Y.; Doyle, A. G. *J. Am. Chem. Soc.* **2015**, *137*, 5638-5641. (c) Pratsch, G.; Lackner, G. L.; Overman, L. E. *J. Org. Chem.* **2015**, *80*, 6025-6036.
7. For examples using Rh, see: (a) Taylor, S. J.; Duffey, M. O.; Morken, J. P. *J. Am. Chem. Soc.* **2000**, *122*, 4528-4529. (b) Russell, A. E.; Fuller, N. O.; Taylor, S. J.; Aurriset, P.; Morken, J. P. *Org. Lett.* **2004**, *6*, 2309-2312. (c) Bocknack, B. M.; Wang, L.-C.; Krische, M. J. *Proc. Natl. Acad. Sci. USA* **2004**, *101*, 5421-5424. (d) Fuller, N. O.; Morken, J. P. *Synlett* **2005**, *9*, 1459-1461. (e) Nishiyama, H.; Shiomi, T.; Tsuchiya, Y.; Matsuda, I. *J. Am. Chem. Soc.* **2005**, *127*, 6972-6973. (f) Jung, C.-K.; Krische, M. J. *J. Am. Chem. Soc.* **2006**, *128*, 17051-17056. (g) Han, S. B.; Krische, M. J. *Org. Lett.* **2006**, *8*, 5657-5660. (h) Ito, J.; Shiomi, T.; Nishiyama, H. *Adv. Synth. Catal.* **2006**, *348*, 1235-1240. (i) Shiomi, T.; Ito, J.; Yamamoto, Y.; Nishiyama, H. *Eur. J. Org. Chem.* **2006**, *24*, 5594-5600. (j) Shiomi, T.; Nishiyama, H. *Org. Lett.* **2007**, *9*, 1651-1654. (k) Hashimoto, T.; Shiomi, T.; Ito, J.; Nishiyama, H. *Tetrahedron* **2007**, *63*, 12883-12887. (l) Hashimoto, T.; Ito, J.; Nishiyama, H. *Org. Lett.* **2007**, *9*, 1651-1654. (m) Bee, C.; Han, S. B.; Hassan, A.; Iida, H.; Krische, M. J. *J. Am. Chem. Soc.* **2008**, *130*, 2746-2747. (n) Shiomi, T.; Adachi, T.; Ito, J.; Nishiyama, H. *Org. Lett.* **2009**, *11*, 1011-1014.
8. For an example using Ir, see: Zhao, C.-X.; Duffey, M. O.; Taylor, S. J.; Morken, J. P. *Org. Lett.* **2001**, *3*, 1829-1831.
9. For examples using Cu, see: (a) Lam, H. W.; Murray, G. J.; Firth, J. D. *Org. Lett.* **2005**, *7*, 5743-5746. (b) Lam, H. W.; Joensuu, P. M. *Org. Lett.* **2005**, *7*, 4225-4228. (c) Chuzel, O.; Deschamp, J.; Chausteur, C.; Riant, O. *Org. Lett.* **2006**, *8*, 5943-5946. (d) Deschamp, J.; Chuzel, O.; Hannedouche, J.; Riant, O. *Angew. Chem. Int. Ed.* **2006**, *145*, 1292-1297. (e) Zhao, D.; Oisaki, K.; Kanai, M.; Shibasaki, M. *Tetrahedron Lett.* **2006**, *47*, 1403-1407. (f) Zhao, D.; Oisaki, K.; Kanai, M.; Shibasaki, M. *J. Am. Chem. Soc.* **2006**, *128*, 14440-14441. (g) Lipshutz, B. H.; Amorelli, B.; Unger, J. B. *J. Am. Chem. Soc.* **2008**, *130*, 14378-14379. (h) Deschamp, J.; Riant, O. *Org. Lett.* **2009**, *11*, 1217-1220. (i) Kato,

- M.; Oki, H.; Ogata, K.; Fukuzawa, S. *Synlett* **2009**, 8, 1299-1302. (j) Ou, J.; Wong, W.-T.; Chiu, P. *Tetrahedron* **2012**, 68, 3450-3456.
10. For an example using Co, see: Lumby, R. J.; Joensuu, P. M.; Lam, H.W. *Tetrahedron* **2008**, 64, 7729-7740.
  11. For an example using Ru, see: Doi, T.; Fukuyama, T.; Minamino, S.; Ryu, I. *Synlett* **2006**, 18, 3013-3016.
  12. For an example using Pd, see: Kiyooka, S.; Shimizu, A.; Torii, S. *Tetrahedron Lett.* **1998**, 39, 5237-5238.
  13. For intermolecular reductive aldol reactions converting  $\alpha,\alpha$ -disubstituted enones, see: (a) Revis, A.; Hilty, T. K. *Tetrahedron Lett.* **1987**, 28, 4809-4812. (b) Ghosh, A. K.; Kass, J.; Anderson, D. D.; Xu, X.; Marian, C. *Org. Lett.* **2008**, 10, 4811-4814.
  14. For intermolecular reductive aldol reactions converting examples of  $\alpha,\beta$ -diisubstituted enones, see: (a) Lipshutz, B. H.; Chrisman, W.; Noson, K.; Papa, P.; Sclafani, J. A.; Vivian, R. W.; Keith, J.M. *Tetrahedron* **2000**, 56, 2779-2788. (b) Matsuda, I.; Takahashi, K.; Sato, S. *Tetrahedron Lett.* **1990**, 31, 5331-5334. (c) Lipshutz, B. H.; Papa, P. *Angew. Chem. Int. Ed.* **2002**, 41, 4580-4582.
  15. For selected intramolecular examples, see: (a) Joensuu, P. M.; Murray, G. J.; Fordyce, E. A. F.; Luebbbers, T.; Lam, H. W. *J. Am. Chem. Soc.* **2008**, 130, 7328-7338. (b) Sloan, L. A.; Baker, T. M.; Macdonald, S. J. F.; Procter, D. J. *Synlett* **2007**, 20, 3155-3159. (c) Chiu, P.; Szeto, C.-P.; Geng, Z.; Cheng, K.-F. *Org. Lett.* **2001**, 3, 1901-1903. (d) Lipshutz, B. H.; Amorelli, B.; Unger, J. B. *J. Am. Chem. Soc.* **2008**, 130, 14378-14379.
  16. Denmark, S. E.; Beutner, G. L. *Angew. Chem. Int. Ed.* **2008**, 47, 1560-1638.
  17. (a) Sugiura, M.; Sato, N.; Kotani, S.; Nakajima, M. *Chem. Commun.* **2008**, 29, 4309-4311. (b) Sugiura, M.; Sato, N.; Sonoda, Y.; Kotani, S.; Nakajima, M. *Chem. Asian J.* **2010**, 5, 478-481.
  18. (a) Denmark, S. E.; Su, X.; Nishigaichi, Y. *J. Am. Chem. Soc.* **1998**, 120, 12990-12991. (b) Denmark, S.E.; Pham, S.M. *Helv. Chim. Acta* **2000**, 83, 1846-1853. (c) Denmark, S. E.; Pham, S. M.; Stavenger, R. A.; Su, X.; Wong, K.-T.; Nishigaichi, Y. *J. Org. Chem.* **2006**, 71, 3904-3922.
  19. For a recent example of tandem  $\text{SiCl}_3\text{H}$  reactivity, see: Chen, L.; Du, Y.; Zeng, X.-P.; Shi, T.-D.; Zhou, F.; Zhou, J. *Org. Lett.* **2015**, 17, 1557-1560.
  20. See Supporting Information for details.
  21. (a) Martín, R.; Romea, P.; Tey, C.; Urpi, F.; Vilarrasa, J. *Synlett* **1997**, 12, 1414-1416. (b) Concellón, J. M.; Rodríguez-Solla, H.; Méjica, C.; Blanco, E. G. *Org. Lett.* **2007**, 9, 2981-2984. (c) Dhoro, F.; Kristensen, T. E.; Stockmann, V.; Yap, G. P. A.; Tius, M. A. *J. Am. Chem. Soc.* **2007**, 129, 7256-7257. (d) Concellón, J. M.; Rodríguez-Solla, H.; Díaz, P. *J. Org. Chem.* **2007**, 72, 7974-7979. (e) Lin, K.-W.; Tsai, C.-H.; Hsieh, I.-L.; Yan, T.-H. *Org. Lett.* **2008**, 10, 1927-1930. (f) Concellón, J. M.; Rodríguez-Solla, H.; del Amo, V.; Díaz, P. *Synthesis* **2009**, 15, 2634-2645. (g) Rye, C.; Barker, D. *Synlett* **2009**, 20, 3315-3319.
  22. (a) Nuhant, P.; Allais, C.; Roush, W. R. *Angew. Chem. Int. Ed.* **2013**, 52, 8703-8707. (b) Allais, C.; Tsai, A. S.; Nuhant, P.; Roush, W. R. *Angew. Chem. Int. Ed.* **2013**, 52, 12888-12891.

23. DePorre, Y. C.\*; Annand, J. R.\*; Bar, S.; Schindler, C. S. *Org. Lett.* **2018**, 2580.  
\*Authors Contributed Equally

## Appendix 1-Chapter 2 Supplementary Information

The synthesis of pharbinilic acid and original Luciferase methodology has been published.<sup>1</sup> The following section will describe the synthesis of unpublished gibberellins as well as the full biological data and methods.

### General Method 2A EDC coupling of the B-ring Carboxylic Acid

The following protocol was used to prepare **2-47**, **2-48**, **2,49**, **2-53**, **2-54**, and **2-85**.

Gibberellic acid (**2-1**) is treated with 10 eq of alcohol or amine coupling partners, 1.1 eq EDC, and 0.2 eq DMAP in DCM (0.1 M) for 14 hr at room temperature with stirring under an inert atmosphere. The reactions are quenched with saturated ammonium chloride extracted twice with DCM. The combined organic extracts were washed twice with saturated sodium bicarbonate and once with brine, dried over sodium sulfate and concentrated. The crude solids were purified by gradient column chromatography to yield white solids. Samples were purified by HPLC on a Phenomenex RPC18 column before being subjected to biological evaluations.

### General Method 2B Dess Martin Periodinane oxidation of enols to enones

The following protocol was used to prepare **2-50**, **2-51**, **2-52**, **2-55**, **2-56**, **2-71**, **2-72**, **2-74**, **2-76**, **2-79**, **2-80**, **2-81**, and **2-86**.

The enol starting material was dissolved in THF (0.1 M) to which was added 2 eq Dess Martin Periodinane, which had been prepared according to published protocols,<sup>2</sup> 10 eq sodium bicarbonate, and 1 eq of *tert*-butanol. The reaction was allowed to proceed for 4 hr or until the

starting material had been consumed by TLC. The reaction was diluted in ether, 1:1 saturated sodium bicarbonate: saturated sodium thiosulfate was added and the mixture was sonicated for 10 minutes. At which point the mixture was extracted with ether the organic layers were washed with brine, dried over magnesium sulfate and concentrated yielding a white solid or foam often not needing further purification. When purification was required gradient column chromatography over silica was employed. Samples were purified by HPLC on a Phenomenex RPC18 column before being subjected to biological evaluations.

#### General Method 2C Riley oxidations

The following protocol was used to prepare **2-65**, **2-66**, **2-67**, **2-68**, **2-69** **2-70**, **2-73**, and **2-75**

Gibberellins and 1 eq selenium dioxide were dissolved in DCM (0.1 M) to which 4.5 eq *tert*-butyl hydroperoxide (2 M in decanes) was added. After 2 hr at room temperature, or when starting material was consumed by TLC, the reaction was concentrated water was added and the reaction was sonicated for 30 minutes at 10 °C. Organic molecules crystallized out from the aqueous mixture upon standing overnight. They were purified by gradient column chromatography over silica and samples were purified by HPLC on a Phenomenex RPC18 column before being subjected to biological evaluations.

Often upon purification or standing some lactoization of **2-65** and **2-66** to **2-67** to **2-68** would occur in part. If this is desired the crude mixture of alcohol diastereomers could be suspended in DMF (0.1 M), treated with 0.1 eq toluenesulfonic acid and heated to 50 °C for 4 hr. At this point most **2-65** and **2-66** is consumed leaving **2-69** and **2-70** unreacted.

#### General Methods 2D allogibberellic acid epimerization and alphas-methenylation



The following protocols were used in the synthesis of **2-59**, **2-60**, **2-61**, **2-62**, **2-63**, **2-64**

Epimerization of the C/D ring of allogibberellins was achieved by refluxing the gibberellins in toluene (0.1 M) with 0.1 eq toluene sulfonic acid for 2 hr. Cooling to room temperature, and washing with saturated sodium bicarbonate and brine. Upon drying over sodium sulfate and concentrating to dryness the epimerized gibberellins could be obtained, often without further purification. Samples were purified by HPLC on a Phenomenex RPC18 column before being subjected to biological evaluations.

C/D-epi-gibberellins were dissolved in THF (0.1 M), cooled to -78 °C and 1 eq of freshly prepared LDA (0.5 M in THF) was added dropwise. 1.5 eq of Eschenmoser's salt was added as a solution (0.5 M in THF) to the resultant lithium enolate. The reaction was allowed to come to room temperature over 60 minutes, quenched with saturated sodium bicarbonate, and extracted with ether. The combined extracts were washed with saturated sodium bicarbonate and brine, dried over magnesium sulfate, and concentrated. The N,N-dimethylamino gibberellins were purified by HPLC on a Phenomenex RPC18 column before being subjected to biological evaluations.

N,N-dimethyl amino gibberellins were dissolved, crude, in THF and treated with 4 eq iodomethane at room temperature for 8 hr. 2 eq DBU was added and the reaction was refluxed for 90 minutes. The reaction was cooled to room temperature quenched with ammonium chloride, and extracted with ether. The combined extracts were washed with brine, dried over magnesium sulfate, and concentrated to dryness. The alpha-methylated gibberellins were purified by gradient column chromatography over silica. Samples were purified by HPLC on a Phenomenex RPC18 column before being subjected to biological evaluations.

## Synthesis of **2-27**

Gibberellin **2-29** was dissolved in Pyridine (0.5 M) and 2.5 eq of freshly distilled triflic anhydride was added. The reaction was allowed to proceed until the starting material was consumed and was quenched with saturated ammonium chloride. The resulting mixture was extracted with ether, washed extensively with 0.1 M HCl, then brine. The combined extracts were dried over magnesium sulfate, concentrated to dryness and then the aryltriflate was redissolved in DMF. To the aryltriflate was added 0.1 eq palladium acetate, 0.2 eq triphenyl phosphine and a solution of 10 eq 1:1 triethylamine:formic acid (1 M in DMF). The solution was heated to 90 °C for 4 hours, cooled to room temperature and then quenched with a 5% (w/v) solution of lithium chloride. The mixture was extracted with ethyl acetate, and the combined extracts were washed with saturated sodium bicarbonate, 1 M HCl, 5% (w/v) lithium chloride and brine, dried over sodium sulfate and concentrated. Gibberellin **2-57** was purified by gradient column chromatography over silica. **2-57** was purified by HPLC on a Phenomenex RPC18 column before being subjected to biological evaluations.

Methyl allogibberellic ester **2-57** was dissolved in THF (0.1 M) and 2.5 eq of potassium trimethylsiloxide was added. The reaction was allowed to stir for 24 hr before being quenched with 0.5 M HCl, and extracted with ethyl acetate. The combined extracts were dried over sodium sulfate and concentrated to dryness yielding **2-27** as a white powder. Allogibberellic acid **2-27** was purified by gradient column chromatography over silica. **2-57** was purified by HPLC on a Phenomenex RPC18 column before being subjected to biological evaluations.

## General Method 2E Epimerization by halogenation

The following method was used to prepare **2-76**, **2-77**, **2-78**, **2-82**, **2-83**, **2-84**

10 eq of N-chlorosuccinimide, N-bromosuccinimide, or N-iodosuccinimide was added to a solution of **2-36** (0.5 M in THF) or 17.5 eq of N-chlorosuccinimide, N-bromosuccinimide, or N-iodosuccinimide was added to a solution of **2-30** (0.5 M in THF) and heated at reflux for 30 minutes. The reactions were, cooled, quenched with saturated sodium bicarbonate, and extracted with ether. The combined extracts were washed with 1 M HCl, saturated sodium bicarbonate and brine, dried over magnesium sulfate and concentrated. The halogenated gibberellins were purified by gradient column chromatography over silica and samples were purified by HPLC on a Phenomenex RPC18 column before being subjected to biological evaluations.

#### TNF $\alpha$ induced HEK293 Luc2P Luciferase Assay

This assay was conducted in GloResponse<sup>TM</sup> NF- $\kappa$ B-RE-*luc2P* HEK293 cells which were purchased from Promega (Product Number E8520) and cultured according to the manufacturer's specifications with hygromycin B to maintain stable transfection. The cells were seeded at 5000 cells/well in a sterile TC-treated white clear bottom 384 well plate in 20  $\mu$ L of DMEM containing 10% FBS, penicillin and streptomycin. It should be noted that 4 wells were excluded having only cell growth media but no cells to serve as a control for background luminescence. 0.2  $\mu$ L of Assay compounds, along with Parthenolide and Lactocysteine B, as positive controls, were dosed in quadruplicate as 6 point 4x dilution curves from 100  $\mu$ M to 0.098  $\mu$ M and the cells were allowed to incubate for 30 minutes at 37  $^{\circ}$ C. TNF $\alpha$  was added in 5  $\mu$ L of DMEM to a final concentration of 20 ng/mL in the assay well. It should be noted that 4 wells, preincubated with DMSO alone, were excluded from TNF $\alpha$  induction to serve as a positive assay control and to these wells were added 5  $\mu$ L of DMEM alone. The cells were allowed to be induced for 1 hour at 37  $^{\circ}$ C. One volume, 25  $\mu$ L, of Firefly OneGlo assay solution

was added, incubated with rocking for 3 minutes, careful not to create bubbles, and the luminescence was read out.

#### High Throughput Cell Titre Glo Viability Assay Protocol

These experiments were done by the Dr. Jamie Cheah at the Koch Integrative Cancer Research Institute of MIT in the High Throughput Screening core facility. Cells were plated at 2000 cells/well in 384 well plates in 50  $\mu$ L of growth media as recommended by their manufacturers. To these cells in duplicate plates, in duplicate curves were pinned 500 nL of assayed cell lines from 100  $\mu$ M to 100 nM and the cells were incubated for 3 days at which point they were assayed by a commercial Cell Titre Glo kit and read by luminescence. MG-132, a known proteasome inhibitor, was employed as a positive control.



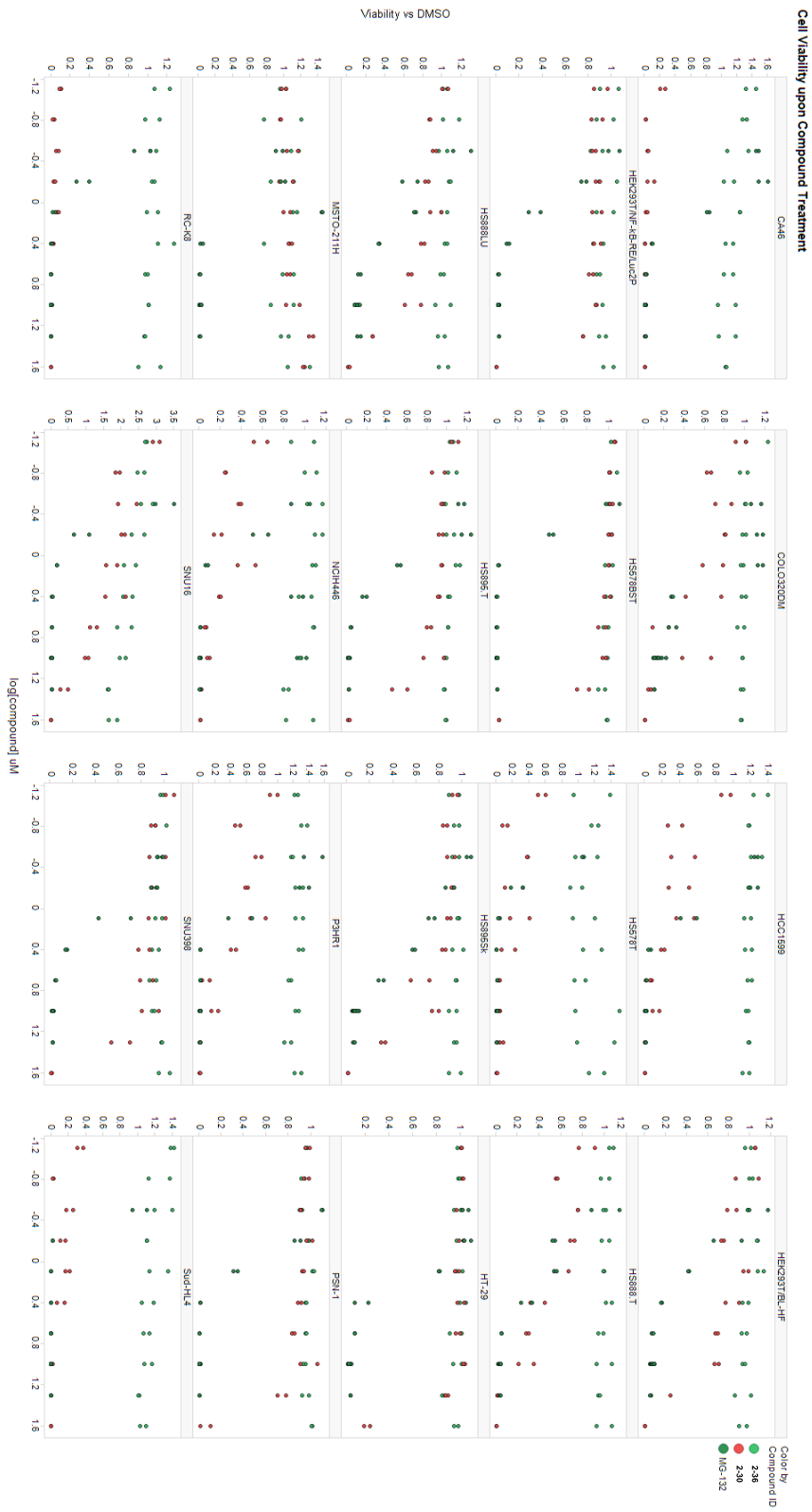


Figure S2- Dose response curves of active inhibitor 239 and inactive analog 236 against a variety of cell lines as determined by a Cell Tite Glo viability assay.

## Nuclear Translocation Assays

Confocal microscopy was conducted on HeLa cells that has been plated on 6 well tissue culture treated microscope slides at 50,000 cells/well in 200  $\mu$ L DMEM complete. After incubation at 37 °C overnight cells were preincubated with **2-30**, **2-36** or DMSO for 1 hour at 1% DMSO final concentration. The cells were induced with TNF $\alpha$  at 20 ng/mL final concentration from a stock solution in PBS. After incubation at 37 °C for 1 hour, the media was removed and the cells were fixed by addition of 37 °C 4% formaldehyde, 16% methanol. After 10 minutes the fixation solution was removed and the cells were washed with PBS. 0.2% Triton X-100 in PBS was added and incubated for 10 minutes to permeabilize the fixed cells. The permeabilization solution was removed and the cells were washed twice with PBS. The cells were blocked with 10% normal goat serum in PBS for 30 minutes and then the blocking buffer was discarded and the cells were washed again with PBS. The cells were incubated with Alexafluor tagged antibodies at the manufacturer's specified dilutions (in most cases 1:500) in 1.5% normal goat serum in PBS. The cells were washed with 0.1% Tween in PBS twice. The cells were incubated with 0.2% DAPI, 1.5% normal goat serum in PBS for 1 hour. The cells were washed twice with 0.1% Tween in PBS and stored at 4 °C in the dark under PBS. The cells were imaged with a Nikon A1 High Sensitivity confocal microscope with the assistance of the Biomedical Research Core Facilities at the University of Michigan.

Fluorescent Microscopy was conducted as above except that the cells used were HUVEC cells. The antibodies used were not conjugated to AlexaFluor so the incubation with DAPI also contained secondary antibodies that were conjugated to AlexaFluor fluorescent dyes. The microscope used was a TX5000 at the Koch Integrative Cancer Research Institute at MIT.

## Appendix 2-Chapter 3 Supplementary Information

Model System Studies:

### 3-148

2-oxocyclohexanecarboxylic acid was cooled to 0 °C and 3 eq of acetone and 3.3 eq acetic anhydride were added to it. 3 drops of concentrated sulfuric acid was added and the reaction was allowed to stir at 0 °C until starting material was consumed by TLC. The reaction mixture was diluted in ether and quenched with saturated sodium carbonate, extracted with ether, and the combined organic fractions were dried of magnesium sulfate and concentrated. The mixture was crudely purified by column chromatography and **3-148** was recrystallized as a white solid from hexanes.

### 3-149

Ethyl acetoacetate was dissolved in benzene (0.5 M) and 1.5 eq triethyl amine was added followed by 1.5 eq chlorotrimethylsilane. The reaction was stirred at room temperature until the starting material was consumed by TLC and the reaction was concentrated. **3-149** was purified from the reaction mixture by vacuum distillation.

### 3-152

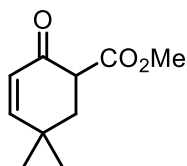


Neat ethyl acetoacetate was treated with 3 eq trimethyl orthoformate and catalytic concentrated sulfuric acid. Upon completion by TLC the reaction was neutralized with quinoline and **3-152** was crudely distilled from the reaction mixture.

### **3-150 and 3-153**

In the most successful photochemical protocols **3-148** and 5 eq of **3-149** or **3-152** were dissolved in acetone (0.1 M) and cold sparged for 90 minutes. The sparged reaction was placed under an inert atmosphere and was passed through FEP tubing via a flow apparatus around a 450 W mercury arc lamp at 50 mL/min while the photochemical setup was being cooled with an isopropanol chiller set to 7.5 °C. **3-150** or **3-153** were purified by silica gel chromatography and the product crystallized out of the fractions therefrom.

### **3-157**



**A-1**

4,4 dimethyl cyclohex-2-ene-1-one was added, slowly, over 2 hr, as a solution in DME (2.4 M) to a suspension of 5 eq of dimethyl carbonate and 2 eq sodium hydride in DME (0.8 M) at reflux. After the addition was complete the reaction continued at reflux for 2 hour and was then cooled to 0 °C. The cooled reaction was quenched, dropwise, with 10% acetic acid and extracted with ethylacetate. The combined organic layers were washed with saturated sodium bicarbonate, brine, dried and concentrated. Purification by column chromatography yielded **A-1**.

**A-1** was dissolved in a suspension of methanol (0.5 M) and 0.1 eq 10% palladium on carbon. The reaction was vacuum sparged with hydrogen and stirred under an atmosphere of hydrogen overnight. The reaction mixture was filtered over Celite and concentrated to yield pure **3-157**.

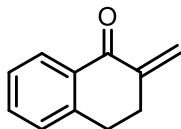
### **3-159 (R = H)**

**A-1** was dissolved in ether (0.1 M) and was treated with 2 eq lithium aluminum hydride portion wise at 0 °C. The reaction was allowed to proceed until the starting material was consumed by TLC and was worked up following the Fieser method. The crude product was dissolved in dioxane (0.1 M) and 1.9 eq DDQ was added. The reaction was allowed to stir 12 hours at which point DHQ was filtered away and the flow through was washed with saturated thiosulfate, brine, dried and concentrated. Yielding a slightly impure orange compound which was further chromatographed over silica gel to provide a clean **3-159 (R = H)**.

### **3-155**

Cyclohexene-1-carboxylic acid was suspended in DCM (0.2 M) with 1.1 eq EDC and 0.1 eq DMAP for 5 minutes to which 1 eq **3-159 (R = H)** was added as a solution in DCM (1 M). The resulting solution was allowed to stir at room temperature until **3-159 (R =H)** was found to be consumed by TLC. At which point the reaction was washed with saturated sodium bicarbonate, brine, dried over sodium sulfate, and concentrated. **3-155** was purified by silica gel chromatography.

### **3-168**



**A-2**

Tetralone and 4 eq of paraformaldehyde were suspended in THF (1.2 M) to which was added 1 eq diisopropylammonium trifluoroacetate and 0.1 eq trifluoroacetic acid. The reaction was allowed to stir for 2 hr at reflux. It was then cooled to room temperature and a second addition of 4 eq paraformaldehyde was added and the reaction was allowed to stir for an additional 12 hr at reflux. The mixture was cooled the solvent was removed and the mixture was resuspended in ether washed with 1 M HCl, 1 M NaOH, and brine before being dried with magnesium sulfate, concentrated and purified by silica gel chromatography to provide **A-2**.

To a 0 °C suspension of **A-2** and 1 eq cerium trichloride in methanol (0.3 M) was slowly added 1.5 eq sodium borohydride and the reaction was allowed to come to room temperature. After 10 minutes the suspension gelled and stirring ceased. The gel was dissolved in methanol, cooled to 0 °C and quenched by slow addition of water. The mixture was extracted with ethyl acetate and the combined extracts were washed with brine and concentrated. The crude reaction products were dissolved without purification in DCM (assumed 0.3 M) cooled to 0 °C and 1.5 eq recrystallized mCPBA was added to it. The reaction was allowed to come to room temperature overnight at which point it was quenched with 1 M NaOH and extracted with DCM. The combined extracts were washed with brine, dried over sodium sulfate, and concentrated to yield **3-168** as a mixture of diastereomers which were separated by column chromatography.

**3-165**

**3-168** was dissolved in DMSO (0.3 M) and 1.5 eq freshly prepared IBX was added to it and the mixture was allowed to stir for 3 hr. The mixture was separated between saturated sodium bicarbonate and ether and filtered through Celite. The organic layer was washed with water and brine, dried over magnesium sulfate and concentrated to provide **3-165** after purification by column chromatography.

**3-169** (and general procedure for titanocene epoxide reductions)

In a protocol adapted from the literature<sup>2</sup> we dissolved **3-165** in air-free, dry, distilled THF (0.05 M) with 1.5 eq activated zinc and 3 eq 2,4,6 trimethyl pyridine HCl salt. 0.2 eq titanocene dichloride was added as a suspension in THF every 3 hr for 24 hr. The reaction was quenched with saturated ammonium chloride, filtered through Celite. The resulting biphasic mixture was extracted with ether and the combined extracts were washed with brine, dried over magnesium sulfate, and concentrated yielding **3-169** after purification by silica gel chromatography.

Heck Reaction Optimization Data:

In collaboration with Merck Process Chemistry Enabling Technologies Group and Dr. Danielle Schultz we conducted high throughput reaction optimization in which 200  $\mu$ L reactions were set up in a glovebox under an argon atmosphere in 96 well plate formats enabling  $\mu$ mole scale reactions to be rapidly evaluated and analysis of conversions of **3-230** as well as yields of **3-236** were ascertained by UPLC-MS using di-tertbutyl biphenyl as an internal standard. Unfortunately, we did not have an authentic standard of Heck products **3-231**, **3-232**, **3-233**, **3-234** were unavailable at the time of the evaluation. However subsequent analyses established XPhos as a uniquely suitable ligand for the formation of these Heck products.

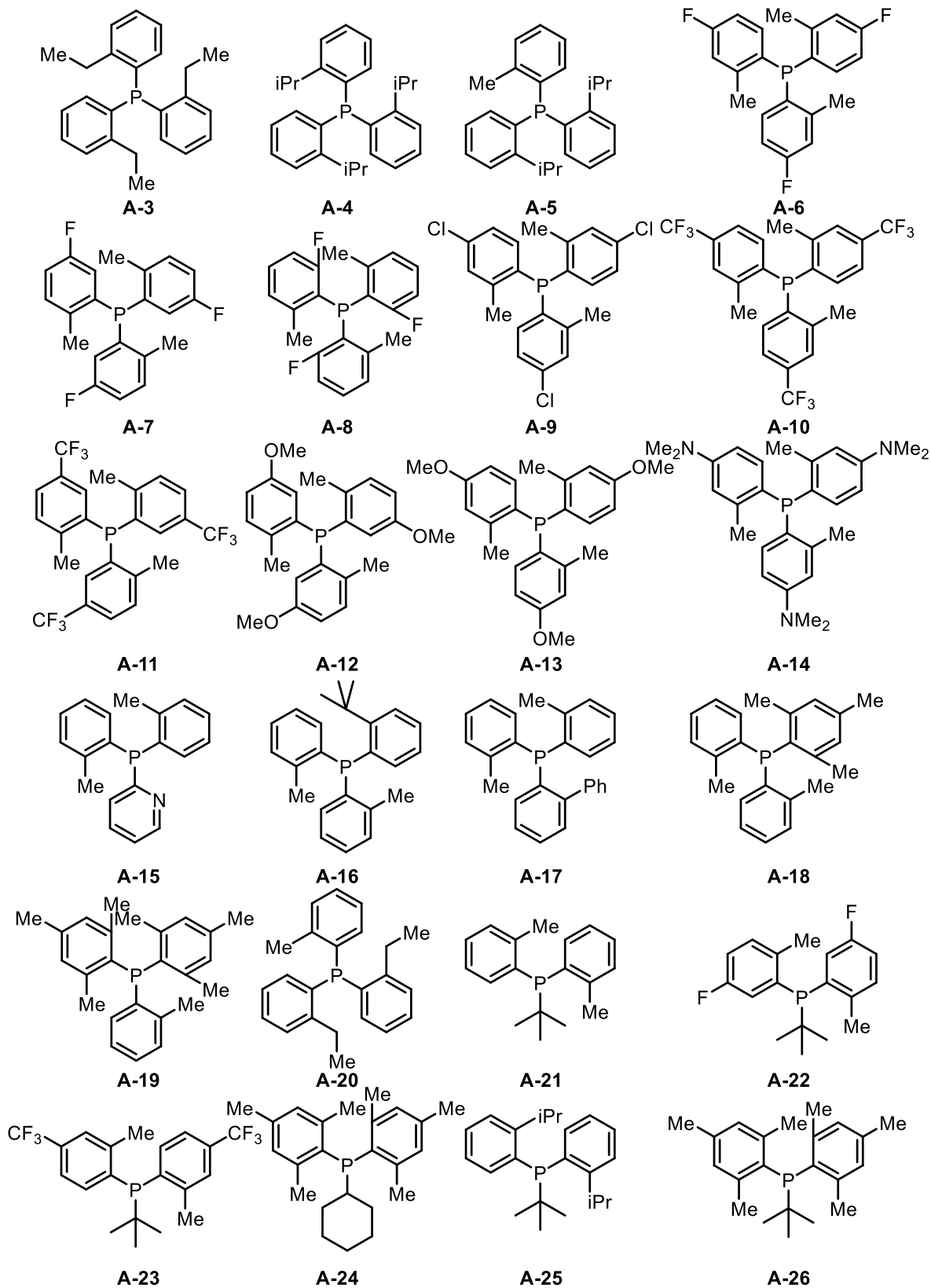


**Figure S3-** Merck Heck monodentate ligands.

0.2 eq Heck monodentate ligands. Rows A, C, E, and G are **A-3** to **A-14**  
 3 eq base Rows B, D, F, and H are **A-15** to **A-26** solvent (0.05 M)

Ag3PO4	21.1	24.4	16.6	11.4	5.54	8.41	10.8	13.7	8.62	19	-0.8	-0.8	DMA
	24.3	24.7	9.94		5.9	2.02	1.32	11	8.65	20	1.02	5.38	
Cy2NMe + AgNO3	11.8	25.8	8.41	5.39	10.5	15.6	7.23		14.7	8.2	1.85	3.22	MeCN
	10.5	14.8	11.9	0.13	11.5	3.21	9.93	9.46	25.9	-1.9	11.7	2.09	
Ag3PO4	19.4	28.1	20.6	19	19.2	9.12	-0.3	27.1	10.5	10	16.9	15.8	MeCN
	16.2	30.5	25.9	13.6	16.5	22.8	24	19.3	26.9	8.1	10.9	-0.1	
Cy2NMe + AgNO3	31.4	25.7	23.6	24.3	32.6	38.4	33.9	39	51.9	21	14.1	19.3	MeCN
	28.3	19.2	37	20.3	31.9	14.9	19.9	13.5	48.1	18	1.58	5.61	

0.1 eq Pd(OAc)<sub>2</sub> as a precatalyst, 12 h, 60 °C

% conversions

3 eq base solvent (0.05 M)

Ag3PO4	46.3	28.6	40.2	35.6	30.4	1.45	30.8	19.3	32.8	50	17.6	24.9	DMA
	37.7	31.4	56.7	39	14	35.6	7.18	40.3	31.8	41	18.2	5.72	
Cy2NMe + AgNO3	55.2	52.8	44.3	45.5	34.5	42	50.9	27.3	56.2	52	31.4	21.4	MeCN
	50	25	75.1	62.2	24	45.3	42.8	40.6	44.4	26	27.3	55.3	
Ag3PO4	46.2	33.5	21.1	26.6	10.3	26.2	37.9	18.5	7.09	1.2	29	32.5	MeCN
	34	12.5	50.5	18.4	34.6	38.7	31.1	16.4	10.1	28	10.4	29.2	
Cy2NMe + AgNO3	59.4	41.8	58.1	58.6	44.5	54.4	58.6	51.2	45.2	41	53	53.7	MeCN
	65.1	47.6	81.8	52.7	42.4	49.6	48.2	55.7	15.2	44	47.3	73.7	

0.1 eq Pd(OAc)<sub>2</sub> as a precatalyst, 12 h, 110 °C

% conversions

3 eq base solvent (0.05 M)

Ag3PO4	0	0	0	0	0	0	0	0	0	0	0	0	DMA
	0	0	5.94	0	0	0	0	0	0	0	0	0	
Cy2NMe + AgNO3	0	7.31	0	0	0	0	0	0	0	0	0	0	MeCN
	0	0	9.64	6.13	0	0	0	0	0	0	0	0	
Ag3PO4	0	0	0	0	0	0	0	0	0	0	0	0	MeCN
	0	0	0	0	12.3	0	0	0	0	0	0	0	
Cy2NMe + AgNO3	0	0	0	0	0	8.67	7.45	10.1	7.52	0	0	5.77	MeCN
	5.83	0	9.91	0	0	0	5.07	7.82	10.4	0	4.11	3.3	

0.1 eq Pd(OAc)<sub>2</sub> as a precatalyst, 12 h, 110 °C

% yield **3-236**

**Figure S4-** HTE screens of Heck ligands under palladium catalyzed Heck reaction conditions.

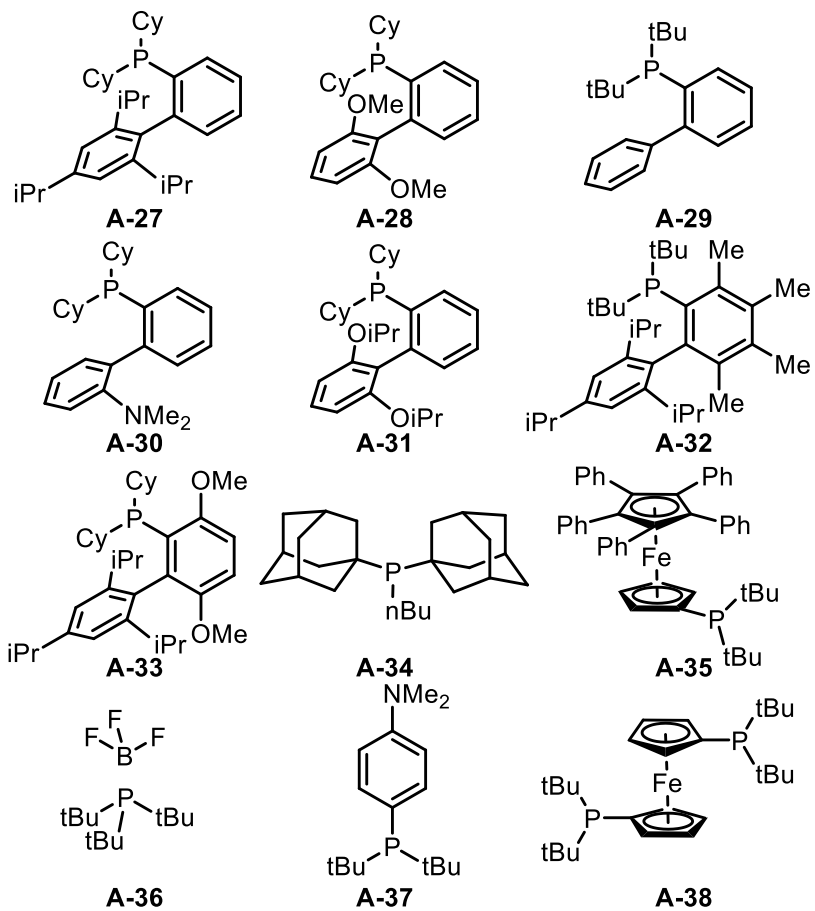


**Figure S5-** The structures of Merck's A-ligands which were compiled based upon their ability to promote myriad cross-coupling reactions.

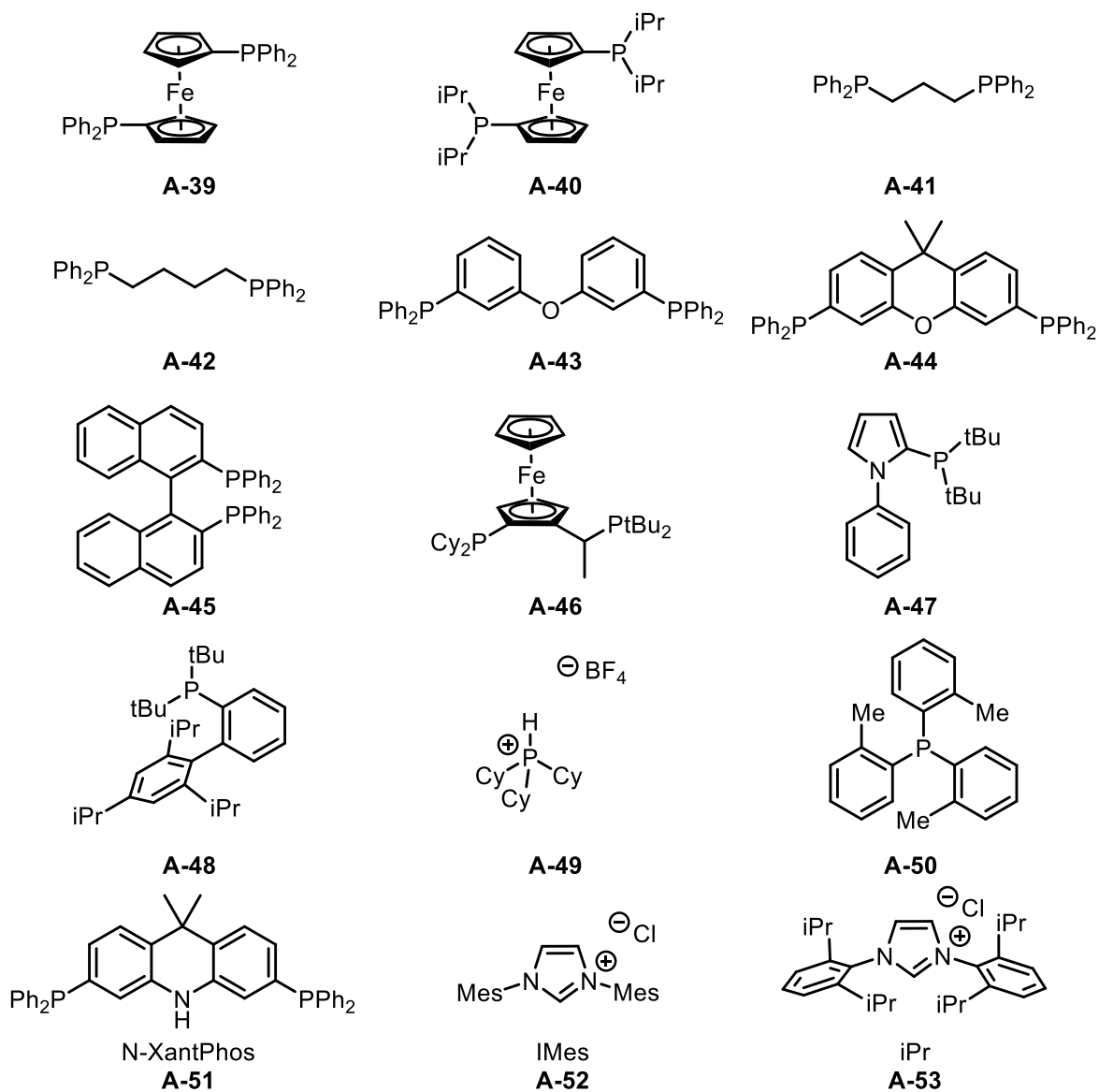


**Figure S6-** Merck's B ligands which were selected based upon their ability to promote myriad cross coupling reactions. Additionally the structures of N-XantPhos, IMes, and IPr are shown.



0.2 eq of Merck A/B ligands. Rows A, C, E, and G are **A-27 to A-38**  
 3 eq base Rows B, D, F, and H are **A-39 to A-50** solvent (0.05 M)

Ag3PO4	88.3	17.2	39.6	33.4	25.9	46.2	55.1	52.4	56.9	52	14.9	20.4	DMA
	39.5	23.3	14.5	-25	8.82	6.06	8.85	-8.3	-67	-43	13.8	-1.6	
Cy2NMe + AgNO3	58.7	-38	62.6	-19	-11	9.66	45.3	-5	53.9	24	42	-1.4	MeCN
	55.9	35.9	58.8	49.9	74.4	52.7	69	31.1	69.5	50	61.2	56	
Ag3PO4	50.5	56.6	46.7	35.9	12.1	45.4	62.6	52.1	58.6	45	42.9	21.7	MeCN
	47	42.1	47.8	50	69.4	53.6	56.6	49.3	36.9	30	12.2	26	
Cy2NMe + AgNO3	65.7	56.4	67.5	50.1	55.4	65.1	62.5	78.1	62.8	49	63	54.2	MeCN
	51.5	45.6	65.1	58.7	100	48	57.4	63.4	65.9	57	65.9	64.3	

0.1 eq Pd(OAc)<sub>2</sub> as a precatalyst, 12 h, 110 °C % conversions  
 3 eq base solvent (0.05 M)

Ag3PO4	0	0	0	0	0	0	0	0	0	0	0	0	DMA
	0	0	0	0	0	0	0	0	0	0	0	0	
Cy2NMe + AgNO3	0	0	0	0	0	0	5.85	0	0	0	0	0	MeCN
	0	0	0	0	0	0	0	0	5.97	0	0	0	
Ag3PO4	0	0	0	0	0	0	0	0	8.76	0	0	0	MeCN
	0	0	0	0	0	0	0	0	0	0	0	0	
Cy2NMe + AgNO3	0	0	5.31	0	0	6.78	0	4.57	7.42	0	0	0	MeCN
	7.06	5.11	4.58	0	3.7	0	5.94	0	7.4	0	0	6.59	

0.1 eq Pd(OAc)<sub>2</sub> as a precatalyst, 12 h, 110 °C % yield **3-236**  
 solvent (0.05 M) 3 eq

	A/B Ligands Except A10 and B7 including in column 12 IMes and lpr with KHMDS												
dioxane	-36	-7.8	-3.4	-3	-20	21.6	82.3	37.5	15.3	-12	12.4	-16	+AgNO3
	8.73	-9.5	19.9	87.4	30.6	32.5	57.5	11.3	5.38	0.5	3.96	6.76	
toluene	16.9	54.6	1.66	8.2	10.7	24.7	84.6	46.3	28.5	26	24.1	35.4	-AgNO3
	87.2	31.3	36.8	87.5	47.5	34.5	20.2	11.9	-4.4	19	12.9	9.94	
dioxane	23.3	22.7	1.99	46.4	40.9	7.18	91.9	66.2	41.7	21	15.2	-3.5	-AgNO3
	-41	-21	17.6	76.4	83.7	100	38.8	-1.8	-5.6	35	17	-11	
toluene	7.94	-29	-12	-6.1	29.3	21	66.2	34.2	12.6	5.4	8.28	7.55	+AgNO3
	-38	2.67	22	73.8	47.6	37.9	77.7	21.4	15.1	12	8.64	9	

0.1 eq Ni(COD)<sub>2</sub> as a precatalyst, 3 eq Cy<sub>2</sub>NMe, 12 h, 110 °C % conversions  
 solvent (0.05 M) 3 eq

	A/B Ligands Except A10 and B7 including in column 12 IMes and lpr with KHMDS												
dioxane	0	0	0	9.62	24.4	2.24	0	1.57	1.46	2.5	1.63	2.55	+AgNO3
	0	0	1.96	0.34	2.25	0	0	0	0	0	0	0	
toluene	0	0	0	0	21	0	0	0	0	0	0	0	-AgNO3
	25.6	16.8	0	14.8	14.2	17.8	8.27	0	0	0	0	0	
dioxane	5.07	3.35	3.53	0	10	2.6	0.85	1.47	0	0	3.04	2.35	-AgNO3
	17.7	7.42	5.92	35.3	35.1	87.9	27.8	11.7	10.9	9.1	7.22	5.21	
toluene	0	0	0	0	0	0	0	0	0	0	0	0	+AgNO3
	0	0	0	7.87	0	12.8	0	0	0	0	0	0	

0.1 eq Ni(COD)<sub>2</sub> as a precatalyst, 3 eq Cy<sub>2</sub>NMe, 12 h, 110 °C % conversions

**Figure S7-** HTE screens of Heck A/B ligands under palladium and nickel catalyzed Heck reaction conditions.

0.2 eq of selected ligands. Column 1 and 7 **A-42**, 2 and 8 **A-43**, 3 and 9 **A-44**, 4 and 10 **A-51**,  
5 and 11 CyDPEPhos, 6 and 12 tBuXantPhos

3 eq Base solvent (0.05 M) solvent (0.05 M) 3 eq Base

K3PO4	MeCN	2.04	2.29	3.12	1.07	2.88	1.69	2.67	8.14	1.06	2	4.63	4.22	dioxane	K3PO4
26Lutidene		12.6	11.8	18.8	21	7.99	0	0	11	0	0	9.18	10.7		26Lutidene
Hunigs Base		4.26	18.6	13.1	12	10.3	0	6.82	12.3	10.2	7.2	10.6	7.19		Hunigs Ba:
Cy2NMe		9.97	34.6	8.93	26.4	4.76	0	7.17	20.9	13.8	0	8.64	10.3		Cy2NMe
K3PO4	DMA	2.04	3.55	1.43	3.27	0.81	1.19	5.74	3.29	5.2	0	4.32	2.72	tamylOH	K3PO4
26Lutidene		8.52	16	16.7	18	5.7	10.5	9.71	17	19	11	8.65	8.65		26Lutidene
Hunigs Base		27.4	38.4	21.2	25.8	11.3	8.6	10.9	17.4	29.7	13	16.2	13.4		Hunigs Ba:
Cy2NMe		37.6	56.9	12.6	23.9	5.56	8.17	11	10	26.6	19	27.8	9.85		Cy2NMe

% yield **3-236**

3 eq Base solvent (0.05 M) solvent (0.05 M) 3 eq Base

K3PO4	MeCN	100	100	98.3	100	100	100	100	100	96.8	100	100	100	dioxane	K3PO4
26Lutidene		87.8	86.1	48.2	41.7	60.7	48.2	19.8	86.8	29	45	70.8	43		26Lutidene
Hunigs Base		81.1	57.2	38.4	41.5	80.1	43.3	49.1	36.1	38.6	29	67.1	15.3		Hunigs Ba:
Cy2NMe		93.5	84.9	77.4	61.5	81.8	61.3	47.4	20.5	41.4	26	75.2	33.9		Cy2NMe
K3PO4	DMA	100	100	100	100	100	100	100	99	99.5	98	100	97.6	tamylOH	K3PO4
26Lutidene		61.1	67.4	25.8	68.2	70.5	28.9	54.1	66	74.1	57	95.1	33.7		26Lutidene
Hunigs Base		87.6	24.8	33.2	45	66.5	42.6	60.8	46.4	58.4	38	76.3	33.3		Hunigs Ba:
Cy2NMe		98.5	81	79.4	56	83	73.5	92.4	52.3	53	48	100	37.5		Cy2NMe

% conversion

0.1 eq Ni(COD)<sub>2</sub> as a precatalyst, 12 h, 110 °C

**Figure S8-** HTE screens of selected ligands in nickel catalyzed Heck reaction conditions.

			MeCN			DMF			dioxane					
			no ligand	dtbbpy	box	n-xantphos	no ligand	dtbbpy	box	n-xantphos	no ligand	dtbbpy	box	n-xantphos
(Ir[dF(CF <sub>3</sub> )ppy] <sub>2</sub> (dtbbpy))PF <sub>6</sub>	Cy <sub>2</sub> NMe	Ni(COD) <sub>2</sub>	11	11	41	26	11	23	41	17	12	9.7	46	15
		NiCl <sub>2</sub> -dme	10	9.4	14	19	7.8	12	28	25	11	20	20	9.5
	Cs <sub>2</sub> CO <sub>3</sub>	Ni(COD) <sub>2</sub>	5.5	4.7	6.5	9.6	6.6	8.9	8.8	3	2	2.4	4.7	3
		NiCl <sub>2</sub> -dme	2.1	1.7	5.1	6.5	4.7	8.6	4.5	3.1	1.7	1.5	1.1	1.9
no photo-catalyst	Cy <sub>2</sub> NMe	Ni(COD) <sub>2</sub>	2.3	2.2	3.1	4.8	4	8	4.7	2.9	2.3	2.6	2.3	0
		NiCl <sub>2</sub> -dme	0	1.9	0	0	0	0	0	0	0	0	0	2.4
	Cs <sub>2</sub> CO <sub>3</sub>	Ni(COD) <sub>2</sub>	2.5	2.9	6.4	5.1	6.7	5.8	7.7	2.9	2.4	2.3	1.9	2.4
		NiCl <sub>2</sub> -dme	0	0	6.1	4.6	3.9	4.4	3.8	2	1.7	1.7	1.7	37

% yield **3-236**

			MeCN			DMF			dioxane					
			no ligand	dtbbpy	box	n-xantphos	no ligand	dtbbpy	box	n-xantphos	no ligand	dtbbpy	box	n-xantphos
(Ir[dF(CF <sub>3</sub> )ppy] <sub>2</sub> (dtbbpy))PF <sub>6</sub>	Cy <sub>2</sub> NMe	Ni(COD) <sub>2</sub>	87	83	89	89	96	78	96	98	71	66	90	96
		NiCl <sub>2</sub> -dme	69	74	82	81	94	82	94	96	97	81	96	90
	Cs <sub>2</sub> CO <sub>3</sub>	Ni(COD) <sub>2</sub>	53	66	52	86	90	95	93	96	71	69	61	73
		NiCl <sub>2</sub> -dme	41	51	43	68	86	90	90	96	60	61	58	54
no photo-catalyst	Cy <sub>2</sub> NMe	Ni(COD) <sub>2</sub>	45	29	35	37	38	37	27	33	40	27	23	28
		NiCl <sub>2</sub> -dme	15	17	14	25	23	21	24	30	15	24	20	15
	Cs <sub>2</sub> CO <sub>3</sub>	Ni(COD) <sub>2</sub>	18	43	27	63	76	81	83	88	51	48	47	48
		NiCl <sub>2</sub> -dme	19	24	11	53	78	83	85	90	54	41	38	32

% conversion

**Figure S9-** HTE follow up investigations in nickel catalyzed photochemical Heck reaction conditions. 1% photocatalyst loading.

		dppf	dppf	dppp	dppb	DPEPhos	Xantphos	R-Bnnp	SL-J03-1	N-phenyl dibenzosilolepyridine	Cy3P-HEF4	lo-dppp	NIXantphos
Cy2NMe	(Ir[dF(CF3)ppy]2(dtbpy))Cl	10	5.1	37	16	20	39	9.5	6.9	5	6.4	5.1	32
	Ru(bpy)3Cl2	11	7.9	35	17	13	22	10	7.1	6.7	8.2	5.4	15
	dark & (Ir[dF(CF3)ppy]2(dtbpy))Cl	4.4	3.1	2.4	3.3	4	2.7	1.8	1.2	0	2.6	1.9	2
	no photocat	2.9	2.5	6.5	9.5	6.1	6.3	3	2.5	1.9	0	1.8	2.3
K3PO4	(Ir[dF(CF3)ppy]2(dtbpy))Cl	1	1.8	11	13	6.9	16	5	3.1	2.7	4.8	2.9	4.2
	Ru(bpy)3Cl2	1.8	1.7	8.7	9.5	7	13	3.5	2.6	2.3	3.3	0	5.5
	dark & (Ir[dF(CF3)ppy]2(dtbpy))Cl	0	1.9	3.4	4.3	2.4	2.9	2.8	2.7	2.9	1.9	0	2
	no photocat	2.6	1.8	10	6.4	6.1	13	3.2	2.4	0	2.3	0	4.4

% yield 3-236

		dppf	dppf	dppp	dppb	DPEPhos	Xantphos	R-Bnnp	SL-J03-1	N-phenyl dibenzosilolepyridine	Cy3P-HEF4	lo-dppp	NIXantphos
Cy2NMe	(Ir[dF(CF3)ppy]2(dtbpy))Cl	87	83	89	89	96	78	96	98	71	66	90	96
	Ru(bpy)3Cl2	69	74	82	81	94	82	94	96	97	81	96	90
	dark & (Ir[dF(CF3)ppy]2(dtbpy))Cl	53	66	52	86	90	95	93	96	71	69	61	73
	no photocat	41	51	43	68	86	90	90	96	60	61	58	54
K3PO4	(Ir[dF(CF3)ppy]2(dtbpy))Cl	45	29	35	37	38	37	27	33	40	27	23	28
	Ru(bpy)3Cl2	15	17	14	25	23	21	24	30	15	24	20	15
	dark & (Ir[dF(CF3)ppy]2(dtbpy))Cl	18	43	27	63	76	81	83	88	51	48	47	48
	no photocat	19	24	11	53	78	83	85	90	54	41	38	32

% conversion

		dppf	dppf	dppp	dppb	DPEPhos	Xantphos	R-Bnnp	SL-J03-1	N-phenyl dibenzosilolepyridine	Cy3P-HEF4	lo-dppp	NIXantphos
26Lutidene	(Ir[dF(CF3)ppy]2(dtbpy))Cl	8.2	3.1	7	6.6	11	10	5	2.6	8	6.1	8.3	6.2
	Ru(bpy)3Cl2	3.6	2.4	3.4	3.3	4.2	6.1	3.5	2.7	3.6	3.3	3.4	4.8
	dark & (Ir[dF(CF3)ppy]2(dtbpy))Cl	3.4	2.3	8	5	2.8	3.8	3.2	5.6	9.8	2.9	8.1	3.6
	no photocat	5.4	2.1	9	8.4	9.2	7.8	2.6	3	6	2.6	4.5	5.6
DIPEA	(Ir[dF(CF3)ppy]2(dtbpy))Cl	5.2	3.6	30	18	15	14	5.8	3.6	3.9	5.4	4.5	17
	Ru(bpy)3Cl2	7.7	5.8	26	15	13	18	7.3	6.4	9.8	9.2	8	15
	dark & (Ir[dF(CF3)ppy]2(dtbpy))Cl	4.7	3.3	7.4	3.4	3.7	2.6	2.4	3	3.9	5.8	2.7	2.5
	no photocat	2.8	2.2	11	10	3.5	3.2	2.4	2.3	3.5	2.2	1.8	3.1

% yield 3-236

		dppf	dppf	dppp	dppb	DPEPhos	Xantphos	R-Bnnp	SL-J03-1	N-phenyl dibenzosilolepyridine	Cy3P-HEF4	lo-dppp	NIXantphos
26Lutidene	(Ir[dF(CF3)ppy]2(dtbpy))Cl	4.6	14	-6	-0.4	22	16	3.5	38	45	15	32	20
	Ru(bpy)3Cl2	23	23	16	15	18	16	10	30	24	15	25	14
	dark & (Ir[dF(CF3)ppy]2(dtbpy))Cl	27	21	18	15	22	14	9.7	13	21	11	25	19
	no photocat	15	19	18	16	19	14	8.8	22	21	26	27	18
DIPEA	(Ir[dF(CF3)ppy]2(dtbpy))Cl	29	22	65	53	39	33	17	25	31	16	48	33
	Ru(bpy)3Cl2	26	28	55	49	30	33	14	25	48	27	38	40
	dark & (Ir[dF(CF3)ppy]2(dtbpy))Cl	28	18	22	33	17	11	7.1	11	17	17	23	13
	no photocat	24	19	28	34	11	6.9	11	14	13	13	21	37

% conversion

Figure S10- HTE follow up investigations nickel catalyzed photochemical Heck reaction conditions 0.01% photocatalyst loading.

## Bibliography

1. Annand, J. R.; Bruno, P. A.; Mapp, A. K.; Schindler, C. S. *Chem. Commun.* **2015**, *51*, 8990.
2. Dong, L.; Deng, L.; Lim, Y. H.; Leung, G. Y. C.; Chen, D. Y.-K. *Tetrahedron* **2011**, *40*, 4070.